ICCESEN-2024

11th International Conference on Computational and Experimental Science and ENgineering

Antalya-TURKEY

25-28 October 2024

iccesen2024@gmail.com

2024.iccesen.org

Proceedings of ICCESEN-2024

EDITORS

Prof.Dr. İskender AKKURT

Dr. Nurdan KARPUZ

ISBN : 978-605-68728-9-1

ICCESEN 25-27 October 2024 Kemer-Antalya-TURKEY www.iccesen.org

11th International Conference on Computational and Experimental Science and ENgineering

Antalya-TURKEY
25-28 October 2024

Proceedings of ICCESEN-2024

Editors:
Prof.Dr. İskender AKKURT
Dr. Nurdan KARPUZ

ISBN: 978-605-68728-9-1

Proceedings of ICCESEN-2024 ,

11th International Conference on Computational and Eperimental Science and Engineering (**ICCESEN-2024**)

25-28 October 2024, Antalya-TURKEY

Editors:
Prof. Dr. İskender AKKURT
Dr. Nurdan KARPUZ

Published : 31 October 2024
ISBN: 978-605-68728-9-1

TABLE OF CONTENTS

FOREWORD

Dear Colleagues,

It is a great honor for me to host you all in **"11th International Conference on Computational and Experimental Science and Engineering (ICCESEN-2024)"** was taken place in Antalya-TURKEY in the period of 25-28 October 2024.

We are also happy to publish the proceeding of ICCESEN-2024. All papers have been reviewed by two reviewers.

Prof. Dr. İskender AKKURT

Chair for ICCESEN-2024
Editor for Proceedings of ICCESEN-2024

ORGANISATION COMMITTEE

Prof.Dr. Iskender AKKURT (Chair)	Suleyman Demirel University, Isparta -Turkey
Dr. Kadir GÜNOĞLU (secretary)	Isparta Uygulamalı Bilimler University, Isparta -Turkey
Dr. Hakan AKYILDIRIM	Suleyman Demirel University, Isparta -Turkey
Dr. Nurdan KARPUZ	Amasya University, Amasya -Turkey
Dr. Sabiha Anas BOUSSAA	CRTSE-Algeria
Dr. Feride KULALI	Üsküdar University, Istanbul-Turkey
Dr. Osman GÜNAY	Yıldız Technical University, Istanbul -Turkiye
Dr. Feride KULALI	Üsküdar University, Istanbul-Turkey
Dr. Mucize SARIHAN	Okan University, Istanbul-Turkey
Dr. Aycan ŞENGÜL	Akdeniz University, Antalya-Turkey
Lect. Berra Seda SARIHAN	Okan University, Istanbul-Turkey

SCIENTIFIC COMMITTEE

Prof.Dr. Iskender AKKURT (Chair)	Suleyman Demirel University, Isparta –Turkey
Prof.Dr. Majid ABBASPOUR	Sharif University of Technology-Iran
Prof.Dr. Zahid Hussain ABRA	Quadi-E-Awam University, Sindh-Pakistan
Prof.Dr. Abdullah ALAMRI	King Saud University, Saudi Arabia
Prof.Dr. Nezam Mahdavi-AMIRI	Sharif University Iran
Dr. John R.M.ANNAND	Glasgow University, Glasgow-Scotland (UK)
Dr. Majda AOUITITEN	Abdelmalek Essaadi University-Morocco
Prof.Dr. Mohamed Kheireddine AROUA	University of Malaya-Malaysia
Dr. Rachid BELKADA	CRSTSE -Algeria
Dr. Radhey S BENIWAL	CSIR-NISCAIR, New Delhi 110012, India
Dr. Mahmoud Abdullah BENNASER	Kuwait University-Kuwait
Dr. Djoudi BOUHAFS	Centre de Recherche en Technologie -Algeria
Prof. Oleg BURDAKOV	Linköping University Linköping, Sweden
Dr. Yusuf CEYLAN	Selcuk University, Konya-Turkey
Prof.Dr. Lotfi CHOUCHANE	Weill Cornell MEdical College-Qatar
Dr. Manju D CHOUDHARY	Niscair-India
Dr. Nermin DEMİRKOL	Kocaeli University, Kocaeli –Turkey
Prof.Dr. İbrahim DİNÇER	University of Ontario Institue of Technology (UOIT)-Canada
Prof. Dr. Mitra DJAMAL	Institute Teknologi Bandung-Indonesia
Prof.Dr. Mahmut DOĞRU	Bitlis Eren University, Bitlis-Turkey
Prof.Dr. Mohammed Mostafa EL TOKHI	United Arab Emirates University-UAE
Dr. Zuhal ER	Istanbul Technical University, Istanbul-Turkey
Prof.Dr. Mustafa EROL	Dokuz Eylul University, İzmir-Turkey
Prof.Dr. Madjid FATHI	Dept. of EECS University of Siegen- Germany
Prof.Dr. Jan FELBA	Wroclaw University of Technology-Poland
Prof.Dr. S. Mostafa GHIAASIAAN	Mechanical/Nuclear Engineering, Georgia Tech USA
Prof.Dr. Mustafa GÜNAL	Gaziantep University, Gaziantep-Turkey
Prof. Dr. Amir HUSSAIN	University of Stirling- Scotland(UK)
Dr. Nabi IBADOV	Warsaw University of Technology-Poland
Prof.Dr. Fatma KARİPCİN	Nevşehir Hacı Bektaşi Veli University-Turkey
Prof.Dr. Hamdi Ş. KILIÇ	Selcuk University, Konya-Turkey
Dr. Menekşe V. KILIÇARSLAN	İstanbul Aydın University, Istanbul-Turkey

Prof.Dr. Ziya Erdem KOÇ	Selcuk University, Konya-Turkey
Prof. Dr. İsmail KOYUNCU	Istanbul Technical University, Istanbul-Turkey
Dr. Irida MARKJA	Polytechnic University,Tirana-Albania
Dr. F.Zümrüt Biber MÜFTÜLER	Ege University, Izmir-Turkey
Dr. Susan Shukur NOORI	Kirkuk University, Kirkuk-lraq
Prof.Dr. Ravindra NUGGEHALLI	New Jersey Institute of Technology-USA
Prof.Dr. İbrahim ÖRÜN	Aksaray University, Aksaray-Turkey
Prof.Dr. Necati ÖZDEMİR	Balıkesir University, Balıkesir-Turkey
Dr. Zeynep PARLAR	Istanbul Technical University, Istanbul-Turkey
Prof.Dr. Ioana G. Petrisor	ToxStrategies, Inc., Mission Viejo, CA
Dr. Tomasz PIOTROWSKI	Warsaw University of Technology, Warsaw-Poland
Prof.Dr. Javad RAHIGHI	AEOI, Tehran-Iran.
Dr. Abdelmadjid RECIOUI	University of Boumerdes-Algeria
Prof.Dr. Osman SAGDIÇ	Yıldız Technical University, Istanbul-Turkey
Prof.Dr. Miljko SATARIC	Faculty of Technical Sciences Novi Sad-Serbia
Prof.Dr. Saleh SULTANSOY	TOBB University, Ankara-Turkey
Dr. Naim SYLA	University of Prishtina-Kosova
Prof. Dr. Mustafa TAVASLI	Uludag University, Bursa-Turkey
Dr. Huseyin TOROS	Istanbul Technical University, Istanbul-Turkey
Prof.Dr. Ahmad UMAR	Najran University-Saudi Arabia
Prof.Dr. Gerhard-Wilhelm WEBER	Middle East Technical University Ankara-Turkey
Prof.Dr. Erol YAŞAR	Mersin University, Mersin-Turkey

INVITED SPEAKERS

Prof. Dr. Amir HUSSEIN

Edinburgh Napier University, UK

Title: Trustworthy AI-enabled Sustainable Technologies

Prof.Dr. Madjid FATHI

Dept. of EECS University of Siegen, GERMANY

Title: Artificial Intelligent as a Concept or as a System: utilizing and conceptualizing AI in Industrial and health care

Dr. Hayat ARBOUZ

University Saad Dahlab Blida1, Algeria

Title: Investigation of the potential of the double perovskite materials Cs2BX6 and Cs2BB'X6 as absorbers in single and tandem solar cells for high-efficiency photovoltaic conversion

Prof.Dr. Mansour Almatarneh

University of Jordan-Jordan

Title: Sustainable Development in the Global Rankings

Prof.Dr. Gerhard-Wilhelm WEBER

Poznan University of Technology-POLAND

Title: Regime-switching models via stochastic optimal control & robust control theory, with applications in finance and insurance

Magneto-optical transition energy in Kane oscillator

Arif BABANLI[1]✉

[1]Suleyman Demirel University, Physics. Department, Isparta, Turkey
✉ Corresponding author: arifbabanli@sdu.edu.tr.

ABSTRACT

The energy spectrum of carriers in a two-dimensional Kane oscillator in a magnetic field was calculated using the non-minimum interaction method. We calculated the magneto-optical transition energy for InSb-type quantum dots with parabolic potential.

1. INTRODUCTION

Extensive research has been conducted on quantum dots with confinement potentials in two [1] and [2] three dimensions. Modern nanotechnology can control the number of particles in quantum dots, the stiffness coefficient of the confinement potential, and other parameters.

The literature [1] mainly uses infinite deep and parabolic potential to find the energy spectra of charge carriers in quantum dots. The parabolic potential model has been confirmed by suitable calculations [3] and can be applied to quantum dots of not very large size. Currently, quantum dots are mainly made of (InAs, GaAs, InSb, etc.) type semiconductors. Since these semiconductors have a complex band structure, the energy spectra of charge carriers are expressed by multi-zone Hamiltonian. The non-parabolicity of energy spectra of charge carriers can be viewed based on the 8-band Kane model [4]. If the parabolic potential is included as a scalar potential within the 8-band Kane model and solved, it is impossible to analytically solve the obtained equation as in [4] in special approximations.

Moshinski and Szepaniak introduced a new interaction operator to the Dirac equations [5,6]. Thus, he took the momentum operator as a linear function of the coordinate. This type of interaction is called a non-minimal interaction. When the non-minimal interaction is included in the Dirac equations and reduced to one equation, the obtained equation comes to the harmonic oscillator equation in non-relativistic quantum mechanics (with the addition of a constant limit due to the strong spin-orbit interaction). This problem is called the Dirac oscillator in the literature. Since Dirac's equation is a multi-component equation like Kane's equations, the aforementioned non-minimal interaction method can be applied to Kane's equations. In this paper, we use the non-minimal interaction method for the two dimensions of Kane equations with a magnetic field.

The 2D Kane Hamiltonian without spin-orbit interaction has the form [7,8]:

2. MATERIALS AND METHODS

$$H=\begin{pmatrix} \varepsilon_g-\varepsilon & -\frac{Pk_-}{\sqrt{2}} & 0 & \frac{Pk_+}{\sqrt{2}} \\ -\frac{Pk_+}{\sqrt{2}} & -\varepsilon & 0 & 0 \\ 0 & 0 & -\varepsilon & 0 \\ \frac{Pk_-}{\sqrt{2}} & 0 & 0 & -\varepsilon \end{pmatrix} \tag{1}$$

Here, *P* is the Kane parameter and ε_g - is the band gap energy. The zero energy is chosen at the bottom of the conduction band and $k_\pm=-i\partial_x\mp\partial_y$

Let us carry out the non-minimal substitution.

$$k_\pm\to k_\pm-i\left(\beta\frac{m\omega}{\hbar}\pm\frac{1}{2}\frac{m\omega_c}{\hbar}\right)r_\pm;r_\pm=x\pm iy \tag{2}$$

If we replace the components of the wave function only with the components of the conduction zone, we get the following expression:

$$\left(\frac{\varepsilon\left(\varepsilon_g-\varepsilon\right)}{P^2}-\partial_x^2-\partial_y^2+\frac{m^2\rho^2}{\hbar^2}\left(\omega^2+\frac{\omega_c^2}{4}\right)+\frac{m\omega_c}{\hbar^2}L_z+\frac{m\omega}{\hbar}\right)\Psi_1\left(x,y\right)=0 \tag{3}$$

Taking into account relationships [5]

$$\frac{P^2}{\varepsilon_g}=\frac{\hbar^2}{2m} \tag{4}$$

We obtain in polar coordinates as

$$\left(-\frac{\varepsilon\left(\varepsilon_g-\varepsilon\right)}{\varepsilon_g}+\frac{\hbar^2}{2m}\left(\partial_\rho^2+\frac{1}{\rho}\partial_\rho+\frac{1}{\rho^2}\partial_\phi^2\right)-\frac{m\rho^2}{2}\left(\omega^2+\frac{\omega_c^2}{4}\right)+i\hbar\frac{\omega_c}{2}\partial_\phi-\frac{h\omega}{2}\right)\Psi_1\left(\rho,\phi\right)=0 \tag{5}$$

The solution of the form

$$\Psi_1\left(\rho,\phi\right)=e^{in\phi}R\left(\rho\right) \tag{6}$$

Obtaining the radial function equation

$$\left(-\frac{\varepsilon\left(\varepsilon_g-\varepsilon\right)}{\varepsilon_g}+\frac{\hbar^2}{2m}\left(\partial_\rho^2+\frac{1}{\rho}\partial_\rho-\frac{n^2}{\rho^2}\right)-\frac{m\rho^2\Omega^2}{8}-n\frac{\hbar\omega_c}{2}-\frac{h\omega}{2}\right)R(\rho)=0 \tag{7}$$

where $\Omega=\sqrt{4\omega^2+\omega_c^2}$

The energy levels are given by the formula [9]:

$$\frac{\varepsilon\left(-\varepsilon_g+\varepsilon\right)}{\varepsilon_g}=\hbar\Omega\left(n_\rho+\frac{|n|}{2}\right)+\frac{h\omega}{2}+n\frac{\hbar\omega_c}{2}, n_\rho=0,1,..,n=0,\pm1,\pm2,... \tag{8}$$

If we choose zero of energy in the middle of the energy gap $\varepsilon\to\varepsilon+\frac{\varepsilon_g}{2}$, the energy levels of electrons and light holes obtained as

$$\varepsilon=\pm\sqrt{\frac{\varepsilon_g^2}{4}+\varepsilon_g\hbar\Omega\left(n_\rho+\frac{|n|}{2}\right)+\varepsilon_g\frac{h\omega}{2}+n\varepsilon_g\frac{\hbar\omega_c}{2}} \tag{9}$$

Figure 1 shows our theoretical results for the magneto-optical transition energy $(00)\to(01);(00)\to(0,-1);\ h\omega=0.025eV,\varepsilon_g=0.24eV$.

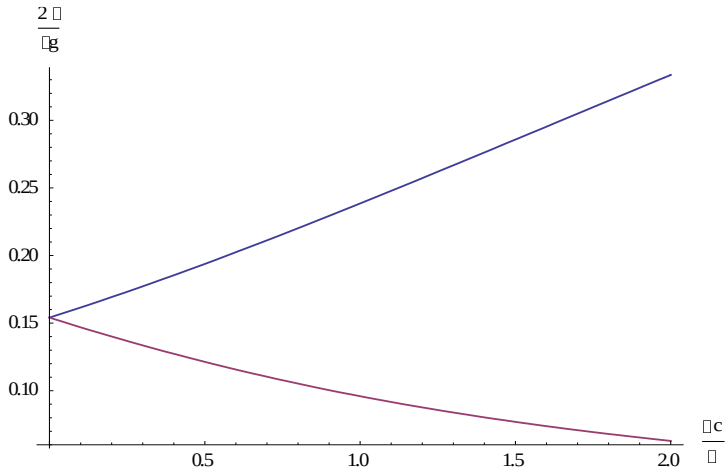

Figure 1. *The dependence magneto-optical transition energy* $(00)\to(01);(00)\to(0,-1);$ *with magnetic field at* $h\omega=0.025eV,\varepsilon_g=0.24eV$.

3. RESULTS AND DISCUSSIONS

Magneto-optical properties of quantum dots in Kane-type semiconductors have been considered using parabolic confinement. The eigen energies of the system have been studied, taking into account the real band structure of materials.

REFERENCES

[1] Chakraborty T., Quantum Dots, Elsevier, Amsterdam, 1999, p.349
[2] Капуткина Н.Е., Лозовик Ю.Е. Шаровые квантовые точки // ФТТ 1998, том.40., №11, с.1753-1759
[3] Darnhofer T. and Rössler U. Effects of band structure and spin in quantum dots // Phys. Rev B, 1993, v.47, p.16020-16023
[4] Bimberg D.,Grundman M., Ledentsov M. Quantum Dot Heterostructures, JOHN WILEY 2001, 299 p.
[5] Moshinsky M. and Szezepanik A . The Dirac oscillator // J.Phys. A: Math.Gen., 1989, v.22, p.L817-L819
[6] Moshinsky M. And A del Sol Mesa The Dirac oscillator of arbitrary spin // J.Phys.A: Math.Gen.,1996, v. 29, p.4217-4236
[7] *Davies John H. The Physics of low-dimensional semiconductors.Cambridge University Press, 1997,438* p.
[8] Babayev A.M. Doctoral thesis1992,Bakı
[9] L.D.Landau and E.M. Lifshitz, Quantum mechanics,1965

Effective g*-factor of electrons in semiconductor quantum dot with wedge disclinations and Rashba spin-orbit interaction

Arif BABANLI[1]✉

[1]*Suleyman Demirel University, Physics. Department, Isparta, Turkey*
✉ *Corresponding author: arifbabanli@sdu.edu.tr.*

ABSTRACT

The present work investigates the effect of topological defects in quantum dots on the effective g*-factor. Using the energy spectrum, we derived the exact analytic expression for the effective g*-factor and studied the variation of the effective g*-factor with the disclination parameter. It was shown that, in the case of n=0,l=-1, as the magnetic field increases, the effective g*-factor changes sign and increases, approaching the value n=0,l=0. In the case of n=0,l=1, it decreases and approaches n=0,l=0. In the case of n=0,l=0, the effective g factor remains constant as the magnetic field changes.

KEYWORDS: *effective g*-factor, quantum dot, wedge disclinations.*

1. INTRODUCTION

In recent years there has been increased interest, both theoretically and experimentally in quantum dot geometry in the presence of a magnetic field. The electron spin plays an important role in the quantum dot design. Spin-dependent effects naturally present in quantum dots are of great importance for the emerging field of spintronic. Spintronic is a new branch of electronics where electron spin is the active element for information storage and transport. An example is Rashba spin-orbit coupling [1], which has recently attracted much attention as it is the basis of a spin-controlled field-effect transistor.

A reasonable model to describe such nonrelativistic quantum dot systems requires a parabolic quantum and the confining potential [2].

In the paper [3], the authors examined the effect of introducing conical disclinations on the thermal and optical properties of a two-dimensional GaAs quantum dot in the presence of a uniform and constant magnetic field.

Katanaev and Volovich's [4,5,6] approach translates the theory of defects in solids into the three-dimensional language. Wedge dislocations are rare in Nature because they require a large amount of medium to be added or removed, which results in a large expenditure of energy. From the qualitative standpoint, creating a wedge dislocation is equivalent to introducing a conical singularity. The authors of the paper[7] investigated the impact of a topological defect and the SOI on the thermomagnetic and optical properties of a two-dimensional quantum dot.

The work [8] obtained the modifications to the traditional Landau-Fock-Darwin spectrum in the presence of conical disclination. The effect of the conical kink on the degeneracy structure of the energy levels was investigated. Topological defects can be the source of changes in a material's electrical, optical, or magnetic properties. The interaction of electron states with the lattice potential in nanocrystals leads to the renormalization of the g-factor [9].In this paper, we consider semiconductor two-dimensional quantum dots with a topological defect given by conical disclinations and Rashba spin-orbit interactions and investigate the effect of disclination on the effective g^*-factor of electrons. We use the Volterra design [10] to model the ring wedge dislocation defect of radius R and the remote wedge dislocation.

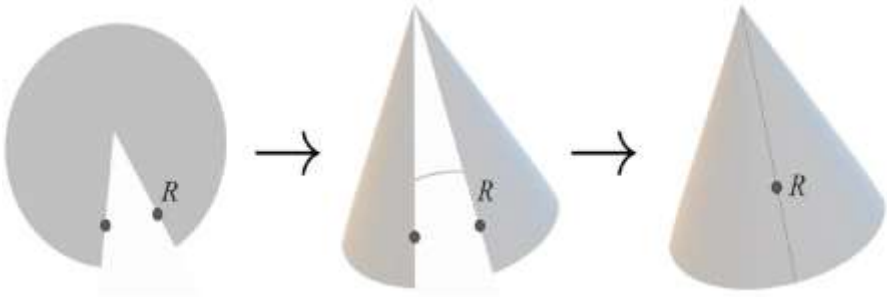

Figure 2. *Volterra construction. A cut planar disk with two radial lines identified point-to-point (marked as bold dots) is isometric to a cone.*

2. MATERIALS AND METHODS

The procedure to create a wedge dislocation is obtained by either removing (positive-curvature wedge dislocation) or inserting (negative-curvature wedge dislocation) an angle $2\pi|\alpha - 1|$ such that the total angle around the *z*-axis is $2\pi\alpha$ instead of 2π.
The conical metric has the form

$$ds^2 = \alpha^{-2}dr^2 + \rho^2 d\phi^2 \tag{1}$$

This is a more frequently used form of the metric for a conical singularity [6].The total Hamiltonian of the system is given by:

$$H = \frac{1}{2m}\left(\vec{P} + e\vec{A}\right)^2 + V_c\left(\alpha, r\right) + H_{RSOI} + H_Z \tag{2}$$

where m is the effective mass of the electrons, and $\vec{A}$ is the vector potential.
The parabolic potential for the quantum dot as

$$V_c(\alpha, \mathrm{r}) = \frac{m\omega^2}{2\alpha^2} r^2 \tag{3}$$

For a uniform magnetic field parallel to the z-axis, the vector potentials in cylindrical coordinates have the components $A_r = 0, A_\theta = \frac{Hr}{2\alpha^2}, A_z = 0$. The Rashba spin-orbital term has the form as [10]

$$H_{RSOI} = \gamma\sigma_z\alpha\frac{dV_c}{dr}\left(-i\frac{1}{r}\frac{\partial}{\partial\theta} + \frac{eHr}{2\hbar\alpha^2}\right) \tag{4}$$

Where σ_z is the Pauli matrix and γ is the Rashba spin-orbit coupling parameter
The wave function of an electron has the form [10]:

$$\Psi(r,\theta) = e^{il\theta} R_{n,l,\sigma}(\mathrm{r}) \tag{5}$$

The eigenvalue

$$E_{nl} = \left(2n+1+\frac{|l|}{\alpha}\right)\hbar\Omega + \frac{1}{2}\frac{\hbar\omega_c l}{\alpha^2} + \frac{\sigma}{2} g^* \mu_B H + \frac{\gamma m\omega^2 l}{\alpha}\sigma \tag{6}$$

The effective g^* -factor can be determined from the Zeeman splitting of subbands:

$$g^* = \frac{E_\uparrow - E_\downarrow}{\mu_B H} \tag{7}$$

Here $E_\uparrow$ $E_\downarrow$ *and* are the electron energy for spin +z and −z directions, respectively.

Let us investigate the effect of the Rashba spin-orbit interaction on the spin splitting of electrons in quantum dots with wedge disclinations. Figure 1 shows the variation of the effective g-factor of electrons in InSb-type quantum dots in the presence of Rashba spin-orbit interaction and wedge dislocations depending on the orbital quantum number l at n=0. We introduce a parameter $y = \frac{\omega_c}{\omega}$ to quantify the magnetic field strength, and $r = \sqrt{\frac{\hbar}{m\omega}}$ =148 $\mathring{A}$. We use the following material constants: $g_0 = 3.2$ for InSb quantum dot $\gamma = 500\,\mathring{A}^2$ [10].In Fig.2 shows the dependence of the effective g^* -factor of the electrons in InSb type quantum dots on the magnetic field parameter y at n=0,l=-1,0,1 for α=0.75.

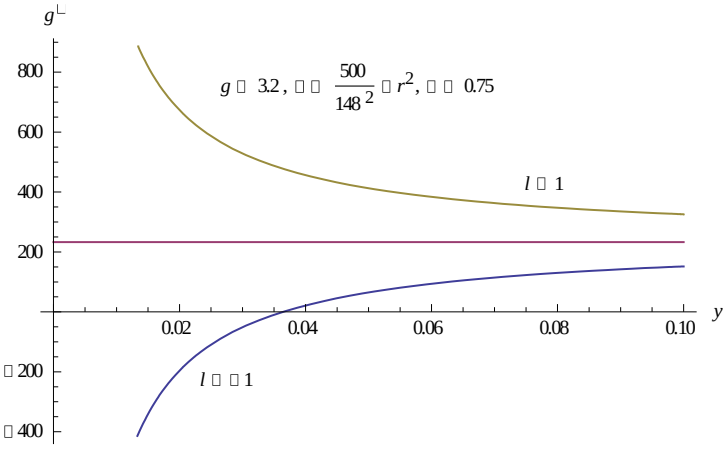

Figure 2. *The dependence of the effective g^* -factor of the electrons in InSb type quantum dots on the magnetic field parameter y at n=0,l=-1,0,1 for α=0.75.*

As can be seen from the figure 2, in the case of n=0,l=-1, as the magnetic field increases, the effective g-factor changes sign and increases, approaching the value n=0,l=0. In the case of n=0, l=1 it decreases and approaches n=0,l=0. In the case of n=0,l=0, the effective g factor remains constant as the magnetic field changes.

3. RESULTS AND DISCUSSIONS

In this study, the energy spectrum and effective g^*-factor of electrons in quantum dots with topological defects were calculated by taking into account the Rashba spin-orbit interaction in the magnetic field. The dependence of the effective g^*-factor on the parameters of the quantum dot and the applied external magnetic field is studied.

REFERENCES

[1] Destefani C F, Ulloa S E and Marques G E 2004 Phys. Rev. B 69 125302
[2] Hashimzade F.M., Babayev A. M., and Mehdiyev B. H. Rashba spin-orbit coupling effects in $Cd_{1-x}Mn_xTe$ quantum dots // Phys. Rev.B,2006, v.**73**, p.245321
[3] N. Candemir, A.N. Özdemir Physics Letters A 492 (2023) 129226,
[4] M.O. Katanaev, I.V. Volovich, Ann. Phys. (NY) 216 (1992) 1.
[5] M.O. Katanaev ,Theoretical and Mathematical Physics, 135(2): 733–744 (2003)
[6] M.O. Katanaev, Physics - Uspekhi 48 (7) 675 - 701 (2005)
[7] Jorge David Castaño-Yepes, D.A. Amor-Quiroz, C.F. Ramirez-Gutierrez, Edgar A. Gómez, Physica E 109 (2019) 56-76
[8] Tridev Mishra, Tapomoy Guha Sarkar, and Jayendra N. Bandyopadhyay, Phys.Rev E **89**, 012103 (2014)
[9] S. Cakmak; A.M. Babayev, E. Artunç, A. Kökce, S. Cakmaktepe, Physica E 18 (2003) 365 – 371
[10] O. Voskoboynikov, C. P. Lee, and O. Tretyak, Phys.Rev B 63, 165306

Determination of Properties of Concretes with Sorel Cement

Şemsettin KILINÇARSLAN[1]✉, Yasemin ŞİMŞEK TÜRKER[1], Nuri IŞILDAR[2]

[1] *Suleyman Demirel University, Department of Civil Engineering, Isparta-TURKEY*

[2]*Suleyman Demirel University, Natural and Industrial Building Materials Application and Research Center, Isparta-TURKEY*

✉ *Corresponding author: semsettinkilincarslan@sdu.edu.tr*

ABSTRACT

Cement is one of the most important sources that accelerate modernization as a basic building material, and cement production is increasing in developing countries within the scope of modernization. However, CO_2 released by the calcination of limestone ($CaCO_3$) during cement production is released into the atmosphere and constitutes approximately 6% of human-induced CO_2 emissions worldwide. Studies are being conducted on low-carbon and environmentally friendly cement alternatives worldwide, and interest in magnesium-containing cement has been increasing, especially in the last 20 years. One of the magnesium-containing cement seen as an alternative to Portland cement is magnesium oxychloride cement, which was discovered by Sorel Frenchman in 1867 and is called Sorel cement in the literature. MOC cement is obtained due to the complex reaction of $MgCl_2$ solution with highly reactive MgO particles at certain rates. In recent years, academic studies have been conducted on Sorel cement as an alternative to eliminate the negative aspects of Portland cement. In this study, the properties of concrete samples produced using Sorel cement were examined. The results were compared with Portland cement-bound concrete samples with the same unit volume mass.

KEYWORDS: *Sorel cement, concrete, properties.*

1. INTRODUCTION

Cement is one of the most important sources that accelerate modernization as a basic building material, and cement production is increasing in developing countries within the scope of modernization. CO_2 released by the calcination of limestone ($CaCO_3$) during cement production is released into the atmosphere and constitutes approximately 6% of human-induced CO_2 emissions in the world [1-5]. Approximately 0.90 tons of CO_2 is released during the production of 1 ton of cement. According to calculations, it is predicted that the amount of CO_2 originating from cement production will increase approximately 2.5 times in 2050 compared to 2010. Cement production in the world increases every year compared to the previous year. While annual cement production in Turkey was 42.79x106 tons in 2005, it increased to 71.41x106 tons by the end of 2015. In parallel with this increase, the amount of CO_2 released increases yearly [6-9].

In recent years, academic studies have been conducted on Sorel cement as an alternative to eliminate the negative aspects of Portland cement. Tan et al., (2014) [10] revealed the effects of H_3PO_4 on the microstructure, uniaxial compressive strength and degree of hydration of the MOC cement in the obtained F5 phase. It was determined that the MOC cements obtained with and without the addition of H_3PO_4 were in the F5 phase, but the MOC produced with the addition of H_3PO_4 had a more needle-like structure. However, the addition of H_3PO_4 caused the setting time of the MOC cement to increase. In addition, the resistance of the MOC cement to water increased, while the uniaxial compressive strength decreased. In their study, Jing et al., (2014) [11] revealed the effects of H_3PO_4

and $Ca(H_2PO_4)_2$ on the uniaxial compressive strength and water resistance of the obtained MOC cement. In this study, the properties of concrete samples produced using Sorel cement were examined.

2. MATERIALS AND METHODS

In this study, CEN standard sand, Portland CEMI 42.5 R cement, MgO, $MgCl_2$, H_2PO_4 were used. In the study, mortar mixtures were made in 2 different groups. The first mortar mixture was mortar samples produced with Portland cement, and the second mixture was mortar samples produced with Sorel cement. $MgO/MgCl_2$ was kept constant in the mixtures so that the mole ratio would be 13. In the literature studies, it is seen that H_3PO_4 increases the water resistance of the produced concrete samples. To increase the water resistance of the mortar samples, H_3PO_4 ratio was added to the mixture in a way that it would be constant in all mixtures.

The test for determining the bending strength of the prepared mortar was carried out according to the TS EN 196-1 standard. 40x40x160 mm samples were prepared for the determination of bending strength. In this test method, the bending strengths of the samples were measured according to the 3-point loading method.

3. RESULTS AND DISCUSSIONS

In this study, mortar samples were produced with the first series Portland cement and the second series Sorel cement. The bending strengths of the samples were determined, and the results are given in Figure 1. On the chart, samples produced with Portland cement are named control, and samples produced with sorel cement are named MOC.

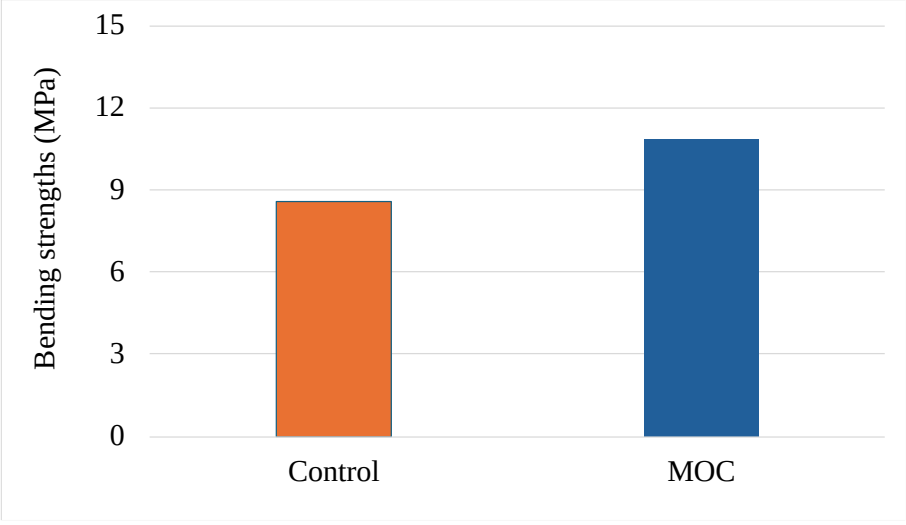

Figure 1. *Flexural properties of mortar mixtures*

When the graph is examined, it was determined that the average flexural strength value of mortars produced with portland cement was 8.56 MPa, and the average flexural strength value of mortars produced with sorel cement was 10.85 MPa.

This result highlights the superior performance of Sorel cement in terms of flexural strength under the conditions of the study. Such findings align with the inherent properties of Sorel cement, which is known for its dense microstructure and high tensile resistance compared to Portland cement.

The higher flexural strength of Sorel cement can be attributed to its unique hydration mechanism, which results in the formation of highly crystalline magnesium oxychloride hydrate phases, such as

$3Mg(OH)_2 \cdot MgCl_2 \cdot 8H_2O$ (Phase 5) and $5Mg(OH)_2 \cdot MgCl_2 \cdot 8H_2O$ (Phase 3). These phases contribute to the cement's compact microstructure and enhanced mechanical properties. Conversely, the hydration products of Portland cement, such as calcium silicate hydrate (C-S-H) gel and calcium hydroxide, while effective for compressive strength, are less robust under tensile and bending stresses, leading to lower flexural strength values.

4. CONCLUSIONS

The superior flexural performance of Sorel cement suggests its suitability for applications requiring higher resistance to bending and tensile stresses, such as in industrial flooring, lightweight structural panels, and decorative elements. On the other hand, Portland cement remains a reliable material for general construction due to its well-documented durability and compressive strength. Future studies should explore the long-term durability of Sorel cement, particularly its sensitivity to moisture, which is a known limitation. Additionally, investigating the influence of various additives and reinforcements on both cements could provide deeper insights into optimizing their respective flexural performances for specific applications. In conclusion, the findings underline the high potential of Sorel cement for applications demanding superior flexural strength, while reinforcing the versatility and robustness of Portland cement in standard construction contexts.

REFERENCES

[1] J. Ma, J. Wang, Y. Zhao, T. Liu, L. Wang, Stabilizationofheavymetals in sewage sludge using Sorel cement. In Chemical, Biological and Environmental Engineering (pp. 69-75) (2010) *DOI: 10.1142/9789814295048_0015.*

[2] Y. Karimi, A. Monshi, Effect of magnesium chloride concentrations on the properties of magnesium oxychloride cement for nano SiC composite purposes, Ceram. Int. 37 (7) (2011) 2405–2410, *DOI: 10.1016/j.ceramint.2011.05.082.*

[3] Gravit, M., Nedryshkin, O., & Zhuravlev, A. (2017). Negative use of finishing materials on Sorel's cement. In MATEC Web of Conferences (vol. 106, p. 03029). EDP Sciences. *DOI: 10.1051/matecconf/201710603029.*

[4] T. Mandal, J.M. Tinjum, T.B. Edil, Non-Destructive Testing Of Cementitiously Stabilized Materials Using Ultrasonic Pulse Velocity Test, Transp. Geotech. 6 (2016) 97–107, *DOI: 10.1016/j.trgeo.2015.09.003.*

[5] A. K. Santra, F. Liang, R. Fitzgerald (2009, January). Sorel Cement for HP/HT Downhole Applications. In SPE International Symposium on Oilfield Chemistry. Society of Petroleum Engineers. *DOI: 10.2118/121102-MS.*

[6] M. Xia, B. Nematollahi, and J. Sanjayan, Compressive strength and dimensional accuracy of Portland cement mortar made using Powder-Based 3D printing for construction applications, in Wangler, T. and Flatt, R.J. (Eds), First RILEM International Conference on Concrete and Digital Fabrication – Digital Concrete 2018, Springer International Publishing, Cham, pp. 245-254, (2019), *DOI: 10.1007/978-3-319- 99519-9_23.*

[7] M. Xia, B. Nematollahi, J. Sanjayan, Influence of binder saturation level on compressive strength and dimensional accuracy of powder-based 3D printed geopolymer, Materials Science Forum, Vol. 939 (2018) 177-183.

[8] M. Jianli, Z. Youcai, W. Jinmei, W. Li, Effect of magnesium oxychloride cement on stabilization / solidification of sewagesludge, Constr. Build. Mater. 24 (2010) 79 *DOI:10.1016/j.conbuildmat.2009.08.011.*

[9] Q. Ye, Y. Han, T. Liu, Y. Bai, Y. Chen, J. Li, S. Q. Shi, Magnesium oxychloride cement reinforced via D-gluconic acid sodium salt for slow-curing, with enhanced compressive strength and water resistance, Constr. Build. Mater. 280 (2021), *DOI: 10.1016/j.conbuildmat.2021.122487.*

[10] Y. Tan, Y. Lıu, L. Grover, Effect Of Phosphoric Acid On The Properties Of Magnesium Oxychloride. Cement And Concrete Research, 56 (2014) 69- 74.
[11] W. Jing, Y. Hongfa, L. Ying, W. Chengyou, D. Jinmei, Effects of Citric Acid on Hydration Process And Mechanical Properties Of Thermal Decomposed Magnesium Oxychloride Cement. Journal Of Wuhan University Of Technology-Mater. Sci. Ed., 29(1) (2014) 114-118.

Determination of the Effect of Regional Change on Mechanical Properties of Standing Trees by Fractometer

Şemsettin KILINÇARSLAN[1]✉, Yasemin ŞİMŞEK TÜRKER[1]

[1] *Suleyman Demirel University, Department of Civil Engineering, Isparta-TURKEY*
✉ *Corresponding author: semsettinkilincarslan@sdu.edu.tr*

ABSTRACT

Building materials must provide certain properties related to heat, moisture, and sound by their intended use. Wood is a natural, renewable, and sustainable resource that has been in human life for thousands of years and has maintained its importance as an engineering material. Wood, whose use dates to the early ages, is now entering people's living spaces intensively with the ever-developing technology and the demand is constantly increasing. There may be a series of deteriorations in wood materials due to moisture content, fungal contamination, insect nesting, chemical damage, and improper protection measures. These can be classified as biological, chemical, photochemical, thermal, fire, and mechanical deteriorations. These ecological factors significantly affect the growth, the annual ring structure formed, and the microscopic, physical, and mechanical properties of the wood. Various properties of wood material, such as thermal conductivity, radiation retention value, and sound absorption coefficient, vary according to the tree species, the tree's fiber direction, density, and the growing environment. In this study, the mechanical properties of the increment cores taken from trees grown in different regions were determined by the fractometer device, which is a semi-non-destructive testing (NDT) method. At the end of the study, it was determined that although the wood materials taken from different regions belonged to the same species, there were slight differences in their mechanical properties.

KEYWORDS: *Building materials, standing tree, increment core, non-destructive method.*

1. INTRODUCTION

For centuries, wood has been a cost-effective and sustainable material for construction [1-4]. Even today, wood serves a variety of purposes, including flooring, furniture, roofing, exterior cladding, barrel production, internal doors, and much more [5]. To determine the most effective applications for this adaptable material, it is crucial to thoroughly assess its properties. Additionally, identifying defects in wood, such as splits, checks, rot, insect damage, and knots, is vital, as these imperfections can significantly affect the material's overall performance. Early detection of these issues, ideally before the final stages of production, can result in considerable cost savings during manufacturing [6,7]. Because decomposition greatly weakens wood, it is a critical factor when assessing tree hazards. The primary goal of such evaluations is to detect signs of rot within a tree and determine the extent and progression of the decay. To accurately map the degree of degradation, various tools and techniques are employed, such as tomography and micro-drills. These methods often provide clear guidance for recommending appropriate actions when the decay is either exceptionally advanced or minimal [8,9]. However, in cases where it is uncertain whether the weakening from decay surpasses an acceptable limit, assessing the quality of the remaining wood becomes a key additional consideration to support decision-making.

The Fractometer II device has been utilized in numerous studies to evaluate the mechanical properties of wood. Ganesan and Hamid (2010) [9] investigated the mechanical properties of 25

different wood species using the Faktometre II instrument. They concluded that the fractometer is a reliable tool for determining the mechanical properties of standing trees.
This study focused on determining the mechanical properties of increment cores collected from Burdur-Golhisar (altitude: 1050 meters) and Antalya-Serik (altitude: 27 meters) using a non-destructive testing device, the fractometer. The research examined how differences in altitude influenced the mechanical characteristics of red pine wood.

2. MATERIALS AND METHODS

In this study, a non-destructive testing method was used to evaluate the mechanical properties of brutian pine trees located in the Antalya and Burdur regions. For the analysis, three increment cores, each 5 mm thick, were collected from five different trees at a height of 1.3 meters above ground level. The cores were carefully removed and placed in plastic tubes, which were then stored in a cooler bag for preservation. The 5 mm diameter cores were subsequently conditioned under controlled conditions of 65±5% relative humidity and 20±2°C until they reached a moisture content of 12%.
The mechanical properties of the increment cores were assessed using the IML Fractometer. This device comprises a measurement unit and an electronic unit. To determine breaking resistance, 5 mm thick increment cores were placed into the measurement unit, and the resistance value was displayed on the screen of the electronic unit. Typically, wood samples are prepared by cutting down trees, and their resistance properties are then measured using universal testing equipment to evaluate the material's strength characteristics.

3. RESULTS AND DISCUSSIONS

In this study, the mechanical properties of 20 increment cores were analyzed, with two cores collected from each of five trees located at an elevation of 1052 meters and another two cores from five trees at an elevation of 25 meters. The average values derived from the evaluation of the bending and compressive strengths of these increment cores are presented in Figure 1 and Figure 2.

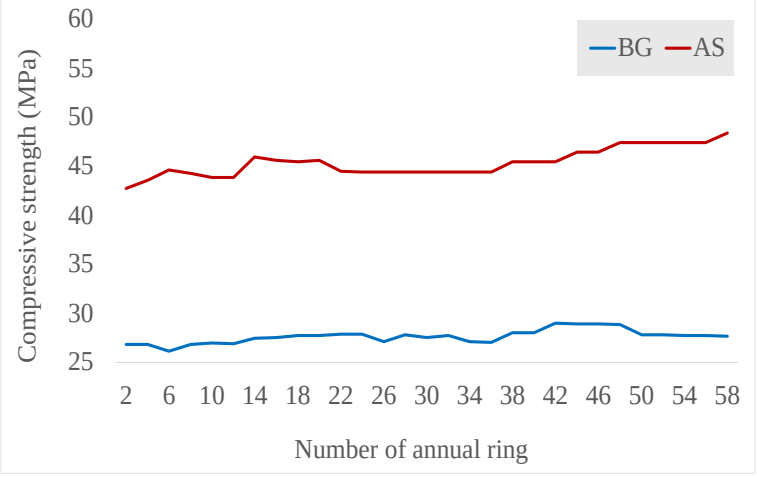

Figure 1. *Compressive Strength Values Based on Annual Ring*

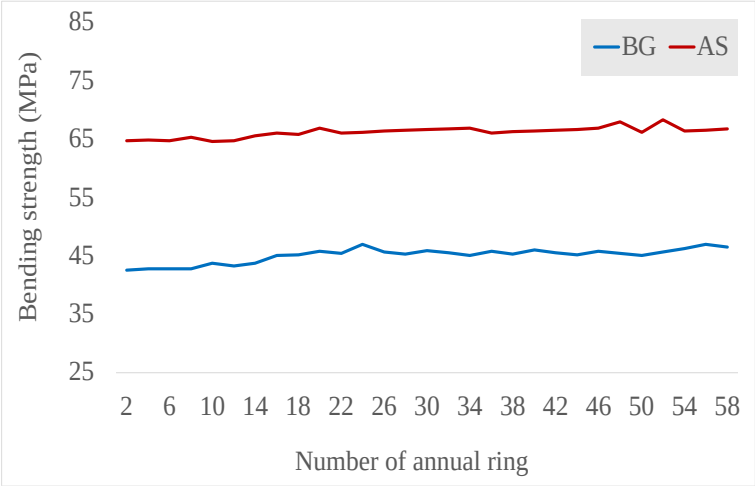

Figure 2. *Bending Strength Values Based on Annual Ring*

The Fractometer II device was used to assess the compressive and flexural strength of brutian pine increment cores, revealing a consistent increase in both properties from the pith (inner region) to the bark (outer region). The compressive and bending strength values of the cores varied between samples taken from Burdur-Golhisar (1052 m) and Antalya-Serik (25 m). The average compressive strength of cores from Burdur-Golhisar was 27.641 MPa, compared to 44.734 MPa for cores from Antalya-Serik. Similarly, differences were observed in bending strength values. The average bending strength was 44.479 MPa for Burdur-Golhisar cores, while Antalya-Serik cores averaged 65.837 MPa.

4. CONCLUSIONS

The bending and compressive strength values of increment cores collected from Burdur-Golhisar and Antalya-Serik were found to differ significantly. As elevation increased, compressive strength declined by approximately 61%, while flexural strength decreased by 48%. Habitat characteristics and ecological factors influence tree growth and, consequently, the structure of the wood. The annual ring structure, formed during the tree's radial growth, varies with environmental factors such as temperature and rainfall. These variations in the annual ring structure impact wood density, which in turn affects its physical and mechanical properties. As is well known, these properties play a critical role in defining the potential applications of wood. To produce trees with high-quality characteristics suitable for meeting the raw material demands of the forest products industry, it is essential to identify optimal growth areas and establish appropriate management schedules. Efforts should focus on determining the regions where superior wood production occurs and implementing necessary silvicultural practices in these areas. Furthermore, fostering collaboration among disciplines such as ecology, silviculture, and wood technology can help address the increasing need for raw materials and support the production of high-quality resources.

REFERENCES

[1] Fang, Y., Lin, L., Feng, H., Lu, Z., Emms, G. W. Review of the use of air-coupled ultrasonic technologies for nondestructive testing of wood and wood products. Computers and Electronics In Agriculture, 137 (2017) 79-87. https://doi.org/10.1016/j.compag.2017.03.015.

[2] Aydemir, D., Gündüz, G., Altuntaş, E., Ertaş, M., Şahin, H. T., Alma, MH. (2011). Investigating changes in the chemical constituents and dimensional stability of heat-treated horn beam and uludag fir wood. BioRes, 6(2) (2011), 1308-1321.
[3] Kaya, A. İ., Yalçin, Ö. Ü., Türker, Y. Physical, Mechanical, and Thermal Properties of Brutian Pine Wood- Gypsum Particleboard. Bilge International Journal of Science and Technology Research, 5(2) (2021) 139-145. https://doi.org/10.30516/bilgesci.956352.
[4] Şimşek Türker Y., Kilinçarslan Ş., Investigation of the Effect of Anatomical Properties on the Technological Properties of Wood Material. ICCESEN 2023, (2023).
[5] Jones, D., Sandberg, D., Goli, G., Todaro, L. Wood Modification in Europe: a state-of-the-art about processes, products, and applications (p. 123), (2019) Firenze University Press.
[6] Bravery, A. F., Berry, R. W., Carey, J. K., Cooper, D. E. Recognising wood rot and insect damage in buildings,3, Watford: Building Research Establishment, 1987.
[7] Akbulut, S., Keten, A., Yüksel, B. Wood destroying insects in Düzce province. Turkish Journal of Zoology, 32(3) (2008) 343-350.
[8] Allison, R. B., Wang, X., Ross, R. J.Visual and nondestructive evaluation of brutian pines supporting a ropes course in the USFS Nesbit Lake Camp, Sidnaw, Michigan. In Proceedings, 15th international symposium on nondestructive testing of wood. Madison, WI: Forest Products Society (pp. 43-48), 2008.
[9] Ganesan, S. K., Hamid, M. A. Survey of wood strength properties of urban trees in Singapore using the Fractometer II. Journal Of Tropical Forest Science, 97-105 (2010).

Comparative Tracking Index of Reinforced Silicone Insulators under Different Pollutant Liquid Exposure Time

Yekta AYDIN [1] , Fatih ATALAR [1✉], Aysel ERSOY [1]

[1] *Department of Electrical and Electronics Engineering, Istanbul University-Cerrahpaşa, 34320 İstanbul/TURKEY*
✉ *Corresponding author: fatih.atalar@iuc.edu.tr*

ABSTRACT

Silicone materials are widely chosen for their electrical insulation properties and thermal stability in high-voltage applications. However, under operational conditions, carbonization and tracking may negatively impact the long-term performance of these materials. The primary objective of this study is to demonstrate the applicability of the leakage current and harmonic analysis method in analyzing the behaviour of electrical insulation materials according to IEC 60112 standard. Carbonization tracks and short-circuit occurrences resulting from pollutant liquid droplets applied for durations of 10, 20, and 30 seconds at 500 and 600 voltage levels. The harmonic analysis, which bases its analysis on group delay in the amplitude-frequency domain of leakage current signals, provides a precise characterization of harmonic components. The results offer a detailed analysis of harmonic distortions under different voltage and water application conditions, contributing to a better understanding of silicone insulation materials' performance. In experiments conducted under 600 V voltage level, serious increases were observed in leakage currents at some points in 20 sec and 10 sec periodic pollutant liquid applications. In addition, increasing disturbances in the waveform of the signal reveal that electrical discharges should be analysed. The 30 sec periodic pollutant liquid application within the scope of CTI is insufficient to create extraordinary environmental conditions. Therefore, in this study, 20 sec and 10 sec periods were selected and more detailed analyses were performed. The findings obtained show that there are more serious and destructive electrical discharges on the surface of the reinforced silicone.

KEYWORDS: *Silicone Insulators, Surface Tracking, Electrical Insulation.*

1. INTRODUCTION

Silicon insulators are dielectric materials that have an important place in the electrical and electronic industry. The energy band gap of these materials is greater than 4 eV between the conduction band and the valence band, and they do not conduct electricity [1-3]. Solid silicon insulators are widely used, especially in electrical power systems. These materials have higher puncture resistance than liquid and gas insulators. Silicone insulators are widely used in the electrical and electronics industries. Silicone-based insulators are preferred in applications requiring high energy, such as high-voltage cables, transformers and capacitors, electric motors. In the automotive industry they are used as engine insulation parts, sensors and sealing elements; in the aerospace industry they are used in applications requiring high temperature and electrical insulation. In addition, silicone insulation materials are indispensable in various fields such as medical devices, food processing equipment and household appliances [4-7].

One of the main challenges faced by silicone insulators in high voltage applications is carbonisation and scarring. This can lead to degradation over time, especially under high electric field and environmental stresses. Carbonisation on the surface of silicone insulators degrades the electrical properties of the material and reduces its insulation. This can increase the risk of short circuits,

especially in high voltage applications. Experts and researchers have been studying the surface degradation of silicone insulators for many years [8-10].

In a study conducted to understand the ageing behaviour of High Temperature Vulcanised Silicone Rubber (HTV-SR) composites under alternating stress, the ageing behaviour of HTV-SR based composites that experienced surface scar formation and erosion due to external contamination and drying belt arc was investigated. Samples loaded with silica and alumina trihydroxide (ATH) fillers were aged in a multi-stress chamber for 5000 hours and then subjected to a scar formation test. The results showed that the fillers improved the scar resistance [11].
In this study, the surface discharge of reinforced silicone sealant was experimentally tested using the CTI method. During the experiments, in addition to the 30 s periodic contaminant drop exposure specified in the CTI application standard, 20 s and 10 s periodic drop applications were also performed. Leakage currents through the surface, rather than the CTI index, were studied in detail in terms of carbonisation, trace formation and drops causing short circuits. As the leakage currents do not contain sufficient information for electrical discharges, the WTMSST method was applied to these current waveforms. The method was used to analyse the intensity and distribution of electrical trace formation in different frequency bands.

2. MATERIALS AND METHODS

CTI Test Setup

The Comparative Surface Tracking Index (CTI) test method, which is widely used to evaluate the surface tracking performance of the reinforced silicone material, was preferred. The electrical circuit diagram of the test setup circuit specified by the IEC 60112 standard [12] for the Comparative Surface Tracking Index test method is shown in the Figure 1. AC voltages of 500 and 600 volts were applied to the sample surface. This voltage creates electrical stress on the surface and initiates the formation of traces. A pollutant liquid which is prepared according to related standard with a certain conductivity (usually ammonium chloride solution) is dropped onto the sample surface. Electrolyte drops are dropped between the electrodes at certain periods (10, 20 and 30 seconds). While the voltage is applied, the leakage current flowing from the sample surface is recorded with a sampling frequency of 48 kHz. For each case, 50 drops of contaminant liquid exposure were applied to the surface separately. During the test, voltages of 500 V and 600 V were applied to the samples. A variac operating with a single-phase supply voltage of 220 V AC was used to adjust the voltage level. This variac was adjusted to provide an output voltage between 0 and 250 V and has a power of 1 kVA. A single-phase transformer with a power of 1 kVA was used in the experimental setup. This transformer has a conversion ratio of 220/1000 V and increases the voltage received from the variac output by approximately 4.55 times. For each case, 50 drops of contaminant liquid exposure were applied to the surface separately.

3. RESULTS AND DISCUSSIONS

600 V and 500 V voltages were applied to our sample at 10 s, 20 s and 30 s intervals, and the harmonic currents of the electrical trace formation caused by our solution modelling the deionised medium, the leakage currents generated during 200 ms from the start of the arc formation and the currents generated during the entire signal were studied. In these investigations, for two different voltage levels, three different groups were examined: the drop where the carbonisation started, the start of the trace formation on the surface and the start of the short circuit. Figure 2 shows a 0.2 second leakage currents of the drops which cause carbonisation, trace formation and short circuit under 600 V application.

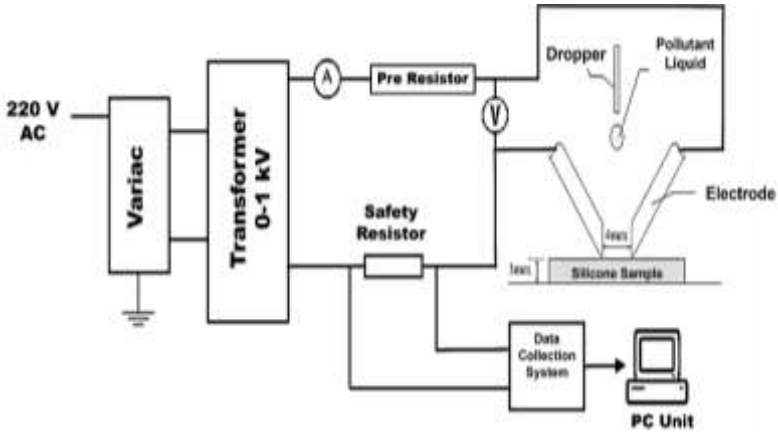

Figure 1. *Block diagram of the experimental set-up.*

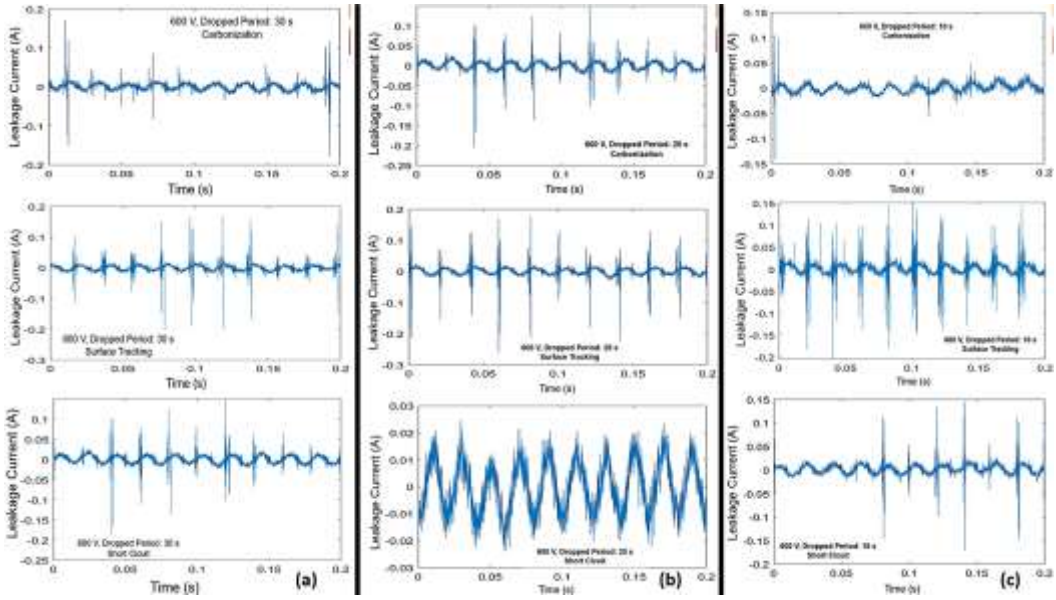

Figure 2. *CTI Test Results of 600V Application. (a) 30 s drop time (b) 20s drop time (c) 10 s drop time*

The leakage current amplitude values were measured as close to each other for all three drops and as a maximum of 0.2 A. Due to its reinforced structure, the silicone rubber material used in the experiments showed a rapid recovery behavior after the contaminant drops came into contact with the surface. The tracking formed after the carbonization of the material surface only created very small deformations on the surface. Even in the event of a short circuit, a similar amount of current flow shows that the material is resistant. Although the current showed a constant behavior during the short circuit, much more electrical jumps (peaks) (10) were observed on the material surface.
It is seen that the leakage current values of the 46th drop where the short circuit started are much lower. The maximum value observed in the 30-second period drop was 0.2 A, while the maximum value in the 20-second period drop was measured at around 0.03 A. In addition, trace formation was observed in the 26th drop in the 30-second period and in the 12th drop in the 20-second period. In

this case, it was formed due to the more frequent pollutant environment on the sample surface. There is a relatively more stable waveform at the time of the short circuit. In the 10-second period when the contaminant liquid is applied most frequently to the silicon surface, the carbonization, trace formation and the drop where short circuit starts are similar to the previous situations. When the leakage current signals are examined, it is observed that very wide and frequent peaks are formed in the case of trace formation. 11 wider amplitude peaks indicating electrical discharges are seen in the leakage current waveform. However, during the short circuit, the material surface tried to resist the current situation more and 5 high amplitude peaks were observed. Under 500 V apllication, maximum leakage currents of around 0.08 A were measured (Figure 3). Since the voltage level is lower and the material surface is very durable, no short circuit was observed in the case of 30 s periodic exposure to pollutant liquid. In the 20 s period contaminant liquid application, a maximum of 0.5 A was measured. In the case of a drop exposure in 20 s, fewer peaks were observed during the formation of the trace. However, there is a large peak of approximately 0.07 A in the negative alternation, which accelerates the ionization. In the 10-sec period case, leakage currents up to 0.1 A were measured in negative alternation at the time of carbonization. In the leakage current signal of the drop where trace formation started under 500 V voltage stress, approximately 9 peaks were observed during the 30-sec period application, approximately 5 peaks were observed in the 20-sec period application, and approximately 11 peaks were observed in the 10-sec period application.

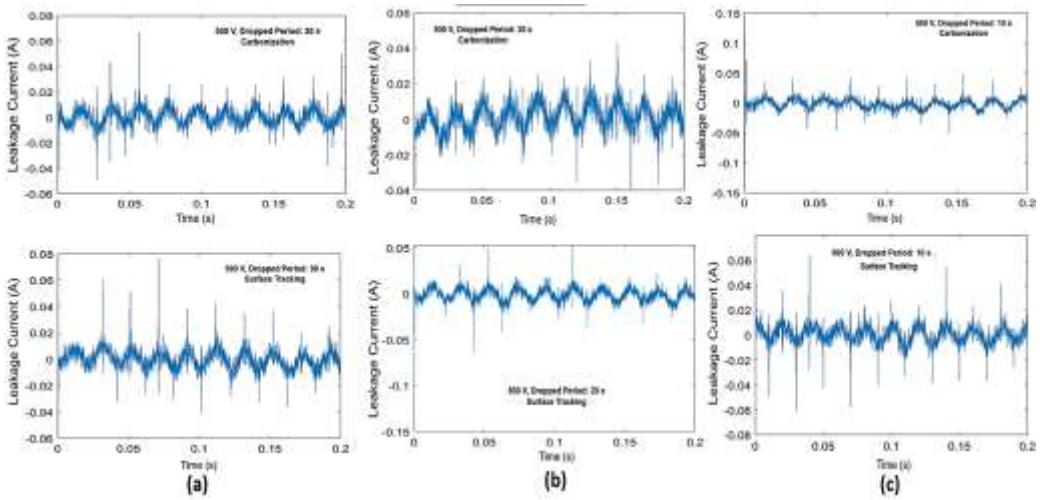

Figure 3. *CTI Test Results of 500V Application. (a) 30 s drop time (b) 20 s drop time (c) 10 s drop time*

Under 500 V application, maximum leakage currents of around 0.08 A were measured. Since the voltage level is lower and the material surface is very durable, no short circuit was observed in the case of 30 s periodic exposure to pollutant liquid. In the 20 s period contaminant liquid application, a maximum of 0.5 A was measured. In the case of a drop exposure in 20 s, fewer peaks were observed during the formation of the trace. However, there is a large peak of approximately 0.07 A in the negative alternation, which accelerates the ionization. In the 10-sec period case, leakage currents up to 0.1 A were measured in negative alternation at the time of carbonization. In the leakage current signal of the drop where trace formation started under 500 V voltage stress, approximately 9 peaks were observed during the 30-sec period application, approximately 5 peaks were observed in the 20-sec period application, and approximately 11 peaks were observed in the 10-sec period application. Total Harmonic Distortion (THD) has been calculated for all specific situations. The THD results are illustrated in Figure 4.

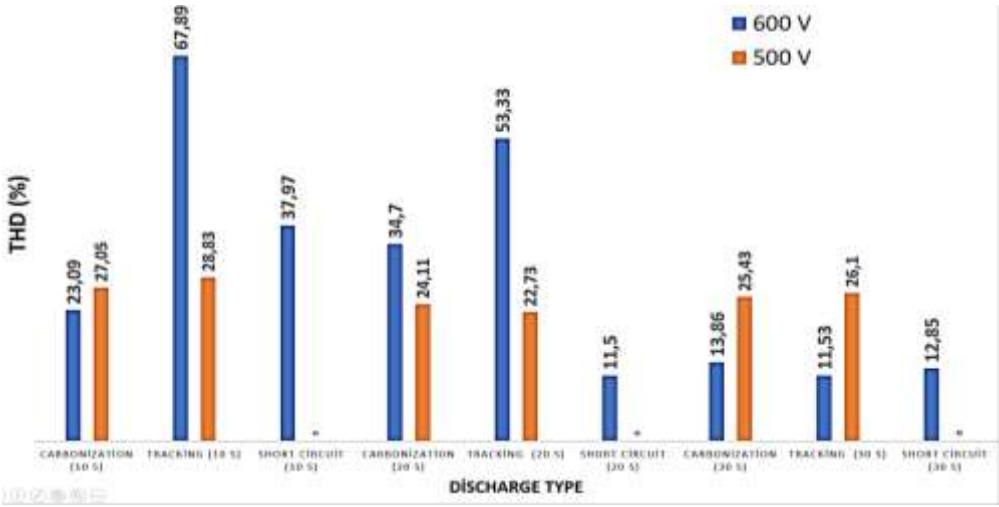

Figure 4. *THD Results of CTI Test of 500V and 600 V Applications*

In general, total harmonic distortion was measured lower under 500 V voltage. In addition, harmonic distortions show a more stable behavior at this voltage value. There is generally a movement between 22%-28%, that is, only in the 6% range. On the other hand, very high distortions up to approximately 68% were measured under 600 V voltage. In 10 and 20 second periodic pollutant liquid applications, total harmonic distortion values were measured very high during trace formation under 600 V voltage. When the application was applied with a 30 seconds periodic period, both the percentage of harmonic distortions generally decreased to around 12 and a more stable distortion behavior was observed.

4. CONCLUSIONS

In this study, the performance of silicone insulation materials was investigated by comparative surface track formation test method. When the liquid drop applications with 30 second intervals given in the standard were reduced to 20 seconds and 10 seconds, as expected, the drop levels at which carbonisation and trace formation occurred decreased. The results show that the formation of tracking and carbonization on the surface are directly dependent on the applied voltage level and the duration of the liquid drops. When the 30-second interval liquid drop applications specified in the standard were reduced to 20 seconds and 10 seconds, the formation of traces and carbonation occurred earlier in strong insulating materials such as silicone. This situation is a factor that negatively affects the durability of the material, especially at high voltage levels. The liquid dropping period and voltage levels used in the trace formation tests for silicone insulating materials need to be adjusted more flexibly. The times and voltage levels specified in the standard may not fully reflect the actual performance of the material in some cases. In cases where strong insulating materials are to be tested in trace formation experiments, sometimes degradation may not occur at times within the standard as expected, in which case it would be appropriate to change the relevant time intervals or voltage levels in the standard. This study is expected to provide guidance for future revision or flexibility of standards, particularly for scientists and engineers involved in trace formation studies.

REFERENCES

[1] Kokalis C-CA, Kontargyri VT, Gonos IF. A Proposal for the Evaluation of HTV Silicone Rubber Composite Insulators. Polymers. 2021; 13(21):3610. Doi:10.3390/polym13213610.

[2] Kamarudin, Najwa, et al. "Mechanical and electrical properties of silicone rubber based composite for high voltage insulator application." *Int. J. Eng. Technol* 7.25 (2018): 452-457.

[3] Ullah, I., Akbar, M., & Khan, H. A. (2022). Enhancement of electrical, mechanical and thermal properties of silicone-based coating with aluminatrihydrate/silica for ceramic insulators. *Materials Chemistry and Physics*, *282*, 125972. Doi:10.1016/j.matchemphys.2022.125972

[4] Schmid, H., and B. Michel. "Siloxane polymers for high-resolution, high-accuracy soft lithography." Macromolecules 33.8 (2000): 3042-3049. DOI: 10.1021/ma982034l

[5] Edelmann, Frank T. "Metallasilsesquioxanes–Synthetic and Structural Studies." Silicon Chemistry: From the Atom to Extended Systems (2003): 383-394. DOI:10.1002/9783527610761

[6] Shit, Subhas C., and Pathik Shah. "A review on silicone rubber." National academy science letters 36.4 (2013): 355-365.

[7] Perry, Robert, et al. "Silicones." Synthetics, mineral oils, and bio-based lubricants. CRC Press, 2020. 235-248.

[8] Loganathan N, Chandrasekar S., "Analysis of Surface Tracking of Micro and Nano Size Alumina Filled Silicone Rubber for High Voltage AC Transmission". Vol. 8, Journal of Electrical Engineering and Technology. 2013. p. 345–53. doi: 10.5370/JEET.2013.8.2.345.

[9] Cherney, E. A., et al. "DC inclined-plane tracking and erosion test of insulating materials." IEEE Transactions on Dielectrics and Electrical Insulation 22.1 (2015): 211-217. doi:10.1109/TDEI.2014.004991

[10] S. Shaukat, A. Arshad and W. A. Shah, "Use of Wavelet Transform to Analyze Leakage Current of Silicone Rubber Insulators Under Polluted Conditions," *2022 2nd International Conference of Smart Systems and Emerging Technologies (SMARTTECH)*, Riyadh, Saudi Arabia, 2022, pp. 118-123, doi: 10.1109/SMARTTECH54121.2022.00037.

[11] Ullah, R., Akbar, M., Ullah, N., Otaibi, S. A., & Althobaiti, A. (2021). Understanding Variations in the Tracking and Erosion Performance of HTV-SR-Based Composites due to AC-Stressed Aging. Polymers, 13(21), 3634. https://doi.org/10.3390/polym13213634

[11] IEC 60112:2003/AMD1:2009 Method for the determination of the proof and the comparative tracking indices of solid insulating materials, 4th edt.

Advanced Decomposition of Leakage Current Signal of Mineral Oil under Non-Uniform Electric Field

Alper AYDOĞAN[1] , Fatih ATALAR[2]✉ , Aysel ERSOY[2]

[1] *Computing & Information Services Office, Muğla Sıtkı Koçman University Muğla-TURKEY*
[2] *Department of Electrical – Electronics Engineering İstanbul University – Cerrahpaşa, Istanbul- TURKEY*
✉ *Corresponding author: fatih.atalar@iuc.edu.tr*

ABSTRACT

In the present study, an experimental laboratory setup was devised utilizing needle and hemispherical electrodes. Two distinct types of needle electrodes were employed: copper needle electrodes and steel needle electrodes equipped with medical tips. Hemispherical electrodes were fabricated in three different sizes, specifically 2 cm, 5 cm, and 6 cm in diameter. A non-uniform electric field was generated between the needle and hemispherical electrodes, and leakage current signals were captured over the ground electrode. Experiments were conducted under varying high voltage levels of 5.4, 7.2, 9, and 10.8 kV. The collected leakage current signals were subsequently processed using advanced signal decomposition techniques, including Empirical Mode Decomposition (EMD), Variational Mode Decomposition (VMD), Ensemble Empirical Mode Decomposition (EEMD), and Multivariate Variational Mode Decomposition (MVMD). Through the application of the EMD method, partial discharge phenomena within the leakage current signal were effectively isolated. Each decomposition technique dissects the signal in unique manners, providing distinct benefits and drawbacks. These methodologies aim to decompose the signal into its intrinsic mode functions, thereby enabling the capture of both high and low-frequency components, and discerning the inherent differences among them. These sophisticated techniques are envisaged as critical tools in elucidating the temporal, amplitude, and frequency characteristics of partial discharge signals, thereby enhancing the detection and analysis of faults and insulation failures by thoroughly examining the behavior of partial discharges.

***KEYWORDS*:** *Transformers faults, Non-Uniform Electric Field, Signal Decomposition.*

1. INTRODUCTION

Transformers are devices used to transmit and supply electrical energy. It is one of the most important players of these parts. Therefore, the continuous and uninterrupted operation of transformers is utterly crucial. The continuity of this process is achieved by preventing faults. Transformers are basically composed of a magnetic circuit, an electric circuit consisting of primary and secondary details, and sections containing cooling and cooling systems. Power transformers are exposed to various stress conditions in the form of electrical, mechanical, temperature and thermal stresses. These stresses are the potential source of various internal and external faults in the power transformer. Most of these failures are due to the high temperature of the thermal system [1].

One of the most important of these temperature and cooling units is transformer oils. transformer oil is the fundamental element of that ensures that the cooling and distribution of temperature in transformers work both safely and efficiently. A safe interval is formed between programs containing high voltage. The risk of electrical explosion is minimized. It does this with its electrical

capacity feature. In addition, the temperature generated in the transformer is effectively distributed and the transformer is prevented from overheating. In this way, the thermal stability of the equipment is maintained. Transformer oil must be of good quality. The quality and cleanliness of the oil ensure good performance and thermal safety. If the oil is dirty and of poor quality, the voltage may be weak. Because of this reason, regular analysis and maintenance of transformer oils is very important for the long and safe operation of transformers. In addition, transformer oils should comply with quality standards. Therefore, it is cared about the life of the electrical grid. It also ensures the economical and efficient operation of electrical energy. Condition monitoring and fault detection in power transformers is important to maintain the continuity and longevity of the transformer system. Many common on-line condition monitoring technologies are used. Dissolved gas analysis (DGA) [24] selection and acoustic analysis [5] , dielectric spectroscopy [6] , differential protection [7] , transformation ratio [8] are some of these techniques. According to these techniques, brightness [9], power factor performance [10], frequency response analysis [11] and resolution resistance [12] are included. Among these techniques, disconnection can be effectively diagnosed with the possibility of transformer connection progress. It is very important for operating and maintenance costs to detect faults in transformer oils in advance and to prevent the fault from growing and making the transformer unusable. There are many types of faults in transformer oils. One of the most important of these faults is partial. Common faults in transformers are separated by the partial discharge (PD) in the electric current, which is the result of continuous thermal insulation. Immediate detection of these faults allows intervention before major failures occur in transformers.

In the present study, an experimental laboratory setup was devised utilising needle and hemispherical electrodes. Two distinct types of needle electrodes were utilised: copper needle electrodes and steel needle electrodes equipped with medical tips. The hemispherical electrodes were produced in three distinct sizes, namely 2 cm, 5 cm, and 6 cm in diameter. A non-uniform electric field was generated between the needle and hemispherical electrodes, and the resulting leakage current signals were captured over the ground electrode. The experiments were conducted under a series of varying high voltage levels, specifically 5.4, 7.2, 9, and 10.8kV. Subsequently, the collected leakage current signals were processed using advanced signal decomposition techniques, including EMD, VMD, EEMD, and MVMD.

2. MATERIALS AND METHODS

Experimental Methodology

2.1 High Voltage Test Setup

An experimental setup for leakage current measurement under a high voltage was established for the laboratory studies. The voltage adjusted by an autotransformer with 5 kVA power and a 0–220 V range at the 50 Hz frequency level was applied to the primary winding of the voltage transformer. The transformer has a conversion ratio of 220 V/40 kV, with a rated power of 1.5 kVA. A 1 MΩ limiting resistance was placed on the high-voltage side of the transformer, as it is typically applied in high-voltage laboratory measurements to protect against high current during breakdown in the testing system The current was measured over a 47 Ω resistor at the Variac output with a Fluke meter 190–504/EU/S, which has 200 MHz bandwidth oscilloscope with a sampling rate of 2.5 GS/s (Giga Sample/second), with an accuracy of 2.1% of reading + 0.04 × range/div. The test chamber is made of plexiglass and has dimensions of 25 × 25 × 10 cm. Mineral oil with a dielectric constant of 2.2 was used throughout the experiments as the dielectric liquid under test. The oil before the beginning of the experiment fulfilled the requirements for the mineral oil specified in the IEC 60296 Standard. During each test, a total number of 30,000 data points was obtained during the 4.8 s of measurement. Thus, the sampling frequency was 6250 Hz. Three different hemispheres made of pure copper with the diameters of 6, 5, and 2 cm were used as the grounded electrodes, respectively. Steel (medical) and copper-pointed needles especially prepared for the experiment, both with a tip radius of 0.1 μm,

were however used as high-voltage (HV) electrodes. The experiments were conducted under four pre-selected voltage levels, which were 5.4, 7.2, 9, and 10.8 kV, respectively.

2.2 Decomposition Methods

In the EMD method, after the peaks in the upper and lower parts of the signal are detected, upper and lower curvatures are produced to make cubic interpolation at these points. After calculating automatically, the average between the two curvatures, a signal with amplitude and modulation is extracted as a result of many cycles for IMF calculation (equation 1).

$$NSD = \sum_{j=1}^{R} \frac{|b_{k-1}(t) - b_k(t)|^2}{b_j^2(t)} \quad (1)$$

Where $b_k(t)$represents the IMF values at each step. When performing a signal decomposition in the EMD method, it is mandatory to have a stopping criterion based on interpolation. This situation has a built that constantly renews itself. EMD decomposes the signal from high frequency to low frequency.

In the VMD method, the input signal is reconstructed by combining the modulated signals which are divided into frequency and amplitude parts. In this method, the signal is decomposed into M modes. The all modes are intensified in their own center frequencies (equation 2).

$$\min_{i_N, v_M} \left\{ \sum_M \left\| \partial_t \left[\left(\sigma(t) + \frac{j}{\pi t} \right) * i_M \right] e^{-jvt} \right\|_2^2 \right\} \quad (2)$$

Here $\sum_M i_M = u$ represents the input signal $i_m(1,2,3, \ldots . L)$ represents each decomposition mode and v_M is the center frequency. In the following stages, the Lagrange multiplier and the penalty term are effectuated. VMD decomposes the signal from low frequency to high frequency.

MVMD extends Variational Mode Decomposition (MVMD) to accommodate multivariate measurement data by transforming single-channel data into multiple channels using the Frobenius norm. The essence of MVMD is to extract *K* oscillatory modes $u_k^+(t)$from the input data containing *N* data channels x(t) as shown in equation 3.

$$\min_{u_k^i, w_k} \sum_{i=1}^{N} \sum_{k=1}^{K} \left\| \frac{d}{dt} \left[\left(x_i(t) - \sum_{k=1}^{K} u_k^i(t) \right) . e^{j\omega_k t} \right] \right\|^2 + \alpha \left(\sum_{k=1}^{K} \left\| u_k^i(t) \right\|^2 \right) \quad (5)$$

To identify multivariate oscillations with a singular common frequency component ω_k in multi-channels, it is necessary to estimate the bandwidth of the modulated multivariate oscillatory signal, by shifting the one-sided spectrum of each channel of $u_k^+(t)$ with center frequency ω_k, utilizing the Frobenius norm to convert single-channel data into multivariate formats.

Ensemble EMD (EEMD), which significantly reduces the chance of undue mode mixing, remarkably enhances the stability of algorithm and reflects the dyadic property of the decomposition for any data. The EMD operation is then performed to decompose $r_i(t)$ into different components $c_{ij}(t)$ by using equation 4.

$$r_i(t) = \sum_{j=1}^{n} c_{ij}(t) + r_{in}(t) \quad (9)$$

Where $c_{ij}(t)$ means the j-th IMF of the i-th added noise signal. This step is then repeated many times, and thus the final result of IMF components is obtained by computing the ensemble mean of the corresponding components. Leakage current signal can be adaptively decomposed with IMFs of

the good time-frequency locality by EEMD according to the signal characteristics. The IMFs obtained by EEMD can well reflect the degradation characteristics of mineral oil.

3. RESULTS AND DISCUSSIONS

The analysis presented in Figure 1(a) corresponds to the decomposition of electrical discharge signals generated under the following experimental setup: a Medical Steel needle was used with an electrode gap of 2 mm and a hemisphere radius of 5 cm, subjected to a voltage level of 10.8 kV. The decomposition process was performed using the EEMD method, which is known for its robustness in isolating signal features while mitigating the effects of noise. The IMFs are ranked from higher frequencies to lower frequencies, capturing transient, oscillatory, and baseline components of the signal.. The high-frequency components, as observed in the first few IMFs (e.g., IMF 1–3), are primarily associated with the transient discharge characteristics and system noise. Of particular importance is IMF 2, which captures the essential dynamics of the electrical discharge with reduced interference, demonstrating the efficacy of the EEMD method. The mid-frequency components, such as those in IMF 4 and IMF 5, show sinusoidal oscillations, which are likely tied to the dominant physical oscillations in the system. These components provide insights into the harmonic behavior of the discharge process. Meanwhile, the low-frequency components (e.g., IMF 6–8) represent the longer-term trends or baseline fluctuations, reflecting the stable, slower-varying behavior of the system after transient effects dissipate. These low-frequency components are devoid of noise, enabling a clear interpretation of the steady-state system dynamics.

The analysis presented in Figure 1(b) pertains to the decomposition of electrical discharge signals using the MVMD method. The experimental setup includes a Medical Steel needle, an electrode gap of 2 mm, a hemisphere radius of 2 cm, and a voltage level of 9 kV. Notably, Mode 2 emerges as a clean sinusoidal waveform, with a clearly defined frequency component. This demonstrates MVMD's ability to isolate and highlight dominant frequency features, which are crucial for understanding the frequency content of the electrical discharge process. Such a mode reflects the primary oscillatory behavior of the discharge, uncorrupted by noise or interference, making it a valuable feature for signal interpretation. Modes 5 and 6 reveal distinct periodic structures with relatively stable amplitudes. These modes likely correspond to the system's harmonic or resonant components, capturing mid-frequency oscillations that are integral to the characterization of electrical discharge dynamics. Their stability across time highlights the robustness of MVMD in preserving coherent signal structures, even in complex discharge conditions.

The analysis presented in Figure 2(a) pertains to the decomposition of electrical discharge signals using the EMD method. The experimental setup includes a copper needle, an electrode gap of 3 mm, a hemisphere radius of 2 cm, and a voltage level of 7.2 kV. The higher frequencies in IMF 1 and IMF 2 suggest they are capturing finer details and rapid fluctuations present in the signal, which might be linked to noise or fast-varying components. In contrast, IMF 4's smooth, periodic nature indicates a more stable, dominant frequency, making it a key mode for understanding the underlying oscillatory processes in the data. These distinctions highlight how the different IMFs decompose the signal into its constituent frequency components.

The analysis presented in Figure 2(b) pertains to the decomposition of electrical discharge signals using the VMD method. The experimental setup comprises a copper needle, an electrode gap of 4 mm, a hemisphere radius of 2 cm and a voltage level of 7.2 kV. Mode 1 exhibits a pronounced, high-frequency sinusoidal waveform, which is presumed to represent the fundamental oscillation of the electrical discharge with pronounced periodic behavior. Mode 1 captures the core, stable frequency of the signal, which is essential for understanding the main characteristics of the discharge. Mode 2, with a slightly lower frequency and amplitude, adds harmonic content or secondary oscillations, complementing Mode 1 by detailing additional frequency components of the process. Collectively, these modes effectively describe the key periodic structure and oscillatory nature of the electrical discharge.

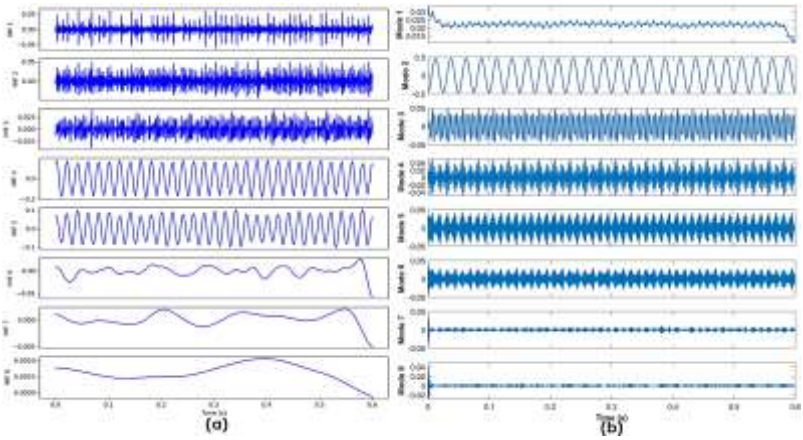

Figure 1. *Leakage Current Decomposition (a): EEMD (b): MVMD*

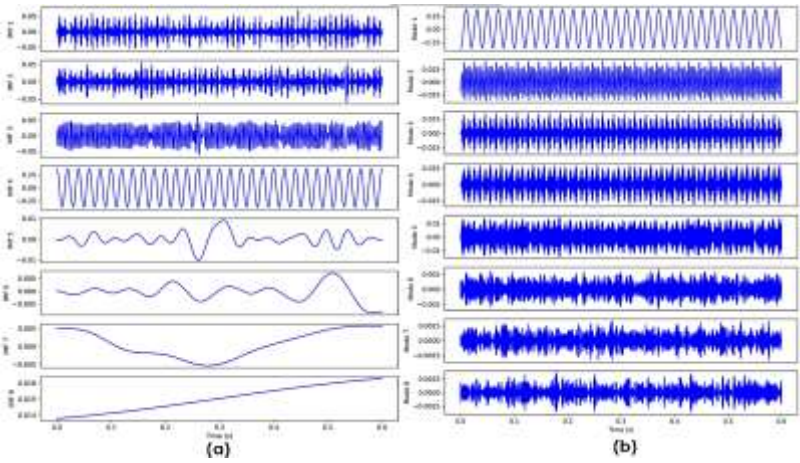

Figure 2. *Leakage Current Decomposition (a): EMD (b): VMD*

4. CONCLUSIONS

In experiments conducted with medical needles, the leakage current signals exhibited greater deformation and a higher number of disturbance points compared to those observed with copper needles. The experiments with copper needles demonstrated a leakage current amplitude that was approximately 10-20% lower, suggesting a less pronounced interaction with the electric field. However, the methods employed in these studies encountered limitations when attempting to analyze scenarios involving the smallest electrode gap of 1 mm and the largest gap of 5 mm. For the smallest gaps, the analysis was impeded by high signal peaks occurring at extremely short intervals, which complicated proper signal separation. Conversely, for the largest gaps, the absence of significant discharges rendered the analysis ineffective. Furthermore, the study revealed that the application of either extremely high or very low voltages is not conducive to effective decomposition of leakage current signals. Maintaining the electric field stress within a moderate range is critical, as it ensures that the disruptive effects are neither excessively large nor negligible.

REFERENCES

[1] Meira, M., Ruschetti, C. R., Álvarez, R. E., & Verucchi, C. J. (2018). Power transformers monitoring based on electrical measurements: state of the art. IET Generation, Transmission & Distribution, 12(12), 2805-2815. http://dx.doi.org/10.1049/iet-gtd.2017.2086

[2] Lopatchenko, G., Groshev, A., Lukonin, A., Kuimov, D., & Yurov, A. (2024). Partial discharges in power transformers. In E3S Web of Conferences (Vol. 583, p. 07001). EDP Sciences. https://doi.org/10.1051/e3sconf/202458307001

[3] Faiz, J., & Soleimani, M. (2017). Dissolved gas analysis evaluation in electric power transformers using conventional methods: A review. IEEE Transactions on Dielectrics and Electrical Insulation, 24(2), 1239-1248. http://dx.doi.org/10.1109/TDEI.2017.005959

[4] Duval, M. (2002). A review of faults detectable by gas-in-oil analysis in transformers. IEEE Electrical Insulation Magazine, 18(3), 8-17. https://doi.org/10.1109/MEI.2002.1014963

[5] Secic, A., Krpan, M., & Kuzle, I. (2019). Vibro-acoustic methods in the condition assessment of power transformers: A survey. IEEE Access, 7, 83915-83931. https://doi.org/10.1109/ACCESS.2019.2924821

[6] Wang, M. V. A. J., Vandermaar, A. J., & Srivastava, K. D. (2002). Review of condition assessment of power transformers in service. IEEE Electrical Insulation Magazine, 18(6), 12-25. http://dx.doi.org/10.1109/MEI.2002.1161455

[7] M. Orlando and A. Suman, 'Application of Discrete Wavelet Transform for Differential Protection of Power Transformers', Discrete Wavelet Transforms - Biomedical Applications. InTech, Sep. 12, 2011. doi: 10.5772/19712.

[8] Yao, C., Zhao, Z., Mi, Y., Li, C., Liao, Y., & Qian, G. (2015). Improved online monitoring method for transformer winding deformations based on the Lissajous graphical analysis of voltage and current. IEEE Transactions on Power Delivery, 30(4), 1965-1973. http://dx.doi.org/10.1109/TPWRD.2015.2418344

[9] M. R. Hussain, S. S. Refaat and H. Abu-Rub, "Overview and Partial Discharge Analysis of Power Transformers: A Literature Review," in *IEEE Access*, vol. 9, pp. 64587-64605, 2021, doi: 10.1109/ACCESS.2021.3075288.

[10] Zhang, S. (2006). Analysis of some measurement issues in bushing power factor tests in the field. IEEE Transactions on Power Delivery, 21(3), 1350-1356. http://dx.doi.org/10.1109/TPWRD.2006.874616

[11] N. Hashemnia, A. Abu-Siada and S. Islam, "Detection of power transformer bushing faults and oil degradation using frequency response analysis," in *IEEE Transactions on Dielectrics and Electrical Insulation*, vol. 23, no. 1, pp. 222-229, February 2016, doi: 10.1109/TDEI.2015.005032.

[12] T. K. Saha, "Review of modern diagnostic techniques for assessing insulation condition in aged transformers," in *IEEE Transactions on Dielectrics and Electrical Insulation*, vol. 10, no. 5, pp. 903-917, Oct. 2003, doi: 10.1109/TDEI.2003.1237337.

Fracture Morphology of Radial Well Fracturing in Glutenite Reservoirs

Yuning Yong[1]✉, Shouceng Tian[1] and Tianyu Wang[1]

[1] *State Key Laboratory of Petroleum Resources and Prospecting, China University of Petroleum (Beijing), Beijing, China*
✉*Corresponding author: yongyn98@163.com*

ABSTRACT

Numerous oil resources have been found in glutenite reservoirs. Radial well fracturing presents a promising technology for efficiently exploiting glutenite reservoirs. This paper experimentally investigates the characteristics of fracture morphology in glutenite reservoirs stimulated by radial well fracturing. The influence of radial borehole azimuths and branches is discussed. The results show that fracture morphologies of radial borehole fracturing in glutenite reservoirs are collectively affected by the in-situ stress, radial borehole, and gravels in glutenite, which contribute to the observed non-planar characteristics of the fracture morphologies. Radial boreholes with the azimuth of 30° and 45° demonstrated the ability to guide directional fracture propagation, potentially leading to the formation of multi-branch fractures. Increasing the azimuth decreases the guiding ability of the radial well. Abundant different pebbles increase fracture tortuosity, which can be mitigated by perpendicularly arranging multiple radial boreholes. This research provides valuable insights into the feasibility of applying radial borehole fracturing for glutenite reservoirs and provides guidance for optimizing the fracturing design.

KEYWORDS: *Hydraulic fracturing, Radial well, Glutenite reservoir.*

1. INTRODUCTION

Glutenite is a sedimentary rock that contains many gravels with a diameter greater than 2 mm. Glutenite reservoirs contain lots of oil resources. Hydraulic fracturing technology is the main way to develop oil reservoirs. Radial well fracturing is a new technology proposed in recent years [1]. The implementation of radial well fracturing technology is to first drill radial horizontal wells with multiple azimuth at different depths of the vertical well, and then fracture each radial well to form multiple directional hydraulic fractures using hydraulic energy. Finally, a complex fracture network in the reservoir is formed and oil production can increase. Radial wellbore fracturing has been successfully implemented in many countries [2] and is expected to promote the efficient development of oil resources in glutenite reservoirs.

A large number of studies on radial well fracturing have been carried out. The team of Professor Tian have achieved fruitful results about this technology [3,4]. They found that radial wells can guide the directional expansion of fractures is because the injection of fracturing fluid into radial wells causes changes in the local stress field, making it easier for the rocks near the radial wells to meet the conditions for fracture expansion. Professor Guo and his team have also carried out a lot of studies on radial well fracturing technology [5,6]. They systematically analysed the effects of radial wellbore parameters, engineering parameter and geological parameter on fracture morphology. In addition, some scholars have conducted studies on the initiation and expansion mechanism of fractures when radial wells are spirally arranged [7,8].

This study aims to carry out experiments on radial well fracturing of glutenite, and study the influence of gravel, radial well azimuth and branches on the fracture propagation in glutenite

reservoirs, in order to provide a theoretical reference for the application of radial well fracturing technology in glutenite reservoirs.

2. MATERIALS AND METHODS

ROCK SAMPLES

The experimental rock sample consists of a glutenite outcrop, a wellbore and an epoxy resin coating, with a size of 100 mm × 100 mm × 100 mm. The glutenite outcrop was collected from the Junggar Basin. The rock sample includes a steel main wellbore and an open-hole radial wellbore. The glutenite outcrop was processed into a cube with 95mm in length, and then a layer of epoxy resin was wrapped around it to fill the uneven surface formed by the falling gravel. Picture of rock samples and wellbores, as well as their dimensions and other details, are shown in Figure 1.

Experimental device and scheme

The experimental device is a true triaxial fracturing experimental device, as shown in Figure 2. The rock samples were fractured by the experimental device according to the same process. In order to avoid damage to the hydraulic fractures, the rock sample was cut cross-sectionally at heights of 30, 50, and 70 mm by wire cutting to obtain the cross-sectional images. Then the 2D hydraulic fractures were outlined in the images and reconstructed in 3D by the software, as shown in Figure 3.

Fracturing experiments were carried out on single-branch radial wells and double-branch radial wells in the same row (well spacing was 40 mm) at azimuths of 30, 45, and 60° (azimuth is the angle between the radial well axis and the maximum principal stress direction). The fracturing fluid used in the experiment was a mixture of glycerol and water with a mass ratio of 4:1 and a viscosity of 100 mpa·s. The fracturing displacement was 30 ml/min. The experimental scheme is shown in Table 1.

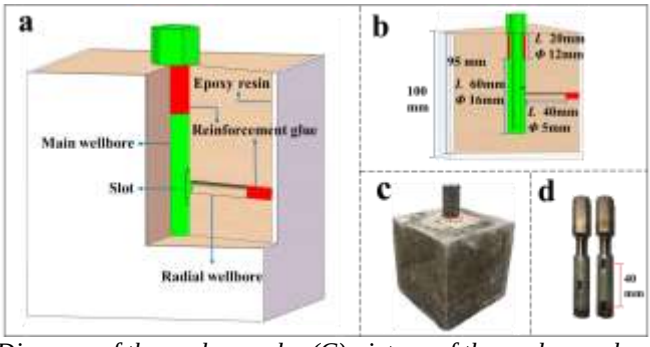

Figure 1. *(a, b) Diagram of the rock sample; (C) picture of the rock sample; (d) picture of the wellbores.*

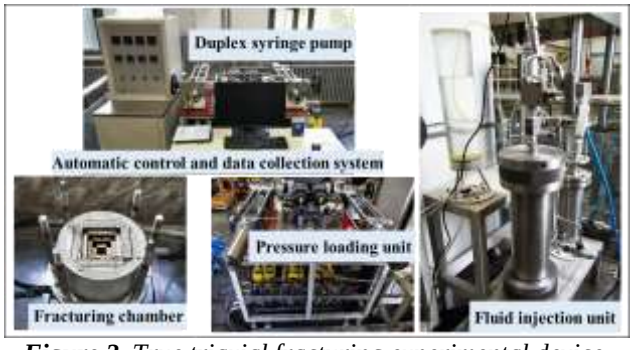

Figure 2. *True triaxial fracturing experimental device.*

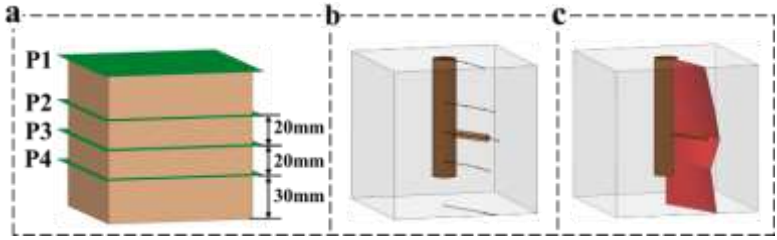

Figure 3. *Schematic diagram of rock sample slices and fracture reconstruction.*

Table 1. *Experimental scheme.*

Rock number	Number of branches	Azimuth (°)	In-suit stress (MPa) σ_V / σ_H / σ_h	Rock number	Number of branches	Azimuth (°)	In-suit stress (MPa) σ_V / σ_H / σ_h
#1	1	30	20/10/5	#4	2	30	20/10/5
#2		45		#5		45	
#3		60		#6		60	

3. RESULTS AND DISCUSSIONS

The experimental results analysed the fracture morphology after fracturing the glutenite with radial wells under different parameters. Fig. 4a-c and d-f shows the fracture morphology after fracturing with single and a row radial wells at different azimuths, respectively.

In the 6 groups of radial well fracturing experiments, the radial wells in 5 groups can effectively guide fracture directionally expansion, while rock sample #4 failed to achieve the expected result due to the interference of natural fractures. The smaller the azimuth of the radial well, the greater the stress change around the wellbore, and the stronger the guiding ability of radial well. When the azimuth is 30° or 45°, the fracture starts at the root of the radial well and can expand along the radial well (Fig. 4a, e). When the azimuth is 60°, the fracture starts at the end of the radial well (Fig. 4f) or does not expand along the radial well direction (Fig. 4c), indicating that the ability of radial well to guide the directional expansion of fractures is reduced. Compared with a single radial well, a continuous plastic zone will be generated between the wells of a row of multiple radial wells, which is more conducive to guiding the directional expansion of fractures. At an azimuth of 45°, the fractures guided by the row of radial wells start from the root of the radial well, and the fractures guided by the single radial well start from the toe of the radial well. In addition, radial wells are also conducive to the formation of branch fractures (Fig. 4f).

Gravel has a great influence on the morphology of fractures in glutenite fracturing. Under the experimental conditions of this paper, three types of fracture extension characteristics were observed: penetrating gravel, bypassing gravel, and bifurcating. Gravel with smaller particle size and content has little effect on the macroscopic fracture path (Fig. 4c, e, and f). As the particle size of gravel increases, it has a significant inhibitory and shielding effect on fractures. When a fracture encounters gravel, the fracture will bypass the gravel or be blocked, and occasionally pass through the gravel (Fig. 4a and b). In addition, the complex expansion behaviour between hydraulic fractures and gravel leads to the formation of non-planar hydraulic fractures with large fracture tortuosity (Fig. 4a). However, row-shaped radial well fracturing can effectively reduce the fracture tortuosity and form a relatively straight hydraulic fracture (contrast of Fig. 4b and e).

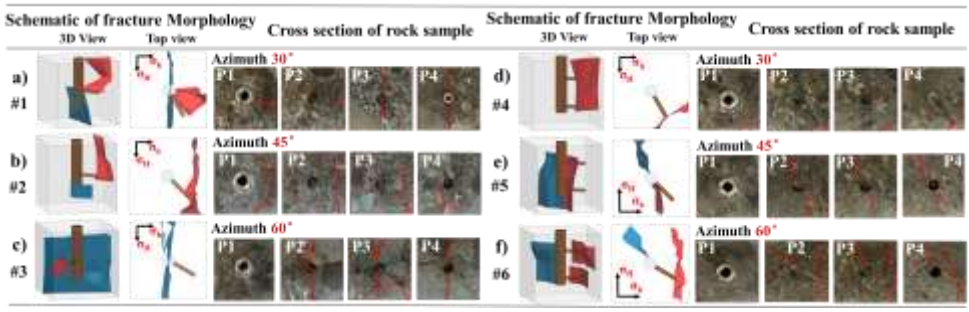

Figure 4. *Schematic diagram of rock sample slices and fracture reconstruction.*

4. CONCLUSION

The fracture characteristics of glutenite fractured by radial wells are studied, and the influence of radial azimuth and branches is explored. The main conclusions are as follows.

(1) Complex expansion behaviours occur between the fracture and gravel when radial well fracturing, which lead to the formation of non-planar fractures with certain tortuosity.

(2) The fracture morphology of glutenite fractured by radial wells is affected by ground stress, radial wells and gravel. Under the combined effect of the three, branch fractures or multiple fractures are easily generated after fracturing, thus forming a complex fracture network.

(3) Radial wells can effectively guide the directional expansion of fractures in glutenite reservoirs, and the guiding ability decreases with the increase of azimuth. Row-shaped multi-branch radial well fracturing can improve the guiding ability of radial wells and reduce the fracture tortuosity.

REFERENCES

[1] Fu, X., Li, G.S., Huang, Z.W. et al., Experimental and numerical study of radial lateral fracturing for coalbed methane. Journal of Geophysics and Engineering. (2015). 12: 875-886. DOI:10.1088/1742-2132/12/5/875

[2] Bruni, M.A., Biasotti, J.H. and Salomone, G.D., Radial drilling in Argentina, Latin American & Caribbean Petroleum Engineering Conference. (2007). OnePetro.

[3] Guo, Z., Tian, S., Liu, Q. et al., Experimental investigation on the breakdown pressure and fracture propagation of radial borehole fracturing. Journal of Petroleum Science and Engineering. (2022). 208: 109169. DOI:10.1016/j.petrol.2021.109169

[4] Yong, Y.N., Guo, Z.Q., Tian, S.C. et al., Fracture geometry and breakdown pressure of radial borehole fracturing in multiple layers. Petroleum Science. (2024). 21: 430-444. DOI:10.1016/j.petsci.2023.09.012

[5] Guo, T., Liu, B., Qu, Z. et al., Study on initiation mechanisms of hydraulic fracture guided by vertical multi-radial boreholes. Rock Mechanics and Rock Engineering. (2017). 50: 1767-1785. DOI:10.1007/s00603-017-1205-3.

[6] Guo, T., Qu, Z., Gong, F. et al., Numerical simulation of hydraulic fracture propagation guided by single radial boreholes. Energies. (2017). 10: 1680. DOI:10.3390/en10101680

[7] Tian, Y., Qu, Z., Guo, T. et al., Theoretical research on radial wells orientating hydraulically created fracture directional extended. International Journal of Hydrogen Energy. (2017). 42: 18358-18363. DOI:10.1016/j.ijhydene.2017.04.179.

[8] Lu, Y.Y., Zuo, S.J., Ge, Z.L. et al., Experimental Study of Crack Initiation and Extension Induced by Hydraulic Fracturing in a Tree-Type Borehole Array. Energies. (2016). 9: 514. DOI:10.3390/en9070514.

The importance of M in STEM

Jana Lipkovski[a], Miroslav Marić[b], Manuela Muzika Dizdarević[c], Aleksandar Lipkovski[b]✉

[a]Institute for Advancement of Education, Belgrade, Serbia
[b]University of Belgrade, Serbia
[c]University of Sarajevo, Bosnia and Herzegovina
✉ *Corresponding author: aleksandar.lipkovski@matf.bg.ac.rs*

ABSTRACT

Organized societies today agree that the most important part of general education for their prosperity is STEM – education in Science, TEchnology and Mathematics.

Already for a couple of decades, the term "STEM" is widely advocated and used in many educational paradigms: Anglo-American, Western European, Eastern European and Asian[i]. There are many attempts of its trivialization and simplification, mostly within western paradigms, interpreting STEM as providing **"**instructional environments for blended learning" and "showing students how the scientific method can be applied in an everyday context**",** thus reducing full education in all STEM disciplines – science, technology and mathematics – to their elementary and trivial applications, and missing the point in profound learning of basic procedures and concepts in science and mathematics. Despite that, STEM educational approach, in its original interpretation in the sense of profound learning of the three disciplines themselves and the connections between them, becomes more and more important. The order of these disciplines, however, reflects only the need for a nice acronym, and does not respect the importance of subjects. We strongly stress the fact that the proper order according to importance must be M-S-T. As Leon Seitelman wrote some time ago (see [1]),

1. Mathematics is vital to the national interests. Strong mathematical capability on a national scale is essential for industrial and technological leadership.

2. Mathematics is an enabler for other disciplines. Virtually all other technology benefits directly from the extension of mathematical knowledge.

3. Mathematical competence is a workplace necessity. Mathematical requirements will increase dramatically for occupations in the information age.

1. INTRODUCTION

The importance of mathematics in the educational process is widely acknowledged: mathematics is the most important school subject. But, when trying to explain the reason behind it, the explanation is usually limited to the notorious fact of its applicability: mathematical knowledge is needed in doing any relevant work in scientific or technological subjects. Actually, there is no scientific or technological educational subject that does not use mathematical tools, concepts and algorithms: not only astronomy and physics, but even sociology, not only mechanical and electrical engineering, but even forestry. There is a popular mathematicians' saying, with its first part claiming that *mathematics is the maid of science*. Or, in the words of Eugene Wigner (see [2]): "The language of mathematics is exceptionally applicable in formulation of physical laws. It is a precious gift, which we do not understand and do not deserve … We are thankful for having it and we hope that we shall continue to use it in future research … Its applicability will grow, bringing us not only joy but also headache."

However, the importance of mathematics in human education is much higher than its mere applicability. The second part of the saying mentioned above is: *mathematics is the queen of science*. This was noticed almost two and a half millennia ago in ancient Greece, explicitly by Plato (see [3]):

"For in the realm of economics, or in affairs of state, or in practical matters, no single subject in our education has such great power as the study of numbers. But its greatest benefit is that it awakens the person who is sleepy and stupid by nature, and makes him easy to teach, retentive, and intelligent, and because of this divine science, he makes progress far beyond his natural endowments..." Here Plato expresses the most important characteristic of mathematical education, which points out that not only clever pupils learn well mathematics, but all pupils should learn mathematics to their intellectual benefit.

If the reader prefers more contemporary quotes, here is one by Conrad Hilton, the founder of the hotel chain business (see [4]): "I'm not out to convince anyone that calculus, or even algebra and geometry, are necessities in the hotel business. But I will argue long and loud that they are not useless ornaments pinned onto an average man's education. ... I found higher *mathematics the best possible exercise for developing the mental muscles* necessary to this process. ... A thorough training in the mental disciplines of mathematics precludes any tendency to be fuzzy, ... and I can only believe that my two years at the School of Mines helped me to see quickly what the actual problem was - and where the problem is, the answer is."

This fact seems to be neglected in the modern western educational paradigms. At schools, the teaching of mathematics is watered down to simple, almost trivial applications. There are no deep concepts anymore, no strict logical conclusions such as the *reductio ad absurdum*, the logical pattern essential for mathematical thinking process. Euclidean geometry is almost completely replaced by coordinate geometry and 3-dimensional Euclidean stereometry completely cut out. The stress is on "applied problems" in mathematics. But, how can one apply something if he doesn't understand its inner structure, relations and connections? Mathematical knowledge is interwoven as a fabric, consisting of multiple layers of procedures and concepts. In the modern western paradigm, the conceptual knowledge in mathematics is diminished by omitting deduction and proofs from the educational process, the procedural knowledge is also diminished due to the fact that all useful mathematical algorithms are now available on computers and there is no direct necessity for deep understanding of mathematical procedures, which involve not only numerical calculation but also differentiation, calculation of integrals or solving differential equations – "the machines will do it for us", and nowadays students at technical and science universities do not know how to calculate triple integrals any more. This is a huge mistake.

The principal *raison d'être* of school mathematics is not its applicability, but its influence on the thinking process and on the development of personal intellectual power of human being. The processes of induction and deduction, analogy, generalization and specialization in mathematics are of utmost importance in the development of human intellectual skills, which then help in understanding the whole world of science and technology, and not only. As Immanuel Kant a long time ago wrote (see [5]): "Ich behaupte aber, daß in jeder besonderen Naturlehre nur so viel eigentliche Wissenschaft angetroffen werden könne, als darin Mathematik anzutreffen ist."

2. MATERIALS AND METHODS

Let us now consider what could be the most important concept in school mathematics. Onecan argue that the question is disputable. It is difficult to answer since there are many crucial concepts in mathematics coming one after another in the educational process, starting with natural numbers and counting. However, we argue that the notion of uncountable infinity (or equivalently, the real numbers, or further on, the straight line) is the most difficult human intellectual concept. There are no infinite things in the real world, so the mathematical infinity "does not really exist". Its most important appearance in education is the transition from rational to real numbers. There are several didactical processes opening the human mind to infinity, and they all originate from ancient Greek mathematics, starting with the "Achilles and the tortoise" paradox (countable infinity), incommensurability of the diagonal of the square with its side (continuum infinity). Here we would like to point out Thales' theorem on similar triangles and its proof(s) as the source of knowledge for

continuum infinity. There are two faces to this theorem and correspondingly two approaches to the proof of the theorem, which are usually not differed. The first one is using only the rational numbers – ratios – and its proof is based solely on triangle congruence. It is usually referred to not as Thales' theorem but as the algorithm of division of a given segment into any given number of equal parts by straightedge and compass. The other is based on the notion of area i.e. the real numbers and bears the name of Thales' theorem. In Euclid's Elements, it is proved in VI.2, much later than the Pythagorean theorem which is proved in I.47. The difference is immense: the first Thales' theorem (we refer to it as "rational" Thales' theorem) appeals only to countable, the other (we refer to it as "full" Thales' theorem) to continuum infinity. The reader can find a detailed exposition of this question in [6]. Here we state just the curious fact that both Thales and Pythagoras were born and lived in an area very close to ICCESEN conference's site in Kemer: the port Miletus between todays' Batıköy and Balat on the Turkish soil, and the Greek island Samos, some 20 nautic miles away, with a time shift of some 50 years.

We have stated our opinion that in the western world today, the level of mathematical education is becoming less and less satisfactory. Let us give a little historical perspective to this fact by comparing examples from the past and today. The examples are chosen from Serbian educational system. The reader should bear in mind that Serbian educational system, after being for a long time on the Russian educational track, has switched to Western track after political changes in the year 2000. This change has its reflection on the mathematical education. Here are some problems from high school algebra graduation exams in Serbia and Yugoslavia almost 100 years ago.

> (1933) One craftsman paid his workers 800 dinars a day. Since he fired 7 workers and reduced the wages of the others by 10 dinars each, he paid 390 dinars a day. How many workers did he have and what was the wage?
>
> (1933) Solve the system of equations $x^5+y^5 = 4149$, $x+y = 9$.
>
> (1933) Solve the equation $x^4-4x^3-3x^2-4x+1 = 0$.
>
> (1938) There is only one equation $x^2+ax+b = 0$ such that their coefficients are equal to its roots. Find it.

Not so easy, isn't it? But today, the education system in Serbia has been reformed according to the European guidelines, and things got much worse. Compare previous examples with authors' recent research results. The research was conducted at two mathematics faculties in Western Balkans (former Yugoslavia) on students' conceptual knowledge as opposed to procedural knowledge of basic algebraic ideas at the beginning of their undergraduate studies (see [7]). It showed very poor results. As an illustration, let us show two examples. The following multiple-choice problem

> Find the equation(s). Encircle letter(s) in front of correct answer(s):
>
> (a) $x^2-3x-2 = 0$;
>
> (b) $3a-0.75 = b$;
>
> (c) $x-y+2ax$;
>
> (d) $(x-y)^2 = x^2-2xy+y^2$;
>
> (e) $(a^2x-2abx+c)/(3x-2y)$;
>
> (f) $3-0.75 = 2.25$.

was answered correctly by only 31%, and 29% responses were not correct (or not answered at all). Even worse were responses to another problem:

Let $P=a+3$ and $Q=3+a$, where a is positive integer. Let $P?Q$. Is it possible to replace the symbol "?" with a symbol of mathematical relation? If yes, explain what mathematical expression is obtained. If no, justify your answer.

There were 31% correct responses and 40% not correct (or not answered). So, the two examples show that less than one third of beginning math students does recognize concepts of mathematical equation or relation. These results show that high-school math education missed the point. And there can be no real knowledge of mathematics without these concepts.

3. RESULTS AND DISCUSSIONS

As a conclusion, we should not allow lowering the importance of mathematics as *general subject* for all students, nor lowering the number of hours or the content of the curriculum; we should not allow the administration's pressure on math teachers in order to increase the average marks: mathematics must be learned. Otherwise, to paraphrase Russian mathematician Vladimir Arnold, the bridges will break and the airplanes crush.

REFERENCES

[1] Leon H. Seitelman, A New Paradigm for Mathematics: Publicity or Perish, Notices AMS, October 1996, 1155-1158

[2] E. Wigner: The unreasonable effectiveness in mathematics. Comm. Pure and Appl. Math., 1960, 13, 1-14

[3] Plato, Laws, Book V, 747 B, from platonicfoundation.org/translation/laws/

[4] C. Hilton, Be My Guest, Prentice-Hall Inc., 1957, p. 71, from Notices of the AMS, 44:8, 1997

[5] I. Kant: Werke, Wilhelm Weischedel [Hrsg.], Insel Verlag, Frankfurt am Main, 1964, Bd. IV: Matematische Anfangsgründe der Naturwissenschaft, S. 470

[6] Липковски А.Т.: Когда преподавать теорему Пифагора, до или после теоремы Фалеса? In: Геометрические аспекты в преподавании математики в высшей и средней школе. Материалы международной конференции (к 100-летию со дня рождения Л.С. Атанасяна). Под общей редакцией Н.И. Гусевой. Москва, 2022. С. 122-129. Available at elibrary.ru/item.asp?id=47813608

[7] Lipkovski A, Muzika Dizdarevic M, Odzak A: Measuring conceptual knowledge of basic algebraic concepts. The Teaching of Mathematics (2024), Vol. XXVII, No.1, pp 32-50. Available at elib.mi.sanu.ac.rs/files/journals/tm/52/tmn52p33-51.pdf

[8] В. И. Арнольд: Математика и физика: родитель и дитя или сестры, Успехи физических наук, 169:12, 1311-1323, 1999.

Heat capacity of electrons confined to a parabolic quantum well in two-dimensional space with conical disclination and Rashba spin-orbit interaction

Arif BABANLI[1]✉

[1]*Suleyman Demirel University, Physics. Department, Isparta, Turkey*
✉ *Corresponding author: arifbabanli@sdu.edu.tr.*

ABSTRACT

In the present work, the effect of topological defects in quantum dots on the heat capacity has been investigated. Using the energy spectrum, we derived the exact analytic expression for the single-particle partition function to determine the heat capacity. It was shown that the effect of the wedge parameter on specific heat is more effective in low magnetic fields. The small value of the wedge parameter gives a small heat capacity value and grows, approaching the peak value. In the high magnetic field regime heat capacity saturate to k_B. This region corresponds to the pure Landau level with the energy spectrum of a 1D oscillator. As a function of temperature, the heat capacity shows at a very low temperature, a sharp peak structure reminiscent of the Schottky anomaly.

KEYWORDS: Diluted magnetic semiconductor, quantum dot, thermodynamic properties.

1. INTRODUCTION

In recent years there has been increased interest, both theoretically and experimentally in quantum dot geometry in the presence of a magnetic field. Since nanostructures have been applied to electronic devices, interest in them has increased.]The reason for this is that in quantum dots there are observed interference effects under the influence of electromagnetic potentials, known as Aharonov-Bohm [1] and Aharonov-Casher [2] effects which have no analog in classical physics. In the paper [3], the modified Kane-Mele Hamiltonian is derived for graphene with wedge disclination and Rashba spin-orbit couplings. The wedge disclination changes the flat lattice into the conical lattice and modifies the spin-orbit couplings. When spin-orbit interaction (SOI) coupling is considered, several new states appear in the electronic structure concerning the electron spin up and spin down. The Rashba SOI coupling [4,5], arises from the asymmetry of the structure and describes the spin-orbit interaction in low-dimensional systems. In authors investigated the impact of a topological defect and the SOI on the thermomagnetic and optical properties in a two-dimensional quantum dot [6].

2. MATERIALS AND METHODS

This study calculated the specific heat of electrons by considering the Rashba spin-orbit interaction in quantum dots with odd topology in the magnetic field. The dependence of the heat capacity depending on the magnetic field, Rashba spin-orbit, and topology parameters was investigated. We use the Volterra design [7,8,9] to model the ring wedge dislocation defect of radius R and the remote wedge dislocation shown in Fig. 1. For this purpose, we obtain the spectrum and the eigenstates of electrons, and then we calculate the partition function of the system. Using the partition function, we obtain the heat capacity of electrons in quantum dots with a wedge dislocation. We consider the quantum dots with a wedge dislocation in an external magnetic field. The metric of the system in polar coordinates for an electron moving in a crystal with a wedge dislocation defect is defined as

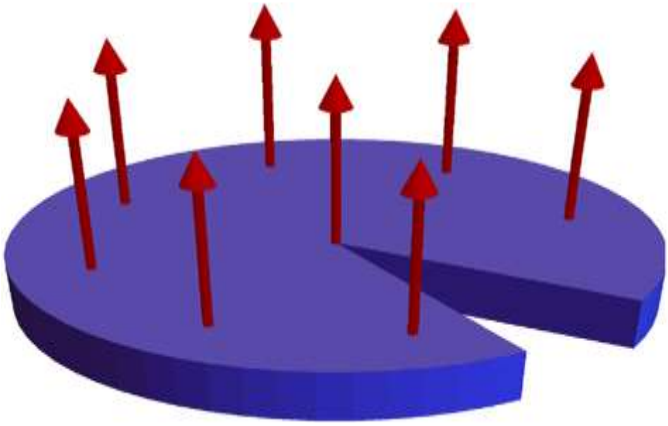

Figure 1. *Volterra process.*

$$ds^2 = \alpha^{-2}dr^2 + \rho^2 d\phi^2 \tag{1}$$

The total Hamiltonian of the system is given by:

$$H = \frac{1}{2m}\left(\vec{P} + e\vec{A}\right)^2 + \frac{m\omega^2}{2\alpha^2}r^2 + H_{RSOI} + H_Z \tag{2}$$

where m is the effective mass of the electrons, and $\vec{A}$ is the vector potential.
For a uniform magnetic field parallel to the z-axis, the vector potentials in cylindrical coordinates have the components $A_r = 0, A_\theta = \frac{Hr}{2\alpha^2}, A_z = 0$. The Rashba spin-orbital term has the form as [10]

$$H_{RSOI} = \gamma\sigma_z\alpha\frac{dV_c}{dr}\left(-i\frac{1}{r}\frac{\partial}{\partial\theta} + \frac{eHr}{2\hbar\alpha^2}\right) \tag{3}$$

Where σ_z is the Pauli matrix and γ is the Rashba spin-orbit coupling parameter
The eigenvalue

$$E_{nl} = \left(2n + 1 + \frac{|l|}{\alpha}\right)\hbar\Omega + \frac{1}{2}\frac{\hbar\omega_c l}{\alpha^2} + \frac{\sigma}{2}g^*\mu_B H + \frac{\gamma m\omega^2 l}{\alpha}\sigma \tag{4}$$

where $\Omega = \sqrt{4\omega^2 + 4\gamma\sigma_z\frac{m}{\alpha}\frac{\omega_c}{\hbar} + \omega_c^2\alpha^{-2}}$

Let us investigate the effect of the Rashba spin-orbit interaction on the heat capacity of electrons in quantum dots with wedge disclamations. The starting point of the thermodynamic analysis is the evaluation of the partition function for the energy spectra given in Eq.(4):

$$Z = \sum_{nl\sigma} e^{-\beta E_{nl\sigma}} = Z^{+} + Z^{-} \tag{5}$$

Where $E_{nk_z\sigma}$ is the energy spectrum of the considered system, $\beta = \frac{1}{k_B T}$ and k_B is the Boltzmann constant, and T is the thermodynamic equilibrium temperature. The sum can be analytically performed and results in the following expression.

$$Z_\sigma = \frac{1}{4} e^{\sigma \frac{1}{2} g \mu_B H} Csch\left[\beta H_\sigma\right] Csch\left[\frac{1}{2}\beta c_\sigma\right] Csch\left[\frac{1}{2}\beta c1_\sigma\right] Sinh\left[\frac{\beta H_\sigma}{k}\right] \tag{6}$$

$$H_\sigma = \hbar\Omega_\sigma = \hbar\omega\sqrt{1+\sigma\gamma\frac{m\omega_c}{\hbar}+\frac{1}{4k^2}\left(\frac{\omega_c}{\omega}\right)^2}\,; c_\sigma = \pm b_\sigma + \frac{\hbar\Omega_1}{\alpha}, \sigma = \pm 1, \tag{7}$$

$$b_\sigma = \mp\frac{\hbar\omega}{r^2}\gamma 1 - \frac{\hbar\omega}{2\alpha^2} y\,; \tag{8}$$

The heat capacity can be obtained by:

$$C = k_B \beta^2 \frac{\partial^2 \ln Z}{\partial \beta^2} \tag{9}$$

Fig. 2 shows the variation of the heat capacity of electrons in InSb-type quantum dots in the presence of Rashba spin-orbit interaction and wedge dislocations depending on the magnetic field at three different values of wedge disclination parameter α=0.3,0,6,1.

3. RESULTS AND DISCUSSIONS

As seen from Figure 1 for a fixed temperature, specific heat initially rises rapidly with the increase in magnetic field, attains a maximum value, and then decreases to k_B. In Fig. 3, we have shown the specific heat of quantum dots as a function of temperature for two different values of disclination parameter for fixed magnetic field y=0.04. As seen from the figure with low magnetic fields, as the temperature is increased from absolute zero, specific heat suddenly increases and then decreases giving a peak-like structure.

The observed peak structure is the well-known Schottky anomaly of the heat capacity, typical for a system where only two states are of importance at low temperatures because thermal energy gained by electrons is enough for only the lowest two levels.

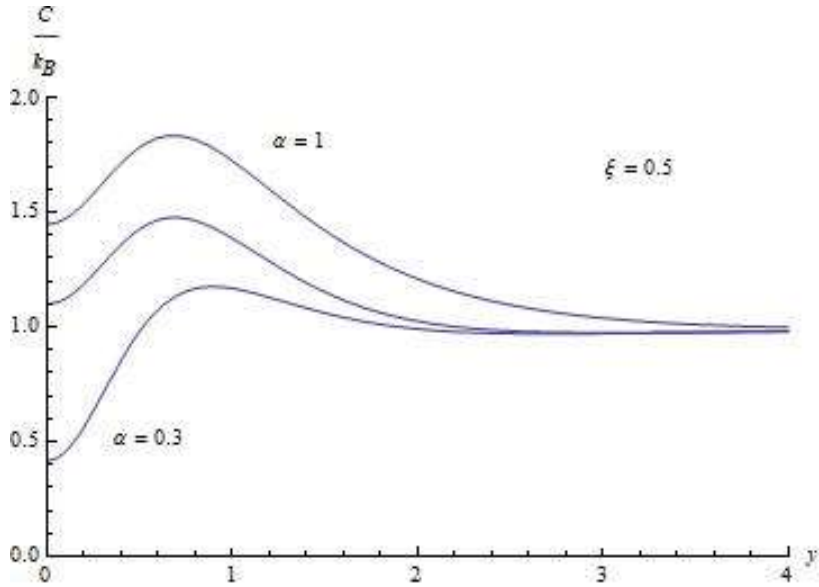

Figure 2. *The variation of heat capacity of electrons in InSb-type quantum dots in the presence of Rashba spin-orbit interaction and wedge dislocations on the magnetic field.*

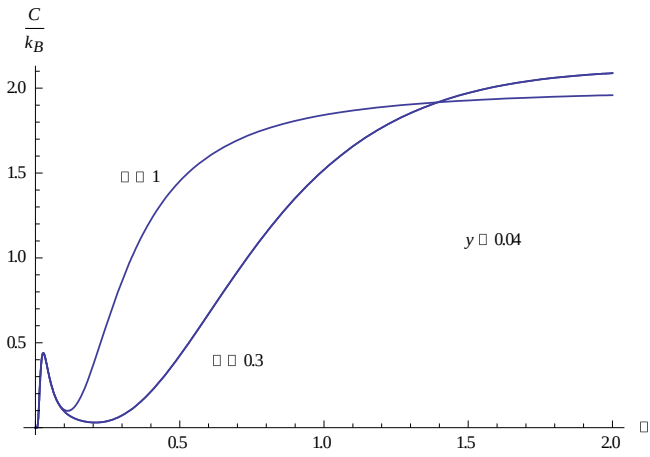

Figure 3. *Variation of specific heat with dimensionless temperature for dimensionless magnetic field y=0.04 at two different disclination parameter*

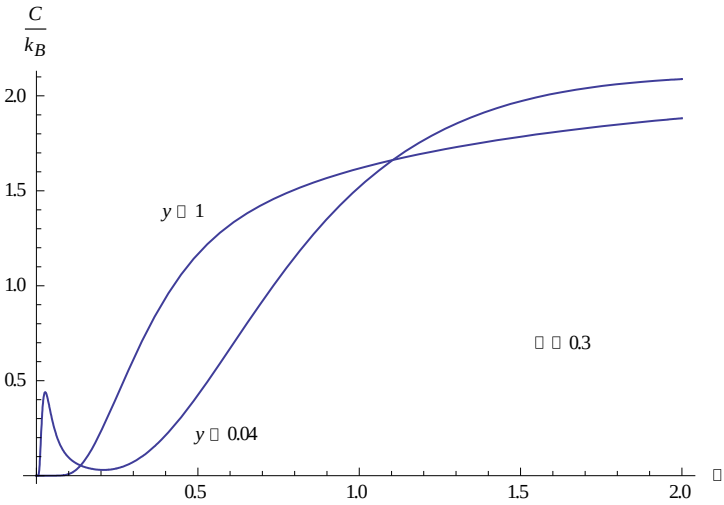

Figure 4. *Variation of specific heat with dimensionless temperature for disclination parameter α=0.3 at two different dimensionless magnetic fields y=0.04,y=1*

Figure 4 shows the variation of heat capacity with temperature for different values of the magnetic field at fixed disclination parameters. As the figure shows, the heat capacity approaches 2 k_B at high temperatures, and the peak of the heat capacity is reached at low temperatures and magnetic fields.

4. CONCLUSIONS

We have studied the heat capacity of the electron gas in quantum dots with topological disclination and Rashba spin-orbit interaction. It was shown that the heat capacity at a high magnetic field approaches k_B. At low magnetic fields, the variation of specific heat with temperature gives a peak-like structure.

REFERENCES

[1] Y. Aharonov and Bohm, Phys. Rev. 115, 485 (1959)
[2] Y. Aharonov and A. Casher Phys. Rev. Lett. 53, 319 (1984)
[3] Vaseghi, B., Malian, M. Energy levels and electron g-factor of spherical quantum dots with Rashba spin-orbit interaction. Phys.Lett. A **2011**, 375, 2747–2753.
[4] Ali, A.A., Shaer, A.; Elsaid, M. , J. Magn. Magn. Mater. **2022**, 556, 169435.
[5] José C.León-González and et.all, Nanomaterials2023,13,1461.
[6] M.O. Katanaev, I.V. Volovich, Ann. Phys. (NY) 216 (1992) 1.
[7] M.O. Katanaev, Physics - Uspekhi 48 (7) 675 - 701 (2005)
[8] Tridev Mishra, Tapomoy Guha Sarkar, and Jayendra N. Bandyopadhyay, Phys.Rev E **89**, 012103 (2014)
[9] O. Voskoboynikov, C. P. Lee, and O. Tretyak, Phys.Rev B 63, 165306

Investigation Of Radiation Properties Of Some Teeth Sample Using GAMOS 6.2 Simulation Code

Aycan Şengül[1], İskender Akkurt[2]

[1] Akdeniz University, Health Services Vocational School, Medical Imaging Techniques, Antalya, Turkey
[2] Suleyman Demirel University, Science Faculty, Physics Department, Isparta, Turkey

ABSTRACT

Tooth enamel is the most mineralized tissue of human body. Its composition is 96% inorganic material and 4% organic material and water. In dentin, the inorganic material represents 70%. Teeth can be exposed to radiation due to head and neck radiotherapy, dental procedures and radiological examinations. Therefore, it is important to study the effect of radiation on teeth. The aim of this study was to evaluate the radiation absorption properties of teeth. Monte Carlo simulation is a crucial tool for obtaining the properties of radiation absorption in a material. We used with 6 different teeth samples defined as D1 (Enamel_outer surface), D2 (Enamel_middle), D3 (Enamel_EDJ), D4 (Dentin_EDJ), D5 (Dentin_middle), and D6 (Dentin_inner). GAMOS 6.2 simulation program was used for simulating the mass absorption coefficients of the teeth. The simulation was repeated,with and without absorber, for 27 energies in the energy range of 10 keV - 20 MeV. The photon was modeled as a point source directed as a parallel beam. Before reaching the NaI detector, beam passed the 0.5 cm thick absorber that was placed. Also, the results have been compared with the calculation that has been done using XCOM computer code and the results were found to be compatible. GAMOS Monte Carlo simulation code is an alternative technique to experimentation for determining the calculations of mass attenuation coefficients of teeth.

***KEYWORDS**: Monte Carlo, the mass attenuation coefficients, Teeth, radiation therapy, GAMOS 6.2*

1. INTRODUCTION

Photons emitted from radioactive sources or produced by radiation devices are widely used in medical and industrial applications because they are a form of ionizing radiation[1-5]. Teeth can be exposed to radiation due to radiotherapy of the head and neck, dental applications and radiological examinations. Therefore, it is important to study the effect of radiation on teeth. The aim of this study was to evaluate the radiation absorption properties of radiation on 6 different dental specimens. Tooth enamel is the most mineralized tissue of human body. Its composition is 96 wt.% inorganic material and 4 wt.% organic material and water. In dentin, the inorganic material represents 70 wt.%. This inorganic material is mainly composed by a calcium phosphate related to the hexagonal hydroxyapatite. All teeth are composed of basic layers such as enamel, dentin, pulp and cementum. However, the thickness, density and mineral content of these layers may vary depending on the type of tooth and the location of the tooth [6-10].

The attenuation coefficient is a measure of the likelihood of photons undergoing scattering or absorption interactions per unit mass of the medium in which they are absorbed. Despite the fact that there are literature studies for μ/ρ that are based on experimental or computational assessments [11-15] The attenuation coefficient μ/ρ quantifies the likelihood of photons engaging in scattering or absorption interactions in relation to the mass of the absorbing medium or during computational assessments. Typically, these are designated for a finite range of substances, approximated at specific energy thresholds.

The goal of this study is to compute μ/ρ data in the energy range of 10 keV-20 MeV for nickel-based metal-organic framework material using the Monte Carlo method and compare it to XCOM data.

2. MATERIALS AND METHODS

Human teeth are exposed to a different point-to-point pressure during mastication. Because the structures that enamel and dentin present, prisms running from the enamel-dentin junction (EDJ) to the surface in the case of enamel and a heterogeneous composite material in the case of dentin, it is easy to imagine that their hardness values are different, even from one site to other inside enamel and dentin themselves; and that they would be chemically dependent. In sound human enamel, it was reported that the hardness values, the mineral content, and the density gradually decrease from the outer surface to the EDJ [16-20].

The approach employs pseudo-random integers and probability distributions in order to approximate the average value of a physical property that is challenging to compute analytically or quantitatively. The inclusion of beam parameters and elemental compositions provides a significant degree of relevance to radiation transport problems [21].

The objective of this study is to employ the widely recognized Monte Carlo method to compute the mass attenuation coefficients of six teeth samples defined as D1 (Enamel_outer surface), D2 (Enamel_middle), D3 (Enamel_EDJ), D4 (Dentin_EDJ), D5 (Dentin_middle), and D6 (Dentin_inner).. GAMOS (Geant4-based Architecture for Medicine-Oriented Simulations) is a variation of the well-known Monte Carlo software Geant4 [22], which is commonly used by medical physicists to model radiation sources in clinical setting [24, 25]. The GAMOS 6.2 software was used to predict the element compositions, geometries, and radiation interaction characteristics of teeth samples in this investigation.

The simulations in this work comprise a point photon source located in a cylinder that generates mono-energetic photons directed parallel toward a cylindrical sample 20 cm distant from the source. The detector was designed as a NaI as shown in Fig 1. The simulations were run with 27 photon energies ranging from 10 keV to 20 MeV. The electromagnetic physics package is the physics package utilized in the simulation. All particles reaching the surface were scoring, and the spectrum was derived using a classifier. The simulation was run with and without absorbing material for each energy. The number of 10^7 photons, which produces sufficient results, is used to boost the precision of Monte Carlo computations and to generate minimal statistical error.

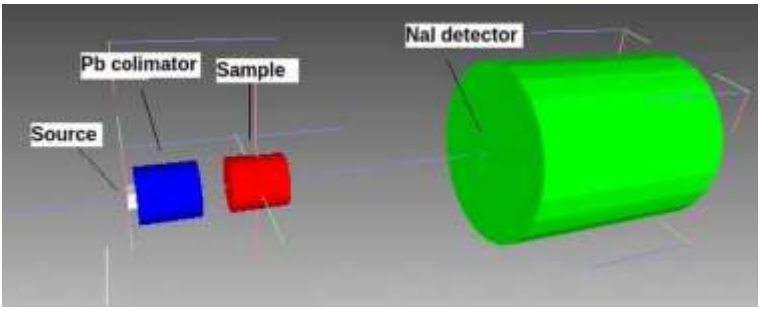

Figure 1. *GAMOS model geometry used for calculation μ /ρ*

The following equation can be used to compute the linear attenuation coefficients (μ) in this procedure.

$$I = I_o e^{-\mu x} \quad (1)$$

I_o is the starting number of gamma ray counts (recorded in the detector), I is the number of gamma ray counts that pass through the absorber, is the linear attenuation coefficient of the shielding material in cm $^{-1}$, and x is the absorber thickness in cm.
EDS results from enamel and dentin. Data in at .% and they are the main values from 3 samples analyzed. EDS analysis was carried out from the outer enamel surface to EDJ in enamel, and from EDJ to the inner dentin layer in dentin. The data for samples are shown in Table 1.

Table 1. *Properties of the teeth sample examined in the study*

	ENAMEL			DENTIN IN		
Element	**Outer Surface**	**Middle**	**EDJ**	**EDJ**	**Middle**	**Inner**
	D1	**D2**	**D3**	**D4**	**D5**	**D6**
C	38.59	36.28	37.05	59	52.27	49.84
O	32.59	34.21	34.51	30.67	30.57	33.54
Na	0.24	0.44	0.66	0.47	0.42	0.36
Mg	0.16	0.23	0.22	0.25	0.34	0.45
P	10.67	10.86	10.46	4.41	6.23	6.32
Cl	0.39	0.25	0.09	0	0	0
Ca	17.36	17.74	16.99	5.19	9.15	9.5

3. RESULTS AND DISCUSSIONS

Linear attenuation coefficients were found by repeated simulations with and without the sample using GAMOS 6.2 Monte Carlo code. μ values is shown for all examples in figure 1. Mass attenuation coefficients were calculated using the material density. μ/ρ at photon energies ranging from KeV to GeV were also calculated using XCOM, which utilizes pre-existing databases for photon interaction [25]. XCOM and GAMOS results for dental samples are compared and shown in figure 2. It can be seen that μ/ρ decreases with increasing energy. It can be seen that D3 has the highest linear absorption coefficient.

4. CONCLUSIONS

Monte Carlo simulations at twenth-seven distinct gamma energies were used in this study to assess the radiation shielding properties of teeth samples. The linear attenuation coefficients of the samples were simulated using the GAMOS 6.2 simulation tool.
The computational data on teeth samples materials allow us to draw the following conclusions:
• The mass absorption coefficient data first reveal a significant decrease in the energy range where photoelectric absorption predominates depending on the atomic number of the material. This tendency can be explained by two factors: first, all materials absorb roughly the same amount of radiation at higher energies; and second, different absorption mechanisms are significant in different energy ranges.
• It can be seen that D3 has the highest linear absorption coefficient.
• When the obtained values were compared to the theoretical values of the XCOM database, a very good agreement ($R^2 = 0.9996$) was established.

These findings show that the Monte Carlo approach can be used safely even in the presence of constraints such as the limited gamma energies that can be used in a lab setting or the inability to perform measurements due to challenges associated with the material's physical production.

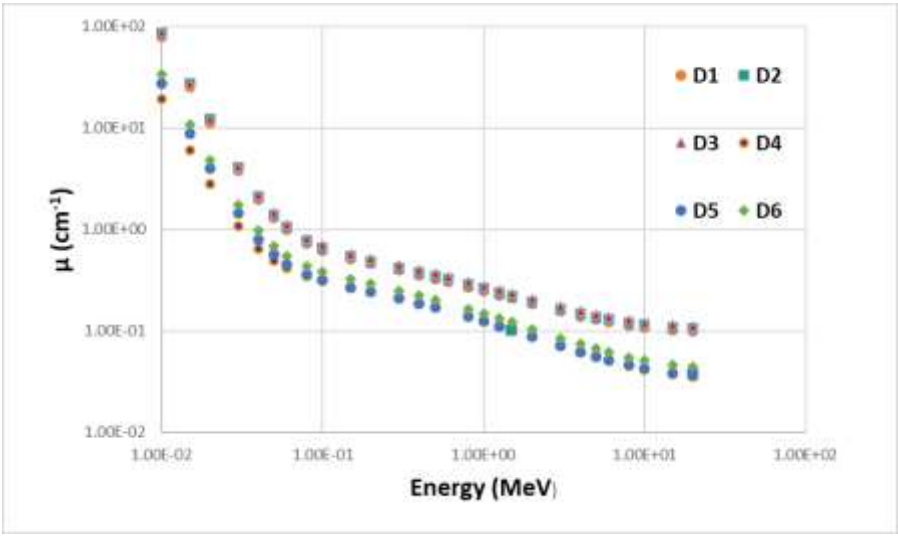

Figure 1. *Comparison of linear attenuation coefficient as a function of gamma energy for samples*

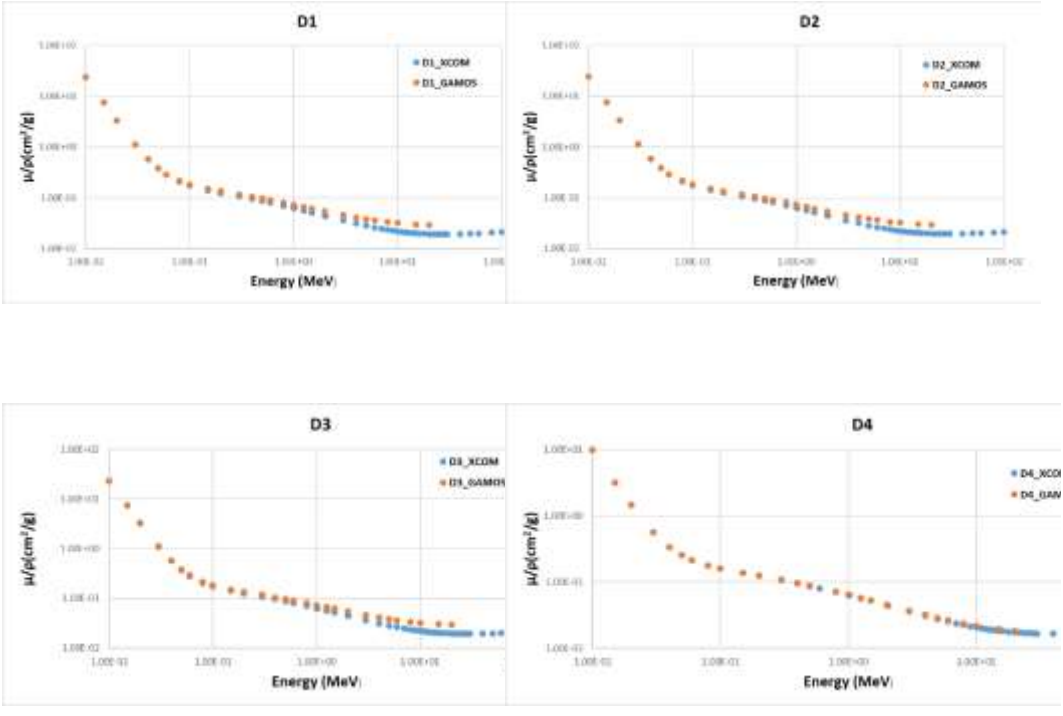

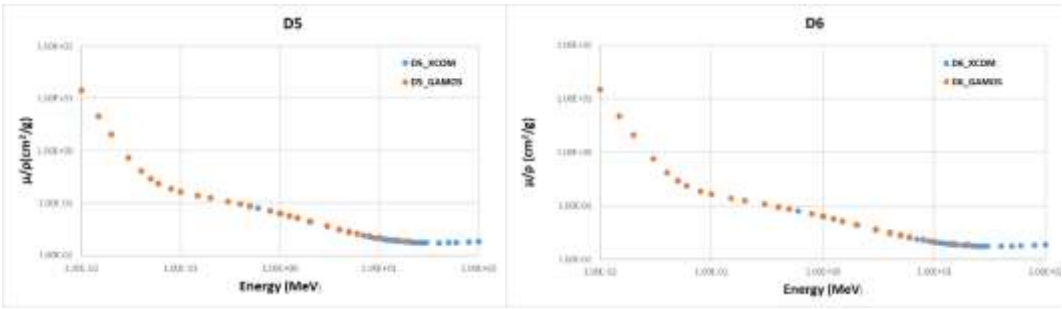

Figure 2. *Comparison of mass attenuation coefficient as a function of gamma energy for samples (XCOM and GAMOS)*

REFERENCES

[1] Al-Buriahi, M.S., H. Arslan, and B.T. Tonguç, *Mass attenuation coefficients, water and tissue equivalence properties of some tissues by Geant4, XCOM and experimental data.* Indian Journal of Pure & Applied Physics (IJPAP), 2019. **57**(6): p. 433-437.

[2] Phelps, M.E., E.J. Hoffman, and M.M. Ter-Pogossian, *Attenuation coefficients of various body tissues, fluids, and lesions at photon energies of 18 to 136 keV.* Radiology, 1975. **117**(3): p. 573-583.

[3] Patterson, D.K., et al., *How parrots talk: Insights based on CT scans, image processing and mathematical models*. Physiology and Function from Multidimensional Images - Medical Imaging 1997, ed. E.A. Hoffman. Vol. 3033. 1997, Bellingham: Spie - Int Soc Optical Engineering. 14-24.

[4] Akkurt, I., R.B. Malidarre, and T. Kavas, *Monte Carlo simulation of radiation shielding properties of the glass system containing Bi 2 O 3.* The European Physical Journal Plus, 2021. **136**(3): p. 1-10.

[5] Akkurt, I., et al., *Monte Carlo simulations study on gamma ray–neutron shielding characteristics for vinyl ester composites.* Polymer Composites, 2021. **42**(9): p. 4764-4774.

[6] Le Geros, R.Z. Calcium phosphates in oral biology and medicine, Howard M. Myers, Ed., San Francisco, California, 1991.

[7] Reyes-Gasga, J.; Alcantara-Rodriguez, C.M.; GonzalezTrejo, A.M.; Madrigal-Colin, A. Acta Microscopica, v. 6, p. 24-38, 1997.

[8] Kinney, J.H.; Balooch, M.; Marshall, S.J.; Marshall. G.W.; Weihs, T.P. Archs Oral Biol., v. 41, p. 9-13, 1996.

[9] Meredith, N.; Sherriff, M.; Setchell, D.J.; Swanson, S.A.V. Archs, Oral Biol. v. 41, p. 539-545, 1996.

[10] Maria del P, Gutiérrez-Salazara, Jorge R, ; Microhardness and Chemical Composition of Human Tooth, Material Research, November 15, 2002; Revised: June 2, 2003

[11] Almisned, G., et al., *Gamma ray shielding properties of CeO2-added hydroxyapatite composite.* Journal of the Australian Ceramic Society, 2022: p. 1-9.

[12] Bozkurt, A. and A. Sengul, *Monte Carlo approach for calculation of mass energy absorption coefficients of some amino acids.* Nuclear Engineering and Technology, 2021.

[13] Ermis, E., et al., *A comprehensive study for mass attenuation coefficients of different parts of the human body through Monte Carlo methods.* Nuclear Science and Techniques, 2016. **27**(3): p. 54.

[14] Akkurt, I. and H. Akyıldırım, *Radiation transmission of concrete including pumice for 662, 1173 and 1332 keV gamma rays.* Nuclear Engineering and Design, 2012. **252**: p. 163-166.
[15] Jawad, A., et al., *Radiation shielding properties of some ceramic wasted samples.* International Journal of Environmental Science and Technology, 2019. **16**(9): p. 5039-5042.
[16] Robinson, C.; Weatherell, J.A.; Hallsworth, A.S. Caries Res., v. 15, p. 70-77, 1981.
[17] Kodaka, T.; Debari, K.; Yamada, M.; Kuroiwa, M. Caries Res., v. 26, p. 139-141, 1992.
[18] Davidson, C.L.; Hoekstra, I.S.; Arends, J. Caries Res., v. 8, p. 135-144, 1974.
[19] Gustafson, G.; Kling, O. Odontol. Tskr., v. 56, p. 23-30, 1948.
[20] Herkströter, F.M.; Witjes, M.; Ruben, J.; Arends, J. Caries Res., v. 23, p. 342-344, 1989.
[21] Andreo, P., *Monte Carlo techniques in medical radiation physics.* Physics in Medicine & Biology, 1991. **36**(7): p. 861.
[22] Glaser, A.K., et al., *A GAMOS plug-in for GEANT4 based Monte Carlo simulation of radiation-induced light transport in biological media.* Biomedical optics express, 2013. **4**(5): p. 741-759.
[23] Arce, P., et al. *GAMOS: A Geant4-based easy and flexible framework for nuclear medicine applications*. in *2008 IEEE Nuclear Science Symposium Conference Record*. 2008. IEEE.
[24] Arce, P., et al., *Gamos: A framework to do Geant4 simulations in different physics fields with an user-friendly interface.* Nuclear Instruments and Methods in Physics Research Section A: Accelerators, Spectrometers, Detectors and Associated Equipment, 2014. **735**: p. 304-313.
[25] Berger, M., et al., *XCOM: Photon Cross Sections Database. NIST, PML, Radiation Physics Division*. 2019.

Effect of Stannous Oxide and Stannic Oxide Additions on the Ball Milling Behavior of Copper Based Composite Powders

Serkan BIYIK✉

Karadeniz Technical University, Abdullah Kanca Vocational School, Department of Machinery and Metal Technologies, Trabzon, Turkey
✉ *Corresponding author: serkanbiyik@ktu.edu.tr*

ABSTRACT

This study investigated the synergetic effect of reinforcement type and milling duration on the synthesis and characterization of copper (Cu) based composite powders. For this purpose, stannous oxide (SnO) and stannic oxide (SnO_2) powders were chosen as reinforcing materials in Cu matrix. Ball milling experiments were carried out using a two stationary planetary type ball mill to synthesize composite powders. Milling parameters were selected to be a milling speed of 300 rpm and a ball-to-powder weight ratio (BPR) of 10:1. By the way, stearic acid was also added in grinding vial at specific milling periods to control heat fluctuations and to establish a balance between cold welding and fracturing. Powder characterization was carried out using scanning electron microscopy (SEM) and laser diffraction analyses (Mastersizer). Accordingly, final size and shape of powder particles are being affected by the type of reinforcement. Considering the evolution of powder morphologies and particle sizes; the usage of SnO_2 was found more efficient than SnO in reducing average particle size.

KEYWORDS: *Ball milling, copper-based composites, particle size, powder technology, stannic oxide, stannous oxide.*

1. INTRODUCTION

Metal matrix composites (MMCs) have superior physical and mechanical properties over conventional materials. Therefore, they have been applied in a wide range of applications including aerospace, automotive, marine, defense, electrical and electronics industries [1-4]. For example, copper (Cu) metal is frequently used as a base material to produce electrical contacts owing to its high formability, high electrical and thermal conductivities, and low cost. However, poor resistance to oxidation and corrosion often pose an obstacle to its further appliance. Hence, to develop its physical and mechanical properties, some reinforcing materials such as oxides, carbides and refractory metals are frequently used with Cu [5-8].

Mechanical alloying (MA) or ball-milling technique can be utilized to synthesize composite powders [9]. However, this process has a number of operational parameters that needed to be optimized [10-13]. Some of them are milling speed, ball-to-powder weight ratio (BPR), materials of both milling vial and grinding balls, type and amount of process control agent (PCA) and milling duration. Apart from the properties of as-received or starting powders, type of the reinforcement also affects the final size and shape of composite powders. Therefore, to investigate the ball-milling behavior of copper; two different types of reinforcements, namely SnO and SnO_2 were separately added to milling vials, and ball-milling experiments were carried out to synthesize composite powders. The effects of different reinforcements on size and shape of composite powders were comparatively studied.

2. MATERIALS AND METHODS

In this study, Cu powder was used as the matrix material whereas SnO and SnO_2 powders were used as the reinforcements. As starting materials, elemental Cu having maximum particle size of 44 μm

and a purity of 99%, SnO having a particle size of 10 μm and a purity of 99.9% and SnO_2 having a particle size of less than 10 μm and a purity of 99.9% powders were used for ball-milling processes. Morphology of as-received powders was investigated by means of scanning electron microscopy (SEM) on a Zeiss Evo LS 10 model (Fig. 1). Table 1 lists the type, particle size and purity of as-received powders used for ball-milling experiments. As described in Table 2, the raw powders with certain mass ratios (90 wt.% Cu and 10 wt.% SnO; 90 wt.% Cu and 10 wt.% SnO_2) were ball-milled for 15 hours in a two stationary planetary-type ball mill (Fritsch Pulverisette 7) with a milling speed of 300 rpm and a ball-to-powder weight ratio (BPR) of 10:1. Stearic acid was also added to powder mixtures as a process control agent (PCA). Ball-milling parameters were listed in Table 3. To inhibit excessive heating of the grinding medium, milling experiments were paused at specified milling cycles until the room temperature attained. Particle size distribution of the powders after milling process was analyzed using a laser diffractometer (Malvern Instruments Mastersizer 2000). Moreover, the interaction between average particle size (APS; d_{50}) and milling duration was investigated using SEM.

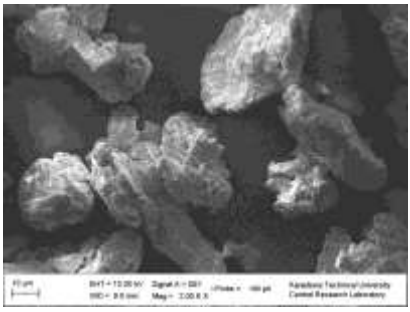

(a)

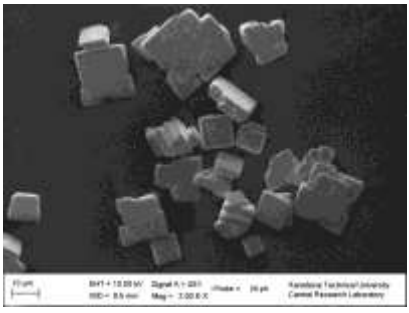

(b)

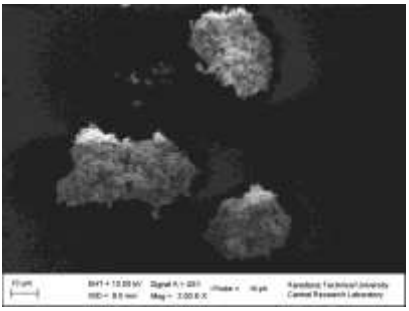

(c)

Figure 3. *Morphology of as-received a) Cu, b) SnO and c) SnO_2 powders.*

Table 1. *Type, particle size and purity of as-received powders used for ball-milling experiments.*

Type of powder	Particle size (microns)	Purity (%)
Cu	max. 44 μm	99%
SnO	10 μm	99%
SnO_2	<10 μm	99.9%

Table 2. *Chemical compositions of the prepared powder specimens.*

No	Matrix (wt.%)	Reinforcement (wt.%)	PCA (wt.%)
P1	Cu - 90%	SnO - 10%	5% stearic acid
P2	Cu - 90%	SnO_2 - 10%	5% stearic acid

Table 3. *Milling parameters used to synthesize Cu10SnO and Cu10SnO_2 composite powders.*

Chemical compositions	Cu10SnO - Cu10SnO_2
Type and amount of process control agent (PCA)	Stearic acid, 5 wt.%
Ball-to-powder weight ratio (BPR)	10:1
Milling speed	300 rpm
Grinding mode	2 min grinding, 1 min pause cycles / reverse mode active
Diameter and material of the grinding balls	10 mm, Tungsten carbide (WC)
Type of ball-mill	Fritsch Pulverisette 7 / 80 ml vials
Milling duration	3, 6, 9, 12 and 15 hours

3. RESULTS AND DISCUSSION

It can be seen from Fig. 1 that, both Cu (Fig. 1a) and SnO_2 (Fig. 1c) powder particles have an irregularly shaped whereas SnO (Fig. 1b) powder has an angular shape with having curved surfaces. Table 4 lists the APS results of powder samples obtained after milling runs. Fig. 2 shows the particle size variation of Cu10SnO and Cu10SnO_2 powder mixtures as a function of milling duration. From

Table 4 and Fig. 2, it can be inferred that for earlier periods of ball-milling, namely up to 3 hours, APS is increased as opposed to decreasing trend with further milling.

Table 4. *Average particle size values of Cu10SnO and Cu10SnO$_2$ powder mixtures as a function of milling duration.*

Chemical composition	Milling time (h) and average particle size (APS, µm)					
	0	3	6	9	12	15
Cu-10SnO 5% stearic acid	28.895	31.596	16.701	14.939	12.821	10.124
Cu-10SnO$_2$ 5% stearic acid	28.895	42.541	21.021	10.959	9.453	5.652

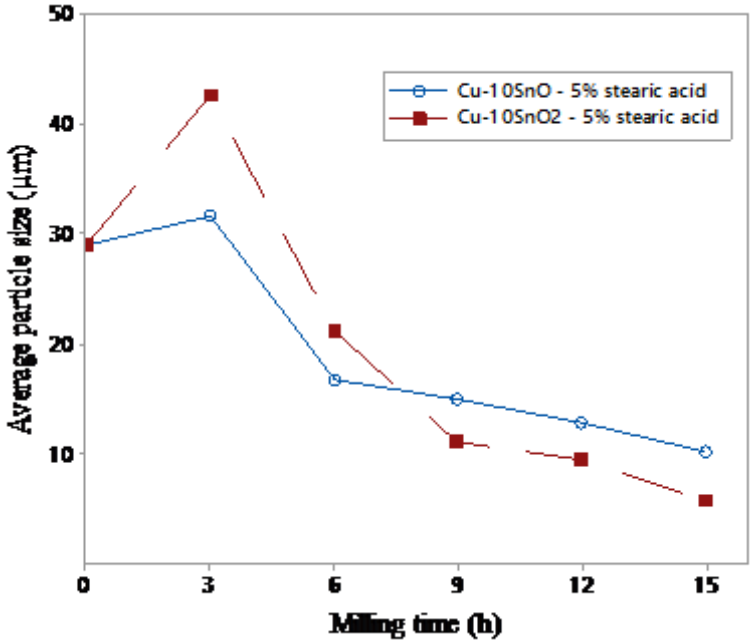

Figure 2. *Particle size variation of Cu10SnO and Cu10SnO$_2$ powder mixtures as a function of milling duration.*

Fig. 3 shows the morphological evolution of the Cu10SnO and Cu10SnO$_2$ both having 5% stearic acid obtained after milling for 3, 6 and 9 h. The first three hours of milling constitute a fluctuation in particle size for both compositions (Figs. 3a and d). With further milling, APS is dramatically reduced until 6 hours of milling, as can be seen from Figs. 3b and e. The fracturing of powders are dominant to cold welding, especially for the specimens having stannic oxide (Fig. 3f) rather than stannous oxide (Fig. 3c) after 9 hours of grinding. The morphological evolution of the Cu10SnO and Cu10SnO$_2$ powder specimens both having 5% stearic acid obtained after milling for 12 and 15 h, was shown in Fig. 4. It should be emphasized that, the decreasing trend of APS comprises for the milling durations corresponding 9 to 15 hours, and consequently APS reduces to 10.124 and 5.652 µm for specimens having stannous oxide (Fig. 4b) and stannic oxide (Fig. 4d), respectively.
As a consequence, considering SEM pictures and particle size values obtained after milling process, stannic oxide was exhibited better milling behavior as compared to stannous oxide addition.

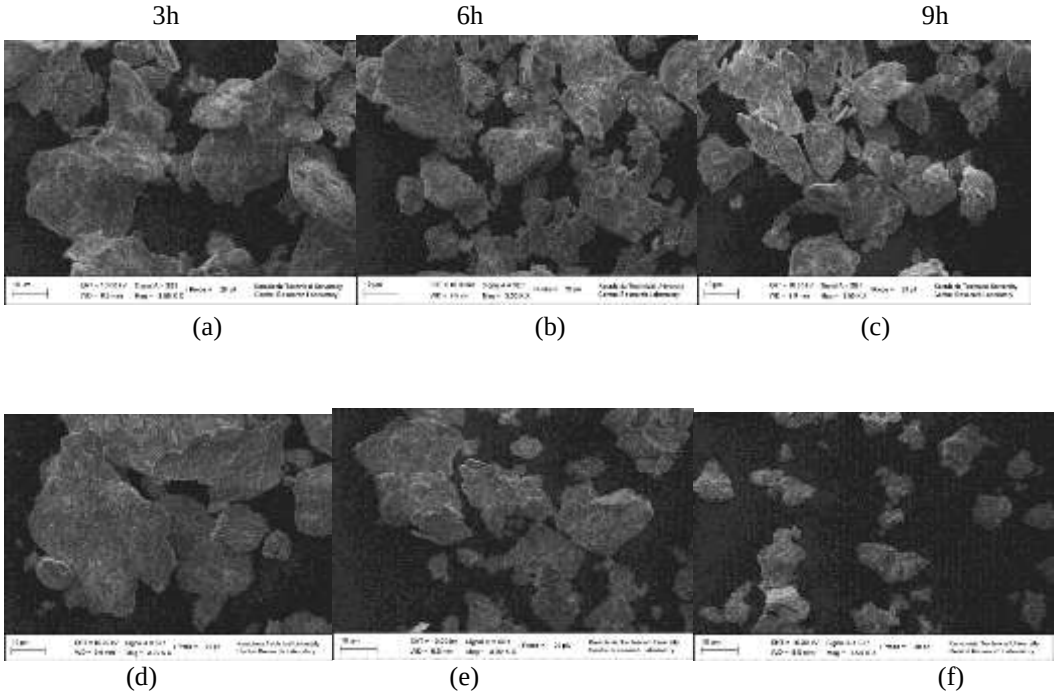

Figure 3. *Morphology of the Cu10SnO having 5% stearic acid after milled for a) 3 h, b) 6 h and c) 9 h; and Cu10SnO$_2$ having 5% stearic acid after milled for a) 3 h, b) 6 h and c) 9 h.*

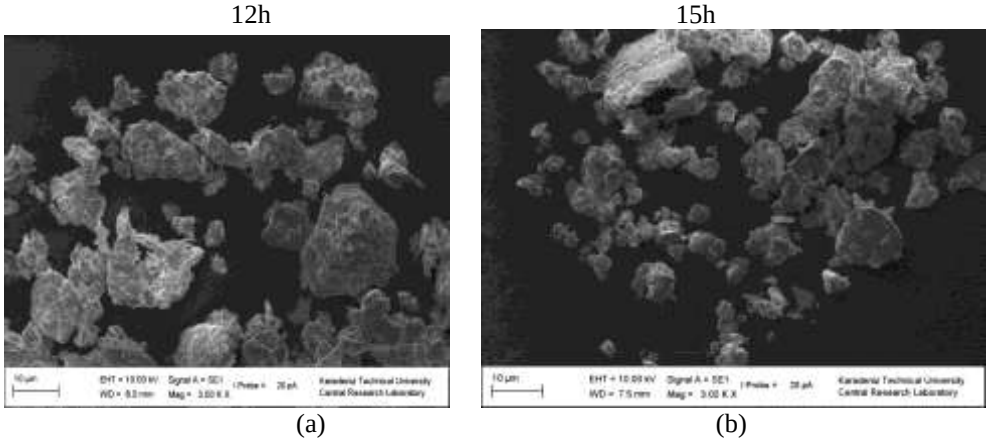

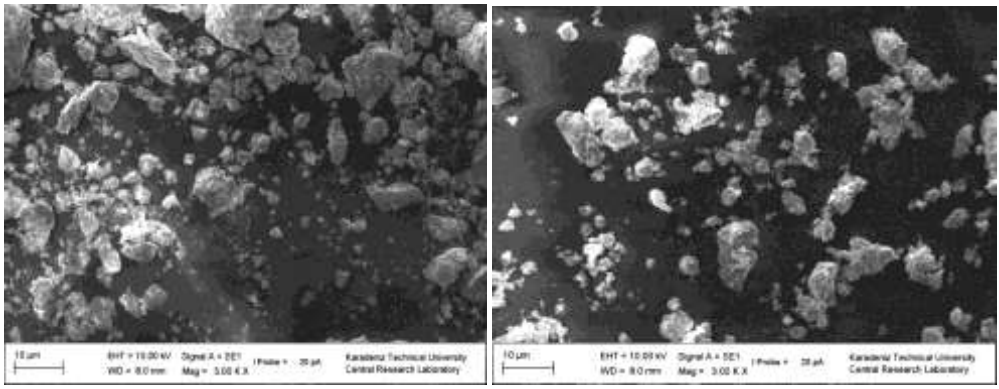

(c) (d)

Figure 4. *Morphology of the Cu10SnO having 5% stearic acid after milled for a) 12 h and b) 15 h; and Cu10SnO₂ having 5% stearic acid after milled for a) 12 h and b) 15 h.*

4. CONCLUSIONS

In this study, the effects of different types of reinforcements were comparatively studied to mill copper (Cu) powder. Particle size values were shown decreasing trends for both compositions, although some fluctuations were observed at first 3 hours of milling process for both specimens. Stearic acid was found effective to reduce average particle size (APS) values. APS values at the end of milling cycles were recorded to be 10.124 and 5.652 µm for stannous oxide and stannic oxide usages, respectively. Considering SEM pictures and particle size values obtained after milling, it was found that stannic oxide addition was exhibited better milling behavior as compared to stannous oxide for the whole milling process, namely up to 15 hours.

REFERENCES

[1] S. Biyik, F. Arslan, M. Aydin, Arc-erosion behavior of boric oxide-reinforced silver-based electrical contact materials produced by mechanical alloying, Journal of Electronic Materials 44 (2015) 457-466. *DOI:10.1007/s11664-014-3399-4*

[2] M. Pehlivan, S. Simsek, S. Ozbek, B. Ozbek, An extensive study on the synthesis of iron based magnetic aluminium oxide nanocomposites by solution combustion method, Journal of Materials Research and Technology, 8 (2019) 1746-1760. *DOI:10.1016/j.jmrt.2018.12.005*

[3] G. ALMisned, K. Günoğlu, H. V. Özkavak, D. Sen Baykal, H. Tekin, N. Karpuz, İ. Akkurt, An investigation on gamma-ray and neutron attenuation properties of multi-layered Al/B_4C composite, Mater. Today Commun. 36 (2023) 106813. *DOI:10.1016/j.mtcomm.2023.106813*

[4] O. Guler, M. Celebi, R. Dalmis, A. Canakci, H. Cuvalci, Novel ZA27/B_4C/Graphite hybrid nanocomposite-bearing materials with enhanced wear and corrosion resistance, Metall. Mater. Trans. A 51(2020) 4632-4646. *DOI:10.1007/s11661-020-05863-5*

[5] S. Biyik, Effect of reinforcement ratio on physical and mechanical properties of Cu-W composites synthesized by ball milling, Mater. Focus 7 (2018) 535-541. *DOI:10.1166/mat.2018.1513*

[6] A. Canakci, T. Varol, H. Cuvalci, F. Erdemir, S. Ozkaya, Development and characterization of bronze-Cr-Ni composites produced by powder metallurgy, Sci. Eng. Compos. Mater. 22 (2015) 425-432. *DOI:10.1515/secm-2013-0262*

[7] S. Biyik, Characterization of nanocrystalline Cu25Mo electrical contact material synthesized via ball milling, Acta Phys. Pol. A 132 (2017) 886-888. *DOI:10.12693/APhysPolA.132.886*

[8] S. X. Zhu, Y. Liu, B. H. Tian, Y. Zhang, K. X. Song, Arc erosion behavior and mechanism of Cu/Cr20 electrical contact material, Vacuum. 143 (2017) 129-137. *DOI:10.1016/j.vacuum.2017.06.002*

[9] C. Suryanarayana, A. A. Al-Joubori, Z. Wang, Nanostructured materials and nanocomposites by mechanical alloying: an overview, Met. Mater. Int. 28 (2022) 41-53. *DOI:10.1007/s12540-021-00998-5*

[10] S. Biyik, M. Aydin, Optimization of mechanical alloying parameters of Cu25W electrical contact material, Acta Phys. Pol. A 132 (2017) 909-912. *DOI:10.12693/APhysPolA.132.909*

[11] S. Biyik, Effect of polyethylene glycol on the mechanical alloying behavior of Cu-W electrical contact material, Acta Phys. Pol. A 134 (2018) 208-212. *DOI:10.12693/APhysPolA.134.208*

[12] S. A. Tunc, A. Canakci, A. H. Karabacak, M. Celebi, M. Turkmen, Effect of different PCA types on morphology, physical, thermal and mechanical properties of AA2024-B_4C composites, Powder Technology 434 (2024) 119373. *DOI:10.1016/j.powtec.2024.119373*

[13] S. Mimouche, M. Azzaz, Study of nanostructured Cu Al Ni alloy produced by high energy mechanical milling, J. Nano Res. 56 (2019) 109-118. *DOI:10.4028/www.scientific.net/JNanoR.56.109*

Investigation of Stopping Power and Dose Distribution in Proton Therapy Using FLUKA Simulation

Rukiye DEMİR[1]✉, Berin Belma ŞİRVANLI[2]

[1] *Gazi University, Institute of Science, Department of Physics, ANKARA - TURKEY*
[2]*Gazi University, Department of Physics, Ankara- TURKEY*
✉ *Corresponding author: rukiye.demir@gazi.edu.tr*

ABSTRACT

This study investigates the stopping power and dose-depth profiles of protons in lung and water environments during proton therapy. Proton therapy is widely used in cancer treatment, particularly due to its advantages in preserving healthy tissues. Using FLUKA Monte Carlo (MC) simulations, stopping power calculations were performed for protons in the energy range of 70–200 MeV in water and lung tissue. These results were compared with reference values from the International Commission on Radiation Units and Measurements (ICRU) and other scientific studies in the literature. The findings revealed that the stopping power of protons varies between water and lung tissues depending on their energy levels. FLUKA simulations produced results consistent with ICRU values in both water and lung environments. Specifically, the results for water showed substantial agreement with ICRU reports, while the results for lung tissue aligned well with other scientific studies in the literature.

Dose-depth profiles were also examined, demonstrating that protons penetrate deeper as their energy increases. The Bragg peak effect of protons emerged as a crucial factor in delivering targeted doses to tumor cells while preserving healthy tissues. This study provides significant findings aimed at improving the accuracy of computational methods used in proton therapy and offers reference data for dosimetry challenges.

KEYWORDS: *proton therapy, radiation dose, FLUKA*

1. INTRODUCTION

Cancer is a disease characterized by uncontrolled and rapid cell growth, leading to tumor formation that damages tissues and blood vessels in the body. As one of the most prevalent diseases globally, cancer remains a significant health issue in Turkey as well. Laryngeal and tracheal, bronchial, and lung cancers rank second among the leading causes of death[1].

Current cancer treatments include surgical interventions, radiotherapy, and chemotherapy, the latter of which can cause toxicity and damage to healthy cells(Baykara, 2016). Radiotherapy employs various modalities using X-rays, gamma rays, and photon particles, but it is known that such interactions can harm normal tissues while controlling malignant cells[2].

In 1946, physicist Robert R. Wilson proposed the use of high-energy protons for cancer treatment. He published a seminal paper explaining that the interactions of protons within the body exhibit a more effective depth-dose distribution compared to X-rays and photons. Wilson also described a method for delivering a uniform dose to an extended target volume by combining several Bragg peaks with varying energy and weight [3,4,5].

Proton therapy is a widely used technique for tumor treatment. The Bragg peak effect and the ability of protons to stop at specific depths enhance the precision of dose delivery to tumors while protecting healthy tissues[6]. Analytical, semi-empirical dose calculation methods, and pencil beam algorithms are commonly employed for treatment planning. However, while these algorithms offer faster

calculations, their accuracy is often uncertain as they do not account for factors like multiple Coulomb scattering and nuclear interactions of charged particles. These limitations can be addressed using Monte Carlo (MC) algorithms and analytical formulas. These methods consider fundamental physical principles, electromagnetic and nuclear interactions, and theoretical models to more accurately predict the dose distributions of charged particles[7,8,9].
In this study, the behavior of protons with energies of 70 MeV, 100 MeV, 120 MeV, 150 MeV, and 200 MeV was examined using FLUKA Monte Carlo simulations in lung and water phantoms. The stopping power and radiation dose analyses were conducted in these phantoms.

2. MATERIALS AND METHODS

In this study, FLUKA version 4-3.0 and its interface FLAIR version 3-1.15 were used to create water and lung phantoms. Calculations for stopping power and dose-depth were performed, and comparisons were made between water and lung-equivalent tissue. Table 1 shows the elemental composition and density data for water and lung tissue, obtained from ICRU 44 and ICRP 66[10,11,12].

***Table 1**. Elemental Composition and Density of Water and Lung Tissue*

Material	**Elements and Composition (%)**	**ρ (g/cm³)**
Lung	H: 10.30, C: 10.50, O: 74.90, N: 3.10, K: 0.20, Na: 0.20, Cl: 0.30, S: 0.30, P: 0.20	1.05
Water	H: 11.2, O: 88.8	1.0

For proton therapy, FLUKA simulations utilized the HADROTHE setting in the DEFAULTS card via the FLAIR interface. This configuration is optimized for hadron therapy applications. The phantom was modeled as a rectangular parallelepiped (20 cm × 20 cm × 40 cm) with a proton source positioned 5 cm from the phantom along the -z axis, delivering 10610^6106 protons. Stopping power was calculated using the USRBIN and DELTARAY cards, while dose-depth calculations were conducted using the DOSE feature of the USRBIN card[13,14,15].

3. RESULTS AND DISCUSSIONS

3.1.Stopping Power Results

Stopping power calculations for protons in water and lung environments were conducted using the FLUKA method and compared with ICRU data. Figure 1 illustrates the stopping power of protons in water and lung environments. The stopping power values in these two media are observed to be closely aligned. Table 2 presents the stopping power values for different proton energy levels in lung and water, along with comparisons to ICRU data[16,17,18].

***Table 2.** Stopping Power of Protons at Different Energies in Lung and Water Environments*

Energy (MeV)	**ICRU (Lung)**	**FLUKA (Lung)**	**MATLAB (Lung)**	**ICRU (Water)**	**FLUKA (Water)**
70	9.47	9.51 ± 0.04	8.43 ± 1.04	9.55	9.61 ± 0.06
100	7.22	7.12 ± 0.07	6.13 ± 1.09	7.28	7.22 ± 0.06

Energy (MeV)	ICRU (Lung)	FLUKA (Lung)	MATLAB (Lung)	ICRU (Water)	FLUKA (Water)
120	6.13	6.63 ± 0.18	5.20 ± 0.93	6.37	6.20 ± 0.17
150	5.44	5.44 ± 0.00	4.25 ± 1.19	5.44	5.44 ± 0.00
200	4.45	4.83 ± 0.38	3.26 ± 1.19	4.49	4.42 ± 0.07

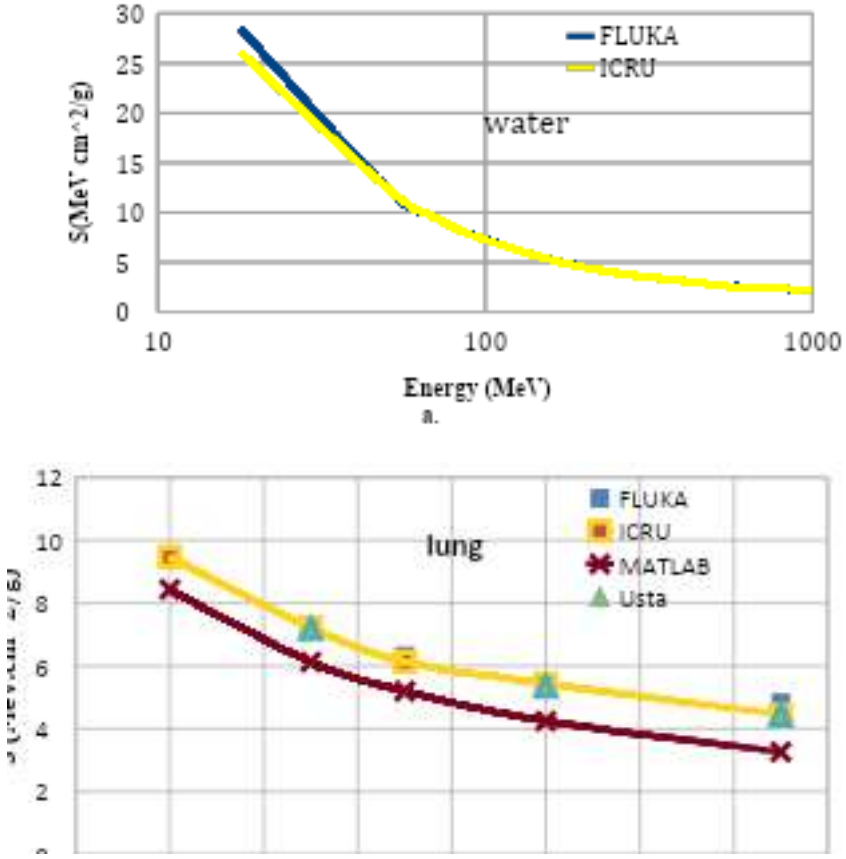

Figure 1. *(a) Comparison of stopping power values of protons in water using FLUKA and ICRU reference data. (b) Comparison of stopping power values of protons in lung tissue using FLUKA, ICRU, and scientific literature data.*

3.2.Dose-Depth Curves

Dose-depth profiles for proton beams in the energy range of 70–200 MeV were simulated in water and lung environments using FLUKA. Figure 2 shows the dose-depth distributions in water and lung environments, revealing minor differences in proton penetration depths between the two media. Table 3 shows the relationship between the dose depth of protons in water and lungs.

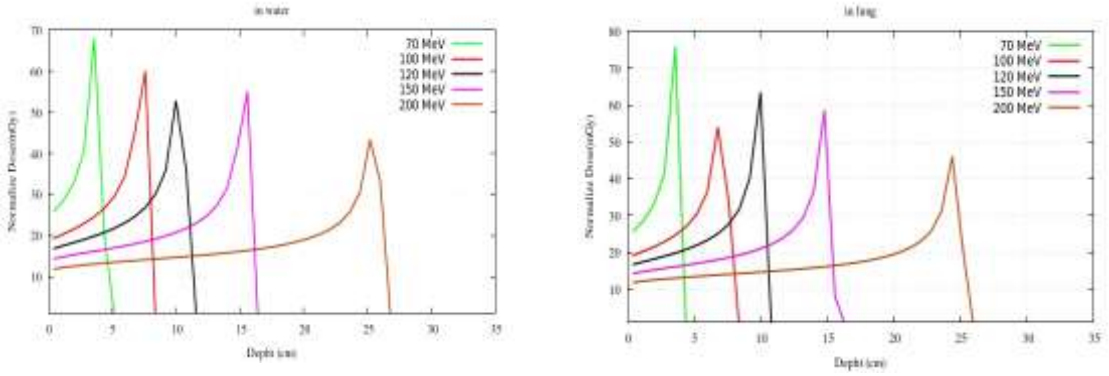

a) b)

Figure 2. *Dose-depth distributions in water(a) and in lung(b).*

Table 3*. Dose-Depth Relationships for Protons in Water and Lung Environments*

Energy (MeV)	ICRU (Lung)	Lung	Difference	ICRU (Water)	Water	Difference
70	3.9	3.5	0.4	4.08	3.6	0.32
100	7.1	6.7	0.4	7.71	7.5	0.21
120	10.5	10.0	0.5	—	10.0	—
150	15.4	14.8	0.6	15.7	15.6	0.1
200	26.0	24.4	1.6	25.99	25.2	0.79

4. CONCLUSION

This study compared theoretical and experimental data. The stopping power and dose-depth relationships of protons with low, medium, and high energy values in water and lung environments were examined using FLUKA. The results are consistent with scientific studies on stopping power and dose-depth relationships.

In radiation therapy, water and water-equivalent materials are used for treatment planning. Analytical dose calculation methods (e.g., pencil beam algorithms) rely on the relative stopping power of water for dose calculations. Monte Carlo (MC) algorithms, however, use material properties such as mass density and mean excitation energy, converted from CT numbers, for tissue-equivalent dose calculations. To accurately compare MC and pencil beam methods and reduce uncertainties in clinical proton beams, energy-dependent relative stopping power calculations should be employed. This study aims to enhance the accuracy of dose calculation algorithms and provide reference data for dosimetry challenges.

REFERENCES

[1] Yılmaz Seçil, Sarıkaya Medine Doğan , Atar Esra , Bağcı Burcu Şen , Kenanoğlu Sercan , Mutlu Nilhan , Yaşar Elif , Önal Ömer , Canöz Özlem, Ö. Y. (2023). Primary Culture of Cancer Cells Derived from Human Lung Tumors.

https://dergipark.org.tr/tr/pub/erciyesfen/issue/77161/1269249
[2] Baykara, O. (2016). Current Modalities in Treatment of Cancer. 154–165. https://doi.org/10.5505/bsbd.2016.93823
[3] Maranci, & Tugrul, A. B. (2017). The chronic dose assessment of three critical organs for liver scintigraphy with using Cr-51. Acta Physica Polonica A, 132(3), 476–478. https://doi.org/10.12693/APhysPolA.132.476
[4] Breuer Hans, S. B. (2000). Proton Therapy and Radiosurgery http://dx.doi.org/10.1007/978-3-662-04301-1
[5] Smith, A. R. (2009). Vision 2020: Proton therapy. Medical Physics, 36(2), 556–568. https://doi.org/10.1118/1.3058485
[6] Epik, H. (2022). Effects of Longitudinal Magnetic Field on Dose Disribution of Proton Beam . 24(71), 351–355. https://doi.org/10.21205/deufmd.2022247101
[7] B, P., E, T., & A, Y. (2011). Klinik proton terapi uygulamaları. Ege Tıp Dergisi, 50(1), 1–6. http://egetipdergisi.com.tr/tr/download/article-file/350460 ER -
[8] Paganetti, Harald. (2017). Proton Beam Therapy (Harald Paganetti (ed.)). 2017. DOI 10.1088/978-0-7503-1370-4
[9] Newhauser, W. D., & Zhang, R. (2015). The physics of proton therapy. Physics in Medicine and Biology, 60(8), R155–R209. https://doi.org/10.1088/0031-9155/60/8/R155
[10] Armutlu B.-Hoş İ. (2019). Proton Therapy Simulations by GATE in the Treatment of Non-Small Cell Lung Cancer (NSCLC) Burcu. 40, 909–916. https://doi.org/10.17776/csj.640079
[11] Mairani, A., Böhlen, T. T., Schiavi, A., Tessonnier, T., Molinelli, S., Brons, S., Battistoni, G., Parodi, K., & Patera, V. (2013). A Monte Carlo-based treatment planning tool for proton therapy. Physics in Medicine and Biology, 58(8), 2471–2490. https://doi.org/10.1088/0031-9155/58/8/2471
[12] Rørvik, E. (2015). A Comparison of Biological Dose Estimates in Proton and Carbon Ion Therapy Based on Averaged and Full Linear Energy Transfer Spectra. July. DOI: 10.1002/mp.12216
[13] ICRP66. (1981). Annals of the ICRP. In ICRP 66,Sowby, F. D. (Vol. 6, Issue 1).https://doi.org/10.1016/0146-6453(81)90127-5
[14] ICRU 44. (1989). Selection Requirements for Tissue Substitutes. https://doi.org/10.1016/j.nimb.2011.04.028
[15] Embriaco, A., Attili, A., Bellinzona, E. V., Dong, Y., Grzanka, L., Mattei, I., Muraro, S., Scifoni, E., Tommasino, F., Valle, S. M., & Battistoni, G. (2020). FLUKA simulation of target fragmentation in proton therapy. Physica Medica, 80(September), 342–346. https://doi.org/10.1016/j.ejmp.2020.09.018
[16] ICRU, 78. (2007). PRESCRIBING, RECORDING, AND REPORTING PROTON-BEAM THERAPY. In ICRU (Vol. 78, Issue 78). https://doi.org/10.1093/jicru/ndm041
[17] Usta, M., Tufan, M. Ç., Aydın, G., & Bozkurt, A. (2018). Stopping power and dose calculations with analytical and Monte Carlo methods for protons and prompt gamma range verification. Nuclear Instruments and Methods in Physics Research, Section A: https://doi.org/10.1016/j.nima.2018.04.045
[18] Almutairi, A. S., & Osman, K. T. (2022). Mass Stopping Power and Range of Protons in Biological Human Body Tissues (Ovary, Lung and Breast). International Journal of Medical Physics, Clinical Engineering and Radiation Oncology, 11(01), 48–59. https://doi.org/10.4236/ijmpcero.2022.111005

Experimental Study on Sand Production Mechanism under Cyclic Loading in Underground Gas Storage

Wenhong Zhang[1], Shouceng Tian[1]✉,Tianyu Wang[1] and Panpan Zhang[2]

[1] *State Key Laboratory of Petroleum Resources and Prospecting, China University of Petroleum (Beijing), Beijing, China*

[2] *College of Petroleum, China University of Petroleum (Beijing) Karamay Campus, Karamay, China*
✉ *Corresponding author: 2021310153@student.cup.edu.cn*

ABSTRACT

Depleted reservoir underground gas storages experience multiple high-flow injection-production cycles annually, leading to cyclic fluctuations in formation pressure that progressively degrade the mechanical properties of the reservoir rock. This degradation has been associated with varying degrees of sand production in numerous reservoirs, which poses significant challenges to the safe operation of gas storage facilities. In this study, we investigate the impact of cyclic stress on sand production in gas storage, using the GCTS triaxial mechanical testing apparatus in conjunction with a sand production simulation device designed for gas storage applications. Based on operational data from China's largest gas storage facility (H storage), the study analyses the sand production in injection-production wells and examines the effects of cyclic loading on sandstone. The findings reveal that cyclic loading significantly weakens the reservoir rock, leading to increased particle cementation disruption, reduced sand clump formation, and a decrease in the grain size of the produced sand. Notably, the results indicate that even gas storage facilities that initially do not produce sand are at risk of encountering sand-related safety issues over extended operational periods. Unlike conventional reservoirs, where stress states tend to stabilize, gas storage rocks are subject to continuous shear damage due to the absence of a stable stress condition. Moreover, high-velocity fluids play a crucial role as sand-carrying agents, further promoting sustained sand production. This study provides essential technical insights and a theoretical framework for the reconstruction and maintenance of gas storage facilities.

KEYWORDS: *Depleted reservoir underground gas storage, sand production, sanding characteristic, cyclic loading.*

1. INTRODUCTION

Underground gas storage (UGS) plays a crucial role in ensuring energy security, especially with the increasing global demand for natural gas[1]. Depleted oil and gas reservoirs are often converted into gas storage facilities due to their existing infrastructure and favourable geological conditions. These gas storages are subjected to multiple high-flow injection-production cycles annually, resulting in fluctuations in formation pressure. This cyclic loading can lead to significant mechanical degradation of the reservoir rock, which, in turn, may induce sand production[2,3]. Sand production in gas storage reservoirs presents a serious operational challenge, potentially affecting the safety and stability of the entire gas storage system.

Over the past few decades, various studies have been conducted to investigate the behaviour of sand production in conventional oil and gas reservoirs. However, the unique conditions in underground gas storage, such as the alternating injection and production cycles and the high fluid velocities, create a different set of challenges. Existing research indicates that cyclic loading exacerbates the mechanical weakening of reservoir rocks, leading to an increased risk of sand production. However,

there is still limited understanding of the specific mechanisms behind this phenomenon in gas storage reservoirs, particularly those undergoing high-frequency cyclic loading.

This study aims to address these gaps by analysing the sand production characteristics in depleted gas reservoirs under cyclic loading conditions. Using a GCTS triaxial mechanical testing device combined with a sand production simulation apparatus, this research simulates the cyclic loading behavior of gas storage rocks and examines the resulting effects on sand production. Through these experiments, we identify the patterns and characteristics of sand production in sandstone subjected to cyclic loading and provide valuable insights into the underlying mechanisms.

The significance of this work lies in its potential to enhance the safety and operational efficiency of underground gas storages. By understanding the sand production mechanisms in these unique environments, this study provides important technical guidance for the design, operation, and maintenance of gas storage facilities. Furthermore, the findings could inform the development of strategies to mitigate sand production, thereby extending the operational lifespan of gas storage sites and reducing the associated risks.

2. MATERIALS AND METHODS

The rock samples used in the experiment were red sandstone outcrops from the Hutubi gas storage site in Xinjiang. The sand production simulation experiment employed thick-walled core samples to simulate downhole perforation holes, as shown in Figure 1. The core had an outer diameter of 50 mm and a length of 100 mm. According to the standard ratio of the outer diameter of the thick-walled core to the perforation hole diameter of 3:1, the simulated perforation hole had a diameter of 16 mm and a depth of 60 mm, with the bottom 40 mm left undrilled [4,5].

Figure 1. *Core samples used in the experiment.*

To investigate the differences in sand production characteristics between the cyclic stress conditions of gas storage reservoirs and conventional single-phase gas reservoir production conditions, this study designed a thick-walled cylinder sand production experiment using the GCTS RTR-1000 rock mechanics testing system. During the experiments, this system provided confining pressure (0–100 MPa) and axial pressure (0–1000 kN) to the thick-walled cylinder sand production units[6], ensuring the stress conditions required for rock failure. The experimental setup is illustrated in Figure 2. The experimental fluid flow rates were determined based on actual data from the Hutubi Gas Storage Reservoir block calculated by Liao Wei, ranging from 1.8 L/min to 13.8 L/min [3]. A flow rate of 2 L/min was selected as the experimental gas injection rate. During the experiment, discrete sand particles at the outlet were collected and weighed using an electronic balance to record the stage sand production and cumulative sand production. Upon completion of the experiment, a Malvern laser particle size analyser was used to perform granulometric analysis of the produced sand, with a measurement accuracy range of 0.02~2000 μm. Additionally, an optical microscope was employed

to observe the microstructural characteristics of the produced sand. To assess damage and failure characteristics of the borehole walls, CT scanning was conducted to recreate the borehole inner surface and visualize the damage features [7].

To study the impact of conventional gas reservoir production conditions and cyclic alternating loading conditions in gas storage reservoirs on sand production, four comparative experiments were conducted, as shown in Table 1.

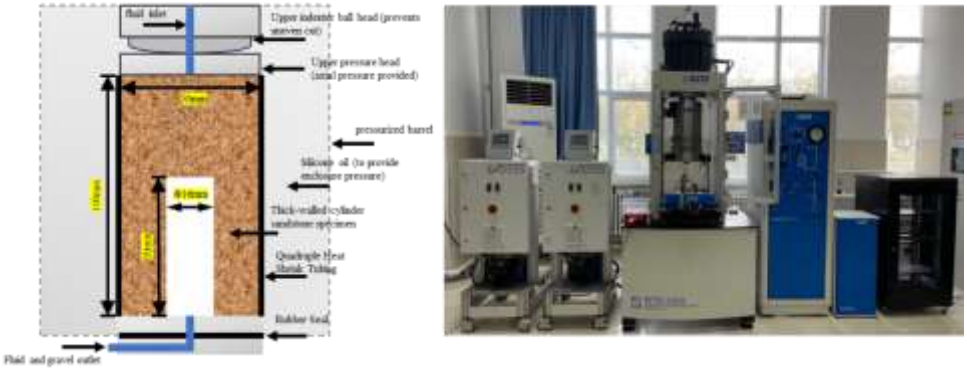

Figure 2. *Experimental equipment and schematic diagram.*

Table 1. *Experimental design program*

id	Simulated working conditions	Critical Sand Cell Pressure	Loading method
Conventional 1	Conventional reservoir production	77MPa	Monotonic loading
Conventional 2		72MPa	
Cycle 1	Cyclic gas storage and injection	60MPa	Triangular wave cyclic loading
Cycle 2			

3. RESULTS AND DISCUSSIONS

From the experimental results, the two repeated experiments under conventional conditions showed nearly identical trends, with the sand production rate following a process of increase, stabilization, and gradual decline to zero. In contrast to conventional production conditions, the cumulative sand production under gas storage conditions increased significantly, exhibiting a sustained sand production phenomenon. After the onset of sand production, the sand production rate remained stable during the early stages of the cyclic loading. Taking Cycle 2 as an example, the sand production rate remained stable within the first 0–35 minutes of the cycle but increased significantly after 35 minutes as the cyclic loading progressed. The particle size distribution curves of sand produced under different operating conditions are shown in Figure 4. The median particle size (D_{50}) of the original formation sand was approximately 72 μm. Under cyclic loading conditions, the median particle size of the produced sand ranged between 120~125 μm, while under conventional conditions, it ranged between 162~193 μm. The median particle size of the sand produced under conventional conditions was 1.35–1.60 times larger than that under cyclic loading conditions and 2.25~2.68 times larger than the original formation sand. The particle size distribution curve for sand produced under cyclic loading conditions was generally lower than that for sand produced under conventional conditions.

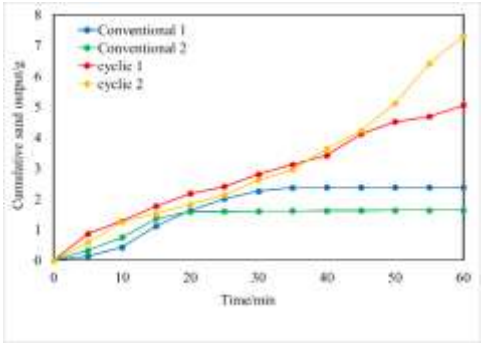

Figure 3. *The cumulative sand production-time relationship diagram under different production conditions.*

As shown in Figure 4, observations under an optical microscope revealed that the sand produced during the experiments existed in an agglomerated particle state. Under conventional conditions, the produced sand exhibited more numerous and larger agglomerates with well-preserved cementing material at the same magnification. In contrast, under cyclic loading conditions, the produced sand displayed fewer agglomerated particles and more thorough fragmentation. Consequently, the sand produced under cyclic loading conditions had a smaller median particle size and overall particle size distribution values compared to the sand produced under conventional production conditions.

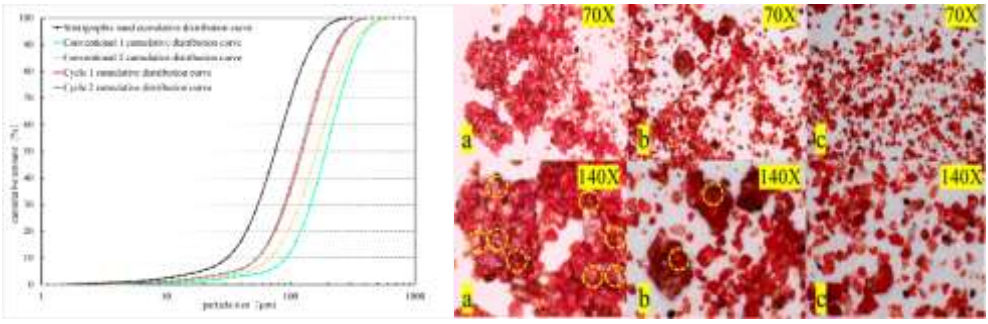

Figure 4. *Magnification of particle size accumulation curve and particle cementation.*

Direct observation and CT scanning methods were used to analyze the damage to the interior and exterior surfaces of the borehole, as shown in Figure 5. The four experimental groups exhibited borehole damage at different scales, with the most severe cross-sections presenting a V-shaped "dog-ear" pattern of failure. Using ImageJ software, the additional fractured area under cyclic loading conditions was analyzed. The fractured areas were measured as 431.17 mm² and 496.59 mm², indicating a significant expansion of the internal control volume. Under conventional conditions, the additional fractured areas were 162.39 mm² and 194.58 mm². The fractured areas under cyclic loading conditions were 2.2~3 times larger than those under conventional conditions. Moreover, the borehole cavity volume, diameter, and extension height increased significantly under cyclic loading conditions, confirming that the presence of cyclic loading exacerbates the sand production phenomenon.

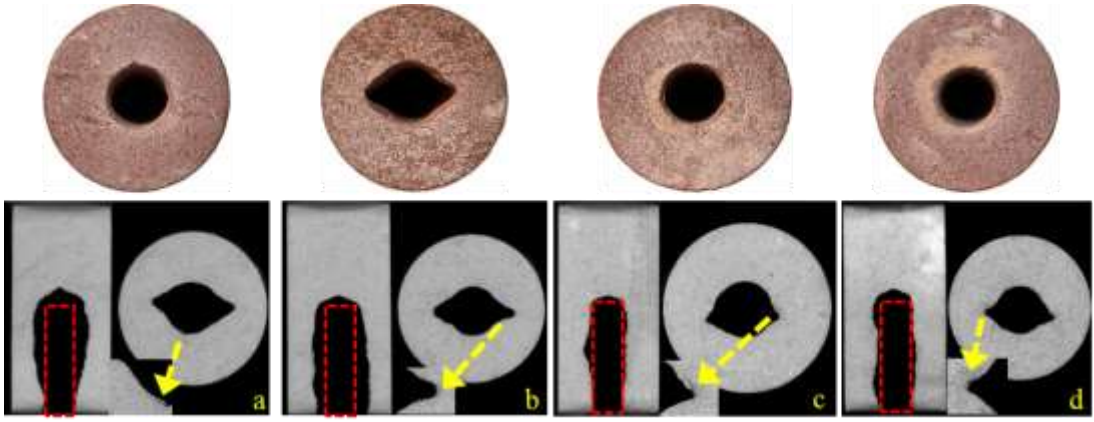

Figure 5. *Hole damage under different working conditions*
(a:cycle 1 b:cycle 2 c:conventional 1 d:conventional 2)

4. CONCLUSION

The sand production mechanism under cyclic injection and production conditions in gas storage reservoirs differs significantly from that under conventional gas reservoir production conditions. Under cyclic conditions, the cumulative sand production from the core increases significantly. Stress fluctuations induced by cyclic injection and production make it difficult for the reservoir to maintain a stable stress state after sand production, leading to sustained sand production. The presence of cyclic loading promotes interparticle dislocation, accelerates particle detachment, and facilitates the separation of cementing materials, resulting in more fragmented sand particles. The borehole is notably affected by changes in operating conditions, with the cavity volume, diameter, and extension height increasing significantly under cyclic loading conditions. This confirms that cyclic loading exacerbates sand production. In gas storage, the unique characteristics of gas storage reservoirs must be considered, particularly when designing injection and production strategies and optimizing sand control parameters.

REFERENCES

[1] DING Guosheng, WANG Jieming. Key points in the reconstruction of an underground gas storage based on a depleted gas reservoir, Natural Gas Industry, 2011, 31(5):87-89.DOI:10.1007/s12182-011-0123-3.

[2] ZHANG Yuda, YUAN Guangjie, DONG Jingnan, et al. Experimental study on sand production of depleted oil and gas reservoirs, FRONTIERS IN EARTH SCIENCE, 2023, 11: 1136695. doi: 10.3389/feart.2023.1136695

[3] LIAO W. Experimental Simulation on the Influencing Factors of Sand Production in H Gas Storage, Xinjiang, China, ACS Omega, 2021, 6(47): 31727-31737. doi: 10.1021/acsomega.1c04419.

[4] Liu Wei. Experimental investigation of sand production in moderately consolidated sandstones, *Petroleum Sci. Bull.* 6 (01), 67–78. doi:10.1021/acsomega.1c04419

[5] Jiangshuai Wang, Gonghui Liu, et al., Study on Temperature Distribution in Wellbore during Drilling, International Conference on Computational and Experimental Science and Engineering (ICCESEN 2018), 12-16 October, 2018 Antalya-Turkey

[6] Zhang, L., et al. Research on sensitivity damage of naturally fractured carbonate reservoirs in Ordos Basin. International Conference on Computational and Experimental Science and

Engineering (ICCESEN 2017), 4-8 October, 2017 Antalya-Turkey. DOI: https://doi.org/10.1007/s12517-019-4805-2

[7] Song, L., et al. Research on reservoir characteristics of Chang7 tight oil based on nano-CT. International Conference on Computational and Experimental Science and Engineering (ICCESEN 2017), 4-8 October, 2017 Antalya-Turkey. DOI: https://doi.org/10.1007/s12517-018-3842-6

Handling Missing Circular EMG Data: Modifying Data Structures for Effective K-NN and EM Imputation

Fatemeh Sarasir[1], Vilda Purutçuoğlu [1,2]✉

[1] *Middle East Technical University/Biomedical Engineering Department, Ankara, Turkey*
[2] *Middle East Technical University/Statistics Department, Ankara,Turkey*
✉ *Corresponding author: vpurutcu@metu.edu.tr*

ABSTRACT

Addressing missing data and imputing the associated values are crucial tasks during the pre-processing phase of data analysis. Electromyography (EMG) data, a fundamental category of biomedical instrumentation data, captures the electrical activity of muscles. This study focuses on imputing missing values in EMG data, which characteristically exhibit periodic patterns. Based on prior analysis, missing observations in these signals are addressed using methods such as Mean and Median imputation, Spline, and Linear interpolation, as well as the EM and K-NN approaches. In the imputation using the aforementioned approaches, the periodic nature of the data is not considered, despite accounting for nonlinearity and high correlation factors in the calculations. However, the periodicity, which can be effectively modelled using circular methods, represents a critical pattern in the data that has the potential to significantly enhance the accuracy of findings.

Hence, this study initially introduces three methods for detecting periodicity in the dataset, namely, Fourier transformation, the Spline model, and the Autoregressive model up to order 10. If the data conforms to any of these models, we will then find the dominant frequency of those datasets which is crucial for employing our new approaches of transforming the time-series data into the circular data.

Finally, we apply the innovative approaches, named Circular-shape and the Circular-time, based on the modification of the data structure applied to time-series EMG datasets. Hereby, we transform the original EMG data into circular EMG form in order to perform effective KNN and EM imputation for missing signals. Subsequently, the performance of the proposed approaches is assessed against non-periodic outcomes, measured in terms of Root Mean Square Error values, CPU-time, and Real-time. The results indicate a significant enhancement in accuracy with the Circular-shape approach with both EM and K-NN imputation. On the other hand, regarding the computational efficiency, the Circular-time method is found to be the best method among the stated proposals in the K-NN based missing imputation.

KEYWORDS: *Missing Imputation, Periodic Patterns, Circular EMG Data*

1. INTRODUCTION

Missingness, the absence of certain data points, is a prevalent issue in statistics and data science, affecting disciplines ranging from surveys to biomedical research. It can lead to bias, reduced statistical power, and decreased generalizability. The appropriate statistical handling of missing data depends on its nature and is essential for drawing valid inferences. Missing data arises primarily due to data collection errors—such as machine malfunctions or calibration issues—and participant dropout, common in longitudinal studies like clinical trials and social research. These factors contribute to gaps in datasets. This study focuses on Electromyography (EMG) data, which measures muscle electrical activity and, in certain cases, is represented as circular data. Circular EMG data exhibits periodic properties, cycling within a defined range (e.g., 0–360°). Proper representation of

this data requires circular statistical methods that account for its cyclical nature. Unaddressed missing values in circular datasets can distort cyclic trends and relationships. For example, missing values in EMG data can obscure peak activity phases, leading to misinterpretations in critical areas like diagnosis and treatment planning. So, addressing missingness is vital for maintaining data integrity. However, common imputation methods such as mean or median substitution, spline, and linear interpolation often fail to account for periodicity. Whereas, circular methods, which model data's cyclic properties, can significantly improve imputation accuracy and preserve cyclic trends. But handling missingness in circular data presents unique challenges due to its wrapped structure (e.g., 0–360° or 0–2π). Thereby, effective techniques must respect this continuity, especially, for variables like wind direction or time of day. Circular-specific approaches offer solutions to these complexities.

The von Mises distribution, a circular analog of the normal distribution, is particularly effective for modeling and imputing circular data. It preserves circular continuity while enabling parameter estimation and missing value prediction. Researchers have advanced these methods by using Bayesian approaches with von Mises or wrapped normal distributions in order to better account for circular data properties [1–6]. Machine learning techniques, such as K-nearest neighbors (K-NN) and neural networks, have also been adapted to handle circular features by encoding angular information in inputs or outputs [7,8]. Machine learning has become an indispensable tool in addressing a wide range of challenges across disciplines, including healthcare, finance, environmental science, and engineering. Its ability to model complex relationships, process large datasets, and adapt to diverse scenarios makes it particularly effective for tasks such as classification, regression, clustering, and predictive modelling [9-13]

This study aims to detect periodicity in time-series EMG datasets, a critical step in identifying data with circular or periodic characteristics. Periodicity detection is a fundamental task across various domains. The Fourier Transform, particularly the Fast Fourier Transform (FFT), decomposes time series into frequency components, revealing dominant periodic patterns [14,15]. Wavelet Transforms, including Continuous (CWT) and Discrete (DWT) variants, analyze periodicities at different scales, making them suitable for non-stationary signals [16]. Autoregressive models (AR, ARIMA) fit time series as combinations of past values and noise [17]. Additionally, autocorrelation and partial autocorrelation methods identify periodicity by measuring time series similarity, with peaks indicating specific intervals [18,19].

We analyze periodicity in time-series EMG datasets using three methods: Fourier transformation, the Spline model, and the Autoregressive model. For datasets conforming to any of these models, we apply the Fast Fourier Transform (FFT) to identify the dominant frequency, which is critical for transforming the data into circular form. We propose two innovative methods—Circular-time and Circular-shape—to restructure time-series EMG data into circular EMG data, enabling more accurate handling of missingness. These methods are applied in conjunction with K-NN and Expectation-Maximization (EM) imputation techniques, which rely on correlations among data samples (columns) to fill missing values. The efficacy of these approaches is evaluated under two missingness patterns: scattered and intermittent.

The paper is organized as follows: Section 2 discusses the significance of Electromyograms and EMG data. Sections 3 and 4 detail the missing data imputation methods. Section 5 presents the results, focusing on imputation accuracy and computational time, and Section 6 provides the conclusion.

DATA

Characteristics of the EMG data

Electromyography (EMG) data records muscle electrical activity during contraction, typically ranging from 0 to 500 Hz, with most power in the 20–150 Hz range. It is essential in diagnosing neuromuscular disorders, guiding rehabilitation, and analyzing movement in biomechanics and

sports science. EMG data also supports myoelectric prosthetics, gesture interfaces, and monitors muscle fatigue for ergonomics and injury prevention. Circular EMG data, used for cyclic or repetitive tasks like walking or cycling, captures rhythmic muscle engagement patterns. It provides insights into the timing, intensity, and duration of muscle contractions, making it valuable for biomechanical analysis, rehabilitation, and optimizing athletic performance.

EMG data description

This study evaluates imputation approaches using two datasets with modified data structures. The first dataset, titled "Surface Electromyographic (sEMG) Signals Collected During Ground Walking," referred to as the "Walking" data, was recorded in 2022 from a 30-year-old able-bodied subject. The data, collected over 5 minutes, consists of sEMG signals from ten leg muscles (five per leg) across 3 channels with a sampling frequency of 2 kHz [20]. The second dataset, named the "Hand Movement" dataset, is from the "Database for Myoelectric Movement," recorded in 2014. It includes surface electromyography signals from the forearm and kinematic data of the hand and wrist during predefined actions and postures. This dataset has 4 channels with a 2 kHz sampling frequency [21]. Figure 1 illustrates the data acquisition procedure.

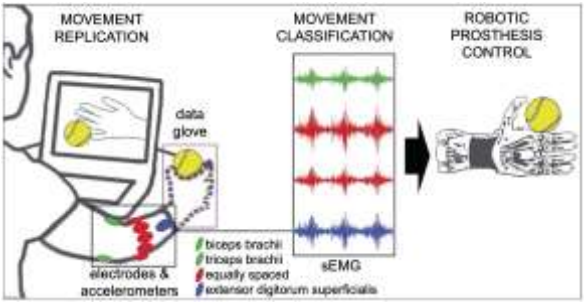

Figure 1. *Database for Myoelectric Movement [16].*

2. MATERIALS AND METHODS

Methods of detecting the periodicity

The purpose of detecting periodicity is to identify EMG datasets with cyclic or harmonic characteristics. In this study, periodicity is detected in time-series EMG data using three methods: Fourier transformation, the Spline model, and the Autoregressive model. These methods are implemented in MATLAB using built-in functions, with detailed theoretical explanations provided in the following subsections. Both the "Walking" and "Hand Movement" EMG datasets conform to all three models, confirming the presence of periodicity in the data.

Fourier transformation

This method detects the periodicity in a signal by transforming it from the time domain into the frequency domain, where periodic components become easier to identify.

Mathematically, for a continuous-time function $\boldsymbol{f(t)}$, the Fourier transform $\boldsymbol{F(\omega)}$ is given by:

$$(\omega) = \int_{-\infty}^{\infty} f(t) e^{-i\omega t}\, dt, \qquad (1)$$

where ω represents the angular frequency and $F(\omega)$ gives the amplitude of the frequency ω present in the signal [22].

Spline model

Detecting periodicity using spline models involves fitting a smooth curve to a set of data points and then, analyzing the behavior of the fitted curve to identify repeating patterns. Unlike Fourier transforms, which analyze periodicity in the frequency domain, spline models work in the time (or spatial) domain by constructing smooth curves that approximate the data. The first derivative of the

spline curve can be used to find local maxima and minima, which correspond to the peaks and troughs of the data and the consistent intervals between these points indicate periodicity. If the intervals between peaks are consistent, it is an indicator of a periodic trend in the data. [23].

Autoregressive model

The Autoregressive (AR) model involves modeling a time series where the current value depends linearly on its previous values. This method can capture periodic patterns in data. Hereby, an AR model of order p uses the last p observations to predict the current observation and, in our study, we consider the order up to 10 (p=10). [24]

Mathematically, an AR model (p=10) can be expressed as;

$$X_t = \emptyset_1 X_{t-1} + \emptyset_2 X_{t-2} + \cdots + \emptyset_{10} X_{t-10} + \epsilon_t. \quad (2)$$

where X_t is the current value of the time series, $\emptyset_1$, $\emptyset_2$, …, $\emptyset_{10}$ are the autoregressive coefficients, and the ϵ_t is white noise (i.e., a random error term).

Methods of handling the missing data

This study focuses on the K-NN and EM methods as imputation techniques. These methods use correlations between data samples (columns) to fill in missing values, which is essential for assessing the accuracy of the Circular-time and Circular-shape approaches.

K-Nearest Neighbor algorithm

The K-Nearest Neighbors (K-NN) algorithm is a non-parametric, instance-based learning method often used for classification, regression, and missing data imputation. For missing data imputation, K-NN operates on the assumption that similar instances (neighbors) will have similar values, allowing it to impute missing values based on the values of its nearest neighbors. Given a dataset with missing values, the K-NN algorithm identifies the k-nearest samples (neighbors) that have values for the missing feature and then impute the missing value based on these neighbors. The key steps in K-NN imputation are as follows:

For each sample with a missing value in feature j, we calculate the distance between this sample and all other samples that do not have a missing value in feature j. The most commonly used distance metric for numerical features is the Euclidean distance:

$$d(x_i , x_p) = \sqrt{\sum_{q=1}^{m} (x_{iq} - x_{pq})^2}\,, \quad (3)$$

where x_i and x_p are the two samples, and $d(x_i , x_p)$ is the distance between them. The k-nearest samples with the smallest distances are identified for the sample with the missing value. Lastly, the missing value x_{ij} can be imputed using the mean or median of the values of the j-th feature for the k-nearest neighbors. [25,26]

Expectation-maximization algorithm

The Expectation-Maximization (EM) algorithm is a parametric imputation technique widely used to estimate parameters in statistical models when data is incomplete or missing values. In the context of imputation, the EM algorithm helps infer likely values for missing data by iteratively estimating missing values and refining model parameters based on observed and estimated data. In our calculation, we assume a multivariate normal distribution when considering the actual magnitude of the EMG data whose program codes were originally developed in MATLAB programming language. The EM algorithm consists of two main steps, the Expectation (E) step and the

Maximization (M) step, which iteratively improves the parameter estimates until convergence [27, 28].

E-Step (Expectation Step): Compute the expected value of the log-likelihood function, concerning the conditional distribution of the latent variables given the observed data and the current parameter estimates:

$$Q\left(\theta\middle|\theta^{(t)}\right) = E_{Z|X,\theta^{(t)}}[\log\ p(X,Z\,|\theta)]. \tag{4}$$

where X is the observed data, Z is the latent variable, θ represents the parameters of the model, $\theta^{(t)}$ is the current estimate of the parameters, and $p(X,Z|\ \theta)$ is the joint probability of the observed and latent variables.

M-Step (Maximization Step): Update the parameters by maximizing the expected log-likelihood obtained in the E-step:

$$\theta^{(t+1)} = \arg\max Q(\theta|\theta^{(t)}). \tag{5}$$

Lastly, we check for convergence by assessing whether the change in the log-likelihood or parameters is below a certain threshold. If not converged, return to the E-step.

3. RESULTS AND DISCUSSIONS

The objective of this study is to evaluate the effectiveness of imputation in addressing missing patterned EMG data by novel transforming methods of time series into circular EMG data. A masking algorithm is employed to produce simulated both randomly missing values amounting to 15%, and partly missing in the whole data segment within the pre-processed dataset comprising complete recordings utilizing the algorithm that is executed in MATLAB. In order to test imputation methods, only one subject is chosen per data type, with each dataset containing varying numbers of rows and columns subsequent to matrix reorganization.

For accuracy measures, the three criteria are used to assess the performance of each imputation method by Circular-time and the Circular-shape transforming approaches. The two of them are the control of visual similarity that is based on graphical representation, and the root mean square error simply RMSE is applied to quantify the numerical value of the error between the actual and imputed values. Finally, the last criterion is the runtime comparison that is computed for both the central processing unit and real-time.

Imputation plots

The visual comparisons between the imputation outcomes and the actual data depicted in plotting figures offer valuable insights. Figures 2, 3, 4, and 5 are selected sample figures that exhibit the process of filling in the absent values in the EMG data using the EM and the K-NN imputation techniques, applied to Circular-Shape and Circular-Time transforming approaches which were missed within two scenarios of Randomly (15%) and the Partly missing patterns. These imputation methods whose mathematical details can be found in the study of Sarasir (2024) [29], are applied to two distinct sets of electromyography (EMG) data utilized in our investigation: "Walking", and "Hand-Movement" signals. The horizontal axis represents the time vector, while the vertical axis, corresponds to the amplitude of the signal in all the figures. When comparing the imputed data to the original data, as shown in the figures, the circular-shape transformation approach performs best with both the EM and K-NN imputation techniques for datasets with a randomly missing 15% pattern and a partially missing pattern. The circular-time approach also closely resembles the original data imputed using the EM and K-NN methods without any data transformation. However, when the EM imputation method is applied to the circular transformation approach for partially

missing time-series (Walking) data, both transformation approaches show similar performance, but, fail to effectively impute the missing segments.

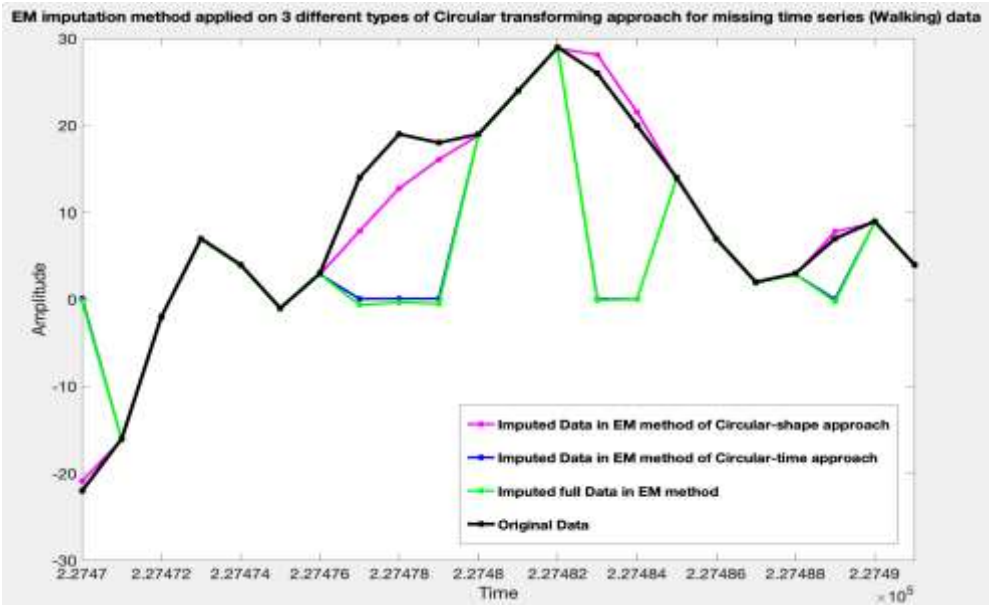

Figure 2. *The EM imputation method applied to Circular transforming approaches for missing time series (Walking) data: Randomly (15%) missing.*

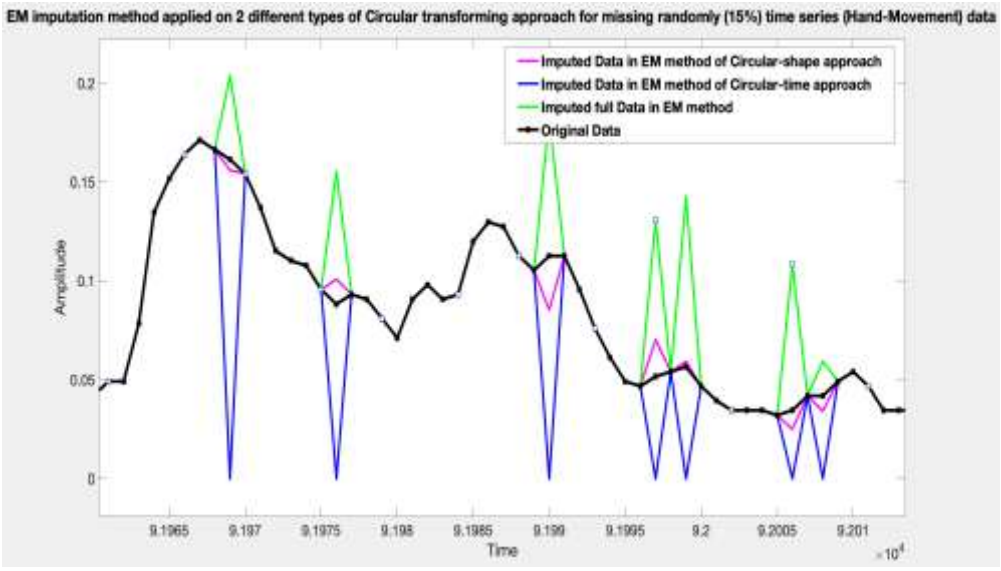

Figure 3. *The EM imputation method applied to Circular transforming approaches for missing time series (Hand-Movement) data: Randomly (15%) missing.*

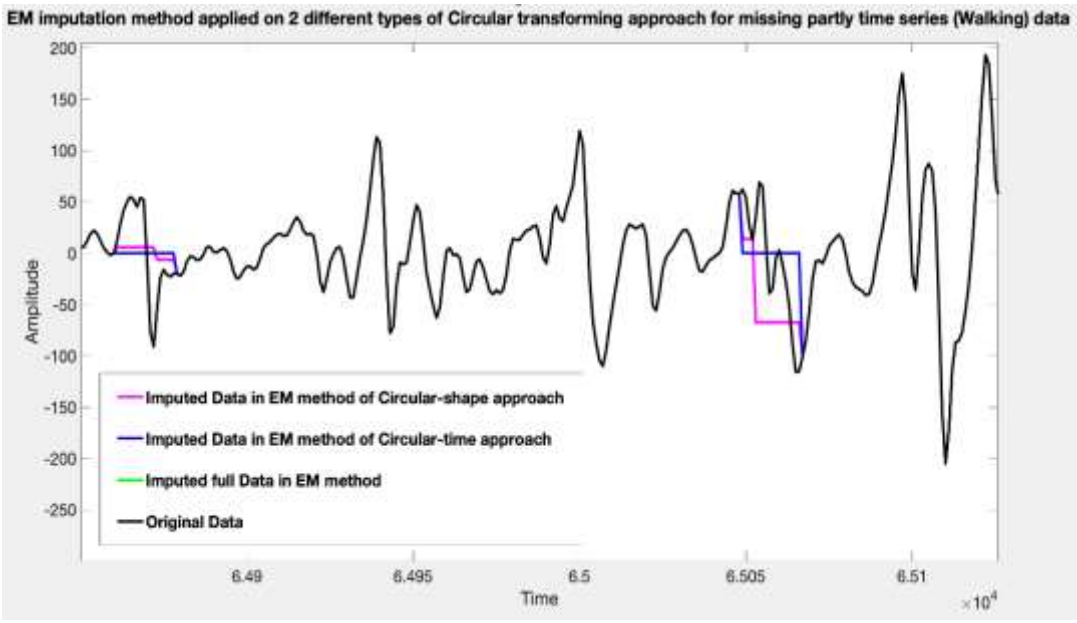

Figure 4. *The EM imputation method applied to Circular transforming approaches for missing time series (Walking) data: Partly missing.*

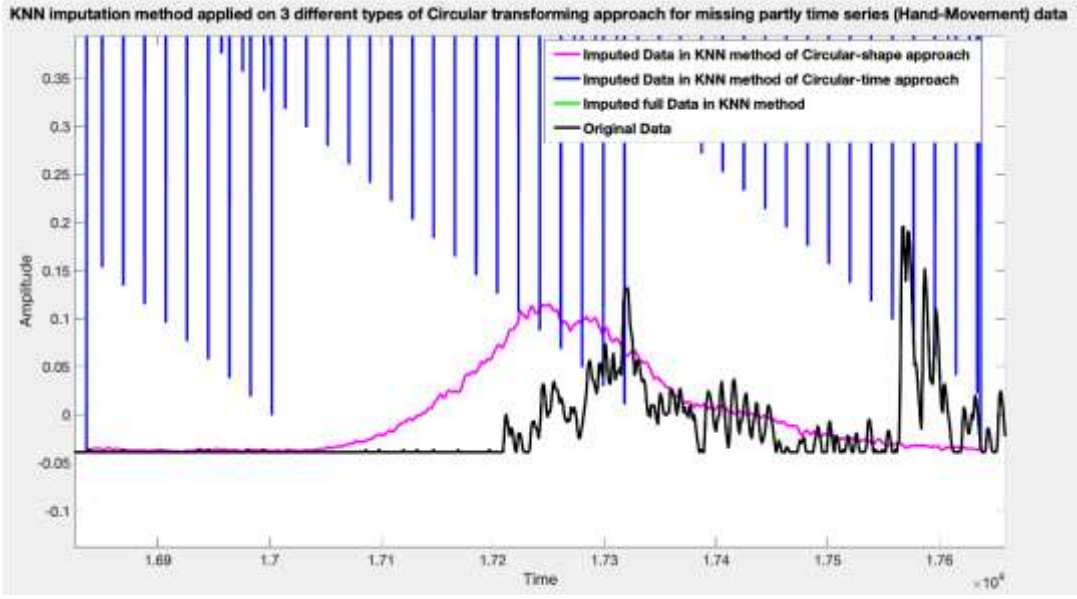

Figure 5. *The KNN imputation method applied to Circular transforming approaches for missing time series (Hand-Movement) data: Partly missing.*

RMSE, CPU-time, and Real-time tables

The tables below display the evaluation results for RMSE, CPU time, and real-time processing in imputing missing values in two circular EMG datasets: "Walking" and "Hand-Movement" signals.

Furthermore, the assessment focuses on the performance of the EM and K-NN imputation techniques, applied to the Circular-Shape and Circular-Time transformation methods. The evaluations were performed under two conditions: Randomly missing with 15% of the data and partially missing patterns.

Table 1. *RMSE, CPU time, and Real-time values of the "Walking" dataset with random missingness.*

Methods / Criteria	K-Nearest-Neighbor (K-NN)			Expectation Maximization (EM)		
	Circular-Time	**Circular-Shape**	**Original Data**	**Circular-Time**	**Circular-Shape**	**Original Data**
RMSE	8.4732	**7.3175**	8.7843	8.5387	**6.2924**	8.5393
CPU time	**0.4200**	9.7400	0.8400	65.3700	674.8800	**25.7800**
Real time	**0.2303**	2.1884	0.3829	60.3039	112.2243	**22.6589**

Table 2. *RMSE, CPU time, and Real-time values for the "Walking" dataset with partly missingness.*

Methods / Criteria	K-Nearest-Neighbor (K-NN)			Expectation Maximization (EM)		
	Circular-Time	**Circular - Shape**	**Original Data**	**Circular-Time**	**Circular-Shape**	**Original Data**
RMSE	6.8402	**5.9479**	Not computable	6.7116	**6.1460**	6.7116
CPU time	**0.4400**	7.3700	Not computable	54.7300	563.9000	**21.9000**
Real time	**0.1777**	2.1089	Not computable	50.0609	91.3863	**19.1875**

Table 3. *RMSE, CPU time, and Real-time values for the "Hand-Movement" dataset with random missingness.*

Methods / Criteria	K-Nearest-Neighbor (K-NN)			Expectation Maximization (EM)		
	Circular -Time	**Circular - Shape**	**Original Data**	**Circular -Time**	**Circular-Shape**	**Original Data**
RMSE	1.4076	**0.0518**	0.0976	0.0580	**0.0108**	0.0377
CPU time	**0.5900**	1.1800	0.8900	44.7100	309.2900	**15.4200**
Real time	**0.3411**	0.8691	0.3728	438.6718	46.9035	**13.3956**

Table 4. *RMSE, CPU time, and Real-time values of the "Hand-Movement" dataset with partly missingness.*

Methods / Criteria	K-Nearest-Neighbor (K-NN)			Expectation Maximization (EM)		
	Circular -Time	**Circular - Shape**	**Original Data**	**Circular -Time**	**Circular-Shape**	**Original Data**
RMSE	0.7901	**0.0248**	Not computable	0.0340	**0.0314**	0.0340
CPU time	**0.5700**	0.9100	Not computable	36.5000	60.2500	**11.2600**
Real time	**0.2213**	0.4834	Not computable	29.3401	9.7858	**9.5804**

The RMSE values indicate that both the EM and K-NN methods exhibit superior performance with the Circular-Shape approach, as they produce lower errors for both the "Walking" and "Hand-Movement" datasets under both random and partial missing patterns. In contrast, the Circular-Time approach and the original data, which imputes missing values without modifying the structure, result in similar, albeit slightly higher, error values. In the case of the K-NN imputation method, the original data fails to meet the evaluation criteria under the partially missing pattern, primarily because K-NN relies on neighboring values. When substantial sections of data are missing (e.g., due

to sensor disconnection), K-NN faces difficulty in imputing values. However, the Circular-Shape and Circular-Time approaches, which modify the data structure, facilitate K-NN in identifying relevant neighbors and accurately filling the gaps. Regarding CPU usage and real-time performance, the Circular-Time approach proves to be the most efficient for K-NN imputation, as it demands less processing time and memory for imputing the two columns (i.e., data and angle) due to the structural changes. In contrast, the EM method demonstrates faster performance with the original data, likely because it does not involve modifications to the data structure.

4. CONCLUSION

The objective of this study is to integrate considerations of the circular patterns observed in certain EMG datasets into our imputation methodologies, with the goal of determining whether accounting for the recurring and oscillatory nature of the data can enhance imputation accuracy. By utilizing Fourier transformation, Spline, and Autoregressive models, we identify the dominant frequencies in periodic data and propose two circular approaches—Circular-shape and Circular-time—that alter or reshape EMG datasets with inherent periodic patterns in order to improve imputation performance. Modifying the data structure refers to reorganization or adjustment of the data to better align with specific processing techniques or enhance algorithmic performance. In the context of imputation, this modification may involve transforming the data into a different format or reshaping it, which can help methods like KNN to more effectively identify relevant neighboring data points. Additionally, it allows imputation techniques like EM to operate more efficiently, as these methods depend on the correlation between signals within the dataset, a requirement for applying Circular-shape and Circular-time approaches. By altering the data structure, imputation methods may overcome challenges posed by missing data, particularly, in scenarios where traditional techniques face difficulties. As a result, our analyses of two circular EMG datasets demonstrate that the Circular-shape approach enhances accuracy for both EM and K-NN imputations, while the Circular-time approach offers greater computational efficiency, especially for K-NN, across both random and partial missing patterns.

REFERENCES

[1] Fisher, N. I. (1995). Statistical Analysis of Circular Data. Cambridge University Press. Doi: 10.1017/CBO9780511564345.

[2] Jammalamadaka, S. R., & SenGupta, A. (2001). Topics in Circular Statistics. World Scientific.doi:10.1142/4031.

[3] Pewsey, A., Neuhäuser, M., & Ruxton, G. D. (2013). Circular Statistics in R. Oxford University Press.ISBN: 978-0-19-165077-2.

[4] Batschelet, E. (1981). Circular Statistics in Biology. Academic Press.ISBN:9780120810505.

[5] Abe, T., & Pewsey, A. (2011). Sine-skewed circular distributions. Statistical Papers, 52(3), 683-707.doi:10.1007/s00362-009-0277-x.

[6] Downes, M. J., & Mengersen, K. L. (2010). Bayesian estimation of the concentration parameter of the von Mises distribution. Statistics and Computing, 20(4), 433-444. doi:10.1007/s11222-009-9114-0.

[7] Azimi, S., & Tamazian, G. (2021). Missing value imputation of circular data using neural networks. Journal of Applied Statistics, 48(6), 1086-1104.doi:10.1080/02664763.2020.1844249.

[8] Chierici, M., et al. (2020). Deep learning for circular data. International Journal of Computational Intelligence Systems, 13(1), 723-739.

[9] Akkurt, I. Special issue of the "International Conference on Computational and Experimental Science and Engineering (ICCESEN)". Int. J. Environ. Sci. Technol. 16, 4997 (2019). https://doi.org/10.1007/s13762-019-02463-8

[10] Dekhandji, F. (2017). Signal processing deployment in power quality disturbance detection and classification. *Acta Physica Polonica A*, *132*(3), 415-419.doi:10.12693/APhysPolA.132.415

[11] Cömert, Z., & Kocamaz, A. D. N. A. N. (2017). Comparison of machine learning techniques for fetal heart rate classification. *Acta Physica Polonica A*, *132*(3), 451-454.doi:10.12693/APhysPolA.132.451

[12] Tekın, H., Altunsoy, E., Manici, T., & Yilmaz, B. (2017). Quantitative characteristic X-ray analysis for different compound samples by using Monte Carlo method. *Acta Physica Polonica A*, *132*(3), 439-441. doi: 10.12693/APhysPolA.132.439

[12] Yüksel, A., Çankaya, Ş., & Üncü, I. (2017). Design of a machine learning based predictive analytics system for spam problem. *Acta Physica Polonica A*, *132*(3), 500-504.doi: 10.12693/APhysPolA.132.500

[13] Oppenheim, A. V., & Schafer, R. W. (2009). Discrete-Time Signal Processing. Pearson.

[14] Bloomfield, P. (2000). Fourier Analysis of Time Series: An Introduction. Wiley.ISBN:978-0-471-88948-9.

[15] Addison, P. S. (2017). The Illustrated Wavelet Transform Handbook. CRC Press. ISBN:9780750306928.

[16] Hyndman, R. J., & Athanasopoulos, G. (2018). Forecasting: Principles and Practice (2nd ed.). OTexts.

[17] Box, G. E., Jenkins, G. M., Reinsel, G. C., & Ljung, G. M. (2015). Time Series Analysis: Forecasting and Control. Wiley.doi: 10.1002/9781118674918.

[18] Brockwell, P. J., & Davis, R. A. (2016). Introduction to Time Series and Forecasting. Springer. ISBN : 978-3-319-29852-8.

[19] Di Nardo, F., Morbidoni, C., & Fioretti, S. (2022). Surface electromyographic signals collected during long-lasting ground walking of young able-bodied subjects. (version 1.0. 0). PhysioNet.doi:10.13026/9q7v-6016.

[20] Atzori, M., Gijsberts, A., Kuzborskij, I., Elsig, S., Hager, A. G. M., Deriaz, O. & Caputo, B. (2014). Characterization of a benchmark database for myoelectric movement classification. IEEE Transactions on Neural Systems and Rehabilitation Engineering, 23(1), 73-83.doi:10.1109/TNSRE.2014.2328495.

[21] Cooley, J. W., Lewis, P. A., & Welch, P. D. (1969). The fast Fourier transform and its applications. IEEE Transactions on Education, 12(1), 27-34.doi:10.1109/TED.1969.300275.

[22] Ligun, A. A. (1980). Approximation of periodic functions by splines of minimal defect. Ukrainian Mathematical Journal, 32(3), 259-261.

[23] DRoy, A., & Karmakar, S. (2021). Time-varying auto-regressive models for count time series. Electronic Journal of Statistics, 15(1), 2905-2938.doi: 10.1214/21-EJS1851.

[24] Troyanskaya, O., Cantor, M., Sherlock, G., Brown, P., Hastie, T., Tibshirani, R., ... & Altman, R. B. (2001). Missing value estimation methods for DNA microarrays. Bioinformatics, 17(6), 520-525.

[25] Batista, G. E. A. P. A., & Monard, M. C. (2003). An analysis of four missing data treatment methods for supervised learning. Applied Artificial Intelligence, 17(5–6), 519–533. doi:10.1080/713827181.

[26] Johnson, R.A., Wichern, D.W. 2007. Applied Multivariate Statistical Analysis, Pearson Press, 6th edition.

[27] McLachlan, G. J., & Krishnan, T. (2007). The EM Algorithm and Extensions (2nd ed.). Hoboken, NJ: Wiley. [ISBN: 978-047120170 0]

[28] Sarasir, F. (2024). The imputation of missingness in circular and non-circular electromyography signaling data (Master's thesis). Middle East Technical University, Ankara, Turkey.

Influence of Stearic Acid and Milling Speed on the Synthesis of Cu-B_4C Composite Powder

Serkan BIYIK✉

Karadeniz Technical University, Abdullah Kanca Vocational School, Department of Machinery and Metal Technologies, Trabzon, Turkey
✉ *Corresponding author: serkanbiyik@ktu.edu.tr*

ABSTRACT

In this study, the effect of milling speed on the synthesis of boron carbide (B_4C) doped copper (Cu) based composite powders, was investigated. For this aim, elemental Cu and B_4C powders were used as matrix and reinforcement phases, respectively. Before milling runs, stearic acid was also added to prepared powder mixtures at specified mass ratios. Mechanical alloying process was carried out using a two-stationary planetary type ball mill. Two different milling speeds, namely 100 and 200 rpm were chosen to explore the effect of milling speed on characterization of milled powders, including particle size and shape. Characterization of both starting and milled powders was carried out using scanning electron microscopy (SEM) and laser diffraction analyses (Mastersizer). Accordingly, milling speed was significantly affected grinding efficiency. The milling speed value of 200 rpm was found much more effective in terms of achieving particle size reduction, as compared to that of 100 rpm. Besides, at lower milling speeds, inhomogeneous distribution of particles was occurred due to the inadequate kinetic energy input.

KEYWORDS: *Boron carbide, copper-based composites, mechanical alloying, particle size, powder technology, stearic acid.*

1. INTRODUCTION

Powder metallurgy (PM) method is used to produce composite materials having compositional flexibility for wide range of industrial applications [1-4]. The manufacturing route of PM includes powder preparation techniques such as V-Turbula mixing, mechanical alloying (MA) or ball-milling, followed by compacting by a hydraulic press, sintering and applying some optional secondary treatments such as surface polishing and repressing. Powder preparation techniques are important to achieve a desired microstructure having uniform particle size distribution and enhanced homogeneity [5]. MA or ball-milling technique is successfully used in the development of dispersion-strengthened materials, composite powders and nanomaterials [5, 6]. However, there are many operational parameters that could be varied during MA. The synthesis of aforementioned materials can be realized by careful selection of these process parameters. Otherwise, it will take much longer processing times that inherently cause increasing product costs. Hence, optimization of the process parameters is mandatory to shorten milling durations in an economical and cost-effective manner [7]. Some of these processing parameters include milling speed, type and amount of process control agent (PCA), ball-to-powder weight ratio (BPR), milling duration and materials of both milling vial and grinding balls [8-11]. Milling speed is one of the most important parameters affecting the size and shape of powder particles during MA. To shorten milling durations for achieving a desired composite powder, the effects of milling speed must be studied for a given chemical composition. Therefore, the aim of the study is to determine optimal milling speed value via observing morphological changes and particle size values for Cu-B_4C composite powder.

2. MATERIALS AND METHODS

Elemental Cu (max. 144 μm) and B_4C (less than 10 μm) powders were used to prepare powder mixtures. Cu powder was used as the matrix material whereas B_4C as the reinforcement. Fig. 1 shows the scanning electron microscopy (SEM) images reflecting the morphology of starting powders. The characteristics of as-received powders were given in Table 1. Morphology of as-received powders was investigated by means of SEM on a Zeiss Evo LS 10 model. Before ball-milling processes, 5 wt.% of stearic acid was also added to each powder specimen as a PCA. Table 2 lists the chemical composition of the prepared powder specimens. These prepared powder mixtures were then milled using a two stationary planetary-type ball-mill (Fritsch Pulverisette 7). Powder mixtures were ball-milled for 15 hours with various milling speeds, namely 100 and 200 rpm; and ball-to-powder weight ratio (BPR) was 5:1 for both specimens. Table 3 lists the parameters used to synthesize Cu-B_4C composite powders. A laser diffractometer (Malvern Instruments Mastersizer 2000) was used to detect average particle size (APS, d_{50}) values throughout the milling tests.

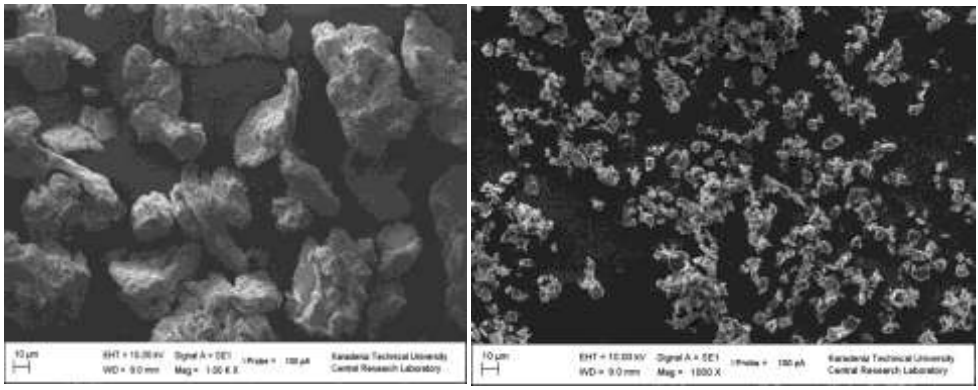

(a) (b)

Figure 1. *Morphology of as-received a) Cu and b) B_4C powders.*

3. RESULTS AND DISCUSSIONS

Considering SEM pictures shown in Fig. 1, Cu (Fig. 1a) powder particles have an irregular shape whereas B_4C (Fig. 1b) powder particles have a polygonal shape. Table 4 lists the APS vales with varying milling speeds and duration. Particle size variation of Cu-B_4C powder mixtures as functions of milling speed and duration is shown in Fig. 2.

Table 1. *Type, particle size and purity of as-received powders used for ball-milling experiments.*

Type of powder	Particle size (microns)	Purity (%)
Cu	max. 44 μm	99%
B_4C	<10 μm	99.7%

Table 2. *Chemical composition of the prepared powder specimens.*

Cu (wt.%)	B_4C (wt.%)	PCA

		(stearic acid, wt.%)
96 %	4 %	5 %

Table 3. *Milling parameters used to synthesize Cu-B_4C composite powders.*

Chemical composition	Cu-B_4C
Type and amount of process control agent (PCA)	Stearic acid, 5 wt.%
Ball-to-powder weight ratio (BPR)	5:1
Milling speed	100 rpm and 200 rpm
Grinding mode	2 min grinding, 1 min pause cycles / reverse mode active
Diameter and material of the grinding balls	10 mm, Tungsten carbide (WC)
Type of ball-mill	Fritsch Pulverisette 7 / 80 ml vials
Milling duration	3, 6, 9, 12 and 15 hours

Table 4. *Average particle size values of Cu4B_4C powder mixtures as a function of milling duration.*

Chemical composition / Milling speed	**Milling time (h) and average particle size (APS, µm)**					
	0	3	6	9	12	15
Cu-4B_4C 5% stearic acid / 100 rpm	28.895	22.232	23.730	23.490	22.314	20.592
Cu-4B_4C 5% stearic acid / 200 rpm	28.895	23.113	24.275	20.258	18.566	11.249

In this study, two different milling speed values, namely 100 and 200 rpm, were comparatively studied to synthesize Cu-B_4C composite powder. Accordingly, APS values described in Fig. 2 and Table 4 were fluctuated at both milling speeds for the range that corresponds to milling durations between 3 and 6 hours. It can be seen from Fig. 2 that APS values for lower milling speeds (100 rpm) remain almost stable (approximately 22 to 20 µm) with later stages of milling. On contrary, at 200 rpm, APS values are constantly decreased until the completion of milling runs. Fig. 3 shows the morphological evolution of Cu-B_4C composite powders obtained after milling for 3, 6 and 9 h with PCA content of 5% stearic acid. Accordingly, efficiency of milling is too low and APS is almost stable for the powder specimen milled at 100 rpm (Figs. 3a-c). In spite of this, the powder specimen milled at 200 rpm is exhibited continuous reduction in the particle size (Figs. 3d-f). APS values for the specimens milled at 100 and 200 rpm after 9 h of grinding are recorded to be 23.490 and 20.258 µm, respectively. Fig. 4 represents the morphology of the Cu-B_4C powder specimens grinded at 100 and 200 rpm speeds after milled for 12 and 15 hours. Stearic acid addition as a PCA, was found effective to reduce APS, especially for the specimen milled at 200 rpm (Figs. 4c and d). At lower milling speeds, inhomogeneous distribution of particles (Figs. 4a and b) was occurred due to the inadequate kinetic energy input. APS values at the end of milling cycles were recorded to be 20.592 and 11.249 µm for milling speeds of 100 and 200 rpm, respectively. As a consequence, the milling speed value of 200 rpm was found much more effective in terms of achieving particle size reduction, as compared to that of 100 rpm.

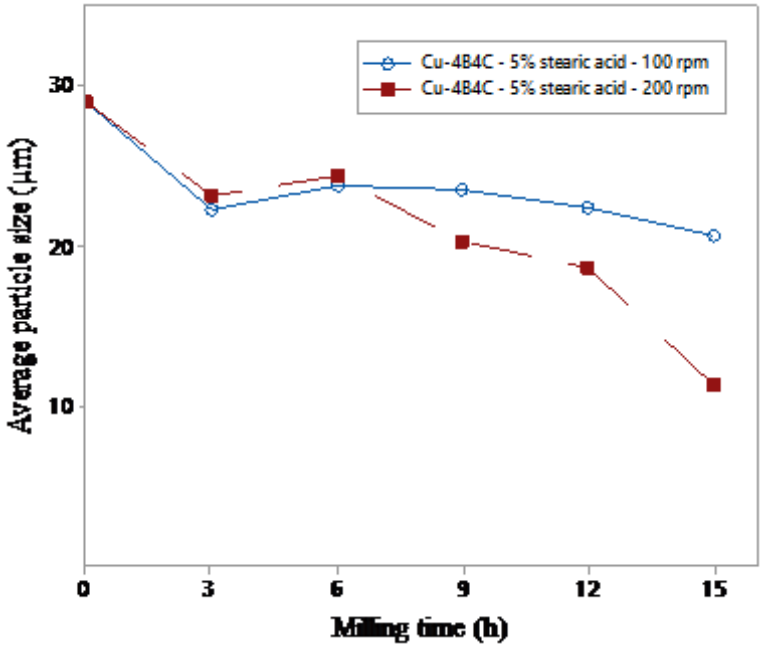

Figure 2. *Particle size variation of Cu-B_4C powder mixtures as functions of milling speed and duration.*

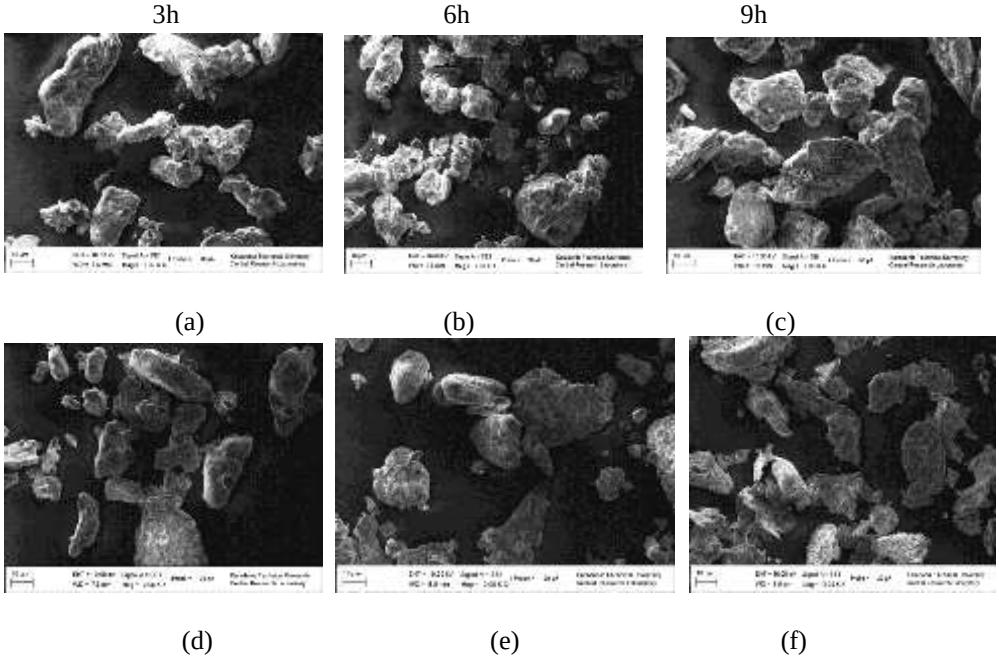

Figure 3. *Morphology of the Cu-B_4C having 5% stearic acid after milled for a) 3 h, b) 6 h and c) 9 h at 100 rpm; and Cu-B_4C having 5% stearic acid after milled for a) 3 h, b) 6 h and c) 9 h at 200 rpm.*

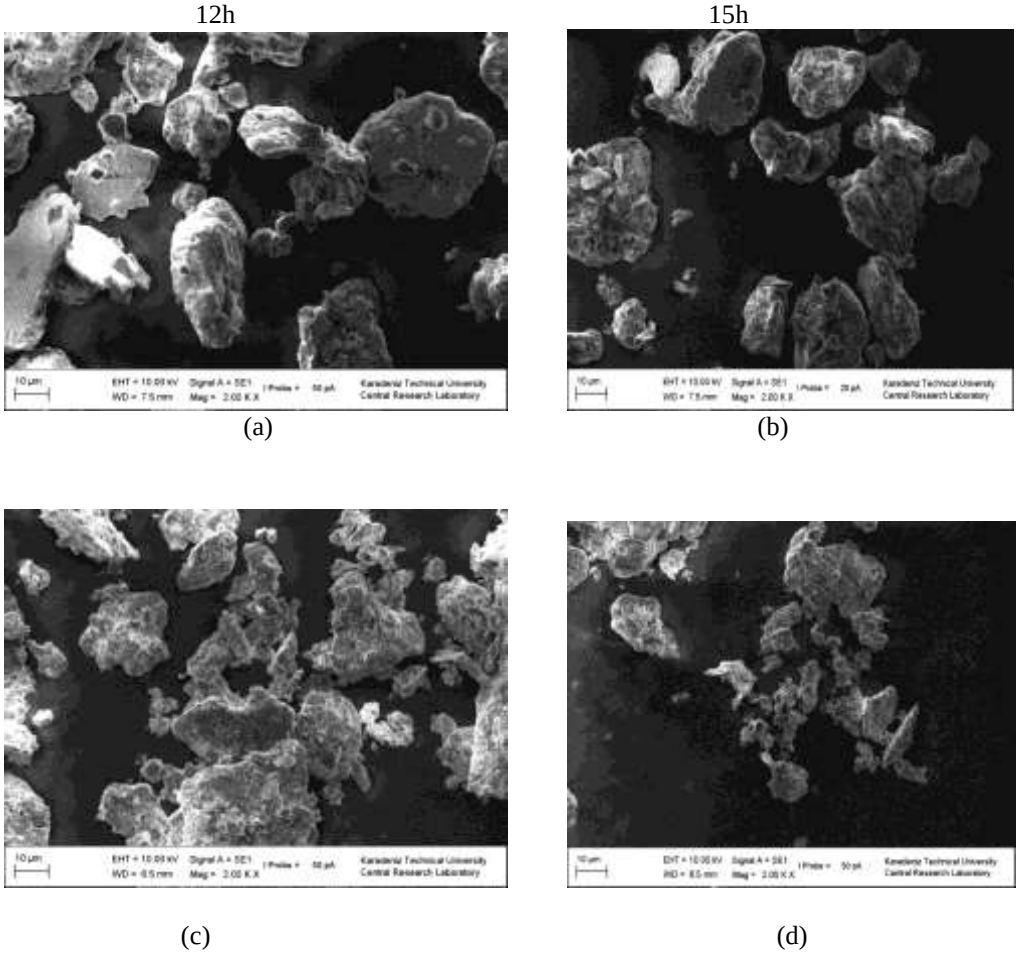

Figure 4. *Morphology of the Cu-B_4C having 5% stearic acid after milled for a) 12 h and b) 15 h at 100 rpm; and Cu-B_4C having 5% stearic acid after milled for a) 12 h and b) 15 h at 200 rpm.*

4. CONCLUSIONS

In this study, two different milling speed values, namely 100 and 200 rpm, were comparatively studied to synthesize Cu-B_4C composite powder. Average particle size (APS) values were fluctuated at both milling speeds for the range that corresponds to milling durations between 3 and 6 hours. Efficiency of milling is too low and APS is almost stable for the powder specimen milled at 100 rpm. On the other hand, the powder specimen milled at 200 rpm is exhibited continuous reduction in the particle size, especially at certain values corresponding to 6 – 15 hours. Stearic acid addition as a PCA, was found effective to reduce APS, especially for the specimen milled at 200 rpm. APS values at the end of milling cycles were recorded to be 20.592 and 11.249 μm for milling speeds of 100 and 200 rpm, respectively. Considering SEM pictures and particle size values obtained after

milling, it was found that 200 rpm of milling speed was determined to be optimum condition to synthesize Cu-B_4C composite powder.

REFERENCES

[1] ASM Handbook, Vol. 7, Powder Metal Technologies and Applications, ASM International Materials Park, Ohio, 1998.

[2] S. Biyik, Effect of cubic and hexagonal boron nitride additions on the synthesis of Ag–SnO_2 electrical contact material, J. Nanoelectron. Optoe. 14 (2019) 1010-1015. *DOI:10.1166/jno.2019.2592*

[3] S. Biyik, Effect of reinforcement ratio on physical and mechanical properties of Cu-W composites synthesized by ball milling, Mater. Focus 7 (2018) 535-541. *DOI:10.1166/mat.2018.1513*

[4] S. Biyik, F. Arslan, M. Aydin, Arc-erosion behavior of boric oxide-reinforced silver-based electrical contact materials produced by mechanical alloying, Journal of Electronic Materials 44 (2015) 457-466. *DOI:10.1007/s11664-014-3399-4*

[5] S. Biyik, Characterization of nanocrystalline Cu25Mo electrical contact material synthesized via ball milling, Acta Phys. Pol. A 132 (2017) 886-888. *DOI:10.12693/APhysPolA.132.886*

[6] C. Suryanarayana, A. A. Al-Joubori, Z. Wang, Nanostructured materials and nanocomposites by mechanical alloying: an overview, Met. Mater. Int. 28 (2022) 41-53. *DOI:10.1007/s12540-021-00998-5*

[7] S. Biyik, M. Aydin, Optimization of mechanical alloying parameters of Cu25W electrical contact material, Acta Phys. Pol. A 132 (2017) 909-912. *DOI:10.12693/APhysPolA.132.909*

[8] S. Biyik, M. Aydin, The effect of milling speed on particle size and morphology of Cu25W composite powder, Acta Phys. Pol. A 127 (2015) 1255-1260. *DOI:10.12693/APhysPolA.127.1255*

[9] S. Biyik, Effect of polyethylene glycol on the mechanical alloying behavior of Cu-W electrical contact material, Acta Phys. Pol. A 134 (2018) 208-212. *DOI:10.12693/APhysPolA.134.208*

[10] S. A. Tunc, A. Canakci, A. H. Karabacak, M. Celebi, M. Turkmen, Effect of different PCA types on morphology, physical, thermal and mechanical properties of AA2024-B_4C composites, Powder Technology 434 (2024) 119373. *DOI:10.1016/j.powtec.2024.119373*

[11] S. X. Zhu, Y. Liu, B. H. Tian, Y. Zhang, K. X. Song, Arc erosion behavior and mechanism of Cu/Cr20 electrical contact material, Vacuum. 143 (2017) 129-137. *DOI:10.1016/j.vacuum.2017.06.002*

A multi-task learning-based method for gas well production prediction in multilayer tight sandstone reservoirs

Dawei Liu [1]✉, Shiqing Cheng [1], Zexuan Xu [1], han Wang [2], Yang Wang[1]

[1] *School of Petroleum Engineering, China University of Petroleum (Beijing) , Beijing, China*
[2] *Sinopec Nortn china Petroleum Bureau, Zhenzhou, China*
✉ *Corresponding author: liudw1995@163.com*

ABSTRACT

Aiming at the poor effect of existing machine learning methods in predicting the production capacity of gas wells in multi-layer tight sandstone reservoirs under small sample conditions, this paper proposes a multi-task learning production capacity prediction method based on Copula entropy theory, residual neural network and progressive hierarchical extraction. The method can not only adaptively extract nonlinear features, but also autonomously select features for different prediction tasks, which improves the accuracy of gas well production prediction in multilayer tight sandstone reservoirs under small sample data. The initial daily production and the first-year cumulative production are taken as the prediction targets, and a multi-task gas well production prediction model is established, which is applied to the production prediction of 50 gas wells in a tight sandstone reservoir. Compared with the single-task model and the classical machine learning model, the accuracies of gas well production prediction of multi-layer tight sandstone reservoirs with multi-task learning under the small-sample data are both substantially improved.

KEYWORDS: *Multi-layer tight sandstone gas reservoir; Gas well production forecasts; Progressive layered*

1. INTRODUCTION

Production capacity prediction is an important step in evaluating the production capacity of gas wells and making decisions on gas reservoir development planning. At present, there are various methods for capacity prediction of gas wells in multilayer reservoirs, such as capacity test well [1-3] and analytical method [4-11]. The capacity test well method is widely used in the field, but it requires long testing time, and many wells cannot be tested due to the cost; the analytical method evaluates and predicts by deriving the capacity equation, in which there are many assumptions in the capacity equation, and the influence of the physical parameters of each small layer on the production is not sufficiently taken into account, which leads to a large deviation of the prediction results from the actual values. Multi-layer tight sandstone gas reservoirs can obtain high production after fracturing, but there is a big difference between the layers of the reservoir, the production rate of gas wells decreases rapidly, and with the extension of production time, the formation pressure decreases, and the contribution of each small layer to the production is different, so it is difficult to quickly and accurately predict the production rate of the wells with the conventional production prediction method.

With the rapid development of artificial intelligence in recent years, machine learning and deep learning algorithms such as support vector machines and neural networks have been applied in oil and gas well production prediction [12-19]. However, at the early stage of tight sandstone gas reservoir development, the number of gas wells is small, and the geological information, fracturing data, and production data owned are also small, and all the above mentioned oil and gas well production prediction algorithms need a large amount of data for support, which leads to limited

applications. Multi-task learning can learn the correlation between different tasks by sharing model parameters, and use the data of multiple related tasks for training, thus expanding the training data and improving the generalization ability of the model, which can effectively alleviate the problem of small number of data samples.

To address the above problems, this paper proposes a multi-layer tight sandstone reservoir gas well production prediction method based on Progressive Layered Extraction (PLE) based on multi-layer tight sandstone reservoir reservoir reservoir physical properties, gas well fracturing and production history data, using Copula entropy and residual neural network methods for feature selection (MTRP) to realize gas well production prediction of multilayer tight sandstone reservoirs under multi-task learning.

2. MATERIALS AND METHODS

Small Sample Prediction Problem with Traditional Machine Learning Methods

When traditional machine learning methods are used in small sample prediction, the amount of data available for training is limited, and the model cannot fully learn the features and patterns of the data, and may face problems such as dimensionality catastrophe, overfitting, and difficulty in feature selection, which leads to poor prediction results [20-23]. Data enhancement, feature selection and dimensionality reduction engineering, integration learning, and transfer learning are widely used in small-sample prediction, but in capacity prediction research, data enhancement modifies data inputs and is not applicable to actual oil and gas well capacity prediction; feature selection and dimensionality reduction engineering require operators to have a large amount of a priori knowledge and experience of the target reservoir; integration learning requires training multiple models that are suitable for oil and gas well capacity prediction of the target reservoir, and the computational complexity may be high. Integration learning requires training multiple models that are suitable for predicting the production of oil and gas wells in the target reservoir, which may have high computational complexity and consume a long time; and migration learning requires oil and gas reservoir data that are similar to the characteristics of the target reservoir, which is highly demanding for data accuracy. Therefore, for small-sample oil and gas well production prediction, it is necessary to find a more suitable prediction method.

Gas Well Production Prediction Model for Progressive Layered Extraction

Multi-task learning improves the performance of small-sample prediction by establishing a unified framework and utilizing the similarity and shared information between different tasks, which reduces the risk of overfitting and improves the data utilization at the same time, and solves the problem of small-sample prediction by data augmentation and other techniques in traditional machine learning methods.In this paper, Copula entropy theory, ResNet model and PLE method are applied to gas well production prediction in multilayer tight sandstone reservoirs.

Copula entropy feature selection strategy

Copula entropy is a method of calculating mutual information or correlation between variables by minimizing the entropy corresponding to mutually independent random variables and is used to measure linear and nonlinear relationships between random variables [24]. Copula entropy can better detect the nonlinear relationship between two random variables compared to Pearson correlation coefficient method [25]. Hampel entropy is a threshold criterion for Copula entropy algorithm [26-28], which is defined by the Eq (1).

$$H_j = \frac{d_j}{1.4826 d_j^{(50)}} \quad d_j = \left| C_{PMI} - C_{PMI}^{(50)} \right| \tag{1}$$

H_j is the Hampel distance, 1.4286 is the normalization factor that makes H_j equal to the standard deviation of the data series, d_j is the absolute value of the difference between the biased mutual information and the median of the biased mutual information, $d_j^{(50)}$ is the median of d_j ; C_{PMI} is the partial mutual information, $C_{PMI}^{(50)}$ s the median of the partial mutual information. Based on the 3x standard deviation criterion [28], When H_j is greater than 3, the feature is selected.

ResNet deep feature extraction strategy

ResNet can further extract the deep potential relationship between features and variables after Copula entropy feature selection. It embeds the residual unit into the network structure, and introduces a "shortcut connection" in addition to the ordinary stacked convolution operation, which directly transfers the input tensor to the output tensor, realizing the constant transformation [29-30], avoiding the problem of gradient explosion and gradient disappearance of the convolutional neural network with the increase of the depth, which leads to the worse effect of feature extraction. The structure of ResNet is shown in Figure 1.

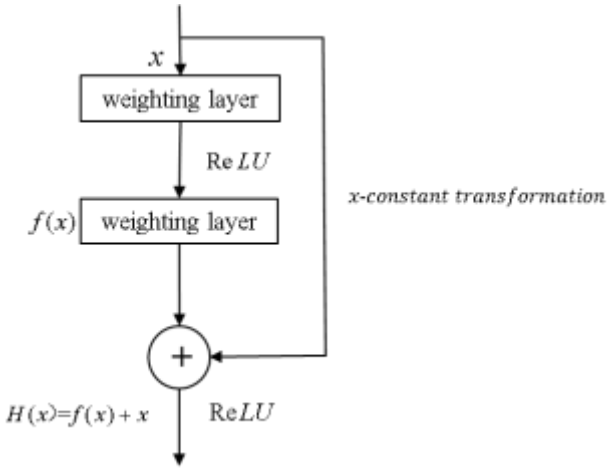

Figure 1. *ResNET structure*

Progressive Layered Extraction Method

In this paper, the PLE model [31] is used to solve the above problems.The PLE model consists of a feature extraction network composed of an underlying shared network and a specific expert network, a gating unit, and an upper tower network.

Compared with the traditional multi-task learning methods, the PLE model has the following unique advantages: (1) The PLE model utilizes the data information extraction process of the expert network and the shared network, which enables the gating unit to obtain the data information in a deeper way before delivering it to the tower network, realizing a deeper level of information extraction for different tasks, thus improving the generalization ability. (2) In the PLE model, there are indirect associations between the tower network and other task-specific expert networks, which allows different types of expert networks to efficiently focus on learning the knowledge of their respective tasks without interference from other tasks, thus better handling the balance between task and sample relevance. (3) The PLE model realizes adaptive assignment to different task data through gating units, which avoids computational complexity and improves computational effectiveness.

In PLE, shared experts and task-specific experts are selectively fused through gated networks. The structure of the gated network is based on a single-layer feed-forward network with SoftMax as the activation function, and the weighted sum of the selected vectors is calculated as the output of the expert network.

MTRP Gas Well Production Forecasting Model

The MTRP model is shown in **Figure 2**. Utilizing Coupla entropy for feature selection, the result after feature selection is input into ResNet to extract deep features, the output of ResNet enters into PLE, different expert networks and shared networks are established, and the output of expert network and shared network is obtained through the fusion of sub-network processing under different tasks, and the processing result is input into different tower network layers after the gating unit, and the prediction outputs of different tasks are obtained.

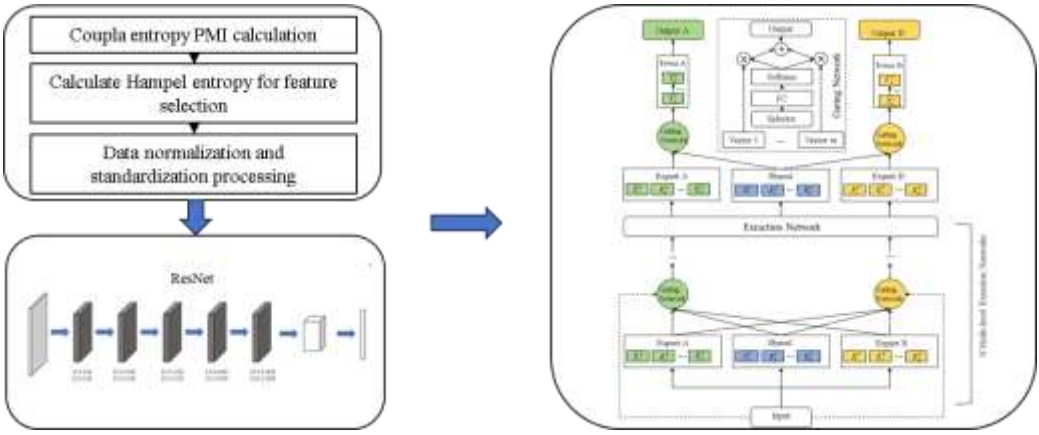

Figure 2. *MTRP model framework*

In this paper, the initial production of a gas well is defined as the first month of gas well production, the initial production of a gas well is defined as the average daily gas production within one month of gas well production, and the first-year cumulative production is defined as the cumulative gas production within 12 months of gas well production. Since the production time of gas wells in the target blocks is generally longer than one year, the initial production corresponds to the short production time of gas wells, which can reflect the influence of fracturing effect on the production of oil and gas wells, while the first-year cumulative production can reflect the influence of different factors on the production capacity of gas wells during the production process of gas wells, based on the above considerations, the initial production and the first-year cumulative production are selected as the targets of multi-task prediction. For the convenience of presentation, initial production and first-year cumulative production prediction are taken as task one and task two respectively in this paper. Therefore, MTL is set as 2 sub-tasks, containing 2 sub-inputs and 2 sub-outputs respectively. Considering the computational speed and accuracy of the model, the residual learning unit is set to be 5, the number of layers of extraction network is 2, and the activation function of expert network layer and shared network layer is Linear. In addition, the computational unit of the tower neural network is Deep-Learning Neural Network (DNN), the number of units is 64, 64, the initial learning rate is 0.01, the learning rate decreases at a frequency of 0.2/10 iterations, and the maximum number of iterations is 100, and the activation function of the network is Relu. the optimizer uses Adam, and the loss function is the Root Mean Square Error (RMSLE), and the metrics are the Mean Squared Error (MSE) and the Absolute Coefficient (R^2).

Example analysis of gas well production prediction in multilayered tight sandstone gas reservoirs

Data sources and pre-processing

The 50 joint wells in the eastern part of a multilayered tight sandstone gas field have the same production layers, which are He 8 section, Shan 2 section and Benxi Formation. The thickness of the gas layer in He 8 section is set as h_1, the thickness of the gas layer in Shan 2 section is set as h_2, and the thickness of the gas layer in Benxi Formation is set as h_3. Other reservoir physical parameters and fracturing parameters, gas well production dynamic parameters are also named in the same way, with a total of 29 features. The initial yield and the first-year cumulative yield are taken as dependent

Table 1. *Copula entropy feature selection*

features	Hampel entropy of characteristics and initial yield	Characterization and Hampel entropy of first year cumulative production	Whether or not to be used as a Resnet input
h_1	3.34	3.27	yes
h_2	3.28	3.34	yes
h_3	3.21	3.05	yes
k_1	3.32	3.29	yes
k_2	3.28	3.32	yes
k_3	3.15	3.21	yes
ϕ_1	2.91	2.94	no
ϕ_2	2.94	2.85	no
ϕ_3	2.83	2.89	no
Sg_1	1.56	1.5	no
Sg_2	1.47	1.53	no
Sg_3	1.55	1.61	no
FR_1	3.08	2.39	no
FR_2	3.08	2.57	no
FR_3	3.17	2.37	no
IW_1	3.27	3.43	yes
IW_2	3.31	3.31	yes
IW_3	3.11	2.91	yes
PF_1	3.32	3.38	yes
PF_2	3.27	3.37	yes
PF_3	3.15	2.98	yes
T_1	2.74	2.74	no
T_2	2.22	2.19	no
Gn_1	2.14	2.96	no
Gn_2	1.64	3.11	yes
Pt_1	3.44	3.01	yes

Pt_2	2.67	3.27	yes
Pc_1	3.36	3.39	yes
Pc_2	2.81	3.11	yes

variables y_1 and y_2, and the above characteristics are taken as independent variables x_i, and the Copula entropy value of each independent variable and dependent variable is calculated, supplemented by the Hampel threshold criterion, to filter out the indicators that have a greater impact on the initial yield and the first-year cumulative yield. The Copula entropy value and Hampel threshold value of 29 characteristics were calculated, and the calculation results are shown in Table 1.

There are some features in Table 2 that have a Hampel entropy value greater than 3 for one task but less than 3 for another (Gn_2 et al.). In single-task learning, features with Hampel entropy values less than 3 can be deleted because they adversely affect the prediction performance of the task. However, in multi-task learning, deleting these features will cause the input information to be incomplete, and the "seesaw" phenomenon is likely to occur in the model performance analysis. From the perspective of Copula entropy theory, these features only have a better effect on the prediction of one task, but will have a negative effect on the prediction of another task. For the sake of completeness of the input information, this paper also summarizes these features as the input feature library of the multi-task learning model, and uses Resnet network and PLE to carry out deep feature extraction and autonomous feature extraction, so as to avoid the negative influence of the features with the entropy value of Hampel less than 3 on the prediction effect of the model.

Performance Comparison of MTRP and Classical Machine Learning Models

In order to further evaluate the effectiveness of the MTRP model, four types of K-nearest neighbor (KNN), Random Forest (RF), Support Vector Machine (SVM), and XGBoost (Extreme Gradient Boosting) were established classical machine learning models, which utilize the feature selection results to predict the initial yield and the first year cumulative yield, respectively. Since machine learning can only support single-task prediction, it is necessary to establish prediction models for the two tasks separately, and the prediction results are the mean values of 500 runs of the model, and the above machine learning algorithms have been optimized with Bayesian optimization algorithm with hyperparameters.

Figure 3(a) and Figure 3(b) show the prediction results of MTRP and Support Vector Machine, K Nearest Neighbor, Random Forest and XGBoost for task one, respectively. The horizontal coordinates in the figure are the real initial production and the first year cumulative production value respectively, the vertical coordinate is the model prediction value, and the black dashed line is the 45° diagonal, the smaller the angle between the fitted line and the diagonal of the prediction result is, the higher the model prediction accuracy is.The prediction results of MTRP are closer to the 45° diagonal for both tasks, and the prediction result is superior to that of the classical machine learning algorithms.

Table 2 compares the MSE and R^2 of Support Vector Machine, K Nearest Neighbor, Random Forest and XGBoost and MTRP models for Task 1 and Task 2, and the MTRP model achieves the minimum error in both tasks. In the case of limited training data, the traditional machine learning algorithms are limited by the single-task prediction mode, which is difficult to fully learn the change rule of yield, and the prediction accuracy is significantly lower than that of the MTRP model.

3. RESULTS AND DISCUSSIONS

Impact of different feature classes on capacity forecasting results

Reservoir physical properties represent the geological characteristics of gas wells, fracturing parameters reflect the fracture formation and expansion status, which in turn affects the production capacity of gas wells, and engineering parameters represent the impact of changes in the working system on the production capacity of gas wells. In order to clarify the influence of different feature categories on the production capacity, reveal the relationship law between different features and production capacity, and improve the production capacity of gas wells in tight sandstone reservoirs, the above feature categories were input into the MTRP prediction model to judge the influence of different feature categories on the production capacity of gas wells.

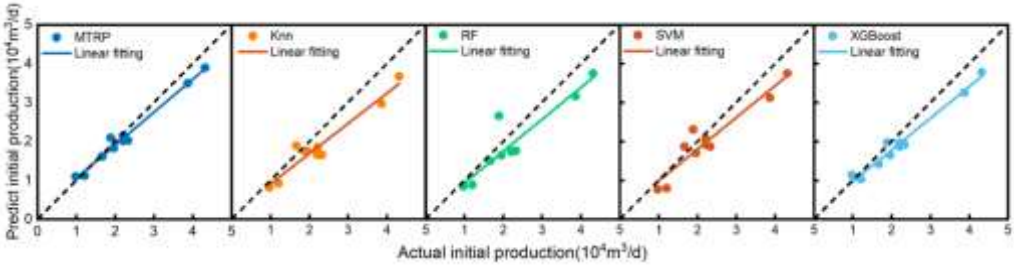

(a) Comparison of Predictions of Different Models on Task 1

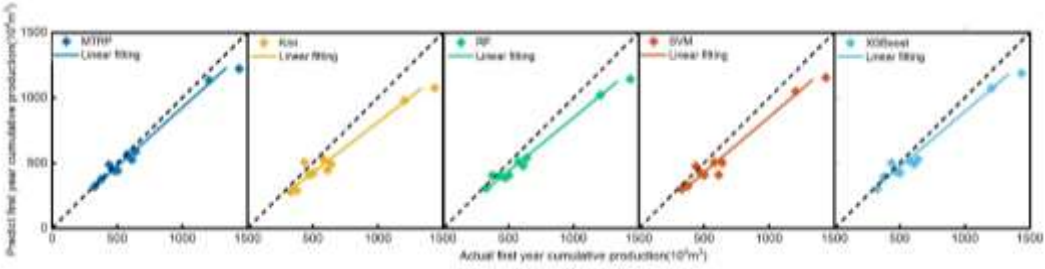

(b) Comparison of Predictions of Different Models on Task 2

Figure 3. *Prediction results of MTRP model and classical machine learning model*

Table 2. Comparison of mean prediction errors between MTRP and classical machine learning

Task	Evaluation indicators	MTRP	Knn	RF	SVM	XGBoost
Task 1	MSE($10^4m^3/d$)	0.09	0.33	0.23	0.23	0.19
	R^2	0.78	0.52	0.65	0.66	0.68
Task 2	MSE($10^4m^3/d$)	7700.28	23032.52	19626.20	12302.93	12963.266
	R^2	0.77	0.48	0.52	0.61	0.6

Figure 4 compares the prediction performance of the MTRP model with different feature categories input. The production dynamic parameters contribute the least to the performance of Task 1. This is due to the relatively consistent pressure drop in each well at the beginning of production and the small change in the nozzle parameters. The production dynamic parameters have the largest contribution to Task 2, which may be due to the good correlation between the oil jacket pressure and gas well production in long-term production of gas wells, whereas the operational changes such as

switching on and off wells and replacing nozzles contain dynamic information related to production fluctuations, which constrains the overall trend of long-term production of the gas wells. The influence of geological parameters on both Task 1 and Task 2 is small, which reflects the strong inhomogeneity and strong inter-well variability of reservoirs in tight sandstone gas reservoirs, and the large gap between the mean and median values of k , h , and φ in the reservoir physical properties in Table 1 indicates that the distribution of these characteristics is more sporadic between the maxima and the minima, whereas the small gap between the mean and the median values of the gas wells' initial daily production and the first year's cumulative production leads to a small difference in the correlation between the characteristics and the The correlation of these features with the initial daily production and first year cumulative production is poor compared to other features, and there may be human errors in the initial entry. However, the influence of fracturing parameters on Task 1 and Task 2 is larger, which indicates that the fracturing parameters can reflect the production status of gas wells in the initial and long-term production periods wells, and the reasonable fracturing parameters have a greater influence on the production capacity of gas wells in multilayered tight sandstone reservoirs.

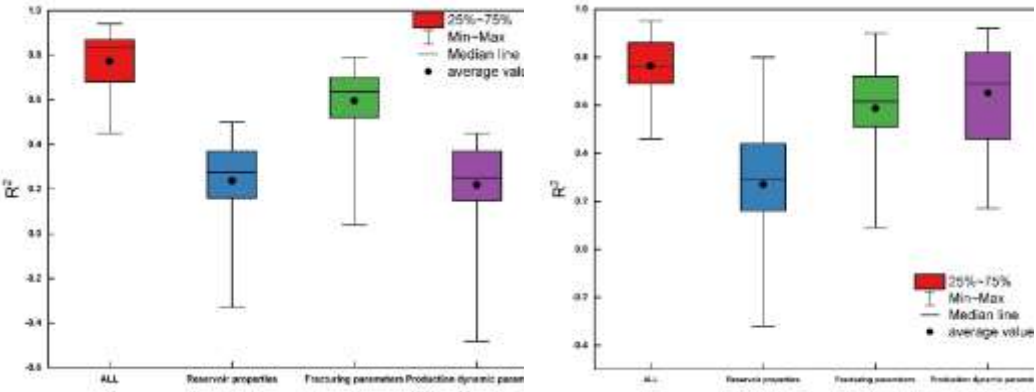

(a) Comparison of prediction results for different feature class inputs in Task 1

(b) Comparison of prediction results for different feature class inputs in Task 2

Figure 4. *Comparison of production capacity prediction results for different feature categorie*

4. CONCLUSIONS

(1) In this paper, a multi-layer tight sandstone reservoir gas well production prediction (MTRP) model based on Coupla entropy, ResNet and progressive layered extraction multi-task learning is proposed. The model adopts Coupla entropy for feature extraction, ResNet neural network is used to further extract the depth relationship between features and variables, progressive hierarchical extraction avoids the interference of weakly correlated information on different tasks, and is able to better utilize the coupling relationship between the data, and the input features can more accurately reflect the changes of the initial production and the first-year cumulative production of gas wells in multilayered tight sandstone reservoirs, which makes the model has stronger stability.

(2) Compared with the classical machine learning model, the MTRP model improves the prediction accuracies of the initial production and the first-year cumulative production of 50 gas wells in multilayered tight sandstone reservoirs in a certain block, which suggests that multi-task learning significantly improves the model's generalization ability under the condition of small samples, and effectively mitigates the problem of the small number of data samples.

(3) The results of different characterization categories for predicting the production capacity of gas wells in multilayered tight sandstone reservoirs show that the production dynamic parameters and fracturing parameters have a greater impact on the long-term production capacity of the gas wells, the fracturing parameters significantly affect the initial production capacity of the gas wells, and the geologic parameters have a lesser impact on the production capacity due to the influence of the strong non-homogeneity in the tight sandstone reservoirs.

REFERENCES

[1] Chen Yuanqian. A simple method to determine the absolute unobstructed flow rate of gas wells . Natural Gas Industry,1987,7(1):59-63.

[2] Wang Weihong, Shen Pingping, Ma Xinhua, et al. Research on the Analysis Method of Gas Well Production Test Data for Low Permeability Gas Reservoirs [J]. Natural Gas Industry, 2005 (11): 76-78+153.

[3] Shi Juntai, Li Qian, Zhang Lei, et al. Reasons and correction methods for abnormal production capacity indicator curves in multi-layer co production gas wells [J]. Natural Gas Industry, 2018, 38 (03): 50-59.

[4] Kucuk F, Karakas M, Aestaran L. Well Testing and Analysis Techniques for Layered Reservoirs[J].Spe Formation Evaluation, 1986, 1(4):342-354.

[5] Kucuk F, Wilkinson D J.Transient PressNre Behavior of Commingled Reservoirs[J]. Spe Formation Evaluaation, 1991, 6(1):111-120.

[6] Yue Jianwei, Duan Yonggang, Chen Wei, et al. Study on the productivity of fractured gas wells with multiple vertical fractures [J]. Daqing Petroleum Geology and Development, 2004 (03): 46-48+91-92 .

[7] He Ying, Xu Lianyu, Lv Wanwan, et al. Analysis of Production Capacity of Fractured Wells in Low Permeability and Permeable Reservoirs [J]. Special Oil and Gas Reservoirs, 2006 (05): 59-61+107.

[8] Liang Bin, Li Min, Zeng Fanhua, et al. Research on Production Capacity Analysis Methods for Tight Gas Reservoirs [J]. Fault Block Oil and Gas Fields, 2005 (01): 30-33+90-91.

[9] Wang Tao, Yu Haiyang, Zhao Pengfei, et al. Evaluation of post fracturing production capacity of tight gas wells based on unstable pressure well testing analysis [J]. Special Oil and Gas Reservoirs, 2023,30 (04): 122-130.

[10] Bai Wenpeng, Cheng Shiqing, Wang Yang, et al. Prediction method for unstable production of multiphase flow in tight condensate gas wells [J]. Petroleum Exploration and Development, 2024,51 (01): 154-160.

[11] Wang Xiangzeng, Feng Dong, Li Xiangfang, et al. Evaluation of tight gas well productivity considering time-varying effects: A case study of Yan'an gas field [J]. Journal of Petroleum, 2019,40 (11): 1358-1367.

[12] Han Kening, Wang Wei, Fan Dongyan, et al. Production prediction of atmospheric shale gas wells based on the coupling of production decline and LSTM [J]. Oil and Gas Reservoir Evaluation and Development, 2023,13 (05): 647-656. DOI: 10.13809/j.cnki. cn32-1825/te. 2023.05.012.

[13] Lin Hun, Sun Xinyi, Song Xixiang, et al. Research on shale gas well production prediction model based on improved artificial neural network [J]. Oil and Gas Reservoir Evaluation and Development, 2023,13 (04): 467-473. DOI: 10.13809/j.cnki. cn32-1825/te. 2023.04.008.

[14] Pang Lansu, Wang Yang, Jiang Wei, et al. Research on Short Production Cycle Carbonate Gas Well Production Prediction Based on Machine Learning [J]. Special Oil and Gas Reservoirs, 2023,30 (02): 134-141.

[15] He Youwei,He Zhiyue,Tang Yong,Qin Jiazheng,Song Junjie,Wang Yong. Production evaluation and prediction of shale gas wells based on machine learning [J]. Petroleum Drilling and Production Technology,2021,43(04):518-524 .DOI:10.13639/j.odpt.2021.04.016.

[16] Ma Xianlin,Fan Yilong. Production prediction model of fracturing vertical well based on machine learning [J].Mathematical Practice and Understanding,2021,51(19):186-196.

[17] Wenpeng Bai, Shiqing Cheng, Xinyang Guo, Yang Wang, Qiao Guo, ChaoDong Tan,Oilfield analogy and productivity prediction based on machine learning: Field cases in PL oilfield, China,Petroleum Science,2024,,ISSN 1995-8226,https://doi.org/10.1016/j.petsci.2024.02.018.

[18] Xuechen Li,Xinfang Ma,Fengchao Xiao,Cong Xiao,Fei Wang,Shicheng Zhang. Time-series production forecasting method based on the integration of Bidirectional Gated Recurrent Unit (Bi-GRU) network and Sparrow Search Algorithm (SSA)[J].Journal of Petroleum Science and Engineering, Volume 208, Part A,2022,109309. https://doi.org/10.1016/j.petrol.2021.109309.

[19] Wang Yang, Cheng Shiqing, Zhang Fengbo, et al. Big Data Technique in the Reservoir Parameters' Prediction and Productivity Evaluation: A Field Case in Western South China Sea. Gondwana Research, 2021, 96(2021): 22-36.

[20] Kokol P, Kokol M, Zagoranski S. Machine learning on small size samples: A synthetic knowledge synthesis. Science Progress. 2022;105(1). doi:10.1177/00368504211029777 Shorten, C., & Khoshgoftaar, T. M. (2019). A survey on image data augmentation for deep learning. Journal of Big Data, 6(1), 60.

[21] Kokol P, Kokol M, Zagoranski S. Machine learning on small size samples: A synthetic knowledge synthesis. Science Progress. 2022;105(1). doi:10.1177/00368504211029777.

[22] R. Larracy, A. Phinyomark and E. Scheme, "Machine Learning Model Validation for Early Stage Studies with Small Sample Sizes," 2021 43rd Annual International Conference of the IEEE Engineering in Medicine & Biology Society (EMBC), Mexico, 2021, pp. 2314-2319, doi: 10.1109/EMBC46164.2021.9629697.

[23] Chao Li, Lei Wang, Jie Li, Yang Chen,Application of multi-algorithm ensemble methods in high-dimensional and small-sample data of geotechnical engineering:A case study of swelling pressure of expansive soils,2024,ISSN 1674-7755.

[24] MA J, SUN Z. Mutual information is Copula entropy[J].Tsinghua science and technology,2011,16(1): 51-54.

[25] Jian Ma. Discovering association with Copula entropy[J].arXiv preprint arXiv:1907.12268, 2019.

[26] Fernando,T.M.K.G,Maier H.R,Dandy G C.Selection of input variables for data driven models:An average shifted histogram partial mutual information estimator approach[J].Journal of Hydrology,2009,367:165-176.

[27] MAY Robert J,Maier Holger R,Dandy Graeme C,Fernando T.M.K. G.Non-linear variable selection for artificial neural networks using partial mutual information[J].Environmental modeling & Software,2008,23:1312-1326.

[28] Li Xiaoqi, Zheng Dong-Jian, JU Yi-peng. Factor optimization of dam seepage statistical model based on Copula entropy theory [J]. Journal of Hohai University (Natural Science Edition), 2016, 44 (04): 370-376.

[29] Song Songbai, CAI Huanjie, Jin Juliang et al. Copulas Function and Its Application in Hydrology [M]. Science Press,2012.

[29] Kaiming He, Xiangyu Zhang, Shaoqing Ren, Jian Sun.Deep Residual Learning for Image Recognition[J].arXiv:1512.03385.

[30] TANG Hongyan,LIU Junning,ZHAO Ming,et al. Progressive layered extraction (PLE) : a novel multi-task learning (MTL) model for personalized recommendations[C]//Proceedings of the 14th ACM Conference on Recommender Systems. New York,USA : ACM,2020 : 269-278.

Impact of Photovoltaic Systems in Garment Companies of Albania

Elmira DUMISHLLARI✉

Polytechnic University of Tirana, Department of Textile and Fashion , Tirana-ALBANIA
✉ *Corresponding author: edumishllari@fim.edu.al*

ABSTRACT

Electricity stands as the foremost energy source for garment production companies in Albania, powering all their machinery. These companies have demonstrated a strong interest in adopting energy-efficient solutions, such as photovoltaic systems. This strategic investment offers a host of benefits, including the absence of harmful greenhouse gas emissions, protection of groundwater from pollution, and preservation of natural resources. The primary objective of this paper is to use a compelling business case to assess the transformative impact of photovoltaic systems on energy consumption within garment production companies in Albania.

The research indicates that the introduction of a photovoltaic system has resulted in decreased electricity usage, leading to lower overall production costs. The implementation of the photovoltaic system has reduced electricity usage by 49.85%. This study suggests a novel approach for garment production companies in Albania to enhance their energy efficiency by considering photovoltaic systems as a viable option. Utilizing energy more effectively presents the most efficient and economical means of saving money.

KEYWORDS: *Energy, energy consumption, production, efficiency, Photovoltaic systems.*

1. INTRODUCTION

Electricity stands as the foremost energy source for garment production companies in Albania [1-4]. Energy efficiency is closely related to quality improvement and productivity [5, 6]. In order for this textile industry sector to thrive, energy efficiency is crucial [6]. Energy consumption in garment factories is very important, as all machines run on electricity. Replacing electricity with other energy sources would not bring profit, due to their high cost [7, 8]. If clothing companies invest in solar panels, they will gain many benefits. When PV solar panels generate electricity, they do not emit harmful greenhouse gases, pollute groundwater, or deplete any natural resources. [9, 10, 11]. Referring to other studies, garment production industry should go solar because of cost reduction, compliance with renewable purchase obligations (RPO), availability of roof space, energy savings, reducing carbon footprint [12, 13].

The main purpose of this paper is to determine through a business case the impact that PV system has on energy consumption and production. This study consists in verification of the hypothesis that the implementation of new options; as PV systems, can significantly improve energy efficiency.

This research was conducted in Albanian garment production companies that operate full package. The data was collected from one of these companies

The production data and energy usage for the past year were recorded, and after installing the PV system, data on monthly energy consumption and production was gathered, showing a reduction in energy usage.

2. MATERIALS AND METHODS

For this study purpose the data of production and energy consumption for 12 months are taken. Energy consumption bills and data of production for 12 months are used. Energy consumption is

given in kWh and production in pieces. Invoices from suppliers, receipts/bills, inventory, weighbridge data and incoming goods records are materials that are used in this study as sources of information.

The method used in this research consists in verification of the hypothesis that the implementation of PV systems, can significantly improve energy efficiency. The method includes:

1. Production data and energy consumption for the last year were obtained
3. After installing a PV system, the data for energy consumption and production in pieces for 12 months were retrieved.
4. Discussion of results and the impact that photovoltaic system has on electricity consumption in actual values.

The criteria for selecting the research object have been a garment production company that operates full package, that is interested in energy efficiency, that implemented a PV system.

3. RESULTS AND DISCUSSIONS

The first source of energy in garment production companies in Albania is electricity taken from the grid. The main purpose of this paper is to determine, through a business case the impact that PV system, has on electricity consumption and production. The data of two years are compared; before and after implementing a PV system.

As mentioned before, first, the data on production and electricity consumption for 12 months were obtained. The data are taken from; invoices from suppliers, receipts/bills, inventory, weighbridge data and incoming goods records [14, 15]

The table 1 presents the monthly electricity consumption and production for 12 months, before PV implementation.

Table 1. *Electricity consumption per month and total production before implementing a PV system.*

No.	Month	Elec. consumption kWh/month	Total production [pcs/month]
1	November 2021	10700	24000
2	December 2021	11950	22000
3	January 2022	15650	14 750
4	February 2022	13150	16 284
5	March 2022	9100	8 000
6	April 2022	7050	9 000
7	May 2022	11900	8 500
8	June 2022	10550	15 000
9	July 2022	20300	12 500
10	August 2022	19750	25 500
11	September 2022	13850	26 000
12	October 2022	12950	28 000

The figure 1, shows the production vs. energy consumption for 12 months and a trendline before implementing PV system.

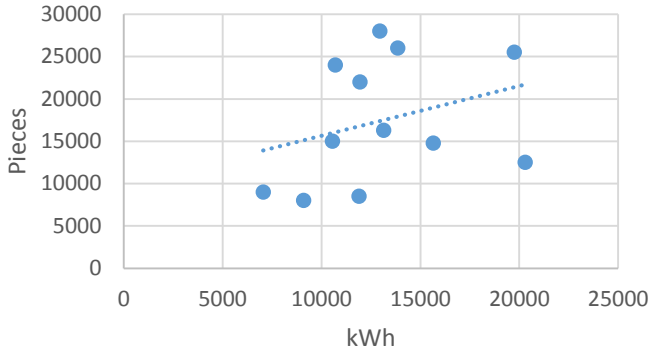

Figure 1. *Production vs. energy consumption and a trendline*

Figure 2 shows electricity consumption before implementing PV plant. July and August are the months with the highest electricity consumption, but are not the months with the higher production. September and October are the months with the higher production in pieces.

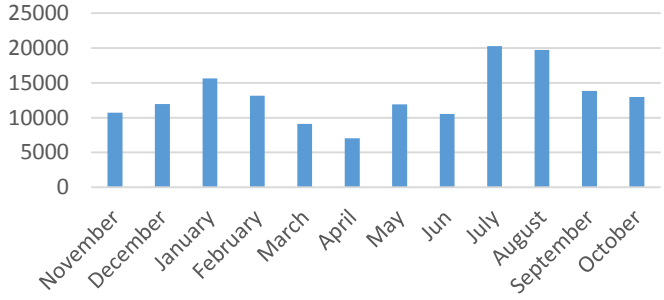

Figure 2. *Energy consumption kWh/month*

The figure 3, presents electricity consumption vs. production levels in 12 months.

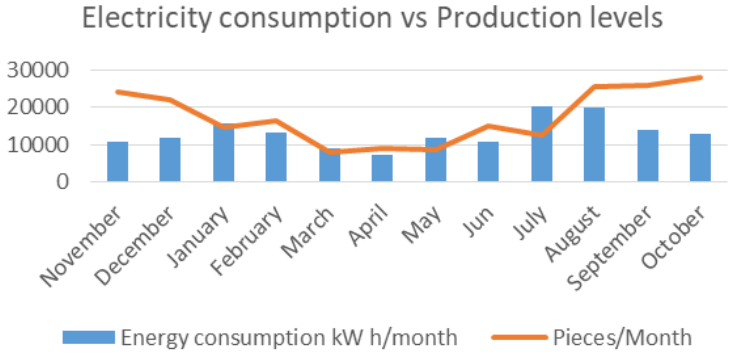

Figure 3. *Energy consumption vs. production*

There is not a proportional relationship between energy consumption and production level. Different factors can influence, for example, defects, months of the year (different need for lighting or use of air conditioning, machinery conditions, etc.). This also indicates the need for reducing the number of batches, idle time, training of operators, switching off idle equipment [16. 17, 18].
After installing a PV plant, the data for energy consumption and production in pieces for 12 months were retrieved. The tab. 2, shows energy consumption (kWh/month) and total production (pcs/month).

Table 2. *Electricity consumption per month and production after installing PV system*

No.	Month	Elec. consumption [kWh/month]	Tot. production [pieces/month]
1	Nov. 2022	5366	24000
2	Dec. 2022	5992	22000
3	Jan. 2023	7848	14 750
4	Feb. 2023	6594	16 284
5	Mar. 2023	4563	8 000
6	Apr. 2023	3535	9 000
7	May 2023	5967	8 500
8	Jun. 2023	5290	15 000
9	Jul. 2023	10180	12 500
10	Aug. 2023	9904.6	25 500
11	Sep. 2023	6945.7	26 000
12	Oct. 2023	6494.4	28 000

The figure 4, presents electricity consumption after PV system implementation in 12 months. July and August are the months with the highest electricity consumption, but are not the months with the higher production Installation of PV system has contributed to the reduction of electricity consumption and in increasing energy efficiency.
The figure 5, shows electricity consumption versus production level. We see that for the same production level, electricity consumption is lower (approximately the electricity consumption is halved). The implementation of the photovoltaic system has reduced electricity usage by 49.85%. Energy efficiency means using less energy to produce the same production level [19] So, this proves the hypothesis that implementation of PV systems can significantly improve energy efficiency.

This study proposes a new method for garment production companies in Albania to improve their energy efficiency, as photovoltaic systems are a new option for them. Using energy more efficiently will bring the fastest, most cost-effective ways to save money.

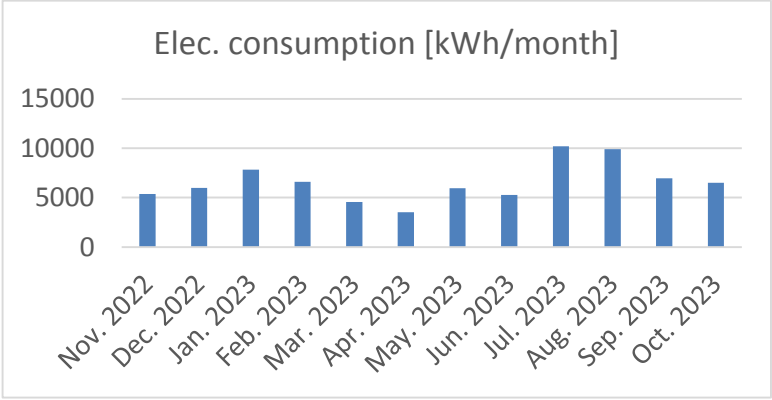

Figure 4. *Energy consumption after PV system implementation*

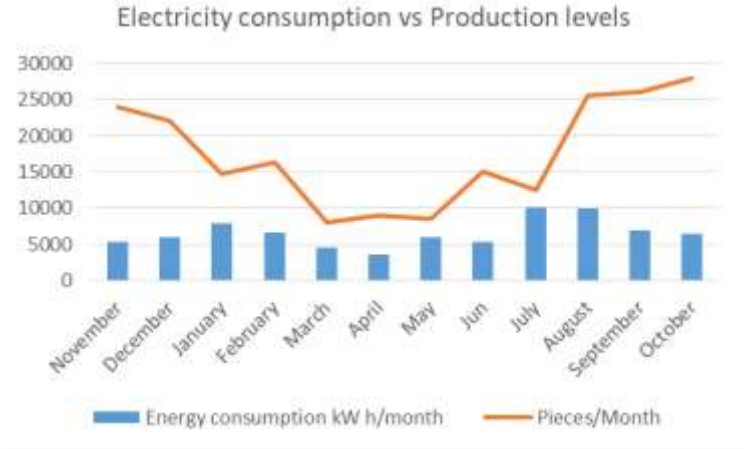

Figure 5. *Energy consumption vs. production*

This shows that the company has achieved a decrease in energy cost, optimization and decrease in product cost.

4. CONCLUSION

Results show that, there is not a proportional relationship between energy consumption and production level. Different factors can influence, for example, defects, months of the year (different need for lighting or use of air conditioning, machinery conditions, etc.). This also indicates the need for reducing the number of batches, idle time, training of operators, switching off idle equipment.

Due to the use of less energy to perform the same task or produce the same result, PV system implementation has contributed in better energy efficiency.

By implementing PV systems in a garment production company, energy consumption will be reduced and energy efficiency is increased. This means that the cost of production will be lower. From results, implementing of PV system has decreased electricity consumption 49.85 %.

This study proposes a new method for garment production companies in Albania to improve their energy efficiency, as photovoltaic systems are a new option for them. Using energy more efficiently will bring the fastest, most cost-effective ways to save money.

Comparison with other studies has shown that energy efficiency is a very important issue in now days, especially in companies that use energy like a key input in production. Application of solar energy in garment companies has the potential of saving. Referring to other studies, garment production industry should go solar because of cost reduction, compliance with renewable purchase obligations (RPO), availability of roof space, energy savings, reducing carbon footprint

It is recommended that in order to increase the energy efficiency clothing production should be focused on solar energy.

There are some limitations in applying the results to other apparel manufacturing companies in Albania such as investment cost, company profile, space for the system installation.

ACKNOWLEDGMENT

This study is realized in the framework of project "Resource Efficient and Cleaner Production", conduced by UNIDO, in Albania. Also, authors thanks Polytechnic University of Tirana for financial support.

REFERENCES

[1] DUMISHLLARI, E., SHEHI, E. (2022) Resource Efficient and Cleaner Production in-plant-assessment in the company SAM shpk, final report..

[2] DUMISHLLARI, E., GUXHO, G. (2015) Energy Economy In the apparel sector. AJNTS (Journal of Natural and Technical Sciences), vol, XX (1), pp. 151-157.

[3] DUMISHLLARI, E., GUXHO, G. (2012) Ndikimi i kohës së punës dhe kontrollit te proceseve ne konsumin e energjisë ne ndermarrjet e prodhimit te veshjeve. Proceedings of the 5 Th International Textile Conference, Tirana, Albania, pp 51.

[4] DUMISHLLARI, E., GUXHO, G. (2014) Assessment of energy consumption in the garment production. 6Th International Conference Of Textile, pp. 148-162 ISBN: 978-9928-171-14-6, 2014.

[5] DUMISHLLARI, E., SHEHI, E, SPAHIJA, S. (2023) "Energy efficiency impact in garment Companies of Albania", published in JOURNAL OF SOUTHWEST JIAOTONG UNIVERSITY, Vol. 58 (4), July 2023

[6] JANANTHAN, R., AMEER, S., AND SHIYAMINI, R. (2006) Comparative Study Of Energy Assessment From Apparel Industries: The Context Of Srilanka. First International Conference on Industrial and Information Systems, pp. 217-220,2006 https://doi.org/10.1109/ICIIS.2006.365726

[7] DUMISHLLARI, E. (2015) PhD Ekonomizimi i lëndës së parë, kohës, energjisë, në kalimin nga prototip në produkt të gatshëm. Doctoral thesis, Polytechnic University of Tirana, Faculty of Mechanical Engineering, Department of Textile and Fashion, Albania.

[8] DUMISHLLARI, E., DRUSHKU, S. (2010) Alternativat më të mira për optimizimin dhe reduktimin e konsumit të ujit dhe energjisë në industrinë tekstile. 4 th International Textile Conference, Tirana, Albania, pp 98-106, ISBN: 978-99956-94-46-3.

[9] HOSENUZZAMAN, M., RAHIM, N.A., SELVARAJ, J. ET AL. (2015) Global prospects, progress, policies, and environmental impact of solar photovoltaic power generation. Elsevier, Renewable and Sustainable Energy Reviews, 41, pp. 284-297.
[10] DAS, U.K., TEY, K.S., SEYEDMAHMOUDIAN, M., MEKHILEF, S., IDRIS, M.Y.I., VAN DEVENTER, W., HORAN, B., STOJCEVSKI, A. (2018) Forecasting of photovoltaic power generation and model optimization: A review. Elsevier, Renewable and Sustainable Energy Reviews, 81, part 1, pp. 912-928.
[11]. BOSNJAKOVIC, M., SANTA, R., CRNAC, Z.,BOSNJAKOVIC, T. (2023) Environmental Impact of PV Power Systems, published in Special Issue Solar Energy Utilization and Sustainable Development), 15(15), 11888; https://doi.org/10.3390/su151511888
[12] BADBADE, P., UJ PATIL, Dr.(2017) Application of Solar Energy in Textile Industry. International conference on Technical and Green Textiles, Bannari Amman Institute of Technology, Sathy, Coimbatore.
[13] GUPTA, K., SOLAR, O. (2023) Why Textile Industry/ Clothing industry should go for solar power. Available: https://ornatesolar.com/blog/why-textile-industry-clothing-industry-should-go-for-solar.
[14] FRESSNER, J. (2010) PRE-SME - Promoting Resource Efficiency in Small & Medium Sized Enterprises Industrial training handbook. United Nations Environment Programme.
[15] FRESNER, J. (2022) EU4Environment, Resource Efficient and Cleaner Production (RECP).
[16] BRUDAN, A. (2015) The KPI Institute, smartKPIs.com, The Production and Quality Management KPI Dictionar, CreateSpace Independent Publishing Platform.
[17] SALONITIS, K. (2020) Energy Efficiency of Manufacturing Processes and Systems. (First edition). Basel, Switzerland: Mdpi AG.
[18] DORNFELD, D., LINKE, B., SUTHERLAND, J. (2018) Energy Efficient Manufacturing: Theory and Applications. (First edition). Hoboken, New Jersey, U.S: Wiley-Scrivener
[19] European Environment Agency. (2024) Energy Efficiency

Stability Analysis of a Multi-input Multi-Output Cardiovascular system

Kessal Farida✉

Faculty of Electrical and Computer engineering /Biomedical Department, Tizi Ouzou, Algeria
✉ *Corresponding author: farida.kessal@ummto.dz*

ABSTRACT

This paper presents the stability analysis of a cardiovascular system using modern control theory tools, it will be sought to determine the context situation of two classes of subjects, hypertensive patients and patients with normal blood pressure. Multiple inputs multiple outputs dynamical systems can be described with many representations: state space equations, transfer function, or matrix fraction description. In state space model, the modal decomposition of the state matrix into its eigenstructure is very useful as it defines the stability and the dynamic behavior of a linear multivariable system. Analysing the state of the arterial wall as a function of compliance is achieved by using the controllability criterion. The unit step response of the multiple-input multiple-output system model illustrates different results and the effectiveness of the method.

KEYWORDS: *cardiovascular system, feedback gain matrix, controllability, stability, transfer function.*

1. INTRODUCTION

Multiple input multiple output systems allow us to work in the state-space without restrictions. The use of the Modern Control Theory let to specify new behaviors of complex structures. MIMO dynamical systems can be described with many representations: state space equations, transfer function, or matrix fraction description.

Modeling the cardiac system with tools of the modern control theory, allows analysis of cardiovascular dynamics using equations of state and multiple transfer functions.

This work presents the stability analysis of a cardiovascular system using modern control theory tools, it will be sought to determine the context situation of two classes of subjects, hypertensive patients and patients with normal blood pressure. Analyzing the state of the arterial wall as a function of compliance is achieved by using the controllability and the observability criteria. Compliance is the parameter that specifies the elastic nature of the blood vessels. It is defined as the incremental change in volume that would result from an incremental change in pressure [1].

A well-known model to operate with the vascular characteristics is the Windkessel model[2,3].

RP: total peripheral resistance
C : arterial compliance
RC : resistance to blood flow
L : an inertial element
D1: valve

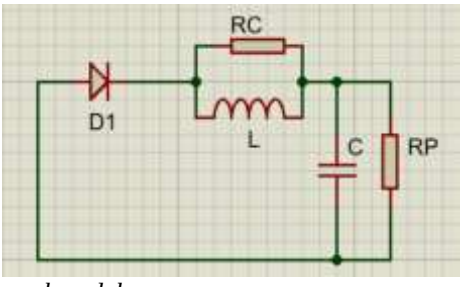

Figure 1. *Windkessel model.*

This model consists of a parallel connection of resistor and capacitor. The resistor Rp represents the total peripheral resistance and the capacitor C represents the compliance of the vessels. Rc, simulates the resistance to blood flow due to the aortic or pulmonary valve. L is an inertial element in parallel with the characteristic resistance Rc.

$$\begin{cases} \dot{x}(t) = Ax + Bu \\ y(t) = Cx \end{cases} \quad (1)$$

$\dot{x}(t)$: state vector A : state matrix

$y(t)$: output vector B : input matrix

$u(t)$: input vector C : output matrix

$$\begin{bmatrix} \dot{x}_1 \\ \dot{x}_2 \\ \dot{x}_3 \\ \dot{x}_4 \end{bmatrix} = \begin{bmatrix} 0 & 1 & 0 & 0 \\ -\frac{1}{C} & -\frac{1}{\tau} & 0 & 0 \\ 0 & 0 & 0 & 1 \\ 0 & 0 & -\frac{1}{L} & -\frac{\tau}{L} \end{bmatrix} \begin{bmatrix} x_1 \\ x_2 \\ x_3 \\ x_4 \end{bmatrix} + \begin{bmatrix} 0 & 1 \\ \frac{1}{C} & 0 \\ 1 & 0 \\ 0 & \frac{1}{L} \end{bmatrix} \begin{bmatrix} u_1 \\ u_2 \end{bmatrix} \quad (2.a)$$

$$\begin{bmatrix} y_1 \\ y_2 \end{bmatrix} = \begin{bmatrix} 1 & 0 & 0 & 0 \\ 0 & 0 & 1 & 0 \end{bmatrix} \begin{bmatrix} x_1 \\ x_2 \\ x_3 \\ x_4 \end{bmatrix} \quad (2.b)$$

where $\tau = R_p C$

u_1 : compliance , u_2 : inertia of blood flow

x_1: systolic pressure , x_2 : blood density

x_3: diastolic pressure , x_4 : arterial wall resistance

y_1: systolic pressure , y_2: diastolic pressure

2. MATERIALS AND METHODS

Procedure

Controllability

Constructing a controllability matrix

$$C(A,B) = [A \quad AB \quad A^2B \quad \cdots \quad A^{n-1}B] \quad (3)$$

Checking

$rank\, C(A,B) = rank([A \quad AB \quad A^2B \quad \cdots \quad A^{n-1}B]) = n$

Hence system (2) is controllable [2].

- General controller canonical form algorithm

In order to construct a similarity transformation (change of basis), n linearly independent vectors in $C(A,B)$ should be found.

Let k_i be the number of linearly independent vectors of $C(A,B)$ corresponding to b_i . k_i is called the controllability index or the kronecher index.

$k_1 \triangleq$ number of linearly independent vectors corresponding to b_1

$b_1, Ab_1, A^2b_1, \ \dots\dots\dots, A^{n-1}b_1$

Now we suppose we have determined the controllability indices k_i , i = 1,2, … , m. We can now construct the controllability base matrix $\bar{C}(A,B)$.

$$\bar{C}(A,B) = \begin{bmatrix} b_1,\ Ab_1\ ,\ A^2b_1,\ \dots\ , A^{k_1-1}\ b_1\ ,\ b_2\ ,\ Ab_2\ ,\ A^2b_2\ ,\ \dots, \\ A^{k_2-1}\ b_2\ ,\ \dots\dots,\ Ab_m\ ,\ A^2b_m,\ \dots\ ,\ A^{k_m-1}b_m \end{bmatrix} \tag{4}$$

We can construct a similarity transformation T_C such that $x_C = T_C x$, where

$$T_C = \begin{bmatrix} p_1\ p_1A\ \dots\ p_1A^{k_1-1}\ p_2\ p_2A\ \dots \\ p_2A^{k_2-1}\ \dots\ p_m\ \dots\ p_mA^{k_m-1} \end{bmatrix}^T$$

and $p_i = \sigma_i{}^{th}$ row of $\bar{C}(A,B)^{-1}$, i = 1,2, … , m , and $\sigma_i = \sum_{j=1}^{i} k_j$

The general controller canonical form of the matrices A, B and C are as follows:

$$A_C = T_C A T_C{}^{-1} = \begin{bmatrix} 0 & 1 & \cdots & 0 & & & & & & & \\ \vdots & \vdots & & \vdots & & & (0) & & & (0) & \\ 0 & 0 & \cdots & 1 & \cdots & & & & & & \\ x & x & \cdots & x & & x & \cdots & x & x & \cdots & x \\ & & \vdots & & \ddots & & & & & \vdots & \\ & & \vdots & & & & \ddots & & & \vdots & \\ & & & & & & & & 0 & 1 & \cdots & 0 \\ & & (0) & & & & (0) & & \vdots & \vdots & & \vdots \\ & & & & \cdots & & & & 0 & 0 & \cdots & 0 \\ x & x & \cdots & x & & x & \cdots & x & x & x & x & x \end{bmatrix}$$

$$B_C = T_C B = \begin{bmatrix} 0 & 0 & \cdots & 0 \\ \vdots & \vdots & & \vdots \\ 1 & x & \cdots & x \\ 0 & 0 & \cdots & 0 \\ \vdots & \vdots & & \vdots \\ 0 & 1 & \cdots & x \\ & \vdots & \vdots & \\ 0 & 0 & \cdots & 0 \\ \vdots & \vdots & & \vdots \\ 0 & 0 & \cdots & 1 \end{bmatrix} \text{ and } C_C = CT_C{}^{-1} = \begin{bmatrix} C_P & C_{P-1} & \dots & C_1 \end{bmatrix}$$

Pole Placement Using State Feedback

The pole placement method used is based on transforming the system into general controller form. We assume that all state variables are measurable and are available for feedback and that the pair

(A, B) is completely controllable, a desired closed-loop matrix Ad is constructed using the desired poles. Computing the feedback gain matrix K_C such that $(A_C - B_C K_C)$ has the desired set of eigenvalues. Finally we compute K from K_C, such that $K = K_C T_C$.

Transfer function

Consider a linear time invariant system (1). Using Laplace transfor

$$Y(S) = C(SI - A)^{-1} \times BU(S) \tag{5}$$

$$H(S) = \frac{Y(S)}{U(S)} = C(SI - A)^{-1} \times B \tag{6}$$

where I is an identity matrix

3. RESULTS AND DISCUSSIONS

Simulation and RESULT

3.1 Controllability for two categories of patients

3.1.a Normotensive subject

Table 1 list the data for patient with normal blood pressure and columns 2 and 3 show systolic and diastolic pressures, respectively. In column 4, the average pressure, Column 5 shows the pulse wave velocity and Column 6 lists the compliance calculated for each record. The values in column 7 indicate the inertia of the system, a parameter that is calculated by subtracting the diastolic pressure from the systolic pressure.

Table 1. *The data list for patient with normal blood pressure [5]*

Normotensive patients	Ps $mmHg$	Pd $mmHg$	Pm $mmHg$	VOP m/s	Cm $e^{-4}\ cm/mmHg$	L $mmHg$
1	93	57	69	10.39	4.03	36
2	127	80	96	12.25	4.15	47
3	104	66	79	9.05	5.03	38
4	120	89	99	10.78	3.43	31
5	91	75	80	10.94	3.14	16
6	97	70	79	11.11	3.57	27
7	118	66	83	9.28	5.36	52
8	85	51	62	7.80	6.40	34
9	96	61	73	8.83	4.08	35
10	117	77	90	9.80	3.62	40
11	119	64	82	10.69	4.00	55

- Using normotensive subject: patient 8
-

$c = 6.40$ $L = 34$ $\tau = 0.73$

Controllability matrix :

$$C(A,B) = \begin{bmatrix} 0 & 0.1563 & 1.0000 & 0 \\ 0.1563 & -0.2140 & 0 & -0.1563 \\ 1.0000 & 0 & 0 & 0.0294 \\ 0 & -0.0294 & 0.0294 & -0.0006 \end{bmatrix}$$

$$rank\, C(A,B) = 4$$

$$A_C = \begin{bmatrix} 0.0000 & 1.0000 & 0 & 0 \\ 0.0137 & -0.1765 & 0.0351 & -0.0875 \\ 0.0000 & 0.0000 & -0.0000 & 1.0000 \\ -0.1865 & -1.4649 & -0.1426 & -1.2149 \end{bmatrix}, B_C = \begin{bmatrix} 0.0000 & 0.0000 \\ 1.0000 & -0.0000 \\ -0.0000 & -0.0000 \\ 0.0000 & 1.0000 \end{bmatrix}$$

$$C_C = \begin{bmatrix} 1.6211 & 0.0001 & 1.2149 & 1.0000 \\ 0.1765 & 1.0000 & 0.1170 & 0.0000 \end{bmatrix}$$

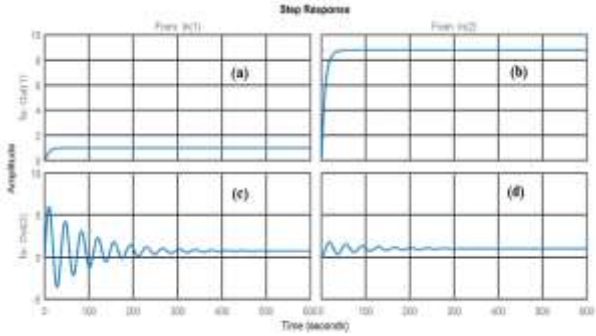

Figure 2. *Step response - normotensive patient.*

3.1.b Hypertensive subject

Table 2. *The data list for hypertension patient[5]*

Hypertensive patients	Ps $mmHg$	Pd $mmHg$	Pm $mmHg$	PWV m/s	Cm $e^{-4}\ cm/mmHg$	L $mmHg$
1	146	96	113	15.21	2.00	50
2	106	84	91	14.58	2.21	22
3	116	65	82	10.07	3.49	51
4	157	89	112	11.15	3.76	68
5	166	98	121	14.25	2.68	68
6	164	92	116	16.26	2.22	72
7	127	82	97	11.44	3.76	45
8	155	92	113	17.16	2.48	63
9	155	70	98	10.83	3.70	85
10	139	100	113	11.28	4.04	39
11	134	84	101	10.27	4.82	50
12	114	75	88	11.31	3.12	39
13	117	78	91	14.07	2.31	39
14	125	83	97	14.78	1.68	42

➢ Using hypertensive subject: patient 5

$c_h = 2.6800 \qquad \tau = 0.7300 \qquad L_h = 68$

- Controllablity matrix : $C(A,B)_h = \begin{bmatrix} 0 & 0.3731 & 1.0000 & 0 \\ 0.3731 & -0.5111 & 0 & -0.3731 \\ 1.0000 & 0 & 0 & 0.0147 \\ 0 & -0.0147 & 0.0147 & -0.0002 \end{bmatrix}$

$rank\ C(A,B)_h = 4$

- System (2) is controllable

$$A_{Ch} = \begin{bmatrix} 0.0000 & 1.0000 & 0.0000 & 0.0000 \\ 0.0001 & -0.3723 & 0.0147 & -0.2532 \\ 0.0000 & 0.0000 & 0.0000 & 1.0000 \\ -0.3722 & -0.9935 & -0.2787 & -1.0083 \end{bmatrix},\ B_{Ch} = \begin{bmatrix} -0.0000 & -0.0000 \\ 1.0000 & -0.0000 \\ -0.0000 & 0.0000 \\ 0.0000 & 1.0000 \end{bmatrix}$$

$$C_{Ch} = \begin{bmatrix} 1.6211 & 0.0001 & 1.2149 & 1.0000 \\ 0.1765 & 1.0000 & 0.1170 & 0.0000 \end{bmatrix}$$

Response for the hypertensive patient

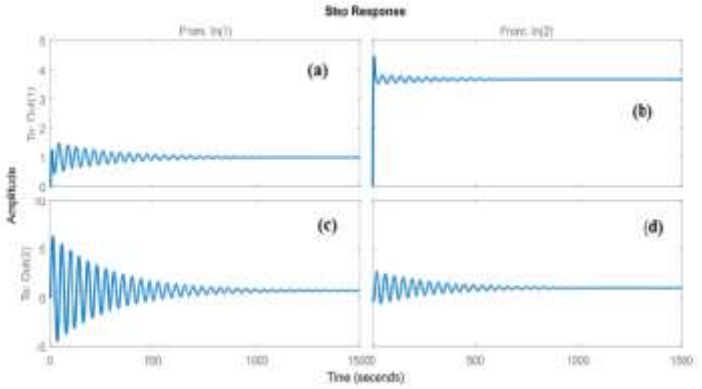

Figure 3. *Step response - hypertensive patient.*

3.1.c Comparison

Response for the two categories of patients

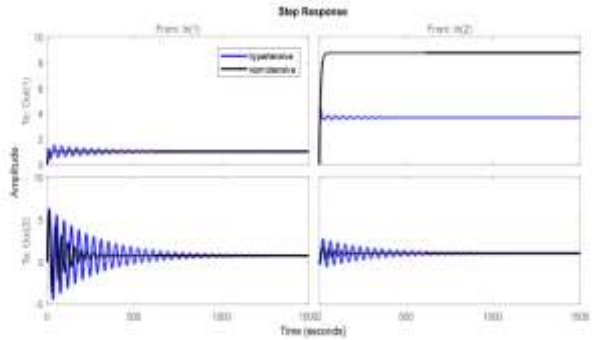

Figure 4. *Step response - two categories of patients.*

The recovery time of the arterial wall shown by the inertia of the blood flow is longer than the recovery time modeled for normotensive patients. The variation of compliance for diastolic pressure is higher for hypertensive patient.

3.2 Pole assignment using State feedback

The input controller $u = -Kx$

- For normotensive patient

with $K_c = \begin{bmatrix} -0.5 & -1.45 & 0.035 & -0.09 \\ -0.19 & -1.47 & 8 & -7 \end{bmatrix}$

the original gain matrix $K = K_c T_c = \begin{bmatrix} -0.4508 & -1.9830 & -1.1525 & -15.489 \\ -16.4787 & -105.4518 & 15.0806 & 323.878 \end{bmatrix}$

its norm is 341.687

- For hypertensive patient

With $K_c = \begin{bmatrix} -0.53 & -2.04 & 0.015 & -0.25 \\ -0.37 & 1 & 17.8 & 8 \end{bmatrix}$

the original gain matrix $K = K_c T_c = \begin{bmatrix} 0.2410 & --3.3992 & -1.5089 & -16.6944 \\ -13.3840 & -52.3699 & 9.1820 & 727.0308 \end{bmatrix}$

its norm is 729.280

The closed-loop matrix is $A_{cl} = A - BK$

Discussion

Small system feedback gains minimize the control energy, and prevent saturation of the controller elements and noise amplification. The norm of a matrix can provide a scalar measure to the magnitude of the matrix.

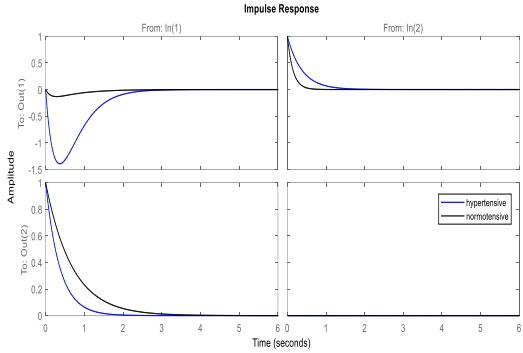

Figure 5. *Impulse response - closed-loop matrix.*

This figure shows the variation of compliance in time for systolic pressure and hypertensive patient presents higher peak pressure.

.

3.3 Transfer function

- Normotensive patient

$$H_{11}(s) = \frac{15.625}{100s^2+137s+16}$$

$$H_{12}(s) = \frac{100s+137}{100s^2+137s+16}$$

$$H_{21}(s) = \frac{100s+2}{100s^2+2s+3}$$

$$H_{22}(s) = \frac{2.94}{100S^2+2s+3}$$

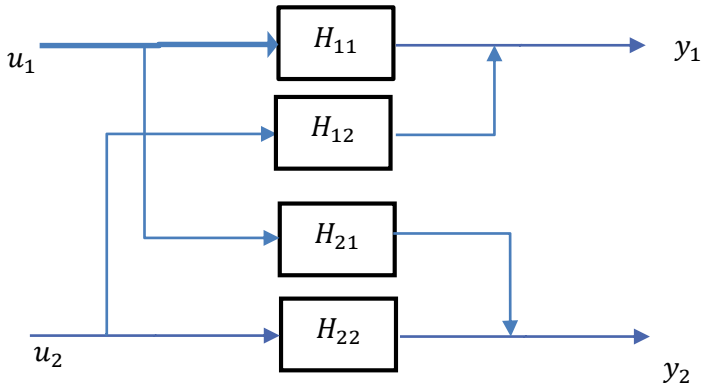

The response using Bode diagram

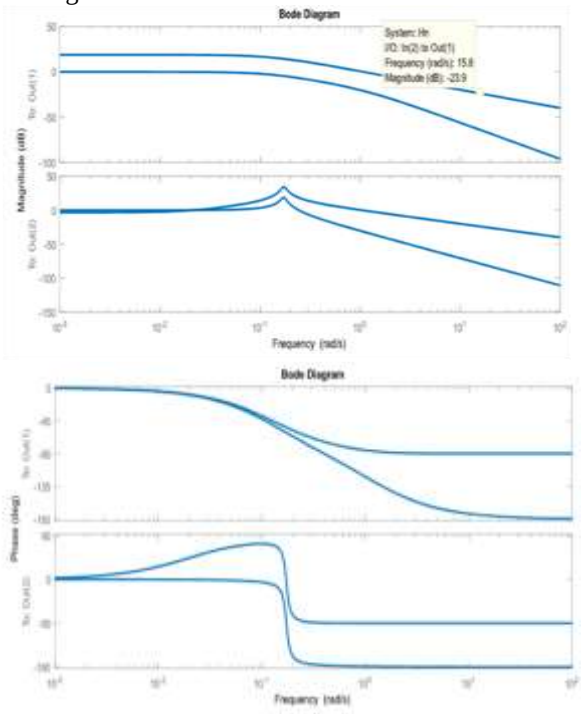

Figure 6. *Phase and magnitude - normotensive patient.*

- Hypertensive patient

$$H_{11}(s) = \frac{40}{100s^2+137s+40}$$

$$H_{12}(s) = \frac{100s+137}{100s^2+137s+40}$$

$$H_{21}(s) = \frac{10^4 s+107}{10^4 s^2+107s+150}$$

$$H_{22}(s) = \frac{150}{10^4 s^2+107s+150}$$

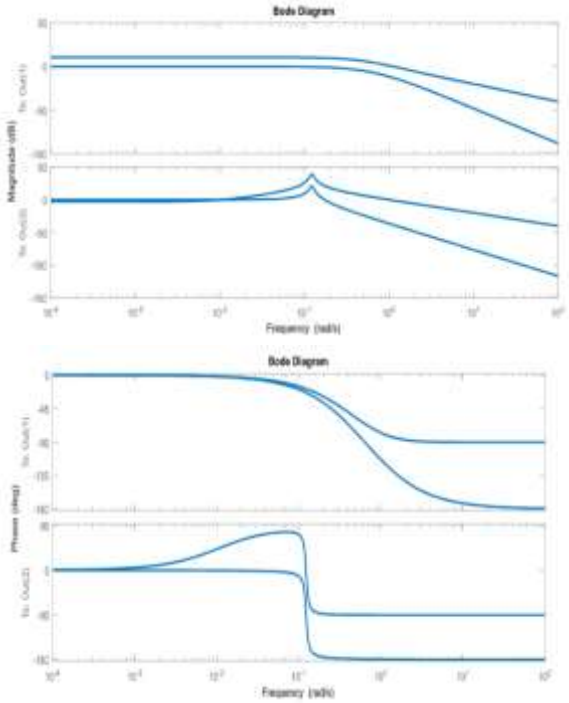

Figure 7. *Phase and magnitude - hypertensive patient.*

- Comparison

In this figure we can see that the phase angle of the normotensive patient is less than that of the hypertensive patient and the amplitude in frequency of the signal of the normotensive patient is greater than that of the hypertensive.

4. CONCLUSION

Our objective is to describe the dynamics of the cardiovascular system and perform an analysis of the associated stability by searching for input-output relationships in state space.

It is important to note that the K matrix is not unique to a given system, but depends on the desired positions of the closed-loop poles or the desired characteristic equation (which determine the speed and damping of the response.

All these results that are accessed from the use of the control tools, serve as a reference, a complementary observation when making a diagnosis or treatment by the medical professional and biomedical engineers.

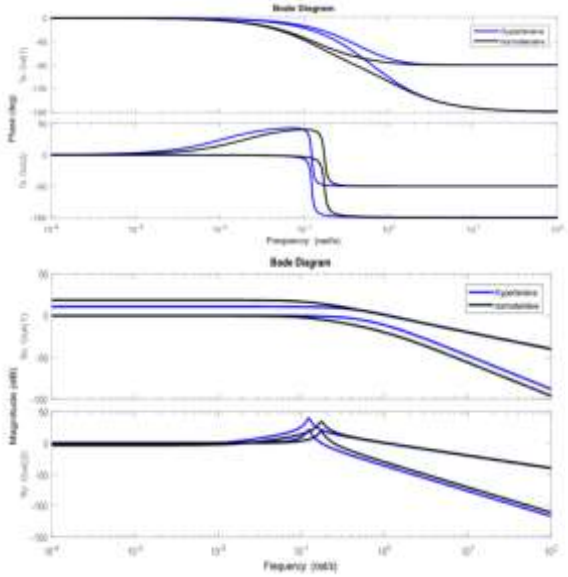

Figure 8. *Phase and magnitude - two categories of patients.*

REFERENCES

[1] JE Monzón., et al. "A multiple-input multiple-output system for modeling the cardiac dynamics". Proceedings of the 33th Annual International Conference of the IEEE-EMBS 2011.

[2] Alvarez P. C., Piacenza Á. E. , Schlesinger ., Luciana and Chiozza J. Á., Stability Control Applied to the Cardiovascular System. Analysis of its Internal Dynamics, Acta Scientific MEDICAL SCIENCES (ISSN: 2582-0931), Volume 8 Issue 3 March 2024.

[3] D. R. Kerner. "Solving Windkessel Models with MATLAB". 2009.

[4] K.Ogata ., Modern Control Engineering, Fifth Edition, Prentice Hall, 2010.

[5] Carlos Alvarez Picaza., et al. "The Effect of the Transfer Matrix Applied to MIMO Systems in the Analysis of Cardiovascular Dynamics". Acta Scientific Medical Sciences 5.8, 2021.

The impact of digitalization on the banking system

Valma PRIFTI[1] , Irida MARKJA[2], Dea SINOIMERI[3]

[1,2,3] *Polytechnic University of Tirana, Production and Management Department, Tirana-ALBANIA*
✉ *Corresponding author: vprifti@fim.edu.al*

ABSTRACT

Digitalization is a process of changing business models through the use of digital technologies to create revenue and value. This includes the integration of digital tools in management, communication, production, and customer service. The main objective of the research is to analyze the impact of digitalization on banking business and operations, discussing how this transformation will positively or negatively affect the bank. This study evaluates the efficiency of digitalizing banking services, identifies the advantages that digitalization brings to the banking business, and makes recommendations for improving the digitalization of business and banking operations.The information and data for this study are obtained through primary data from a survey of bank customers and secondary data from articles, reports, and websites. The research results indicate that digitalization has a positive impact on the bank's business and operations, enhancing service efficiency and customer loyalty. However, to improve digitalization, ongoing development, innovation, and enhancements are needed.

The aim of this study is to provide a clear and sustainable perspective for the future of financial functions in banks and to outline the necessary steps to achieve a financial system better suited for the digital age. The analyses and assessments made will help in crafting a sustainable vision for a financial infrastructure appropriate for our time.

KEYWORDS: *Digitalization, Services, Financial, Technology, Innovation, Adaptation, Efficiency, Customers, Strategy.*

1. INTRODUCTION

Digitization is a fundamental transformation in business modalities, including the use of digital technologies to create value and fulfill business goals. This includes the use of digital tools in business management, internal and external communication, and customer service. For banks in Albania, this process is a challenge and an opportunity to meet customer needs and increase their operational efficiency.Banks in Albania, as part of this change, are investing in technology and developing digital platforms to provide better services to their customers. This includes the development of mobile applications, internet banking platforms and other digital innovations to facilitate access and improve the customer experience.Also, digitization has brought new opportunities for banks in Albania, including digital payments, credit cards with advanced technology and real-time assistance services for customers. This makes banks more suitable to market demands and offer better and efficient services to their customers.Digitization: Digitization is the process of using technology to transform data into a digital format. For the banking industry, the use of digitization is important. Banks can provide better services to their customers by embracing digitalization. Digital technologies: Digital technology includes electronic devices, apparatus, structures, and sets of resources that use it for data processing or archiving, in addition to many other uses that increase employee productivity and efficiency. Banking services: The main functions of a bank include collecting savings, granting loans, helping operations, and offering a range of banking products, such as credit cards, loans, and savings accounts.

2. MATERIALS AND METHODS

Research design is a system or collection of strategies and techniques used to collect and examine data on certain factors in a given research question. In this study, quantitative analysis will be used. The research design of this study involves measuring the impact of digitization on the Bank's business and operations and how it affects the efficiency of services in the bank. Research methodologies are used to gather information or evidence for analysis in an attempt to find new details or develop deeper knowledge about a particular topic. The study population is a group of people who are involved in statistical studies or analyses. In the context of banks in Albania, for this study, the target population is the managers and employees of Credins Bank. Banka Banka Credins is interested in engaging experienced and competent employees and is interested in their career development. In addition, Credins Bank participates in various employee recruitment and training activities to enhance the empowerment of the local workforce. The target population for this analysis is limited to two branches of Credins Bank in Albania, where the number of managers and employees is about 34. For data analysis in the SPSS program, a statistical approach will be used. Credins is interested in hiring experienced and competent employees and is interested in their career development. In addition, Credins Bank participates in various employee recruitment and training activities to enhance the empowerment of the local workforce. The target population for this analysis is limited to two branches of Credins Bank in Albania, where the number of managers and employees is about 34. For data analysis in the SPSS program, a statistical approach will be used. The SPSS program is a programming and data analysis environment that provides a wide range of statistical operations to analyze and interpret data. This methodology of using the SPSS program will be explained in detail in the data analysis phase. Research hypotheses and prediction of results are included in the structure used before data collection, they explain the transitional relationship between independent and dependent variables. Two of the research hypotheses are:

Hypothesis 1: Digitization causes a positive impact on bank performance.

Hypothesis 2: Digitization has a significant impact on the activity, operations and efficiency of services in the bank. This will lead to increased customer loyalty.

Sampling technique

In this study, a probability sampling technique will be used, which is a well-known method of obtaining data from a population. For sample selection, all relevant data elements will be considered. The most common and objective method is simple random sampling, and for this study, a sample of 34 employees from Credins Bank will be used.

Sample Size

The sample size in research determines the number of participants in the study. This is related to the number of respondents in the questionnaire, who represent the study. The questionnaire for this study includes the employees of the Bank, with an estimated number of about 34 employees.

Search Tools

Research instruments include any tool used in a variety of sectors to collect, analyze and evaluate data related to the topic of study.

Data Collection Methods

In this study, the majority data collection technique will be used using a questionnaire created in an online program and then sending it to the employees of the Bank, as this method saves time and effort.

Data Analysis Method

The data analysis method usually involves several steps, such as obtaining, organizing and cleaning the data. In this study, data analysis technology will be used to analyze the research results. This includes the statistical analysis of research and is the process of preparing, designing, collecting

data, analyzing usefully and publishing the results of research, including all statistical methods that are used to help carry out studies.

3. RESULTS AND DISCUSSIONS

Research and findings

In this research, both quantitative and qualitative data collection were used. The sample of this study was 34 respondents. Google Forms in the Google Drive program were used to create the questionnaire, which includes demographic questions and closed questions. The number of respondents to the questionnaire is shown below. The answers were converted into numbers in the Excel program and then entered into the SPSS program. The questions were analyzed using graphs and tables to get clear and accurate information about the impact of digitization on the Bank's business and operations.

3.1 Analysis of the results of the demographic questions (Qualification of respondents)

Gender responses: The results show the number of male respondents 55.9% and female 44.1% who completed the questionnaire. The number of men exceeds the number of women in the Bank.

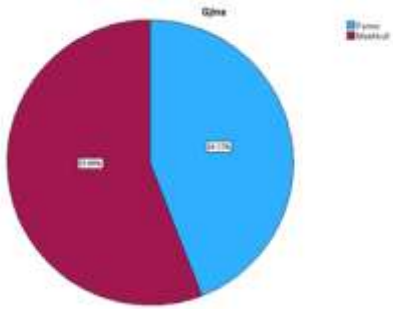

Figure 1. *Gender response (Source: SPSS)*

Age responses: The results show the age of the respondents who completed the questionnaire, as the percentage of respondents who were between 20-29 years old was 32.4%, while those who were between 30-39 years old were 41.2% and those who were between 40-49 years old were 17.6%, while the group aged 49 years and above was 8.8%. The largest age group for Bank employees is between 30-39 years

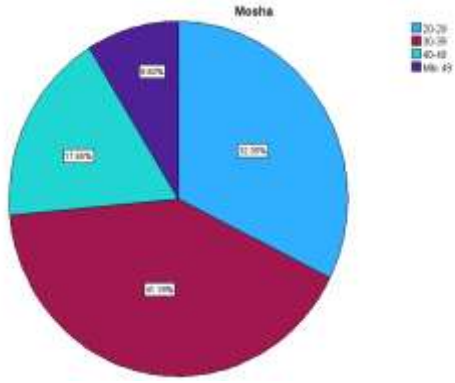

Figure 2. *Age response (Source: SPSS)*

Qualification of respondents: The results show the qualifications of the respondents who completed the questionnaire, such as the percentage of employees who had high school was 5.9%, and their number was 2, the percentage of bachelor's degree was 41.2%, while the percentage of master's degree was 52.9% , and their number was 18. The highest percentage of qualifications of employees in the Bank was a master's degree, which reached 52.9%.

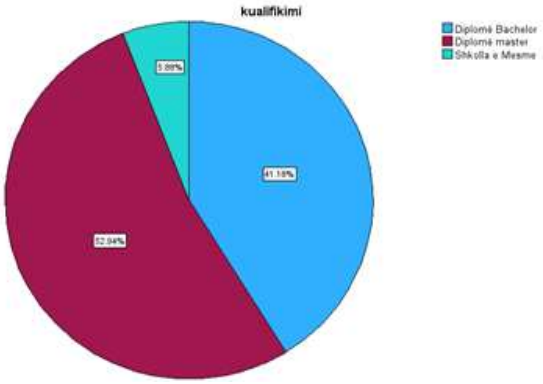

Figure 3. *Qualification of respondents (Source: SPSS)*

3.2 Linear Regression Analysis

Through the SPSS Statistic program, hypothesis testing was done. Below are the results: H0: Digitization causes a positive impact on bank performance; H1: Digitalization has a significant impact on the activity, operations and efficiency of services in the bank, and this will lead to increased customer loyalty. Below is the analysis of H0 and H1, where they are presented in tabular form Model Summary, ANOVA, Coeffients H0 / H1.

Table 1. *Model Summary H0*

Model Summary				
Model	R	R Square	Adjusted R Square	Std. Error of the Estimate
1	.500[a]	.250	.049	.712

R (Multiple Correlation): R = 0.500 indicating a moderate correlation between these variables.
R Square (Coefficient of determination): $R^2 = 0.250$ This indicator shows that 25% of the variation in digitization in bank performance is explained by the model that includes the independent variables.
Adjusted R Square (Adjusted coefficient of determination): Adjusted $R^2 = 0.049$ The value 0.049 indicates that the model explains 4.9% of the variation in the dependent variable.
Std. Error of the Estimate: 0.712 A standard error value of 0.712 indicates the degree of accuracy of the model's predictions. Any lower value of this standard indicates a higher accuracy of the model.

Table 2. *ANOVA,H0*

Model		Sum of Squares	df	Mean Square	F	Sig.
1	Regression	4.396	7	.628	1.240	.317b
	Residual	13.163	26	.506		
	Total	17.559	33			

ANOVA shows that the regression model has an F-test value of 1.240, the P-value (0.317) is greater than the significance level (usually 0.05), which means that the model is not statistically significant. This indicates that there is insufficient evidence to assert that the selected independent variables significantly affect the dependent variable Confidence level.

Table 3. *Coefficients, H0*

Coefficientsa,						
Model		Unstandardized Coefficients		Standardized Coefficients	t	Sig.
		B	Std. Error	Beta		
1	(Constant)	1.759	1.562		1.126	.270
	Technological level	.307	.261	.288	1.177	.250
	Continuous training	-.485	.316	-.335	-1.533	.137
	Advantages of digitization/ Improvement of services	-.202	.184	-.289	-1.100	.281
	Advantages of digitization / Cost reduction	.271	.191	.318	1.422	.167
	Advantages of digitization/Reliability	-.155	.224	-.159	-.692	.495
	Advantages of digitization/ Increased competition	.073	.254	.058	.288	.776
	Bank adjustment	-.195	.626	-.064	-.311	.758
a. Dependent Variable: Confidence level						

H1: Digitalization has a significant impact on the activity, operations and efficiency of services in the bank, and this will lead to increased customer loyalty.

Table 4.*: Model Summary, H1*

Model Summary

Model	R	R Square	Adjusted R Square	Std. Error of the Estimate
1	.825a	.681	.445	.543

R (Multiple Correlation): R = 0.825;
The Pearson correlation between the independent and dependent variables is 0.825. This indicates a strong positive correlation between the variables. An R closer to 1 suggests a stronger relationship between the variables.

R Square (Coefficient of determination): $R^2 = 0.681$;

This shows the percentage of variation explained by the model in the dependent variable (Bank Adjustment in this case). In this case, about 68.1% of the variation in the bank's adaptation level can be explained by the variables included in the model. This is a medium explanation of variation compared to other values, but suggests that the model has a good ability to predict bank adaptation based on the variables included.

Adjusted R Square (Coefficient of determination adjusted): Adjusted $R^2 = 0.445$;

This is a refined version of R Square, considering the number of variables included in the model and the sample size. In contrast to R Square, the lower Adjusted R Square suggests that a large proportion of the variation in bank adjustment is explained by the variables used in the model.

Std. Error of the Estimate: 0.543;

This is a measure of the accuracy of the model's predictions. The lower this value, the better the performance of the model in fitting the data. In this case, a Std. The error of 0.543 indicates that the model predictions have a circular distribution around the true values of bank adaptation.

Table 5. ANOVA,H1

Model		Sum of Squares	df	Mean Square	F	Sig.
1	Regression	11.951	14	.854	2.893	.016b
	Residual	5.607	19	.295		
	Total	17.559	33			

a. Dependent Variable: Confidence level

b. Predictors: (Constant), Challenge for the bank / Adapting to change, Continuous training, Challenge for work / Increasing responsibilities, Adapting the bank, Challenge for customers / Adapting to technology, Challenge for work / Technological services, Challenge for customers / Data privacy, Challenge for Bank / Data Security, Customer Challenge / Accessibility, Work Challenge / Adaptation to Technology, Customer Challenge / Lack of Staff Support, Bank Challenge / Compliance with Laws, Work Challenge / Data Security, Challenge for the bank / Adaptation to technology.

The ANOVA shown shows that your model has a statistically significant impact on the confidence level. The high F-statistic and low p-value (0.016) suggest that the variables used in the model explain a significant portion of the variation in the confidence level.
The data show that some challenges defined as "work" and "customers" have a significant impact on the level of trust, while other variables do not have a statistically significant impact. This analysis

is important to understand which factors may be more critical in adapting the bank to this particular context.

The statistically significant positive correlation between Confidence Level and Work Challenge / Technology Services (-0.371*, p = 0.031) suggests that an increase in challenges identified as "work" is associated with a decrease in confidence level. Whereas, the statistically significant negative correlation between Confidence Level and Work Challenge / Data Security (-0.247, p = 0.159) suggests that an increase in challenges identified as "work" is associated with a decrease in confidence level, however this is not statistically significant at the standard significance level.

4. CONCLUSIONS

In this paper, the survey included 12 questions, spanning demographic questions and questions related to the topic of the study. There were four main objectives.

The first objective was to understand the impact of digitization on the Bank's business and operations. Digitization is a key factor for the bank's success, improving services and trying to meet customers' needs efficiently.

The second objective was to evaluate the efficiency of digital services in the Bank. The Bank works to support the latest technologies to provide more efficient services and to improve existing services.

The third objective was to identify the advantages of digitization in the Bank's business and operations: Digitization facilitates banking processes and increases the sustainability of banking services.

The fourth objective was to provide recommendations for improving the digitalization of the Bank's business and operations. Recommendations include the use of advanced technologies and investments in updated platforms and applications to ensure a better experience for customers.

In conclusion, the study has proven that digitization has a substantial and positive impact on the bank's business and operations. The results of the statistical analysis show a strong connection between the level of digitization and the increase in the efficiency of banking services, also contributing to the increase in customer loyalty. Digitization brings numerous benefits to banks, including improving the speed and accuracy of transactions, reducing operating costs and providing more personalized services to customers. The implementation of new technologies, such as artificial intelligence and big data analysis, allows banks to offer better and safer solutions to their customers.The study has identified some important challenges that banks must face in the digitization process. These include the need for ongoing staff training, operational challenges and addressing customer expectations. Our analysis shows that these challenges have a negative impact on the level of customer loyalty. For example, lack of adequate training can lead to ineffective use of technology, resulting in inadequate customer service.

Research recommendations include improving digitization processes in the bank by addressing identified challenges and focusing on customer benefits and needs. Banks must continuously invest in technology and innovation to improve the customer experience and increase competitiveness in the financial market. Continuous training of personnel and adaptation of services according to customer expectations are necessary steps for success in this process. In conclusion, this study proves that digitization is not only an opportunity, but a necessary requirement for the success of banks in a diverse and fast technological environment.

As banks adapt and evolve to this context, they can ensure a better customer experience and achieve long-term success in the financial industry. Facing the challenges of digitization and taking advantage of the opportunities offered by technology can create a more efficient, safer and more customer-oriented banking system.

Acknowledgment
This study was carried out with the cooperation and financial support of AKKSHI within the National Project "Digitalization of industrial and service companies in Albania" in Polytechnic University of Tirana.

REFERENCES

[1] K. Yeganegi, S. Safaeian, "Design of Project Management Information Systems", International Conference on Industrial Engineering and Operations Management, pp. 3-6, 2012.
[2] A. Kocak, M.C. Taplamacioglu, H. Gozde, "General overview of area networks and communication technologies in smart grid applications", International Journal on Technical and Physical Problems of Engineering, Issue 46, Vol.13, No. 1, pp. 103-110, March 2021.
[3] N. Vurukonda, B.R. Thirumala, T.R. Burramukku, "A secured cloud data storage with access privileges", International Journal of Electrical and Computer Engineering, Vol. 6, No. 5, pp. 2338-2344, 2016.
[4] V. Prifti, "Optimizing a business in e-commerce", American Journal of Multidisciplinary Research and Development, Vol. 4, No. 3, pp. 54-60, 2022.
[5] B. Jabir, N. Falih, "Big Data analytics opportunities and challenges for the smart enterprise", International Journal on Technical and Physical Problems of Engineering, Issue 47, Vol.13, No. 2, pp. 20-26, June 2021.
[6] M.A. Salih, M.M. Hamad, W.M. Jasim, "Optimization feature selection techniques for big data using multi-phase particle swarm optimization algorithm", International Journal on Technical and Physical Problems of Engineering, Issue 56, Vol.15, No. 3, pp. 188–196, September 2023.
[7] V. Prifti, "Optimizing project management using artificial intelligence", European Journal of Formal Sciences and Engineering, Vol. 5, No. 1, pp. 29-37. 2022.
[8] V. Prifti, M. Aranitasi, "E-Commerce Business Model in KLER Enterprise for Shirt Manufacturing", International Journal of Innovative Technology and Interdisciplinary Sciences, Vol. 5, No. 1, pp. 858-864, 2022.
[9] A. El Kihel, H. Gziri, A. Bakdid, "Method of implementing maintenance 4.0 in industry- a case study of an industrial system", International Journal on Technical and Physical Problems of Engineering, Issue 49, Vol.13, No. 4, pp. 78-84, December 2021.
[10] V. Prifti, K. Dhoska, "Information systems in project management and their role in decision making", International Journal on Technical and Physical Problems of Engineering, Issue 53, Vol.14, No. 4, pp. 189–194, December 2022.
[11] V. Prifti, I. Markja, K. Dhoska, A. Pramono, "Management of information systems, implementation and their importance in Albanian enterprises", IOP Conference Series Materials Science and Engineering, Vol. 909, pp. 1-11, 2020.
[12] J.C. Bertot, U. Gorham, P.T. Jaeger, L.C. Sarin, H. Choi, "Big Data", Open government and e-government issues, policies and recommendations Information Policy, Vol. 19, No.1-2 pp. 5-16, 2014.

A Variable density dynamic killing method and simulation system for ultra-deep wells in fractured formations

Wang Chen[1], Jun Li[2] ✉, Hongwei Yang[1], Geng Zhang[1], Biao Wang[1]

[1] China University of Petroleum-Beijing, 18 Fuxue Road, Changping District, Beijing, China
[2] China University of Petroleum-Beijing at Karamay, 355 Anding Road, Karamay District, Karamay City, Xinjiang, China
✉ Corresponding author: lijuncup2007@163.com

ABSTRACT

To address the need for rapidly reducing wellhead back pressure and balancing formation pressure during the well-killing process in ultra-deep fractured formations, this paper integrates the principle of variable density dynamic killing. Based on drift flow theory and transient heat transfer theory between the wellbore and formation, while considering the changes in drilling fluid properties under high-temperature and high-pressure conditions, a transient non-isothermal multiphase flow model suitable for variable density dynamic killing was established. This model enables precise pressure curve calculations and fluid distribution tracking within the wellbore, achieving dynamic simulations of the variable density killing process. Field case validation shows the model achieves a calculation accuracy of over 90%. Furthermore, a variable density dynamic killing simulation software tailored for fractured formations was developed. The results indicate that the proposed method and system can efficiently and accurately design killing parameters and conduct dynamic simulations, providing robust technical support for reducing well control operation risks and improving the success rate of killing. This has significant theoretical and practical implications for well control safety in ultra-deep fractured formations.

KEYWORDS: *Fractured Formations, Ultra-deep Wells, Well Control, Variable Density Dynamic Killing.*

1. INTRODUCTION

China's deep and ultra-deep oil and gas reservoirs are widely distributed, with abundant resources and significant exploration and development potential. In regions such as the Tarim Basin, Sichuan Basin, and Ordos Basin, multiple major oil and gas fields have been discovered and successfully developed[1,2]. Among them, deep carbonate oil and gas reservoirs exhibit immense development potential. However, the exploitation of these reservoirs faces numerous challenges. Due to their long geological history, great burial depth, high bottom-hole temperatures, complex formation pressure systems, and extensive fracturing, the narrow safe pressure window significantly increases the difficulty of handling overflow during drilling[3,4]. This has become a major constraint on the efficient and safe drilling of deep carbonate reservoirs. Statistics show that compared to shallow wells, high-pressure and high-temperature wells have a 20% higher frequency of blowouts and overflow incidents, with non-productive time and economic costs more than tripling[5,6].

When drilling into fractured formations and encountering an influx, conventional well-killing methods, also known as constant bottom-hole pressure methods, are typically employed. These methods maintain bottom-hole pressure equal to or slightly greater than the formation pressure, using circulation to displace formation fluids from the wellbore to the surface, while relying on the hydrostatic pressure of the kill fluid to balance the formation pressure. Based on the characteristics of the well-killing process and circulation time, these methods are further categorized into the

Engineer's Method and the Driller's Method. While both approaches are relatively simple in terms of parameter calculation and operational control, their application in ultra-deep fractured formations carries certain risks[7,8]. For instance, the Engineer's Method, due to its longer shut-in time, can increase the risk of secondary formation fluid invasion, leading to more complex influx scenarios. Conversely, the Driller's Method, while involving shorter shut-in times, often results in excessively high casing pressures at the wellhead during the killing process, potentially causing equipment failure or even formation fracturing.

To address the need for rapidly reducing wellhead back pressure and balancing formation pressure during the well-killing process in ultra-deep fractured formations, a variable density dynamic pressure control method was proposed in the field. This method combines high-density and low-density drilling fluids to quickly lower wellhead pressure, thereby reducing the burden on wellhead equipment. However, the variable density dynamic killing method remains in an exploratory stage. Existing models often neglect the effects of high-temperature and high-pressure conditions on the rheological properties of drilling fluids, which could lead to deviations or failures under the complex conditions of ultra-deep wells.

Therefore, it is essential to further refine the theoretical foundation of variable density dynamic killing and develop dynamic killing models that account for the rheological behavior of drilling fluids, particularly under high-temperature and high-pressure conditions. These advancements will provide more precise and reliable technical support for well control in ultra-deep wells, significantly improving the safety and success rate of well control operations.

2. MATERIALS AND METHODS

Variable Density Dynamic Killing Method

2.1 Well-Killing Principle

Variable density dynamic well killing is a technique in which the density of the kill fluid changes two or more times during the well-killing process (excluding the Driller's Method)[9]. The core principle is to leverage the synergistic effects of kill fluids with different densities to quickly reduce wellhead pressure while preventing formation fracturing. The specific process is as follows:

Heavy Fluid Injection Stage: At the initial stage of the well-killing process, a high-density kill fluid (heavier than the final design density) is pumped into the wellbore. As the high-density fluid gradually enters the drill string and eventually reaches the annulus, the annular pressure drops rapidly, mitigating the risk of excessive wellhead pressure. The objective of this stage is to quickly adjust the static pressure of the fluid column to create safe conditions for subsequent operations.

Light Fluid Injection Stage: After the high-density fluid injection is complete, a low-density kill fluid (designed to achieve the final target density) is pumped into the wellbore to prevent formation fracturing caused by excessive pressure. The low-density fluid gradually balances the downhole pressure, while simultaneously circulating out formation fluids that have invaded the annulus, restoring bottom-hole pressure equilibrium.

As shown in Figure 1, this process typically takes slightly longer than the Engineer's Method in terms of circulation time. However, it results in lower wellhead back pressure and overall wellbore pressure during the influx displacement process, offering a safer and more controlled operation.

2.2 Mathematical Model

For the wellbore flow model[10], the gas-phase and liquid-phase mass conservation equations, along with the mixed-phase momentum conservation equation, are used to describe single-phase and gas-liquid two-phase flow in the wellbore (Eq. (1-3)).

Gas-phase Mass Conservation Equation:

$$\frac{\partial}{\partial t}\left(\rho_g \alpha_g A\right)+\frac{\partial}{\partial t}\left(\rho_g \alpha_g v_g A\right)=0 \tag{1}$$

Liquid-phase Mass Conservation Equation:

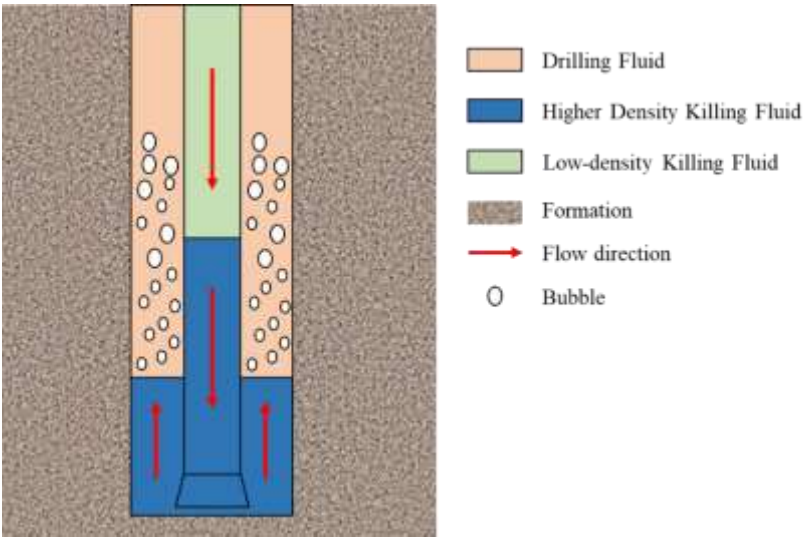

Figure 1. *Variable Density Dynamic Well-Killing Circulation Diagram.*

$$\frac{\partial}{\partial t}\left(\rho_l \alpha_l A\right)+\frac{\partial}{\partial t}\left(\rho_l \alpha_l v_l A\right)=0 \tag{2}$$

Mixed-phase Momentum Conservation Equation:

$$\frac{\partial}{\partial t}\left(\rho_g \alpha_g v_g A+\rho_l \alpha_{l} v_l A\right)+\frac{\partial}{\partial z}\left(\rho_g \alpha_g v_g^2 A+\rho_l \alpha_l v_{l}^2 A\right)+\left(\rho_g \alpha_g+\rho_l \alpha_l\right) g\sin\theta A + \frac{\partial(pA)}{\partial z}+A\frac{\partial p_f}{\partial z}=0 \tag{3}$$

Where, ρ is the density, kg/cm^3； α is the volume fraction； v is the flow rate, m/s; A is the annulus cross-sectional area, m^2; t is the time, s; z is the axial space, m; the subscripts l, g denote the fluid of the drilling mud, the gas, respectively; P is the wellbore pressure, Pa; f is the friction coefficient; d_h is the equivalent diameter, m; g is the acceleration of gravity, m^2/s; θ is the well inclination angle, rad.

Based on the First Law of Thermodynamics, Considering the Joule-Thomson effect of gases, heat exchange between the annular fluids and the surrounding environment, and thermal convection between the formation gas-liquid mixture and the wellbore fluids, energy conservation equations are established for both the drill string and the annulus, as shown in Eq(4) and (5).

Energy Conservation Equation Inside the Drill String:

$$Q_p - \rho_l q_l C_l \frac{\partial T_p}{\partial z} - 2\pi r_{pi} h_{pi} \left(T_p - T_w\right) = \rho_l C_l \pi r_{pi}^2 \frac{\partial T_p}{\partial t} \tag{4}$$

Energy Conservation Equation Inside the Annulus:

$$\begin{aligned} &Q_a + \left(\rho_g C_g\, q_g \alpha_g + \rho_l C_l q_l \alpha_l\right)\frac{\partial T_a}{\partial z} + 2\pi r_{ci} h_{ci}\left(T_c - T_a\right) + 2\pi r_{po} h_{po}\left(T_w - T_a\right) \\ &= \left(\rho_g C_g\, \alpha_g + \rho_l C_l \alpha_l\right)\pi\left(r_{ci}{}^2 - r_{po}{}^2\right)\frac{\partial T_a}{\partial t} \end{aligned} \tag{5}$$

Where: Q is Power of viscous friction, W/m; q is Fluid flow rate, L/s; T is Temperature, K; h is Convective heat transfer coefficient, W/(m²·℃); k is Thermal conductivity, W/(m·℃); c is Specific heat capacity, J/(kg·℃) ; z is Axial coordinate, m; r is Radial coordinate, m; Subscripts: l is Liquid phase; g is Gas phase; p: Drill string; a is Annulus; p_i is Inner wall of the drill string; p_o is Outer wall of the drill string;

In addition, the transient heat transfer model for the formation region, thermal properties of fluids, and convective heat transfer coefficients can be referenced from Document 11[11].

In ultra-deep drilling operations, high temperatures cause fluid expansion, while high pressures result in fluid compression. Under high-temperature and high-pressure conditions, the properties of drilling fluids change, which significantly affects wellbore pressure dynamics[12,13]. Therefore, it is essential to consider the variations in drilling fluid properties under these conditions when analyzing wellbore pressure.

Experimental results on the rheological behavior of drilling fluids under high-temperature and high-pressure conditions indicate that the Herschel-Bulkley rheological model can accurately characterize the fluid behavior. Using multivariate nonlinear regression methods, the rheological parameters of the drilling fluid have been fitted into the following calculation formulas, as represented by Eq(6)–(8).

$$\tau_0 = 2.9644 \times \mathrm{e}^{[2.4\times10^{-3}(T-T_0)-4.9433\times10^{-9}(P-P_0)-2.2170\times10^{-5}(T-T_0)^2]} \tag{6}$$

$$K = 0.7413 \times \mathrm{e}^{[8.7812\times10^{-4}(T-T_0)-1.5552\times10^{-10}(P-P_0)-1.7509\times10^{-6}(T-T_0)^2]} \tag{7}$$

$$n = 0.5440 \times \mathrm{e}^{[-6.5\times10^{-3}(T-T_0)+6.8526\times10^{-10}(P-P_0)+8.1477\times10^{-6}(T-T_0)^2]} \tag{8}$$

Where: T_0 is Initial temperature, ℃; P_0 is Initial pressure, Pa; T is Actual temperature, ℃; P is Actual pressure, Pa; τ_0 is Yield stress, Pa; K is Consistency coefficient, Pa·sⁿ; n is Flow index (dimensionless)

The aforementioned variable density dynamic well-killing model is a highly nonlinear partial differential equation, which makes direct solving difficult. Therefore, a fully implicit finite difference scheme is employed to discretize the governing equations[14]. By iteratively solving the discretized model, the pressure curve can be calculated, and the real-time tracking of fluid

distribution in the wellbore can be achieved, enabling the dynamic simulation of the variable density well-killing process.

3. RESULTS AND DISCUSSIONS

Model Validation

To verify the accuracy of the variable density dynamic well-killing model, the post-overflow well-killing data from well X-1 was used for validation. The parameters of the kill fluids used during different time periods are shown in Table 1.

By comparing the simulated standpipe pressure with the actual riser pressure during the well-killing process (Figure 2), the calculated pressure values closely match the measured values, with an average calculation accuracy of 92.3%.

Table 1. *Kill Fluid Properties for Well X-1.*

Time Period	Killing Fluid Density (g/cm^3)	Viscosity (mPa·s)
a-b	2.23~2.25	20.0
c-d	2.25~2.27	20.0
e	2.27	21.0

The figure highlights two areas with significant discrepancies:Measurement Error (Area ①): During this time, the measurement-while-drilling tool failed to transmit signals, resulting in a large discrepancy between the measured riser pressure and the true value. Operational Error (Area ②): During this time, the pumps were stopped for a 30-minute static observation, causing the measured riser pressure to approach zero. This discrepancy was due to manual intervention.

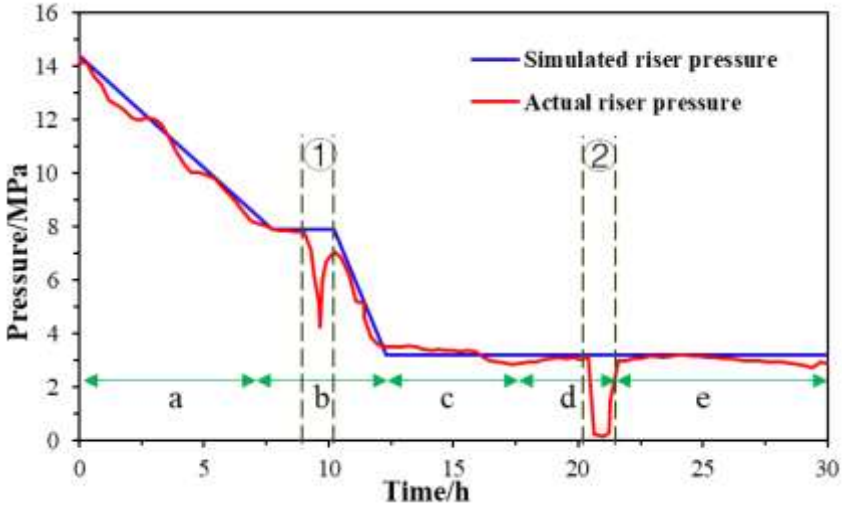

Figure 2. *Comparison of Simulated and Actual Riser Pressure for Well X-1.*

Software Development

Based on the variable density dynamic well-killing mathematical model proposed in this study, a variable density dynamic well-killing calculation software was developed using C#. The software architecture is shown in Figure 3. This software enables convenient calculation of critical well control parameters during the well-killing process, including overflow volume, wellbore pressure, and kill fluid position.

The software architecture is divided into three main components. (1)Data Processing Module: This module is responsible for inputting basic parameters, including well depth, wellbore structure, drill string configuration, and fluid properties. It serves as the foundation for subsequent calculations and simulations. (2)Simulation Calculation Module: Based on the input parameters and mathematical model, this module performs calculations for variable density dynamic well-killing parameters. Key functions include kill fluid density design, pressure curve generation, and fluid position tracking. (3)Data Output Module: This module outputs the calculation results and generates well-killing operation sheets, facilitating practical use during well-killing operations.

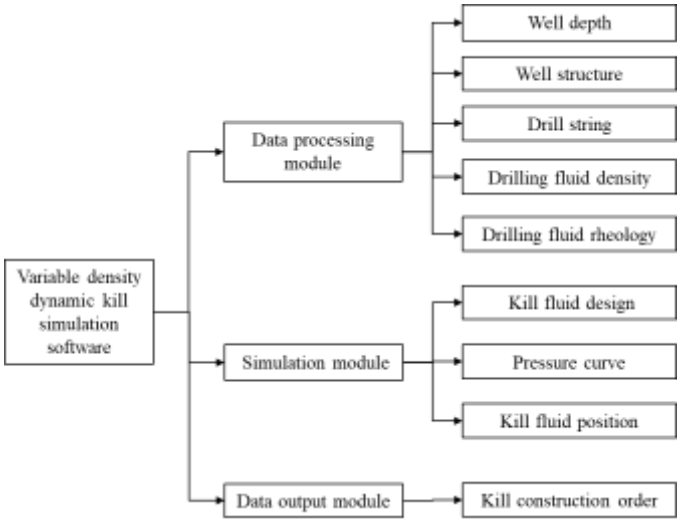

Figure 3. *Variable Density Dynamic Well-Killing Software Architecture.*

4. CONCLUSION

（1）This study addresses the requirements for rapidly reducing wellhead back pressure and balancing formation pressure during the well-killing process in ultra-deep fractured formations, and analyzes the variable density dynamic well-killing process.

（2）It incorporates the effects of high-temperature and high-pressure conditions on the rheological properties of drilling fluids, establishes a variable density dynamic well-killing model, and validates its accuracy and stability through a field well-killing case study.

（3）Based on the mathematical model, a software system with variable density dynamic well-killing calculation functions was developed, enabling convenient and accurate design and simulation of variable density dynamic well killing.

REFERENCES

[1] Y.P. Hu , L. Wang , W.ZH. Ding , et al.A rate decline model for acidizing and fracturing wells in closed carbonate reservoirs[J].Arabian Journal of Geoences, 2019, 12(7). *DOI:10.1007/s12517-019-4348-6.*

[2] L.F. Zhang, F.J. Zhou, J.Y. Mou, et al. Research on sensitivity damage of naturally fractured carbonate reservoirs in Ordos Basin[J].Arabian Journal of Geosciences, 2019, 12(18). *DOI:10.1007/s12517-019-4805-2.*

[3] X.L. Mao, Y.T. Liu, W.L. Guan, et al. Experimental and numerical simulation on the influence of anisotropic fracture network deformation to shale gas percolation[J].Arabian Journal of Geosciences, 2018, 11(20). *DOI:10.1007/s12517-018-3973-9.*

[4] W.K. Zheng, Y.T. Liu, J.SH. Huang, et al. Study on the optimal development method for offshore buried hill fractured reservoirs[J]. Arabian Journal of Geosciences, 2018, 11(20): 1-6. *DOI:10.1007/s12517-018-3965-9.*

[5] Z.H. Li, ZH.M. Yin, D.Q. Tian. Research Progress on Well Control Risk Management Technology for Deep Sea and Ultra-deep Water Drilling [J]. Drilling & Production Technology, 2024,47(04):8-17+6. *DOI ： 10.3969/J.ISSN.1006-768X.2024.04.02*

[6] Y.J. Zhou, X.F. Li, A. Wojtanowicz, et al. Multidimensional Evaluation for Safe and Efficient Killing Using Dynamic Kill Method: A Case Analysis in China[J]. *DOI:10.2118/188636-MS.*

[7] B.J. Sun, CH.S. Wang, G.ZH. Xin, et al.Research on Well Killing Technology in Drilling Complex Pressure System Formation [J]. Drilling & Production Technology, 2024, 47(4):42-50. DOI:10.3969/J.ISSN.1006-768X.2024.04.06.

[8] X.ZH. Wu, Y. Qing, D.H. Li. Research on Quantitative Risk Assessment Method for Kick Handling [J]. Drilling & Production Technology, 2024,47(4): 35-41. DOI: 10.3969/J.ISSN 1006-768X.2024.04.05.

[9] H.B. Zhou, M.G. Sun, X.M. Niu, et al. A Novel Multi-Density Dynamic Well Killing Method for Ultra-Deep Wells and the Simulation System[C]. Abu Dhabi International Petroleum Exhibition & Conference.2018. *DOI:10.2118/193216-MS.*

[10] H.W. Yang,J. Li, G.H. Liu. Development of a Dual-Measured-Points Early Gas Kick Detection Method based on the pressure responses of two PWD tools[J]. Arabian Journal of Geosciences, 2020, 13(16):1-8. *DOI:10.1007/s12517-020-05799-5.*

[11] H.W. Yang, J. Li, G.H. Liu, et al. Numerical analysis of transient wellbore thermal behavior in dynamic deepwater multi-gradient drilling[J]. Energy, 2019, 179(JUL.15):138-153. *DOI:10.1016/j.energy.2019.04.214.*

[12] C.B. Orun, J.U. Akpabio, O.E. Agwu. Drilling fluid design for depleted zone drilling: An integrated review of laboratory,field,modelling and cost studies[J]. Geoenergy Science and Engineering, 2023. *DOI:10.1016/j.geoen.2023.211706.*

[13] P.J. Liu, J.Y. He, Y. Zhang, et al. Study on effects of fluid properties on borehole pressure under temperature and pressure coupling in high temperature deep wells [J]. Drilling Fluid & Completion Fluid, 2024, 41(3):288-295. *DOI: 10.12358/j.issn.1001-5620.2024.03.002*

[14] H. Shi, J.A. Holmes, L.R. Diaz,et al. Drift-Flux Parameters for Three-Phase Steady-State Flow in Wellbores[J]. Spe Journal, 2005, 10(2):p.130-137. *DOI:10.2118/89836-pa*

Comparison of the Performance of SSD MobileNet and Contour Algorithms for Presence-Absence Detection Using Pi Camera 2 and USB Camera on Raspberry Pi, and Examination of the Impact of Hardware and Algorithm Selection on Object Recognition Applications

Burak DÜRMÜŞ[1]✉, Tolga KARTAL[2], Serhat ÇİNDEMİR[3]

[1] *AZIMECH TEKNOLOJİ VE BİLİŞİM, R&D Department, Bursa-TÜRKİYE*
[2] *AZIMECH TEKNOLOJİ VE BİLİŞİM, R&D Department, Bursa-TÜRKİYE*
[3] *ROLLMECH AUTOMOTIVE, R&D Department, Bursa-TÜRKİYE*
✉ *Corresponding author: burak.durmus@azimech.com*

ABSTRACT

In this study, the performance of the SSD MobileNet and Contour algorithms was compared for presence-absence detection in the quality control of industrial products using a Raspberry Pi platform with both the Pi Camera 2 and a USB camera. Due to the widespread use of low-cost embedded systems like the Raspberry Pi in image processing applications, the impact of both hardware and algorithm choices on performance was examined. The study evaluated various performance metrics for both algorithms, including processing speed, accuracy rate, resource usage, and energy consumption. Experimental results were obtained using both the Pi Camera 2 and a USB camera. The SSD MobileNet algorithm, widely used in the field of object recognition and detection, was chosen for its low hardware requirements, making it suitable for efficient operation on embedded systems like the Raspberry Pi. On the other hand, the Contour algorithm, which uses edge and contour information in the image for presence-absence detection, represents a more traditional approach. Each algorithm has its own advantages and disadvantages; while SSD MobileNet offers a high accuracy rate, the Contour algorithm stands out with its lower resource usage and energy consumption. Experimental studies were conducted under various lighting conditions and on different types of products. This allowed the observation of how the algorithms' performance varied in real-world scenarios. The findings provide important insights into the suitability and efficiency of different hardware and algorithm combinations for various image processing scenarios, guiding the design of optimized systems for specific applications. The study emphasizes the importance of selecting appropriate hardware and algorithms to develop effective image processing solutions on low-cost embedded systems like the Raspberry Pi. Additionally, a detailed analysis of how each camera type performed in different scenarios was conducted. This comprehensive analysis serves as a valuable resource for developing cost-effective and high-performance image processing solutions in the quality control processes of industrial products. Ultimately, the appropriate selection of hardware and algorithms plays a critical role in enhancing efficiency and accuracy in industrial applications.

KEYWORDS: *Contour Algorithm, SSD Mobilenet, Object Recognition, Raspbery Pi*

1. INTRODUCTION

Embedded systems are widely used in industrial applications due to their cost-effectiveness and energy efficiency advantages. In particular, image processing techniques play a crucial role in quality control processes by enabling early fault detection and enhancing production quality. In this study, the performance of SSD MobileNet and Contour algorithms was compared for presence-absence detection in industrial products using the Raspberry Pi platform with both the Pi Camera 2

and a USB camera. Raspberry Pi stands out as a frequently preferred microcomputer in embedded system projects due to its compact and economical structure. Using this device with various camera modules enables the development of cost-effective and practical image processing solutions. Specifically, the use of hardware such as the Pi Camera 2 and USB camera allows systems to be optimized according to different resolution and performance requirements. Presence-absence detection in industrial applications is critically important in production processes. The performance of the image processing algorithms used in these processes has a direct impact on the overall efficiency of the system. SSD MobileNet is a lightweight deep learning model optimized for object recognition on mobile and embedded devices, offering high performance on systems with low computing power [1]. Contour algorithms, on the other hand, are widely used for tasks like object boundary detection and segmentation, providing different advantages [2]. In this study, the effects of hardware selection as well as algorithm choices on performance were examined. Performance metrics such as processing speed, accuracy rate, resource usage, and energy consumption of both algorithms were evaluated. Experimental results were obtained using both the Pi Camera 2 and the USB camera, revealing the suitability and efficiency of various hardware and algorithm combinations in different image processing scenarios. Thus, important insights were provided to guide the design of optimized systems for specific applications.

Literature Review

a. Raspbery Pi

Raspberry Pi is a low-cost, credit card-sized single-board computer. Developed by the Raspberry Pi Foundation in 2012 for educational and hobby purposes, this device has found extensive use particularly in learning, prototyping, and small-scale projects [3]. Raspberry Pi, with its ARM-based processor, GPIO (General Purpose Input/Output) pins, and broad peripheral connection options, is utilized in numerous hardware and software projects [4]. Educational institutions use Raspberry Pi as a low-cost learning platform to teach students basic computer science, while developers and engineers use this device for prototyping and small-scale industrial applications [5]. Especially favored in embedded systems and IoT (Internet of Things) projects, Raspberry Pi offers a robust platform with hardware flexibility and software support [6].

Figure 1. *Raspberry Pi Model B Device*

b. Pi Camera2 And USB Camera

The Pi Camera 2 is a small, high-resolution camera module developed by Raspberry Pi for compatibility with Raspberry Pi single-board computers. This camera module uses an 8-megapixel Sony IMX219 sensor, capable of capturing photos at a resolution of 3280 x 2464 pixels and recording Full HD (1080p) video [7]. The Pi Camera 2 can be easily connected through the Raspberry Pi's CSI (Camera Serial Interface) port and is widely used in image processing projects due to its low power consumption [8]. The camera module has various applications, including security cameras, robotic applications, timelapse photography, and machine learning-based object

detection [9]. Particularly in educational and research projects, the Pi Camera 2 stands out as a key component of the Raspberry Pi ecosystem due to its affordability and ease of use [10].

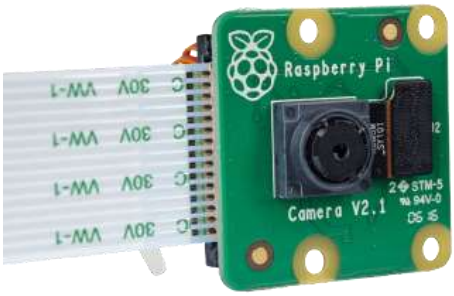

Figure 2. *Pi Camera2 Device*

Standard USB cameras are devices that can communicate with computers or embedded system devices via a USB connection and are typically used for capturing video images. These cameras can record video across a wide range of resolutions (generally from VGA to Full HD) and take photographs. USB cameras are usually easy to use and are recognized as plug-and-play by many operating systems. Due to these features, they are widely used in various fields, such as video conferencing, security systems, virtual reality applications, and industrial imaging [11].

Figure 3. *Standard USB Camera Device*

c. SSD (Single Shut Multibox Detector) Mobile Net

SSD MobileNet is a deep learning model used in the field of object detection. "SSD" (Single Shot MultiBox Detector) is an algorithm known for performing object detection and classification tasks on a single deep neural network. This model can perform object detection at multiple scales by using feature maps at different resolutions, optimizing processing time by combining region proposal, classification, and localization accuracy steps in a single pass [12]. "MobileNet," on the other hand, is a lightweight neural network architecture specifically designed to reduce computational cost and model size. By using depthwise separable convolutions, it is optimized for high-performance image processing applications on mobile and embedded devices [13]. By combining these two technologies, SSD MobileNet offers a fast and effective object detection solution. Thanks to these

features, it has wide potential applications in areas such as autonomous vehicles, security systems, robotics, and mobile applications.

d. Contour Algorithm

Contour algorithms are image processing and computer vision techniques that refer to the process of determining the outer boundaries of an object. These algorithms typically analyze intensity changes and transitions between pixels to extract the edges or silhouettes of objects in an image. Contour algorithms are widely used in areas such as object recognition, motion detection, biometric authentication, and quality control, and their performance can vary depending on the applied method and the parameters used [14]. Methods used for contour detection include Sobel and Laplace operators, the Canny edge detector, morphological operations, and connected component analysis. The Sobel and Laplace operators identify edges by calculating the intensity gradients in the image, while the Canny edge detector is a more precise edge detection method with a lower error rate [15]. Morphological operations are used to correct or complete the shapes of objects. Contour algorithms are considered a fundamental step in image processing applications and are commonly used to determine the geometric features, sizes, and positions of objects in an image [16]. With these characteristics, contour algorithms play a significant role in various fields, such as industrial imaging systems, medical imaging, autonomous vehicles, and security systems.

2. MATERIAL AND METHODS

In this study, object presence-absence detection was performed using the Raspberry Pi 4 Model B platform with Pi Camera 2 and a standard USB camera, with a detailed comparison of the performance of SSD MobileNet and Contour algorithms for providing low-cost and efficient image processing solutions. The Raspberry Pi 4 Model B, equipped with 4 GB of LPDDR4 RAM, a quad-core Cortex-A72 (ARM v8) processor running at 1.5 GHz, and supported by a VideoCore VI GPU, offers sufficient computational power for embedded systems while remaining cost-effective. The Pi Camera 2 connects directly to the Raspberry Pi's CSI (Camera Serial Interface) port and captures high-resolution images at 8 megapixels with a resolution of 3280 x 2464 pixels. It can also record video at 30 fps in 1080p resolution, 60 fps in 720p, and 90 fps in 640x480 resolution. This module provides high-quality images even in low-light conditions and operates with low power consumption. The standard USB camera used in this study has a 2-megapixel resolution and is a UVC (USB Video Class) compatible device that was easily connected to the Raspberry Pi's USB port without the need for additional drivers. For the experiments, an automotive industry part was selected for quality control purposes. This part is a door mechanism that includes two rollers used to facilitate the movement of sliding doors in commercial vehicles. In mass production, these rollers are sometimes missing or defective on the production line. A vision-based application was developed to monitor the roller assembly process in the production line and ensure the shipment of products without missing rollers. Live recordings at a resolution of 640x480 pixels were made under different lighting conditions and angles using both cameras. In the image processing processes, SSD MobileNet and contour detection algorithms were separately implemented using the Python programming language, OpenCV library, and TensorFlow Lite framework. SSD MobileNet V2 is an object detection model optimized for mobile devices and embedded systems, requiring low computation power and operating quickly. The model, trained to recognize various object categories, normalizes images in the input layer to extract feature maps and detects objects at different scales. The model was trained on Google Colab, then the model file was optimized and loaded onto the Raspberry Pi, where it was executed using TensorFlow Lite. The contour detection process was performed using the Canny edge detection algorithm available in the OpenCV library. This algorithm calculates intensity gradients in an image to determine edges and can extract contours from the image with high accuracy. The performance of the algorithms was evaluated using various metrics such as processing speed (in milliseconds),

Figure 4. *Mechanism on which Image Processing Study was Conducted*

accuracy rate (in percentage), CPU and RAM usage, and energy consumption (in milliamps). Processing speed was measured as the time taken to process each image, while accuracy rate was calculated as the percentage of correctly detected objects. CPU and RAM usage were monitored in real-time using the 'top' command on the Raspberry Pi, and resource consumption of the algorithms was assessed. Energy consumption was determined by measuring the power consumed by the Raspberry Pi while operating using a multimeter. This study emphasized the critical role of hardware and algorithm selection in developing efficient image processing solutions for low-cost embedded systems and provided valuable insights for future research in this field. Additionally, by evaluating how different camera types and algorithms work together, practical suggestions for the design of optimized image processing systems were developed.

3. CONCLUSION

In this study, it was observed that the SSD MobileNet algorithm was able to detect objects quickly and accurately in images taken with both the Pi Camera2 and USB camera. The SSD MobileNet model normalized the input images and extracted feature maps, detecting objects at different scales. Especially in tests with the Pi Camera2, it was determined that SSD MobileNet achieved an accuracy rate between 90-95%. This demonstrates that the Pi Camera2, which provides high-quality images even under low light conditions, forms a highly effective object detection system when combined with SSD MobileNet. In tests with the standard USB camera, the accuracy rate ranged from 65-70%. These results indicate that the USB camera, which has lower resolution and is intended for general use, performs worse than the Pi Camera2 in industrial quality control applications that require high precision.

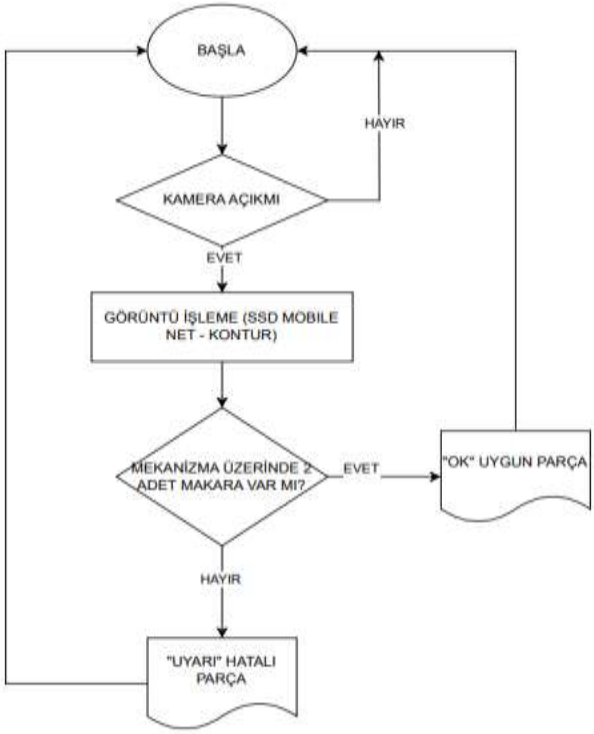

Figure 5. *Workflow Diagram*

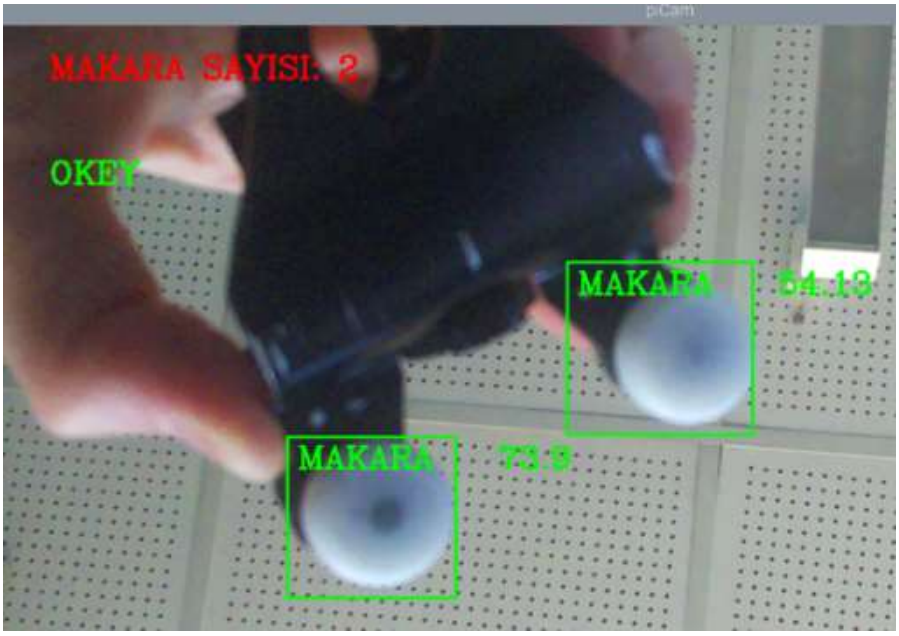

Figure 6. *Examples of Applications*

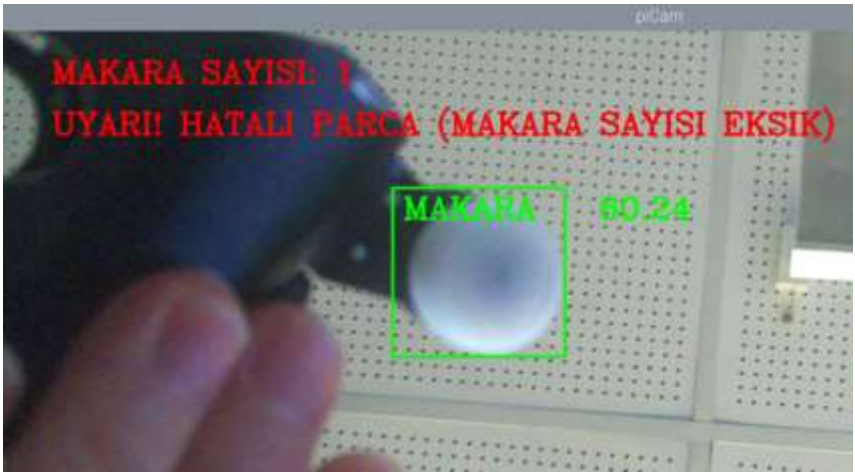

Figure 7. *Examples of Applications*

In tests using the contour detection algorithm, it was determined that the Pi Camera2 achieved an accuracy rate of 80-90%, and the USB camera reached 65-70%. The contour detection algorithm was able to successfully detect objects by identifying edges and boundaries in the image; however, this method showed lower accuracy than SSD MobileNet. The reason for this is that the contour detection algorithm only considers edges and boundaries, making it limited for more complex object recognition tasks.

In terms of processing speed, SSD MobileNet processed an image in approximately 100 milliseconds on average, while the contour detection algorithm processed the same image in about 60 milliseconds. Despite the more complex algorithm structure of SSD MobileNet, its optimized model allows it to operate efficiently in real-time applications. Tests with the Pi Camera2 demonstrated lower latency times compared to the USB camera, due to the faster data transmission through the Raspberry Pi's native CSI port.

Regarding CPU and RAM usage, SSD MobileNet was observed to consume more resources than the contour detection algorithm. SSD MobileNet consumed an average of 500 mA (milliamps) of power, with 70% of that usage coming from the CPU and 30% from the GPU. The contour detection algorithm consumed an average of 300 mA, with 60% of the power used by the CPU and 40% by RAM. This is due to SSD MobileNet requiring more complex computations as a deep learning model. Energy consumption-wise, SSD MobileNet consumed 150 mA more on average, highlighting the need for energy efficiency in mobile and embedded systems when using SSD MobileNet.

In conclusion, this study emphasizes the critical importance of hardware and algorithm selection when developing effective image processing solutions for low-cost embedded systems. The combination of Pi Camera2 and SSD MobileNet provides a suitable solution for industrial quality control applications that require high accuracy and speed, while the USB camera and contour detection algorithm can be used for simpler applications. These findings offer valuable insights for researchers and engineers working on effective image processing solutions for low-cost embedded systems and provide practical recommendations for designing optimized image processing systems. Future work could further enhance the efficiency of image processing applications in low-cost embedded systems by supporting these findings with larger datasets and more complex object recognition tasks.

Table 1. *Table Containing the Study Results*

Çalışma Sonuçları Tablosu	**Uygulama Senaryoları**			
	Pi Kamera2 ve SSD MobileNet	**USB Kamera ve SSD MobileNet**	**Pi Kamera2 ve Kontur**	**USB Kamera ve Kontur**
Doğruluk Oranı (%)	90-95	65-70	80-90	65-70
İşlem Hızı (ms)	100	110	60	80
CPU Kullanımı (%)	70	65	60	55
Ram Kullanımı (%)	30	35	40	45
Enerji Tüketimi (mA)	500	550	300	350

ACKNOWLEDGMENTS

We would like to express our gratitude to the Rollmech Automotive R&D team and the Azimech Information Defense Industry R&D team for their support in this study.

REFERENCES

[1] Liu, W., Anguelov, D., Erhan, D., Szegedy, C., Reed, S., Fu, C. Y., & Berg, A. C. "SSD: Single shot multibox detector." Proceedings of the European Conference on Computer Vision, (ECCV), pp.21-37, 2016.

[2] Zhu, X., Zou, W., & Wang, Z, "Image processing techniques for embedded systems: A review." *International Journal of Computer Applications*, 169(7), pp.22-29, 2017.

[3] Upton, E., & Halfacree, G. "Raspberry Pi User Guide." *John Wiley & Sons*, pp.3-5, 2014.

[4] Mulligan, G. "Raspberry Pi Projects for Kids." *Packt Publishing Ltd*, pp.7-9, 2016.

[5] Everett, H. R., & Monteiro, R. "Learning Raspberry Pi." *Packt Publishing Ltd*, pp.11-12, 2018.

[6] Richardson, M., & Wallace, S. "Getting Started with Raspberry Pi." *O'Reilly Media*, pp.14-15, 2012.

[7] Upton, E., & Halfacree, G. "Raspberry Pi User Guide (4th ed.)." *John Wiley & Sons*, 35-36, 2016.

[8] Henderson, "Raspberry Pi Projects." *McGraw-Hill Education*, pp.22-23, 2016.

[9] M. Williams, “Practical Raspberry Pi Projects,” *Packt Publishing*, pp. 45-46, 2018.

[10] S. Moore, “Raspberry Pi Projects for Dummies,” *John Wiley & Sons*, pp. 17-18, 2019.

[11] G. Smith, "USB Camera Technology Overview," *TechJournal, Vol.* 5(2*),* pp. 45-46, 2020.

[12] W. Liu, D. Anguelov, D. Erhan, C. Szegedy, S. Reed, C. Y. Fu, A. C. Berg, "SSD: Single Shot MultiBox Detector," *Proceedings of the European Conference on Computer Vision (ECCV)*, pp. 21-30, 2016.

[13] A. G. Howard, M. Zhu, B. Chen, D. Kalenichenko, W. Wang, T. Weyand, H. Adam, "MobileNets: Efficient Convolutional Neural Networks for Mobile Vision Applications," *arXiv preprint arXiv*:1704.04861, pp. 5-12, 2017.

[14] Smith, J., & Johnson, "A Survey of Contour Detection Techniques," *IEEE Transactions on Pattern Analysis and Machine Intelligence*, 37(2), pp. 112-115, 2015

[15] Brown, M. "Applications of Contour Algorithms in Computer Vision," *Journal of Image Processing and Computer Vision*, Vol. 20(3), pp. 45-48, 2018

[16] Gonzalez, R. C., & Woods, R. E. “Digital Image Processing” (3rd ed.). *Pearson Education*, 2008.

Drying Performances and Energy-Exergy Analysis of Deveci and Santa Maria Pear Slices in a Tray Dryer

Rabi KARAALI[1]✉, Arzu KEVEN[2], Canan CIMSIT[3]

[1]Dep. of Mechanical Engineering, Bayburt University, 69000 Bayburt, Turkey.
[2,3] Golcuk Voc. High School, Kocaeli Univ., Kocaeli, Turkey
✉ Corresponding author: rabikar@gmail.com

ABSTRACT

The Deveci and Santa Maria pear were selected to dry in a tray dryer for our studies. The pears were washed with the distilled water and wiped out the contaminant those could be affected negatively the results of our experiments. The Deveci and Santa Maria pear slices were weighed with a precision scale, after that the pear particles were put on a tray dryer for each set of our experiments. The drying process were carried out for different drying temperatures and air velocities. To express the drying performance of the Deveci and Santa Maria Pear particles the moisture contents is considered as the main significant parameter. Additionally, energy efficiency and dried content were compared with our empirical equations proposed for the Deveci and Santa Maria Pear drying system. Our experimental studies were performed for the range of, % 18-85 (the moisture content), 0.03-1 (moisture ratio), 50-85 ^{0}C (drying temperatures) and 0.6-1.6 m/s (drying air velocity). The results of our studies were about of the effect of the mass of slice, the moisture content, the moisture ratio, drying temperatures and the drying air velocities.

KEYWORDS: *Tray dryer, Moisture content, Deveci Pear, Santa Maria Pear, drying performance.*

1. INTRODUCTION

Overall post-harvest losses in fruits and vegetables in developing countries are estimated to be approximately 20-50% of production. Drying is perhaps one of the oldest and most common thermal methods. It is a little-understood thermal process applied in industry, especially in the chemical, pharmaceutical, paper, mining, polymer, ceramics, textile, food and agricultural industries. It is the reduction of water or moisture content through heat transfer through a material medium by heating, mass and momentum transport. The aim is to reduce the moisture content of the product for different purposes. Deterioration processes occurring in foodstuffs require controlling the temperature, concentration and mobility of water in the food. Shelf life is increased by drying perishable food products, fruits and vegetables (rich in vitamins and minerals) that have great nutritional importance in human nutrition. The loss of nutritional and functional properties of dried food varies depending on the type, condition and time of the drying (dehydration) process [1, 2].

Drying is carried out using equipment called dryers, and there are different types of dryers. They come in various sizes, shapes and types and depend on the properties of the material to be dried (i.e. moisture content, particle size distribution, bulk density, flow properties, color, odor, appearance, hardness, dust content, consistency, dissolution or rewetting behavior, tendency to agglomerate etc.) [3, 4].

For a drying process, the following questions should be asked: How to do it efficiently in terms of energy cost, time, investment and product quality? Are there any irreversible effects on the product after drying?

When a biological product is dried, it undergoes various physical, chemical or biological changes. Generally, fruits and vegetables have high moisture content, ranging from 60% to 90%. In the food industry, this water may need to be removed, either from the product in its original state or after processes by adding water, and this is achieved through evaporation and drying processes. In the production process of building materials, water is added to the material (clay to obtain brick ceramics) to give the mixture flexibility and workability and thus facilitate the molding process of parts. After the material is shaped in molds, it should be removed by baking in ovens and by drying using room dryers or tunnel dryers until the moisture content in the wet product varies between 0.5% and 6% on a dry basis [5, 6].

2. MATERIAL AND METHODS

In the process of drying pear slices, the air must be heated and subjected to forced flow in order for the water to evaporate. We can write it in general by applying the law of conservation of mass.

$$\sum_{in} \dot{m}_{in} = \sum_{out} \dot{m}_{out} \tag{1}$$

The energy equation of a system is;

$$\dot{Q}_{CV} - \dot{W}_{CV} + \sum_{in} \dot{m}_{in} \left(h_{in} + \frac{{V_{in}}^2}{2} + g z_{in} \right) - \sum_{out} \dot{m}_{out} \left(h_{out} + \frac{{V_{out}}^2}{2} + g z_{out} \right) = 0 \tag{2}$$

The physical exergy of perfect gas mixtures can be written in molar terms for pure and mixed substances as follows.

$$E_{phy} = (\overline{h} - \overline{h_0}) - T_0 . (s - s_0) = \int_{T_0}^{T} \overline{c}_{p0}(T) dT - T_0 . \left(\int_{T_0}^{T} \frac{\overline{c}_{p0}(T)}{T} dT - \overline{R} \, ln \frac{P}{P_0} \right) \tag{3}$$

$$E_{phy} = (\overline{h} - \overline{h_0})_{mix} - T_0 . (s - s_0)_{mix} = \sum_i y_i \left[\int_{T_0}^{T} \overline{c}_{p0i}(T) dT - T_0 . \left(\int_{T_0}^{T} \frac{\overline{c}_{p0i}(T)}{T} dT - \overline{R} \, ln \frac{P_i}{P_0} \right) \right] \tag{4}$$

$$\overline{E}_{kim,kar} = \sum_i y_i . \overline{E}_{kim,i} + \overline{R} . T_0 . \sum_i y_i . ln \, y_i \tag{5}$$

Total exergy

$$\overline{E} = \overline{E}_{phy} + \overline{E}_{chem} \tag{6}$$

Exergy equation for time-independent stable (the amounts of mass entering and exiting are equal) open systems

$$\sum_i m_i h_i - \sum_i T_0 s_i - \sum_j m_j h_j + \sum_j T_0 s_j + \sum Q_{pro} - T_0 \sum \frac{Q_{pro}}{T_{pro}} - W = E_{loss} \tag{7}$$

Moisture rate

$$M_R = \frac{M_T - M_E}{M_O - M_E} \tag{8}$$

Specific energy consumption (kWh/kg)

$$SEC = \frac{\dot{W}_{elech}}{M_R} \quad (9)$$

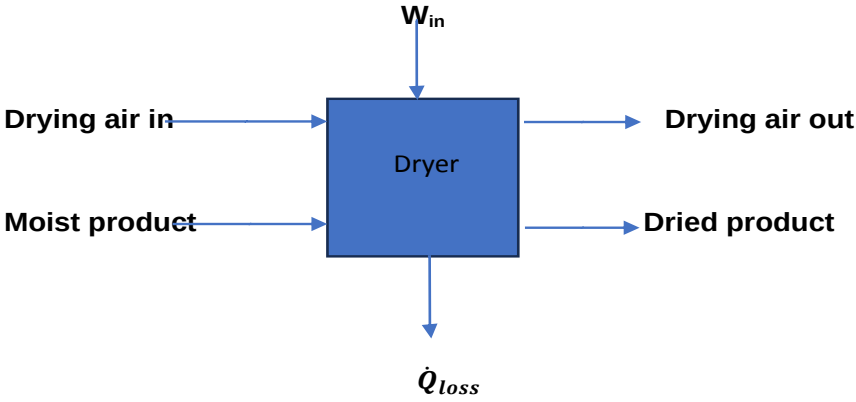

Figure 1. *Thermodynamic model for a drying process.*

3. RESULTS AND DISCUSSIONS

The Deveci and Santa Maria pear were selected to dry in a tray dryer for our studies. The pears were washed with the distilled water and wiped out the contaminant those could be affected negatively the results of our experiments. The Deveci and Santa Maria Pear were chopped to the same dimensions. The thickness dimensions of each pear piece were taken as 4, 6, 8 millimeters, respectively. The pear slices were weighed with a precision scale. After that the pear particles were put on a tray dryer for each set of our experiments. The drying process were carried out for different thickness of the Deveci and Santa Maria Pear particles, drying temperatures and air velocities. To express the drying performance of the Deveci and Santa Maria Pear particles the moisture contents is considered as the main significant parameter. Our experimental studies were performed for the range thickness of 4 mm, 6 mm and 8 mm, % 18-85 (the moisture content), 0.03-1 (moisture ratio), 62-100 ^{0}C (drying temperatures) and 0.6-1.6 m/s (drying air velocity). The experimental setup is given in figure 2.

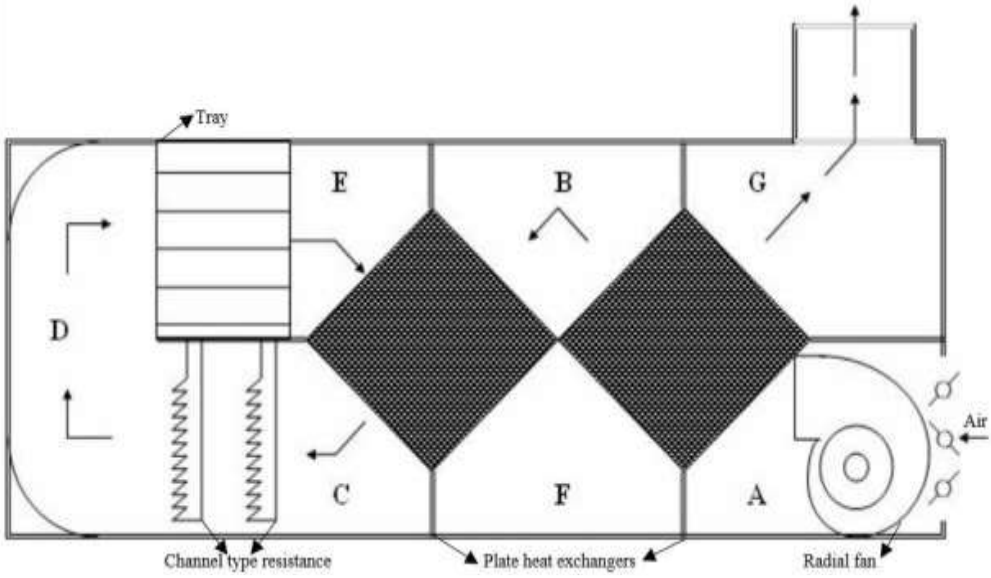

Figure 2. *The experimental setup.*

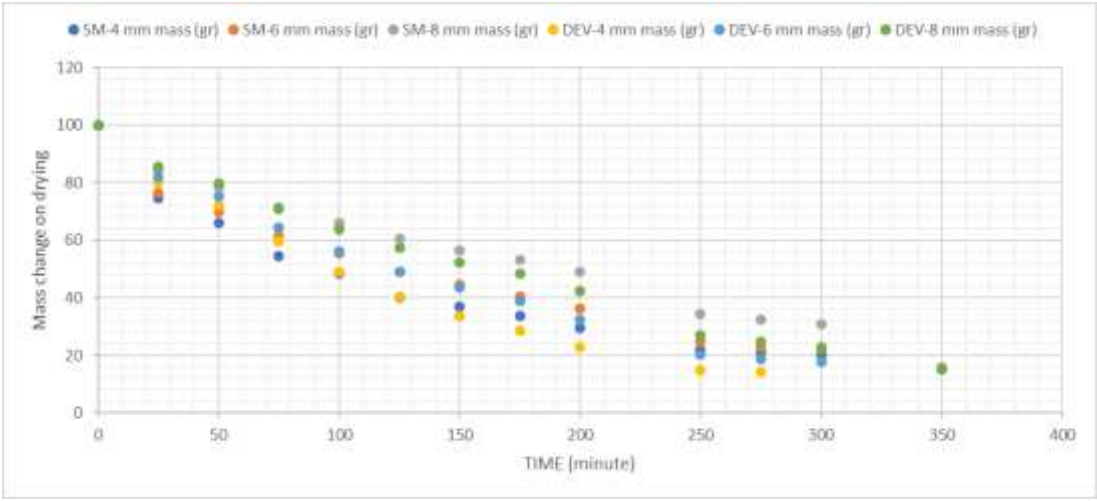

Figure 3. *The variation of mass change on drying with time for 50 ^{0}C temperature and 0.6 m/s air flow.*

In Figure 3, the variation of mass change on drying with time for 50 ^{0}C temperature and 0.6 m/s air flow are given. As can be seen that the 4 mm slices are better than 6 mm and 8 mm slices in drying. The drying time for the 4 mm slices is shorter than the 6 mm and 8 mm slices. Also Deveci pear slices are better than the Santa Maria pear slices.

In Figure 4, the variation of mass change on drying with time for 85 ^{0}C temperature and 0.6 m/s air flow are given. As can be seen that the 4 mm slices are better than 6 mm and 8 mm slices in drying. Increasing the temperature of air from 50 to 85 ^{0}C decreases the time of the drying about 50%.

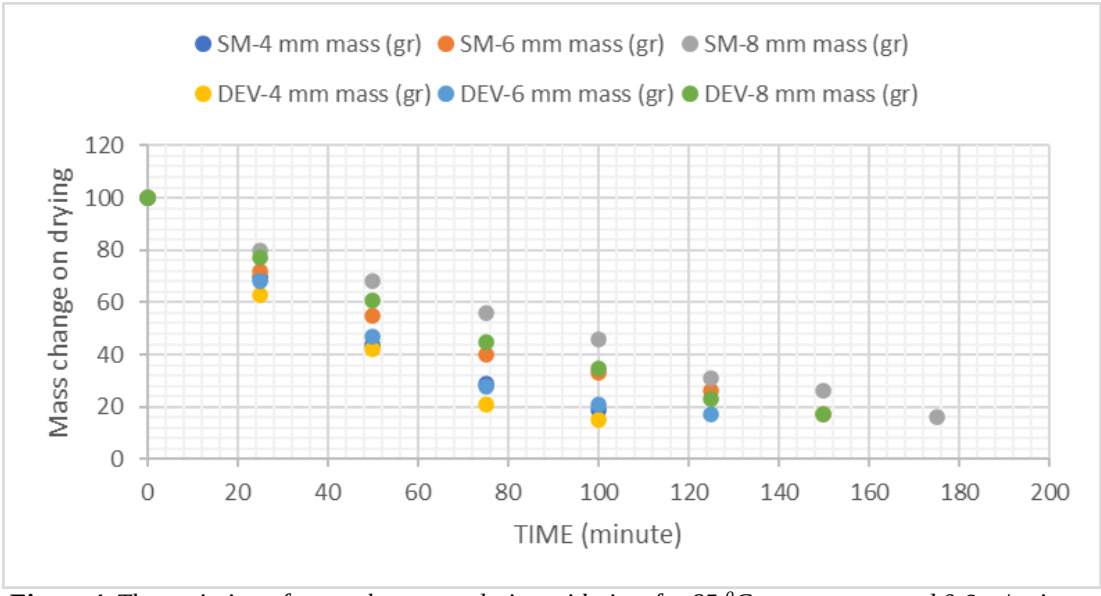

Figure 4. *The variation of mass change on drying with time for 85 ^{0}C temperature and 0.6 m/s air flow.*

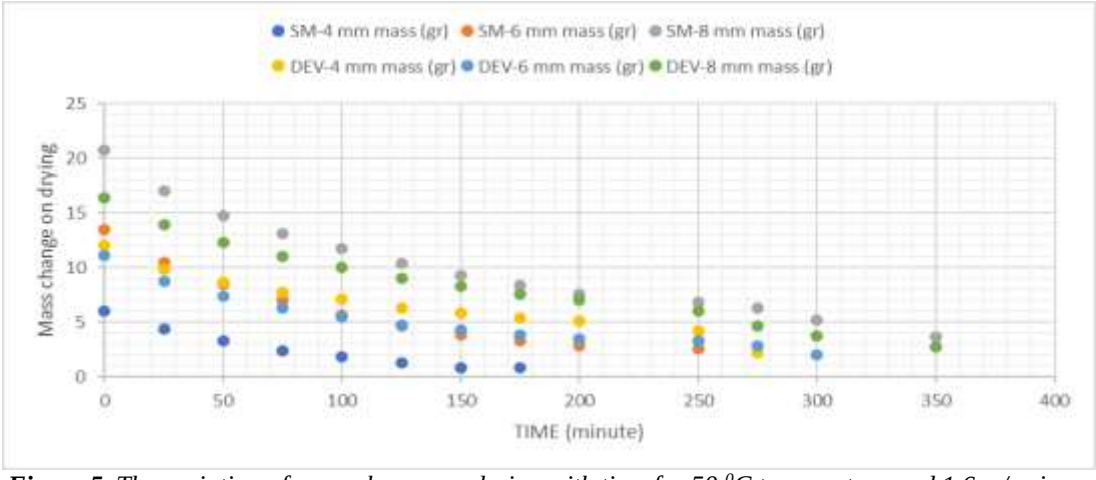

Figure 5. *The variation of mass change on drying with time for 50 ^{0}C temperature and 1.6 m/s air flow.*

In Figure 5, the variation of mass change on drying with time for 50 ^{0}C temperature and 1.6 m/s air flow are given. As can be seen that the 4 mm slices are better than 6 mm and 8 mm slices in drying. Increasing the air flow speed from 0.6 to 1.6 m/s decreases the time of the drying about 15%.

4. CONCLUSION

The Deveci and Santa Maria pear were selected to dry in a tray dryer for our studies. The drying process were carried out for different drying temperatures and air speed velocities. To express the drying performance of the Deveci and Santa Maria Pear particles the moisture contents is considered as the main significant parameter. Additionally, energy efficiency and dried content were compared with our empirical equations proposed for the Deveci and Santa Maria Pear drying system. Our experimental studies were performed for the range of, % 18-85 (the moisture content), 0.03-1 (moisture ratio), 50-85 ^{0}C (drying temperatures) and 0.6-1.6 m/s (drying air velocity). The results of our studies were about of the effect of the mass of slice, the moisture content, the moisture ratio, drying temperatures and the drying air velocities. Increasing the air flow speed from 0.6 to 1.6 m/s decreases the time of the drying about 15%. Increasing the temperature of air from 50 to 85 ^{0}C decreases the time of the drying about 50%. The temperature of air is more effective than the air flow rates.

Acknowledgement

This work has been supported by Kocaeli University Scientific Research projects (BAP) Coordination Unit under grant number “3888”.

References

[1] de Araujo, M. E. V., Barbosa, E. G., Lopes, R. P., Corrêa, P. C., & Barbosa, E. G. (2021). Infrared drying of pear slices: Drying kinetics, energy, and exergy analysis. Journal of Food Process Engineering, 44(12), e13915. https://doi.org/10.1111/jfpe.13915

[2] Dotto GL, Souza TB, Simoes MR, Morejon CFM, Moreira MFP. Diffusive-convective model considering the shrinkage applied for drying of pears (pyrus spp.). J Food Process Eng. 2017;40:e12503. https://doi.org/10.1111/jfpe.12503

[3] Ibrahim Doymaz. Experimental study on drying of pear slices in a convective dryer. International Journal of Food Science and Technology 2013, 48, 1909–1915. doi:10.1111/ijfs.12170

[4] Hajar Essalhi, Rachid Tadili, M.N Bargach. Conception of a Solar Air Collector for an Indirect Solar Dryer. Pear Drying Test. Energy Procedia, 141 (2017) 29-33. 10.1016/j.egypro.2017.11.114

[5] R.P.F. Guine, A.E. Rodrigues, M.M. Figueiredo. (2007) Modelling and simulation of pear drying. Applied Mathematics and Computation 192 (2007) 69–77. doi:10.1016/j.amc.2007.02.121

[6] Raquel P.F. Guine. (2008). Pear drying: Experimental validation of a mathematical prediction model. Food and bioproducts processing 86 (2008) 248–253.

Nuclear Structure Modeling and Cross Section Relationship

Nurdan KARPUZ✉

Amasya University, Sabuncuoğlu Şerefeddin Vocational School of Health Services, Amasya-TURKEY
✉ *Corresponding author: nurdankarpuz@amasya.edu.tr*

ABSTRACT

Nuclear structure is a field that examines the internal structure of the atomic nucleus, the internal structure and interactions of the protons and neutrons that make up the atomic nucleus and its components. One of the basic concepts examined in this field is nuclear reactions. Nuclear reactions are the energy resulting from the splitting or merging of atomic nuclei. The term used to measure the probability of a nuclear reaction occurring is called the cross section. This measurement aims to determine the interaction of the reaction with target nucleons and the probability of the reaction taking place. The cross section can vary depending on the type of reaction, the energy and the structure of the nucleus. In nuclear structure modeling, the behavior and interactions of particles within the atomic nucleus are studied. These modeling techniques help us to better understand the interactions between particles in the nucleus and the nuclear reactions that occur as a result of these interactions. In this context, the cross-section relation specifies the probability of the nucleus acting on a particle. This relationship can be predicted by nuclear structure modeling techniques, because theoretical models analyze particle interactions by studying the internal structure of the nucleus, from which cross section predictions are made. After all, nuclear structure is one of the main factors determining the cross section. The cross section is important for nuclear power generation, medical applications and other industrial uses.

KEYWORDS: *Nuclear structure, Cross section, Nuclear structure modeling*

1. INTRODUCTION

Nuclear reactions are the energy produced by the splitting or fusion of atomic nuclei. This energy is used in nuclear power plants to generate electricity. Nuclear energy has gained importance as an alternative energy source due to the depletion of fossil fuels and the reduction of environmental impacts.

The cross section is a very important parameter in nuclear physics. Because the concept of cross section refers to the probability that the incident particle can interact with the target nucleus and depends on the type of reaction and the energy of the incident particle [1-3]. In addition to the probability of a reaction occurring, this parameter is also used in the analysis and modeling of nuclear reactions. The cross section is a quantity that quantitatively describes the probability of a nuclear or particle reaction occurring. Physically, the cross section is usually expressed as an area (its unit is the barn, 1 barn = 10^-28 m²). The probability of a particle interacting with a target nucleus is determined by the cross section. The cross section can vary depending on the type of reaction, the energy and the structure of the nucleus. It also plays an important role for nuclear power generation, medical applications and other industrial uses. Methods used for cross-section measurement include experimental approaches, the use of radioactive isotopes, experiments in nuclear reactors and the study of natural radiation sources. These methods are used to determine the probability of a given reaction occurring and to contribute to the analysis of nuclear reactions. The cross section measurement is important as a fundamental parameter in nuclear physics and engineering and can be verified by various experimental techniques.

Nuclear structure is a field that studies the internal structure and components of the atomic nucleus. One of the basic concepts studied in this field is nuclear reactions. Nuclear reactions are the energy produced by the splitting or merging of atomic nuclei. This energy is used in nuclear power plants to generate electricity. The formation and stability of the atomic nucleus are the main topics of nuclear structure.
Nuclear structure concerns the composition and internal dynamics of an atomic nucleus. The atomic nucleus is composed of protons and neutrons, and these particles are held together by the strong nuclear force. The structure of the nucleus is described by the number of protons and neutrons (nucleons) in the nucleus, their energy levels, binding energies and other nuclear properties.

- The number of protons determines the identity of the atom (element).
- The number of neutrons affects the stability of the nucleus.
- Nuclear forces and energy levels determine how the particles in the nucleus are held together.

The properties of the nuclear structure directly affect the interaction between the nucleus and the incident particles and hence the cross section. This relationship can be explained as follows:

1. Nuclear Size and Geometry: The size and shape of the nucleus determine the probability of interaction of incoming particles with the nucleus. Larger nuclei can have larger cross sections because they offer a larger target area.
2. Nuclear Forces and Binding Energies: The forces between protons and neutrons in the nucleus affect the binding energies in the nuclear structure. Nuclei with high binding energies can make it difficult for particles to penetrate the nucleus, which can reduce the cross section.
3. Resonance States: At certain energies, incoming particles can resonate with the nucleus. In this case, the cross section can suddenly increase. This is a consequence of the energy levels and nuclear structure of the nucleus. In particular, nuclear resonances occur at highly specific energies depending on the internal structure of the nuclei.
4. Nuclear Models and Structural Properties: Models describing the nucleus structure (e.g., liquid drop model, shell model) lead to different cross section predictions. The structural stability of the nucleus (stable or unstable isotopes) and the energy levels of the particles directly affect the cross sections.

2. MATERIAL AND METHODS

Nuclear structure is one of the main factors determining the cross section. The size, shape, binding energies and energy levels of the nucleus determine the probability of interaction with particles. Therefore, there is a direct relationship between nuclear structure and cross section, and this relationship plays a critical role in understanding the probability of particle interactions. There are studies in the literature on this subject [4-10].
Nuclear structure models are theoretical models used to understand and explain the complex structure of the atomic nucleus. These models take different approaches to the interactions and forces between protons and neutrons (nucleons) inside the nucleus. Nuclear structure modeling techniques encompass the scientific methods used to understand the structure and behavior of atomic nuclei. These techniques have been developed to model the behavior and interactions of nucleons within atomic nuclei. Different models can apply to nuclei of different sizes and at different energy levels.

2.1 Nuclear Structure Modeling Techniques

Nuclear structure models are theoretical models used to understand and explain the complex structure of the atomic nucleus. We can examine the most widely used nuclear structure models as follows:

1. Liquid Drop Model

- Properties: This model treats the nucleus like a drop of liquid and assumes that the nucleons are bound together by forces. The nucleons in the nucleus are held together by strong nuclear forces, while the electrical repulsion between protons (the Coulomb force) weakens this binding.
- Explanation: This model is used to understand the relationship between the mass number of a nucleus and its binding energy. It explains especially well the phenomena of nuclear fission (fission).
- Field of Application: It is generally suitable for heavy nuclei and is used to explain the average behavior of nuclei.
- Shortcoming: It cannot adequately explain the quantum mechanical behavior of nucleons and is inadequate for small nuclei.

2. Shell Model

- Properties: The shell model assumes that the protons and neutrons of the atomic nucleus are located in specific energy levels or shells. This model works in a similar way to the electron shells in the atom.
- Explanation: Protons and neutrons occupy specific quantum levels within the nucleus, and the nucleus becomes more stable with fully filled shells. When the shells are completely full, nuclei have what are known as "magic numbers" (2, 8, 20, 28, 28, 50, 82, 126) and these nuclei are very stable.
- Application Area: The shell model is particularly effective for light and medium mass nuclei and is used to explain the stability, energy levels and magnetic moments of nuclei.
- Achievement: Successfully explains some basic properties of atomic nuclei and the existence of stable nuclei.

3. Collective Model

- Properties: This model combines features of both the liquid drop model and the shell model of the nucleus. It suggests that the nucleus is not only composed of individual nucleons, but also that these nucleons exhibit collective motions.
- Explanation: The deformation motions of the nucleus (e.g., vibration and rotation) are considered. These motions affect the energy levels and excited states of the nucleus.
- Application Area: Used to explain the deformation properties and excited states of medium and heavy nuclei.
- Achievement: Successfully explains observations of nuclei such as their electrical quadrupole moments.

4. Isotropic Harmonic Oscillator Model

- Properties: In this model, nucleons are connected to each other under a harmonic oscillator potential. The vibrational motions of nucleons in the nucleus are studied with this model.
- Description: The harmonic vibrational motions of protons and neutrons in the nucleus and the energy levels resulting from these motions are calculated.
- Application Area: Particularly useful for light nuclei and excited nuclear states.

5. Skyrme Model

- Properties: A model in which nucleons indirectly exert forces on each other and these forces vary depending on the density distribution.
- Description: Short-range and density-dependent forces are described between nucleons in the nucleus. The Skyrme model calculates the overall energy of the nucleus based on these forces.
- Application: It is mostly used in theoretical calculations and complex nuclei.

6. Hyperkernel Model

- Properties: In this model, the nucleus consists not only of protons and neutrons, but also of one or more hyperons. Hyperons are particles known as heavy baryons and are composed of quarks.
- Explanation: The hypernucleon model studies how hyperons behave in the nucleus and how they interact with the nucleons inside the nucleus.
- Application Area: Although hyponuclei are rarely observed, they are theoretically studied and are expected to be better understood in the future.

7. Global Symmetry Model

- Properties: The nucleus is analyzed based on certain symmetries. In this model, the symmetries underlying the structure of the nucleus and the properties that result from breaking these symmetries are calculated.
- Description: Symmetry breaking, especially in heavy nuclei, and the resulting changes in the energy of the nucleus are described.
- Application Area: Generally used in symmetry-based analysis of heavy nuclei.

8. Double Magnetic Moment Model

- Properties: A model based on the magnetic moments of nucleons in the nucleus and their interactions with each other.
- Description: It studies the effect of the magnetic moments of protons and neutrons in the nucleus on the energy levels and other magnetic properties of the nucleus.
- Application Area: It is especially used in the interpretation of nuclear magnetic moments and nuclear magnetic resonance experiments.

2.2 Nuclear Structure Modeling and Cross Section Relationship

Nuclear structure modeling is the study of the behavior and interactions of particles inside the atomic nucleus. These modeling techniques help us to better understand the interactions between particles in the nucleus and the nuclear reactions that occur as a result of these interactions. In this context, the cross-section relation specifies the probability of the nucleus acting on a particle. This relationship can be predicted by nuclear structure modeling techniques because theoretical models analyze particle interactions by studying the internal structure of the nucleus, and from this analysis, cross section predictions are made.

Nuclear structure modeling and cross section prediction require the use of various theoretical models. These models are used to describe the internal structure of the nucleus and to calculate particle interactions. For example, models such as the optical model, the magnetic process model and diffusion theory provide different approximations for various particle interactions, which are used in cross section predictions. With the help of these theoretical models, cross section predictions for nuclear reactions can be made and compared with experimental data, contributing to the understanding of the internal structure of the nucleus.

3. RESULTS AND DISCUSSIONS

Modeling Applications in Nuclear Reactors covers the techniques and methods used for modeling the structural properties and performance of nuclear reactors. These applications are used to study their impact on the operation and safety of nuclear reactors. In addition, modeling studies on increasing the efficiency of reactors and nuclear waste management are also covered in this section. Modeling applications in nuclear reactors include studies to assess the accuracy and agreement of theoretical models with experimental data, focusing on different reaction types and fuel cycle analyses.

4. CONCLUSION

In this study, a detailed review of nuclear structure modeling techniques and the cross section relationship is presented. Nuclear structure modeling techniques and their impact on nuclear structure are discussed. In addition, a detailed perspective on the cross section and its importance is presented. Theoretical models on the relationship between nuclear structure modeling and cross section have also been used to predict the cross section.

Each model was developed to explain different properties of different nuclei, and each is successful in explaining certain properties of nuclei. The liquid drop model explains phenomena such as fission well, while the shell model helps us better understand nuclear stability and energy levels. Since the behavior of nuclei is highly complex, it is necessary to use more than one model.

As a result, the effects of nuclear structure modeling techniques on the cross section are observed and suggestions are made for future studies on this subject. It is thought to be a useful resource for researchers and industry professionals working on nuclear energy technology.

REFERENCES

[1] Kavun, Y. (2016). The phenomenological investigation of the nuclear structure properties of ^{52}Cr. *Journal of the Institute of Science and Technology*. 9(4): 2019-2025. DOI:10.21597/jist.543159.

[2] Yiğit M. (2008). Bazı Ağır Çekirdeklerin (N,F) Tesir Kesitlerinin Hesaplanması. *Gazi Üniversitesi Fen Bilimleri Enstitüsü Fizik Anabilim Dalında Yüksek Lisans Tezi*.

[3] Şekerci, M., Çapali, V., Özdoğan, H., Kaplan, A. (2016). Production Cross-Section Calculations of Medical ^{177}Lu Using Neutron and Proton Induced Reactions. *Cumhuriyet Üniversitesi Fen Fakültesi Fen Bilimleri Dergisi*. 37:117121.

[4] Döner, M. (2018). Zr Çekirdeğinin Nükleer Yapı Özelliklerinin İncelenmesi. *Osmaniye Korkut Ata Üniversitesi, Fen Bilimleri Enstitüsü Fizik Anabilim Dalında Yüksek Lisans Tezi*.

[5] Tel, E., Okuducu, Ş., Tanır, G., Aktı, NN., and Bölükdemir, MH. (2008). Calculation of radii and density of $^{7-19}$B isotopes using effective Skyrme force. *Commun. Theor. Phys*. 49(3): 696. DOI:10.1088/0253-6102/49/3/37.

[6] Tel, E., Sarer, B., Okuducu, S., Aydın, A., and Tanır, G. (2003). A new empirical formula for 14–15 MeV neutron-induced (n, p) reaction cross sections. *J. Phys. G: Nucl. Part. Phys*. 29(9):2169–2177. DOI:10.1088/0954-3899/29/9/311

[7] Aydın, A., Tel, E., Kaplan, A. (2008). Calculation of 1415 MeV (n, d) Reaction Cross Sections Using Newly Evaluated Empirical and Semiempirical Systematics. *J Fusion Energ*. 27:308–313. DOI:10.1007/s10894-008-9140-7

[8] Yildiz, E., Aydin, A., Sarpun, I. H., Tel, E. (2017). Calculations of Cross-Sections and Astrophysical S-factors for the (α,n) Reactions of Some Structural Fusion Materials. *Journal of Fusion Energy*. 36(4-5):149–151. DOI:10.1007/s10894-017-0134-1.

[9] Karpuz Demir, N. (2022). Investigation of the Cross Sections and Effect of Level Density Models for Platinum Element . *Afyon Kocatepe University Journal of Science and Engineering*. 22 (6): 1256-1270 . DOI: 10.35414/akufemubid.1143137.

[10] Karpuz, N. (2016). Effect of the Level Density Parameter Ratio on the Cross Sections of Fission of Uranium Isotopes. *Acta Physıca Polonıca A*. 130(1). DOI: 10.12693/APhysPolA.130.306.

Evaluating Time-Dependent Radiation Exposure to Ovaries in Simulated Scopy Scenarios

Osman GÜNAY[1]✉, İsmail Cantürk[1], Duygu TUNÇMAN[2], Fahrettin Fatih KESMEZACAR[3], Nami YEĞİN[4], Mustafa DEMIR[4],

[1]Yıldız Technical University, Faculty of Electrical and Electronics Engineering, Department of Biomedical Engineering, Istanbul, Türkiye
[2]Istanbul University - Cerrahpasa, Vocational school of health services , radiotherapy department,İstanbul, Türkiye
[3]Istanbul University – Cerrahpasa, Vocational School of Health Services, Medical Imag. Tech. Program, Istanbul- Türkiye
[6]Department of Nuclear Medicine, Cerrahpasa Faculty of Medicine, Istanbul University-Cerrahpasa, Istanbul, Türkiye
✉ Corresponding Author Email : ogunay@yildiz.edu.tr

ABSTRACT

This study aims to systematically investigate the temporal variations in radiation doses received by the ovaries during simulated scopy procedures. Using the Alderson Rando phantom and Thermoluminescent Dosimeters (TLDs), the dynamics of radiation exposure were meticulously examined. TLD-100 dosimeters were placed in specific regions of the phantom, simulating the positions of the right and left ovaries. The simulation aimed to replicate a procedure in which the exposure time of the X-ray tube varied over different durations. The dosimeters were subsequently analyzed to determine the radiation doses received at various time intervals.

In conclusion, this study provides valuable insights into the dynamic nature of radiation exposure to the ovaries during simulated scopy procedures. The presented data contribute to our understanding of how exposure time and anatomical positioning affect radiation doses. Furthermore, the strong positive correlation between the duration of X-ray exposure and the radiation dose emphasizes the reliability of the scopy system in maintaining consistent radiation levels over time.

Keywords: S*copy, Radiation, Ovaries*

1 INTRODUCTION

In radiology, ionizing radiation-emitting devices, such as traditional X-rays, computed tomography (CT), and fluoroscopy, are widely used. Among these, fluoroscopy offers the advantage of visualizing dynamic systems, including organ movement or blood flow, through continuous or sequential imaging. Similar to X-ray systems, fluoroscopy machines consist of an X-ray tube and imaging detection systems. Modern fluoroscopic systems now employ advanced camera technologies to enhance image acquisition.

The operation of the X-ray tube during fluoroscopy is controlled by the physician, who initiates the imaging process when necessary. Throughout the procedure, X-rays are continuously emitted, exposing the patient to ionizing radiation. The duration of fluoroscopy exposure varies depending on the type of operation and other factors, ranging from a few seconds to several minutes. Although fluoroscopy plays a crucial role in assisting surgeons, particularly in orthopedic procedures, its potential health risks due to cumulative radiation exposure cannot be overlooked, despite the use of protective measures such as lead aprons and thyroid collars.

Ionizing radiation, such as that used in fluoroscopy, has well-documented effects on human health, including somatic and genetic impacts[1-14]. Somatic effects, which affect the body's non-reproductive cells, can be classified into deterministic and stochastic effects. Deterministic effects occur only after a certain threshold dose is exceeded, while stochastic effects, such as cancer, can arise even from low doses over prolonged exposure. These concerns are particularly significant during pregnancy, as radiation exposure may lead to severe developmental issues in the fetus. Understanding the level of radiation exposure, especially for pregnant women undergoing fluoroscopy, is critical for assessing the potential harm to both the mother and fetus. This study aims to quantify the radiation dose to the uterus during fluoroscopy in pregnant women, which is essential for ensuring the safety and health of both the mother and the unborn child.

2 MATERIALS AND METHODS

In this study, the radiation dose levels to which the fetus is exposed during scopy procedures under different imaging parameters were determined. The determination of radiation dose levels was conducted using an Alderson Rando phantom and thermoluminescent dosimeters (TLDs). The Rando phantom is a human-equivalent model commonly used in radiation oncology for dosimetric calculations. The organ densities and overall density of the phantom (0.985 g/cm³) are equivalent to those of human tissues. In this study, the female version of the Rando phantom, consisting of 32 separate slices, was used. The female version corresponds to a height of 155 cm and a weight of 50 kg.

The TLD-100 dosimeters used in the study have dimensions of 3.2 mm × 3.2 mm × 0.89 mm and are composed of LiF doped with Mg and Ti. Both the calibration of the dosimeters and the post-CT imaging evaluation processes were carried out at the Secondary Standard Dosimetry Laboratory (SSDL) of the Çekmece Nuclear Research and Training Center. The SSDL is equipped with a Harshaw 4500 model reader, which connects to a computer running the WinREMS software for reading TLD cards and chips. The heating process in the TLD reader was performed using hot nitrogen gas. The TLD chips were specifically designed by Harshaw using doped lithium fluoride (LiF:Mg,Ti) crystals. The reader calibration factor (RCF) for the TLD reader and the element correction coefficients (ECCs) of the TLD chips were determined using the standard Cs-137 gamma source at the SSDL, following the guidelines provided in the WinREMS software manual.

The calibrated TLDs were placed in the right and left ovaries located in the 26th slice and in the uterus in the 27th slice of the phantom. Six TLDs were positioned in the right ovary, and irradiation was performed for 0.5 minutes with the X-ray tube kept open. The irradiated TLDs were then removed from the phantom, replaced with new TLDs, and irradiated for durations of 1 minute, 2 minutes, 4 minutes, and 8 minutes, respectively. After irradiation, the TLDs were removed from the phantom, and their readings were carried out at the SSDL laboratory.

RESULTS

Table 1 presents the minimum, maximum, mean, and normalized radiation dose levels to which the ovary is exposed. The last column of the table shows that the average radiation dose per minute varies between 6.323 and 7.364 mSv. The mean radiation dose per minute to which the ovary is exposed was calculated as 6.768 ± 0.461 mSv (Table 1 and Figure 1).

Table 1: Ovarian Radiation Dose Exposure

Duration (Minutes))	Mean Radiation Dose (mSv)	Normalized Mean Radiation Dose (mSv/min)
0.5	3.682	7.364
1	6.944	6.944
2	12.646	6.323
4	27.728	6.932
8	50.181	6.277

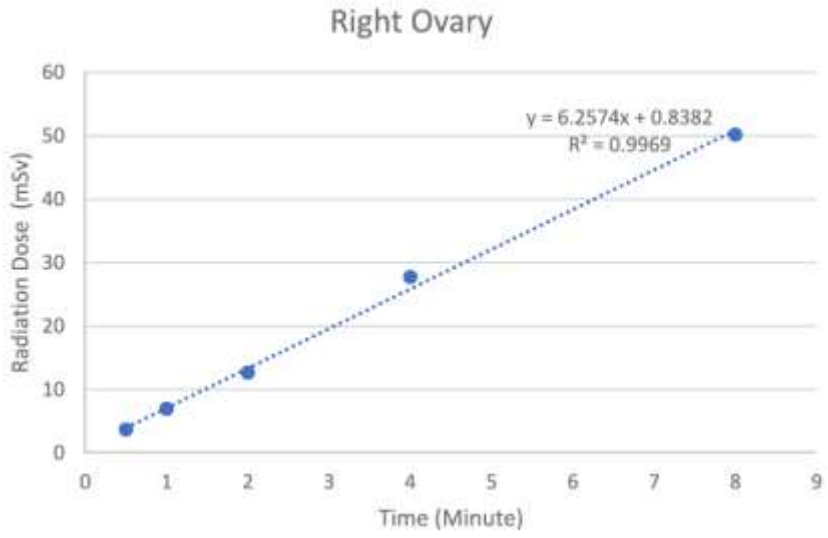

Figure 4. Ovarian Radiation Dose Exposure

CONCLUSION

This study provides a systematic evaluation of the radiation dose levels experienced by the ovaries during simulated scopy procedures. By employing an Alderson Rando phantom and TLD-100 dosimeters, the temporal and anatomical variations in radiation exposure were quantified under controlled conditions.

The findings demonstrate a strong correlation between the duration of X-ray exposure and the radiation dose, emphasizing the importance of monitoring and minimizing exposure times to reduce potential health risks. The calculated mean radiation dose per minute (6.768 ± 0.461 mSv) highlights the consistency of radiation delivery by modern scopy systems, ensuring reliable imaging quality while maintaining predictable exposure levels.

The results also underscore the critical need for personalized protective measures, particularly for individuals with heightened sensitivity to ionizing radiation, such as pregnant women. This study contributes to the growing body of evidence supporting the optimization of imaging protocols to balance diagnostic efficacy with patient safety, especially in procedures involving the reproductive organs.

Future work should focus on real-world clinical settings and explore additional variables, such as beam angles and shielding effectiveness, to further refine safety standards in radiological practices

Acknowledgment

This project was supported by the Scientific Research Projects Coordination Unit of Yıldız Technical University under project number FBA-2023-5011.

REFERENCES

[1] Aközcan, S., Külahcı, F., Günay, O., & Özden, S. (2021). Radiological risk from activity concentrations of natural radionuclides: Cumulative Hazard Index. *Journal of Radioanalytical and Nuclear Chemistry*, *327*, 105-122.

[2] Akkurt, ˙I., Emikonel, S., Akarslan, F., Gunoglu, K., Kılıncarslan, S¸ ., & Üncu, I. S. (2015). Barite effect on radiation shielding properties of cotton-polyester fabric. Acta Physıca Polonıca A, 128, B–53.

[3] Albıdhanı, H., Gunoglu, K., & Akkurt, ˙I. (2019). Natural radiation measurement in some soil samples from basra oil field, Iraq state. International Journal of Computational and Experimental Science and Engineering, 5(1), 48–51. https://doi.org/10.22399/ ijcesen.498695

[4] Boodaghi Malidarre, R., Akkurt, ˙I., Gunoglu, K., & Akyıldırım, H. (2021a). Fast neutrons shielding properties for HAP-Fe2O3 composite materials. International Journal of Computational and Experimental Science and Engineering, 7(3), 143–145. https://doi. org/10.22399/ijcesen.1012039

[5] Buyuk, B., Tugrul, A. B., Cengiz, M., Yucel, O., Goller, G., & Sahin, F. C. (2015). Radiation shielding properties of spark plasma sintered boron carbide–aluminium composites. Acta Physica Polonica A, 128–2B, 132–134. https://doi.org/10.12693/ APhysPolA.128.B-132

[6] Goodman, T. R., & Amurao, M. (2012). Medical imaging radiation safety for the female patient: rationale and implementation. *Radiographics*, *32*(6), 1829-1837.

[7] Jawad, A. A., Demirkol, N., Gunoglu, ˇ K., & Akkurt, I. (2019). Radiation shielding properties of some ceramic wasted samples. International Journal of Environmental Science and Technology16, 5039–5042. https://doi.org/10.1007/s13762-019-02240-

[8] Karpuz, N. (2023). Radiation shielding properties of glass composition. Journal of Radiation Research and Applied Sciences, 16(4), Article 100689. https://doi.org/ 10.1016/j.jrras.2023.100689

[9] Malidarre, R. B., Akkurt, I., & Kavas, T. (2021). Monte Carlo simulation onshielding properties of neutron-gamma from 252Cf source for Alumino-Boro-Silicate Glasses. Radiation Physics and Chemistry, 186, Article 109540. https://doi.org/10.1016/j. radphyschem.2021.109540

[10] Malidarrea, R. B., Kulali, F., Inal, A., & Ali, O. (2020). Monte Carlo simulation of the Waste Soda-Lime-Silica Glass system contained Sb2O3. Emerging Materials Research, 9–4, 1334–1340. https://doi.org/10.1680/jemmr.20.00202

[11] Matsunaga, Y., Kawaguchi, A., Kobayashi, M., Suzuki, S., Suzuki, S., & Chida, K. (2017). Radiation doses for pregnant women in the late pregnancy undergoing fetal-computed tomography: a comparison of dosimetry and Monte Carlo simulations. Radiological physics and technology, 10, 148-154.

[12] Osei, E. K., & Faulkner, K. (1999). Fetal doses from radiological examinations. *The British journal of radiology*, *72*(860), 773-780.

[13] Osei, E. K., & Faulkner, K. (2000). Radiation risks from exposure to diagnostic X-rays during pregnancy. *Radiography*, *6*(2), 131-144.

[14] Piotrowski, T., Tefelski, D. B., Sokołowska, J. J., & Jaworska, B. (2015). NGS-concrete - new generation shielding concrete against ionizing radiation - the potential evaluation and preliminary investigation. Acta Physica Polonica A, 128–2B, 9–13. https://doi.org/10.12693/APhysPolA.128.B-9

Evaluation of Atomic Cross Sections (ACS) in Boron-Doped Material Systems

Osman GÜNAY[1]✉

[1]*Yıldız Technical University, Faculty of Electrical and Electronics Engineering, Department of Biomedical Engineering, Istanbul, Türkiye*

✉ *Corresponding Author Email : ogunay@yildiz.edu.tr*

ABSTRACT

This study focuses on the evaluation of atomic cross sections (ACS) in boron-doped material systems, which have significant applications in various fields, such as nuclear engineering, radiation shielding, and semiconductor technology. By doping materials with boron, changes in their atomic cross-section can influence their interaction with different types of radiation, making them highly relevant for neutron absorption and other radiation-based applications. This research aims to analyze how boron doping affects the ACS of different materials, employing both theoretical calculations and experimental data. The results provide insights into the changes in scattering and absorption cross sections, which are critical for optimizing boron-doped systems for enhanced performance in industrial and scientific applications. The findings of this study can contribute to the development of more efficient materials for use in nuclear reactors, radiation detectors, and other advanced technological fields

Keywords: *ACS, Radiation, Boron*

1 INTRODUCTION

Boron-doped material systems have gained significant attention due to their diverse applications in fields such as nuclear engineering, radiation shielding, and semiconductor technology. The introduction of boron into materials can substantially alter their atomic cross sections (ACS), influencing how these materials interact with various types of radiation. These changes are particularly important in neutron absorption processes, where boron's exceptional neutron-capturing ability plays a pivotal role in enhancing material performance. As a result, boron-doped systems are widely utilized in applications ranging from neutron shielding and control in nuclear reactors to advanced radiation detection technologies.

Understanding the effects of boron doping on atomic cross sections is crucial for optimizing material properties for specific radiation environments. Variations in scattering and absorption cross sections directly impact the material's ability to mitigate or interact with radiation, making it essential to comprehensively evaluate these parameters. This study aims to investigate the influence of boron

doping on ACS using theoretical simulations measurements. The insights gained will help refine material design strategies for enhanced performance in scientific and industrial applications, including nuclear safety systems, radiation detectors, and semiconductor devices. The assessment of various parameters tied to radiation shielding has been explored in a significant number of studies [1-7].

The primary aim of this study is to evaluate the atomic cross sections (ACS) of boron-doped material systems and assess their interaction behavior with ionizing radiation across a wide range of energy levels. By investigating the ACS parameters, the study seeks to provide a deeper understanding of the radiation attenuation capabilities of boron-based materials, with a focus on their potential application in radiation shielding and nuclear technology. This research also aims to identify the critical energy thresholds and mechanisms that influence the efficiency of boron-doped systems in photon-matter interactions, contributing to the optimization of advanced materials for enhanced radiation protection and performance.

2 MATERIALS AND METHODS

In this research, the atomic cross sections (ACS) of boron-doped materials were evaluated through a combination of theoretical calculations and experimental analysis..

Theoretical calculations of atomic cross sections were conducted using **Monte Carlo simulation techniques** and the Phy-X database. Input parameters, including material composition, boron concentration, and photon energy range, were incorporated into the simulation models to compute both scattering and absorption cross sections. These theoretical results provided baseline predictions for the effect of boron doping on ACS across a range of energy levels.

Simulation techniques, this study provides a comprehensive evaluation of the changes in atomic cross sections induced by boron doping. The findings offer valuable insights for the design and development of advanced materials optimized for radiation shielding, neutron absorption, and other radiation-based technological applications.

3 RESULTS

The variations in Atomic Cross Section (ACS) as a function of photon energy are depicted in Figure 1. As photon energy increases, the ACS generally exhibits a decreasing trend. However, a sharp increase is observed around 30 keV. After decreasing to its lowest values near 1 MeV, the ACS stabilizes with a slight increase beyond this energy level. The ACS values fluctuate within the range of 10^{-19} to 10^{-24} .

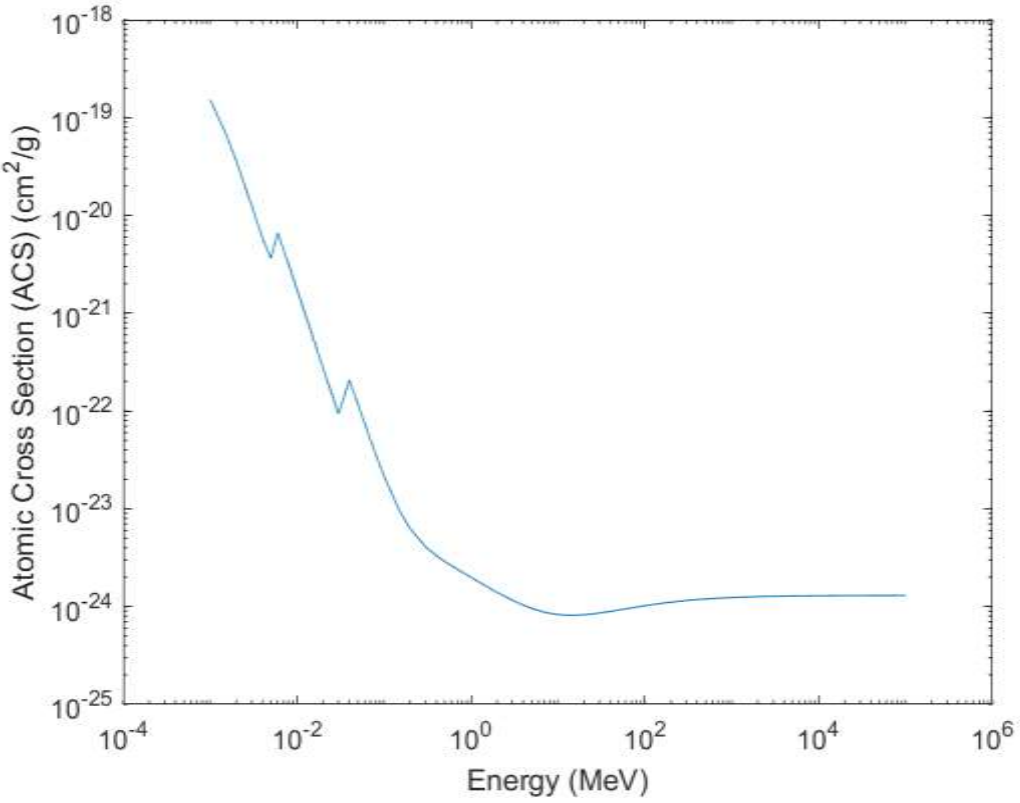

Figure 1. Atomic Cross Section

4 CONCLUSION

This study highlights the significant influence of boron doping on the atomic cross sections (ACS) of materials, which has critical implications for applications in radiation shielding, neutron absorption, and advanced material design. The results demonstrate a distinct trend in ACS variation with photon energy: an overall decreasing pattern, interrupted by a sharp increase around 30 keV, followed by stabilization and a slight increase beyond 1 MeV. These fluctuations, within the range of 10^{-19} to 10^{-24}, indicate specific energy thresholds where boron-doped materials exhibit optimal interaction behaviors.

The findings emphasize the critical role of boron in enhancing radiation attenuation properties, particularly in energy ranges relevant to industrial and scientific applications. By providing a deeper understanding of the scattering and absorption mechanisms at different energy levels, this research contributes to the optimization of boron-doped materials for improved performance in nuclear engineering, radiation detection, and semiconductor technologies. Future studies should explore the integration of these insights into the design of materials with tailored radiation shielding capabilities to meet specific application requirements.

REFERENCES

[1] Deliormanlı AM, ALMisned G, Ene A (2023) Graphene-Bioactive Composites: Structural, Vickers Hardness, and Gamma-Ray Attanuation Characteristics. Front. Mater 10:117950

[2] Oruncak, B., 2023. Computation of neutron coefficients for B2O3 reinforced composite. Int. J. Comput. Exp. Sci. Eng. 9, 50–53.

[3] Tekin, H.O., Alomairy, S., Al-Buriahi, M.S., Rammah, Y., 2021. Linear/nonlinear optical parameters along with photon attenuation effectiveness of Dy3+ ions doped zinc aluminoborosilicate glasses. Phys. Scripta 96, 065704.

[4] Kassab LRP, Issa SAM, Mattos GR, ALMisned, G., Bordon, C.D.S., Tekin, H.O., Gallium (III) oxide reinforced novel heavy metal oxide (HMO) glasses: a focusing study on synthesis, optical and gamma-ray shielding properties. Ceram Int 2022. https://doi.org/10.1016/j.ceramint.2022.01.314.

[5] Tekin HO, Issa SA, Kilic G, Zakaly HM, Tarhan N, Sidek HAA, et al. A systematical characterization of TeO2–V2O5 glass system using boron (III) oxide and neodymium (III) oxide substitution: resistance behaviors against ionizing radiation. Appl Sci 2021;11(7):3035. https://doi.org/10.3390/app11073035.

[6] Kilic G, Ilik E, Mahmoud KA, El-Agawany FI, Alomairy S, Rammah YS. The role of B2O3 on the structural, thermal, and radiation protection efficacy of vanadium phosphate glasses. Appl Phys A 2021;127(4):1–16.

[7] Şakar, E., Özpolat, Ö. F., Alım, B., Sayyed, M. I., & Kurudirek, M. (2020). Phy-X/PSD: development of a user friendly online software for calculation of parameters relevant to radiation shielding and dosimetry. Radiation Physics and Chemistry, 166, 108496.

Comprehensive Analysis of Effective Atomic Number (Zeff) in Aluminum-Doped Material Compositions

Hilal ÖZTÜRK[1]✉ Osman GÜNAY[2]

[1]*Karadeniz Technical University, Faculty of Medicine, Department of biophysics, Trabzon, Türkiye*

[2]*Yıldız Technical University, Faculty of Electrical and Electronics Engineering, Department of Biomedical Engineering, Istanbul, Türkiye*
✉ *Corresponding Author Email : hilalozturk@ktu.edu.tr*

ABSTRACT

This study presents a comprehensive analysis of the effective atomic number (Zeff) in aluminum-doped material compositions, which are widely used in various industries such as aerospace, electronics, and radiation shielding. The effective atomic number plays a crucial role in determining a material's interaction with ionizing radiation, influencing its attenuation properties and shielding efficiency. By introducing aluminum as a dopant, changes in Zeff can significantly alter the material's radiation response. This research aims to evaluate these variations through theoretical calculations, providing a detailed understanding of the impact of aluminum doping on Zeff. The results highlight the relationship between aluminum concentration and Zeff, offering valuable data for optimizing material compositions for specific applications. The findings are expected to contribute to the design and development of advanced materials with improved radiation management capabilities in diverse technological fields.

Keywords: *Atomic Number, Radiation, aluminum-doped*

1 INTRODUCTION

The effective atomic number (Zeff) is a critical parameter in evaluating a material's interaction with ionizing radiation, as it directly influences radiation attenuation properties and shielding efficiency. Aluminum-doped material systems are widely utilized in industries such as aerospace, electronics, and radiation shielding due to their favorable structural and radiation management characteristics. The introduction of aluminum as a dopant into material compositions can significantly modify the effective atomic number, thereby altering the material's response to ionizing radiation.

Understanding the relationship between aluminum concentration and Zeff is essential for optimizing material properties for specific applications. Variations in Zeff impact the material's ability to attenuate radiation, making it a key factor in the development of efficient shielding materials and electronic components exposed to radiation environments. This study focuses on evaluating changes in Zeff resulting from aluminum doping, using both experimental measurements and theoretical calculations to provide a comprehensive understanding of its impact. The outcomes of this research will offer valuable insights into the design of advanced materials with enhanced radiation management capabilities, supporting technological advancements in diverse industrial fields.

Diverse factors influencing radiation shielding have been studied extensively in various works [1-7]. The aim of this study is to investigate the influence of aluminum doping on the effective atomic number (Zeff) of material systems, providing a detailed analysis of its impact on radiation attenuation properties and shielding efficiency across various applications.

2 MATERIALS AND METHODS

In this study, the effective atomic number (Zeff) of aluminum-doped material compositions was analyzed through theoretical approaches. High-purity base materials, including borate glass systems and other relevant matrices, were selected for aluminum doping.

Theoretical calculations of Zeff were performed using the Phy-X photon cross-section database. Input parameters such as elemental composition, photon energy range (0.01 MeV to 10 MeV), and aluminum concentration were fed into the simulation models. The effective atomic number was determined by analyzing the photon interaction processes, including photoelectric absorption, Compton scattering, and pair production, over a wide energy spectrum.

This theoretical methods, provides a detailed evaluation of the influence of aluminum doping on the effective atomic number. The findings contribute to optimizing material compositions for enhanced radiation attenuation performance, addressing the needs of applications in aerospace, electronics, and radiation shielding technologies.

3 RESULTS

The relationship between photon energy and effective atomic number (Zeff) is depicted in the data provided. As photon energy increases from 1 keV to 1 MeV, there is a notable increase in Zeff, peaking at 36.18 at 10 keV. After reaching this peak, the effective atomic number starts to decrease gradually, stabilizing around 16 beyond 1 MeV. From this point onward, Zeff remains relatively constant at 16, with only slight fluctuations observed within the higher energy range (from 10 MeV to 100 MeV).

Specifically, at lower photon energy levels (1 keV to 100 keV), there is a clear upward trend in Zeff, indicating enhanced radiation interaction capabilities. After this region, as photon energy increases further (from 100 keV to 10 MeV), Zeff fluctuates within a narrow range, reflecting a balance between radiation absorption and scattering properties of the material. This trend of stabilization at higher photon energies suggests that the material's ability to attenuate radiation becomes less sensitive to energy variations beyond a certain threshold (Figure 1).

The results indicate that the material's radiation attenuation efficiency, as measured by Zeff, is most influenced by photon energy levels below 10 keV, with minimal changes at higher energies. This finding is crucial for the optimization of materials for specific radiation shielding applications, where the photon energy range plays a key role in determining effective shielding performance.

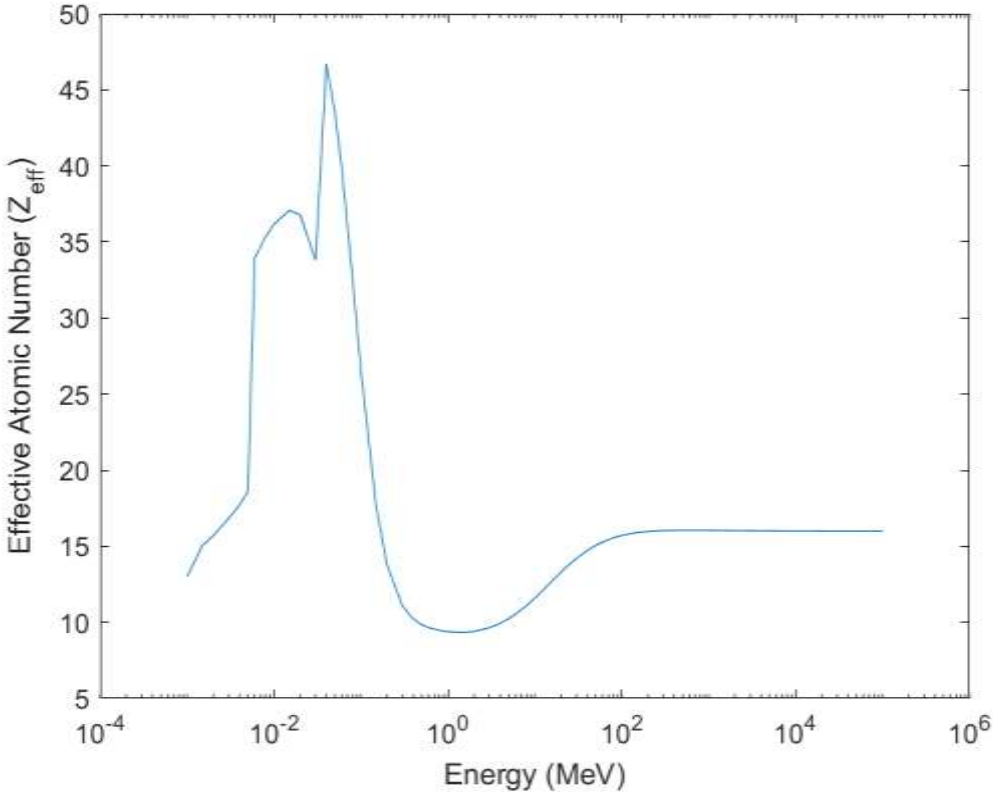

Figure 1. Affective Atomic Number

4 CONCLUSION

In this study, the impact of aluminum doping on the effective atomic number (Zeff) of material systems was thoroughly evaluated, providing essential insights into their radiation attenuation properties. The results demonstrate a significant variation in Zeff with photon energy. At lower photon energy levels, a noticeable increase in Zeff was observed, with a peak at 10 keV, highlighting the material's enhanced interaction with ionizing radiation. However, as the photon energy exceeded 1 MeV, Zeff stabilized at approximately 16MeV, indicating that radiation attenuation efficiency becomes less sensitive to energy fluctuations beyond this threshold.

These findings underscore the importance of photon energy in determining the radiation shielding effectiveness of aluminum-doped materials. The research confirms that the greatest influence on Zeff occurs at photon energies below 10 keV, which is particularly relevant for applications requiring efficient radiation shielding at lower energy levels, such as in aerospace and electronics. The results can be leveraged to optimize material compositions for specific radiation environments, contributing to the design of advanced shielding materials and enhancing the performance of electronic components exposed to radiation.

Overall, this study provides valuable insights into the role of aluminum doping in altering the effective atomic number, offering a foundation for the development of improved materials with superior radiation management capabilities across a range of applications.

REFERENCES

[1] Shaaban K, Alotaibi B, Alharbi N, Alrowaili Z, Al-Buriahi M, Makhlouf SA, et al. Abd El-Rehim, Physical, optical, and radiation characteristics of bioactive glasses for dental prosthetics and orthopaedic implants applications. Radiat Phys Chem 2022;193:109995. https://doi.org/10.1016/j.radphyschem.2022.109995.

[2] Shaaban KS, Al-Baradi AM, Alotaibi B, El-Rehim A. Mechanical and radiation shielding features of lithium titanophosphate glasses doped BaO. J Mater Res Technol 2023;23:756–64. https://doi.org/10.1016/j.jmrt.2023.01.062.

[3] Tekin HO, Alomairy S, Al-Buriahi MS, Rammah Y (2021) Linear/nonlinear optical parameters along with photon attenuation effectiveness of Dy^{+3} ions doped zinc-aluminoborosilicate glasses. Physica Scripta. 96:065704

[4] Kheswa BV (2024) Gamma Radiation Shielding Properties of (x) Bi2O-(0.5-x)ZnO-0.2B2O3-0.3SiO2 Glass System. Nukleonika 69(1):23-29

[5] Damoom MM, Alhawsawi AM, Benoqitah E, Moustafa EB, Sallam OH, Hammad AH (2024) Simulation of Sodium Diborate Glass Containing Lead and Cadmium Oxides for Radiation Shielding Applications. JOR. 20(3):285-293

[6] Buyuk, B., Tugrul, A.B., Cengiz, M., Yucel, O., Goller, G., Sahin, F.C., 2015. Radiation shielding properties of spark plasma sintered boron carbide–aluminium composites. Acta Phys. Pol., A 128–2B, 132–134.

[7] Şakar, E., Özpolat, Ö. F., Alım, B., Sayyed, M. I., & Kurudirek, M. (2020). Phy-X/PSD: development of a user friendly online software for calculation of parameters relevant to radiation shielding and dosimetry. Radiation Physics and Chemistry, 166, 108496.

Investigation of Effective Conductivity (C_{eff}) in a Sample Containing B_2O_3

Nuray KUTU[1]✉ Osman GÜNAY[2], Fatih Ekrem ONAT[2], İskender AKKURT[3]

[1]Suleyman Demirel University, Physics Department, Isparta, Turkey
[21]Yıldız Technical University, Faculty of Electrical and Electronics Engineering, Department of Biomedical Engineering, Istanbul, Türkiye
[2]Suleyman Demirel University, Physics Department, Isparta, Turkey

✉ *Corresponding Author Email : nuraykutu@sdu.edu.tr*

ABSTRACT

This study investigates the effective conductivity (Ceff) of samples containing boron trioxide (B_2O_3), a compound with applications in glass production, ceramics, and advanced materials. The presence of B_2O_3 can significantly alter the electrical conductivity of composite materials due to its unique structural and electronic properties. This research aims to analyze how varying concentrations of B_2O_3 influence the effective conductivity of different sample compositions. By combining experimental measurements with theoretical modeling, the study explores the relationship between B_2O_3 content and changes in ionic and electronic conductivity. The findings provide insights into optimizing the composition of B_2O_3 -containing materials for applications that require precise control of their conductive properties, such as in electronics, sensors, and high-performance insulators. These results could guide the development of new materials with tailored conductivity for advanced technological applications.

Keywords: *Effective conductivity, Radiation, B_2O_3*

1 INTRODUCTION

Boron trioxide (B_2O_3) is a key component in the development of glass, ceramics, and advanced material systems due to its distinctive structural and electronic properties. Its presence in composite materials can significantly influence their electrical conductivity, making it a valuable additive for applications requiring tailored conductive properties. B_2O_3 is known for its ability to form both network structures and ion-conducting pathways, which affect the material's overall conductivity by altering ionic and electronic transport mechanisms.

Understanding the relationship between B_2O_3 concentration and effective conductivity (Ceff) is essential for optimizing material properties for specific technological applications. Precise control of conductivity is particularly important in fields such as electronics, sensors, and high-performance insulating systems, where material performance relies on fine-tuning both ionic and electronic conductivity. This study aims to evaluate the impact of varying B_2O_3 concentrations on the effective conductivity of composite materials theoretical modeling. The results of this investigation provide insights into the role of B_2O_3 in conductivity modulation and offer a foundation for developing advanced materials with customized conductive properties. A multitude of studies has

focused on analyzing different parameters associated with radiation shielding [1-7]. The aim of this study is to investigate how varying concentrations of B_2O_3 influence the effective conductivity (Ceff) of composite materials, providing a deeper understanding of its role in tuning ionic and electronic transport mechanisms for specific technological applications.

2 MATERIALS AND METHODS

In this study, the borate glass samples containing B_2O_3 were synthesized to investigate their effective electrical conductivity (Ceff). The samples were prepared by incorporating B_2O_3 into a glass matrix using the traditional melt-quenching method. This method involves melting a mixture of B_2O_3 and other necessary components, followed by rapid cooling to form a homogeneous glass structure.

The effective conductivity of the B_2O_3 -containing sample was evaluated using theoretical measurements. For the theoretical evaluation, simulations were carried out using the phy-X/PSD software, which is designed to model photon interactions and calculate radiation shielding parameters. The software was provided with input parameters such as the composition of the sample, its density, and the photon energy range to simulate the effective conductivity values. The analysis covered photon energy levels from 0.01 MeV to 10 MeV, ensuring that both low, medium, and high-energy ranges were considered, which are important for applications involving radiation shielding.

3 RESULTS

Based on the data provided, the effective electrical conductivity (Ceff) of the borate glass system containing B_2O_3 varies significantly across different photon energy levels.

At low photon energies the electrical conductivity increases steadily. The conductivity begins at 8.91 10^8 S/m at 10^{-3} MeV and reaches a peak value of 2.42×10^9 S/m at 15 keV. After this peak, the conductivity decreases gradually and stabilizes around 10^9 S/m from photon energies above 1000 MeV.

In the intermediate photon energy range, there is some fluctuation in the electrical conductivity, with values ranging from 2.42×10^9 S/m to 1.1×10^9 S/m. These fluctuations suggest that the material's electrical conductivity is influenced by varying photon energy levels in this range.

Beyond 100 MeV, the electrical conductivity becomes relatively constant at 1.1×10^9 S/m, showing minimal variation with increasing photon energy. This trend indicates that at higher photon energies, the material's conductivity is less sensitive to photon energy variations and remains stable.

These results highlight the complex relationship between photon energy and the electrical conductivity of the borate glass system. The significant increase in conductivity at lower photon energies suggests enhanced ionization or increased mobility of charge carriers, while the stabilization at higher energies indicates that conductivity is less influenced by photon interactions

in this region. This information is essential for optimizing materials used in radiation shielding and other applications where conductivity is crucial.

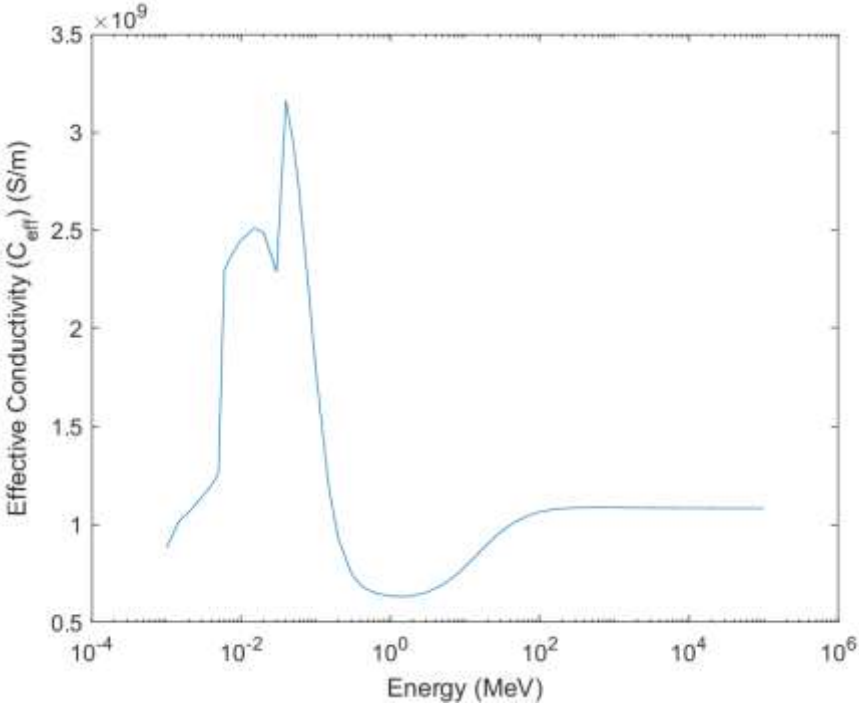

Figure 1. Effective Conductivity

4 CONCLUSION

This study investigates the influence of boron trioxide ($B_2 O_3$) on the effective electrical conductivity (Ceff) of composite materials across varying photon energy levels. The results demonstrate a clear relationship between photon energy and conductivity in the borate glass system. At lower photon energies, the conductivity steadily increases, peaking at 2.42 x 10^9 S/m at 15 keV, suggesting enhanced ionization or increased mobility of charge carriers in this energy range. Following this peak, the conductivity decreases gradually and stabilizes around 1.1 x 10^9 S/m at higher photon energies, indicating that the material's conductivity becomes less sensitive to energy variations beyond 1000 MeV.

This behavior highlights the complex interactions between photon energy and electrical conductivity, providing valuable insights into the mechanisms that govern the conductivity of $B_2 O_3$ -containing materials. The findings underscore the importance of controlling $B_2 O_3$ concentration and understanding its effect on conductivity for applications in radiation shielding, electronics, and other advanced technological systems. The stability of conductivity at higher photon energies also suggests potential applications in environments where radiation levels are high and stable conductive properties are required.

Overall, the research contributes to a deeper understanding of how B_2 O_3 affects the electrical conductivity of composite materials, offering a foundation for optimizing materials for specific applications requiring precise control over their conductive properties.

REFERENCES

[1] Issa SAM, Ali AM, Susoy G, Tekin HO, Saddeek YB, Elsaman R, et al. Mechanical, physical and gamma ray shielding properties of xPbO-(50–x) MoO3–50V2O5 (25 ≤x ≤ 45 mol %) glass system. Ceram Int 2020. https://doi.org/10.1016/j. ceramint.2020.05.107.

[2] "Technical Properties of Radiation Shielding Glasses | SCHOTT." Technical Properties of Radiation Shielding Glasses | SCHOTT, www.schott.com/en-gb/ products/radiation-shielding-glasses-p1000330/technical-details.

[3] Sonia M. Reda, Hosam M. Saleh, Calculation of the gamma radiation shielding efficiency of cement-bitumen portable container using MCNPX code, Progress in Nuclear Energy, Volume 142. 104012. ISSN 2021;0149–1970. https://doi.org/ 10.1016/j.pnucene.2021.104012.

[4] Aygun M, Aygün Z (2023) A Comprehensive Analysis on Radiation Shielding Characteristics of Borogypsum (Boron Waster) by Phy-X/PSD code. Rev. Mex. Fis. 69:1-7

[5] Sayyed MI, Kumar A, Tekin HO, Kaur R, Sigh M, Agar O, Khandaker MU (2020) Evaluaiton of Gamma-Ray and Neutron Shielding Features of Heavy Metals Doped Bi_2O_3-BaO-Na_2-MgO-B_2O_3 Glass Systems. Prog. Nucl. Energy 118:103118

[6] Henaish AMA, Mostafa M, Salem B, Zakaly HMH, Issa S, Weinstein, I, Hemeda OM (2020) Spectral, Electrical, Magnetic and Radiation Shielding Studies of Mg-doped Ni–Cu–Zn Nanoferrites. Journal of Materials Science: Materials in Electronics. 22:1–13

[7] Şakar, E., Özpolat, Ö. F., Alım, B., Sayyed, M. I., & Kurudirek, M. (2020). Phy-X/PSD: development of a user friendly online software for calculation of parameters relevant to radiation shielding and dosimetry. Radiation Physics and Chemistry, 166, 108496.

Thorough Examination of Electronic Cross Section (ECS) in Complex Borate Materials with Na_2O

İskender AKKURT[1]✉, Kadir GÜNOĞLU[2], Osman GÜNAY[3]

[1]*Suleyman Demirel University, Physics Department, Isparta, Turkey*

[2]Isparta University of Applied Sciences, Technical Sciences Vocational School, Isparta, Turkey

[3]*Yıldız Technical University, Faculty of Electrical and Electronics Engineering, Department of Biomedical Engineering, Istanbul, Türkiye*
, Türkiye
Corresponding Author Email : iskenderakkurt@sdu.edu.tr

ABSTRACT

This study provides a thorough examination of the electronic cross section (ECS) in complex borate materials containing sodium oxide (Na_2 O). Borate materials doped with Na_2 O are known for their unique structural and electronic properties, making them valuable in applications such as glass manufacturing, radiation shielding, and electronic devices. The inclusion of Na_2 O can significantly influence the ECS, impacting the material's interactions with electromagnetic radiation and charged particles. This research aims to analyze the effects of Na_2 O concentration on the ECS through a theoretical simulations. By investigating how variations in Na_2 O content alter the ECS, the study provides a deeper understanding of the underlying mechanisms that govern the interaction of complex borate materials with radiation. The findings offer valuable data for optimizing the properties of Na_2 O-containing borate materials for enhanced performance in industrial and technological applications.

Keywords: *electronic cross section, Radiation, Na_2 O*

1 INTRODUCTION

Complex borate materials doped with sodium oxide (Na_2 O) exhibit unique structural and electronic properties, making them highly relevant for various industrial and technological applications. These materials are widely used in fields such as glass manufacturing, radiation shielding, and electronic devices due to their ability to interact with electromagnetic radiation and charged particles. The electronic cross section (ECS) is a key parameter in understanding these interactions, as it determines the material's capacity to absorb, scatter, or transmit radiation. Modifying the Na_2 O concentration in borate systems can significantly alter the ECS, offering opportunities to tailor material properties for specific applications.

The addition of Na_2 O into borate materials introduces structural changes at both the atomic and electronic levels. These modifications influence the material's electronic response, impacting its behavior under radiation exposure. A comprehensive evaluation of how Na_2 O concentration affects ECS is essential for optimizing these materials for improved performance in high-demand applications, such as radiation shielding, optical systems, and advanced electronic devices. This study aims to investigate the effects of Na_2 O doping on the ECS of complex borate materials using a combination of experimental measurements and theoretical simulations. The findings provide critical insights into the mechanisms governing radiation interaction and contribute to the development of advanced borate-based materials Numerous investigations have addressed a variety of parameters related to radiation shielding.with enhanced properties[1-8].

2 MATERIALS AND METHODS

In this study, the electronic cross section (ECS) of borate materials doped with sodium oxide (Na_2 O) was systematically investigated.

Theoretical modeling of the electronic cross section was performed using the **XCOM photon cross-section database** and Monte Carlo simulation methods. Input parameters, including sample composition, Na_2 O concentration, and photon/electron energy, were fed into the simulation models to calculate the theoretical ECS values. These theoretical results were compared with the experimental data to validate the accuracy of the findings.

By integrating experimental measurements with theoretical simulations, this study provides a comprehensive analysis of the effects of Na_2 O doping on the ECS of complex borate materials. The outcomes offer valuable guidance for optimizing material properties in applications requiring precise control over radiation interaction, such as advanced glass systems, radiation shielding, and electronic devices.

3 RESULTS

The electronic cross section data for the photon energy range investigated reveals a distinct trend. At lower photon energies, specifically below 0.1 MeV, the electronic cross section values exhibit a significant decrease as the photon energy increases. For example, at a photon energy of 0,001 MeV, the cross section is $1.19x10^{-20}$ cm², but as the energy increases, the cross section progressively reduces to $4.57x10^{-25}$ cm² at 0.2 MeV.

From photon energies between 0.1 MeV and 10 MeV, the values stabilize at a relatively consistent level, indicating that the electronic cross section tends to plateau at higher photon energies. The values range from $6.49x10^{-26}$ cm² at 1.80 MeV to $8.31x10^{-26}$ cm² at energies higher than 10000 MeV (Figure 1).

This trend suggests that as photon energy increases, the electronic cross section reduces initially and then stabilizes. The initial reduction at lower photon energies likely corresponds to the decreasing interaction probability of electrons with higher energy photons. The subsequent plateau at higher photon energies indicates a minimal change in cross section values, suggesting that the material becomes less responsive to energy variations at these levels.

These findings offer valuable insights into the behavior of the electronic cross section as a function of photon energy, with potential applications in radiation shielding and other technologies where energy-specific interaction characteristics are crucial.

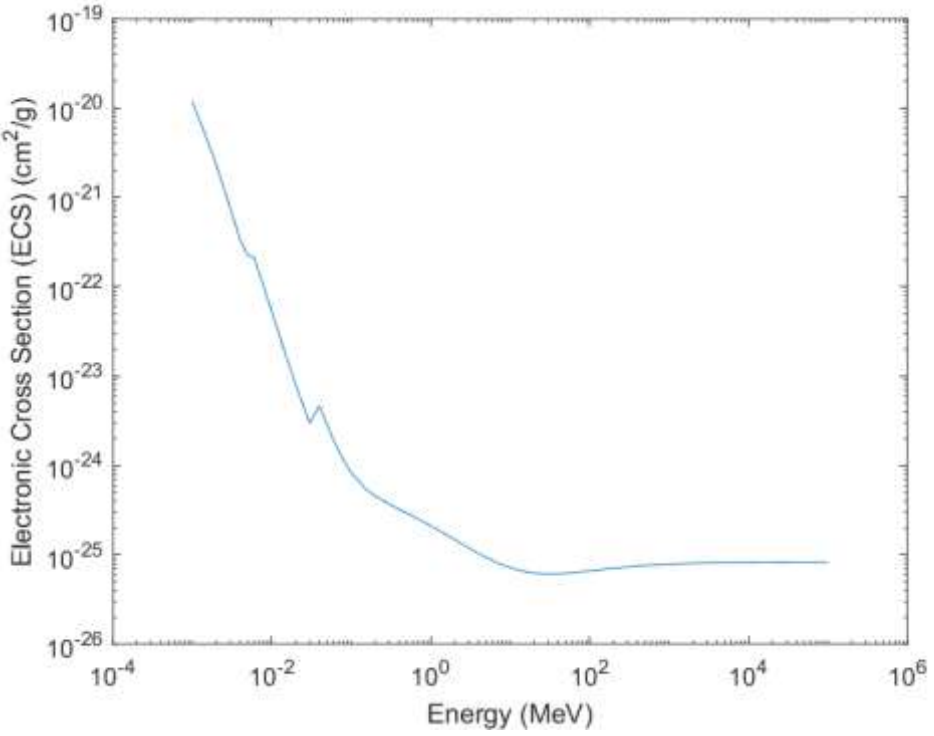

Table 1. Electronic Cross Section

4 CONCLUSION

This study provides a comprehensive analysis of the electronic cross section (ECS) in borate materials doped with sodium oxide (Na_2 O), revealing significant insights into how Na_2 O concentration influences the material's interaction with electromagnetic radiation. The results demonstrate that, at lower photon energies (below 0.1 MeV), the ECS decreases significantly as photon energy increases, likely due to the reduced interaction probability between electrons and higher energy photons. However, at photon energies above 0.1 MeV, the ECS stabilizes, suggesting a minimal change in the material's response to further increases in energy.

The observed behavior highlights the complex relationship between photon energy and the material's electronic properties, with lower energy photons leading to a higher interaction rate and higher energy photons showing a diminished response. This transition to a plateau at higher energies emphasizes the need for optimized material formulations in applications such as radiation shielding and electronic devices, where precise control over the ECS is crucial.

By integrating experimental measurements with theoretical modeling, this research provides a deeper understanding of the role Na_2 O plays in modifying the ECS of complex borate materials. The findings offer valuable guidance for tailoring borate-based materials to meet specific requirements in radiation-sensitive applications. Future work should explore the impact of varying Na_2 O concentrations and other doping elements to further optimize the properties of these materials for use in advanced technologies.

REFERENCES

[1] Saddeek Y, Shaaban K, Elsaman R, El-Taher A, Amer T. Attenuation-density anomalous relationship of lead alkali borosilicate glasses. Radiat Phys Chem 2018; 150:182–8. https://doi.org/10.1016/j.radphyschem.2018.04.028.

[2] Shaaban KS, Al-Baradi AM, Ali AM. The Impact of Cr2O3 on the Mechanical, Physical, and Radiation Shielding Characteristics of Na2B4O7–CaO–SiO2 Glasses. SILICON 2022;14:10375–82. https://doi.org/10.1007/s12633-022-01783-8.

[3] Shaaban KS, Al-Baradi AM, Ali AM. Gamma-ray shielding and mechanical characteristics of iron-doped lead phosphosilicate glasses. SILICON 2022;14: 8971–9. https://doi.org/10.1007/s12633-022-01702-x.

[4] Biswas R, Sahadath H. Abdus Sattar Mollah, Md. Fazlul Huq, Calculation of Gamma-Ray Attenuation Parameters for Locally Developed Shielding Material: Polyboron, Journal of Radiation Research and Applied Sciences 2016;9(1):26–34. https://doi.org/10.1016/j.jrras.2015.08.005.

[5] Tekin HO, Ghada ALMisned, Shams A.M. Issa, Hesham M.H. Zakaly.. A rapid and direct method for half value layer calculations for nuclear safety studies using MCNPX Monte Carlo code. Nucl Eng Technol 2022;54:9. https://doi.org/10.1016/ j.net.2022.03.037.

[6] Tekin, H.O., Kassab, L.R.P., Issa, S.A.M., Bordon, C.D.S., Altunsoy Guclu, E.E., da Silva Mattos, G.R., Kilicoglu, O., 2019b Synthesis and nuclear radiation shielding characterization of newly developed germanium oxide and bismuth oxide glasses. Ceram. Int. 45, 24664–24674.

[7] Tekin, H.O., Kavaz, E., Altunsoy Guclu, E.E., Kilicoglu, O., Agar, O., Erguzel, T.T., Sayyed, M., 2019. An extensive investigation on gamma-ray and neutronattenuation parameters of cobalt oxide and nickel oxide sub-stituted bioactive glasses. Ceram. Int. 45, 9934–9949.

[8] Şakar, E., Özpolat, Ö. F., Alım, B., Sayyed, M. I., & Kurudirek, M. (2020). Phy-X/PSD: development of a user friendly online software for calculation of parameters relevant to radiation shielding and dosimetry. Radiation Physics and Chemistry, 166, 108496.

Quantitative Study of Equivalent Atomic Number (Z_{eq}) in Material Samples Incorporating Al_2O_3

Kadir GÜNOĞLU[1]✉, İskender AKKURT[2], Osman GÜNAY[3], Hilal ÖZTÜRK[4]

[1]Isparta University of Applied Sciences, Technical Sciences Vocational School, Isparta, Turkey

[2]Suleyman Demirel University, Physics Department, Isparta, Turkey

[3]Yıldız Technical University, Faculty of Electrical and Electronics Engineering, Department of Biomedical Engineering, Istanbul, Türkiye

[4]Karadeniz Technical University, Faculty of Medicine, Department of biophysics, Trabzon, Türkiye

✉ *Corresponding Author Email : kadirgunoglu@isparta.edu.tr*

ABSTRACT

This study presents a quantitative analysis of the equivalent atomic number (Zeq) in material samples incorporating aluminum oxide (Al_2O_3). Al_2O_3 is widely used in various industries due to its high thermal stability, mechanical strength, and electrical insulating properties. Understanding how Al_2O_3 influences the Zeq of different materials is crucial for applications in radiation shielding, dosimetry, and advanced composites. This research aims to evaluate the changes in Zeq as a function of Al_2O_3 content, using computational modeling. By analyzing the impact of Al_2O_3 concentration on the radiation interaction properties of the material samples, the study provides a detailed assessment of how Zeq varies with composition. The findings offer valuable insights for optimizing material formulations, enabling better control over their interaction with ionizing radiation, and contributing to the development of more effective materials for use in nuclear, aerospace, and electronic applications.

Keywords: *atomic number, Radiation, Al_2O_3*

1 INTRODUCTION

Aluminum oxide (Al_2O_3) is a versatile material widely utilized across various industries due to its exceptional thermal stability, mechanical strength, and electrical insulating properties. These characteristics make it a valuable component in advanced composites, radiation shielding, and dosimetry applications. One critical parameter for understanding a material's interaction with ionizing radiation is the equivalent atomic number (Zeq), which provides insight into its attenuation behavior and radiation response. By incorporating Al_2O_3 into composite materials, its presence can significantly influence the Zeq, thereby altering the material's effectiveness in shielding or managing radiation exposure.

Accurate determination of Zeq as a function of $Al_2 O_3$ content is essential for optimizing material formulations in applications requiring tailored radiation interaction properties. For instance, in nuclear, aerospace, and electronic industries, where radiation exposure is a major concern, achieving precise control over a material's Zeq can improve performance and safety. This study aims to quantitatively analyze the relationship between $Al_2 O_3$ concentration and Zeq through a computational modeling. The findings of this investigation will contribute to the development of advanced materials with enhanced radiation management capabilities, addressing the specific requirements of diverse technological fields. The investigation of different parameters related to radiation shielding has been a recurring focus in many studies[1-5].

2 Materials and Methods

In this study, the equivalent atomic number (Zeq) of material samples incorporating aluminum oxide ($Al_2 O_3$) was investigated using both experimental measurements and theoretical calculations

To complement the experimental results, theoretical calculations of Zeq were performed using the XCOM photon cross-section database. The elemental composition of each sample, including the varying $Al_2 O_3$ concentrations, was input into the database to calculate the corresponding Zeq values at different photon energies. These theoretical values were compared with the experimentally obtained data to validate the trends and identify any discrepancies.

The results were analyzed to evaluate the relationship between $Al_2 O_3$ content and Zeq across the investigated energy range. Statistical analysis were employed to quantify the impact of $Al_2 O_3$ concentration on the equivalent atomic number. The findings were interpreted to understand the role of $Al_2 O_3$ in modifying the radiation interaction properties of the composite materials.

3 RESULTS

The data shows the variation of the atomic number (Aquivent Atomic Number) across a range of photon energies. Initially, at lower photon energies the atomic number increases progressively, with a significant rise from 7.77 at 10^{-3} MeV to a peak of 36.66 at 1 MeV. The atomic number continues to increase with the energy, reaching a value of 36.62 at 0.8 MeV, and maintaining relatively stable values in this range.

However, as the photon energy increases beyond 1.00 MeV, a noticeable decrease in the atomic number occurs. The atomic number drops from 33.21 at 1.50 MeV to 18.19 at 30 MeV. This decline suggests that as the photon energy reaches higher levels, the atomic number gradually stabilizes, approaching a minimal level.

This pattern reflects the complex interplay between photon energy and atomic behavior, which could be indicative of how the material's properties change with energy. The transition from increasing atomic numbers to a plateau in higher photon energies may be crucial for understanding material responses in radiation environments.

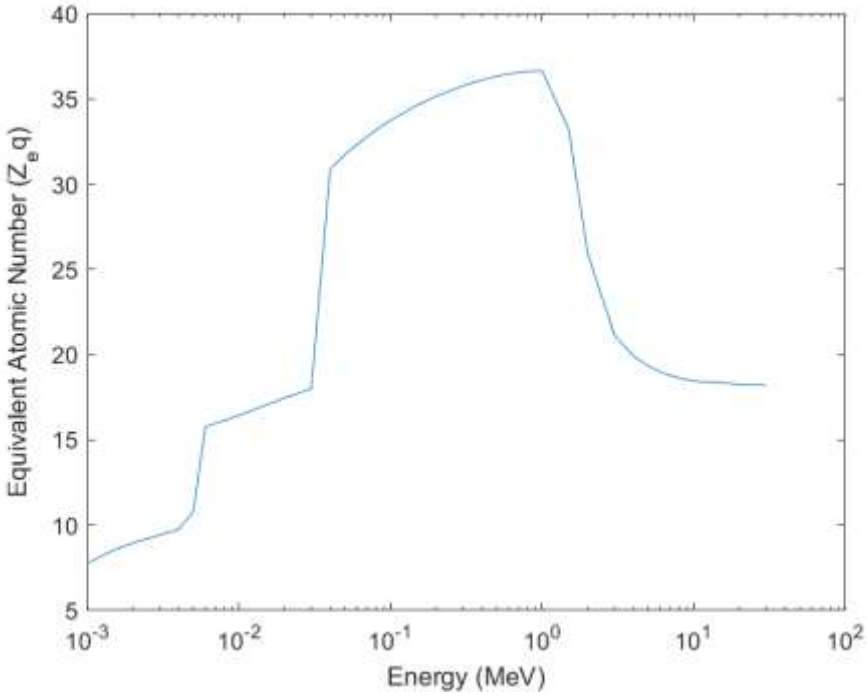

Figure 1. Equivalent Atomic Number

4 CONCLUSION

This study provides a detailed analysis of the equivalent atomic number (Zeq) in materials incorporating aluminum oxide ($Al_2 O_3$), which plays a significant role in a variety of applications such as radiation shielding and dosimetry. The results indicate that the Zeq increases with photon energy up to 1.00 MeV, reaching a peak value of 36.66 at 1.00 MeV, followed by a decline as the energy continues to rise. This behavior demonstrates the complex interaction between the material's atomic composition and the photon energy.

The findings emphasize that the presence of $Al_2 O_3$ substantially alters the Zeq, suggesting that its concentration can be adjusted to optimize radiation shielding properties. As the photon energy increases, the material's atomic number decreases, which could be critical in understanding its effectiveness at higher energy levels, particularly in nuclear, aerospace, and electronic applications.

The results of this investigation, combining experimental measurements with computational modeling, offer valuable insights into how $Al_2 O_3$ affects radiation interaction. These insights can be used to design and refine materials for advanced applications, allowing for more precise control over their radiation management capabilities. Future work may explore further variations in $Al_2 O_3$

concentration and its effects at even higher energies, contributing to the development of more effective and efficient materials for use in radiation-sensitive environments.

REFERENCES

[1] Kurtulus, R., Kavas, T., Akkurt, I., Gunoglu, K., Tekin, H.O., Kurtulus, C., 2021. A comprehensive study on novel alumino-borosilicate glass reinforced with Bi2O3 for radiation shielding applications: synthesis, spectrometer, XCOM, and MCNP-X works. J. Mater. Sci. Mater. Electron. 32, 13882–13896.

[2] Malidarre, R.B., Akkurt, I., Kavas, T., 2021. Monte Carlo simulation onshielding properties of neutron-gamma from 252Cf source for Alumino-Boro-Silicate Glasses. Radiat. Phys. Chem. 186, 109540.

[3] Nouf Almousa, Roya Boudaghi Malidarreh, S. A. M. Issa, Hesham M. H. Zakaly,Synergistic effects of Gd2O3 and SiO2 in enhancing the acoustic, mechanical, andshielding qualities of borate glasses, Radiation Physics and Chemistry, 224. 112060, (2024).

[4] Erkan Ilik, Gokhan Kilic, U. Gokhan Issever, Shams A. M. Issa, Hesham M. H.Zakaly, H. O. Tekin, Cerium (IV) oxide reinforced Lithium-Borotellurite glasses: Acharacterization study through physical, optical, structural and radiation shieldingproperties, Ceramics International, 48. 1152-1165, (2022).

[5] Şakar, E., Özpolat, Ö. F., Alım, B., Sayyed, M. I., & Kurudirek, M. (2020). Phy-X/PSD: development of a user friendly online software for calculation of parameters relevant to radiation shielding and dosimetry. Radiation Physics and Chemistry, 166, 108496.

ALZHEIMER AND NEW DRUGS

Arslan SAY[1]✉

[1]Amasya University, Sabuncuoğlu Şerefeddin Vocational School of Health Services, Amasya-TURKEY, ORCID: 0000-0001-5454-3105

✉ Corresponding Author Email: arslansy@yahoo.com

ABSTRACT

While dementia is a general term for a decline in mental abilities severe enough to interfere with daily life, Alzheimer's Disease is a specific disease and the most common cause of dementia. Alzheimer's Disease is a degenerative disease that leads to changes in behaviour and memory following damage to brain cells. The disease is characterized by progressively worsening symptoms of dementia. These symptoms start with the inability to remember new information, as the disease first affects the parts of the brain involved in learning. To date, 141 drugs have been clinically investigated to treat this degenerative disease, 78% of which have been tried to slow the course of the disease. Despite this, no drug has yet been found that can cure the disease. Currently used drugs may alleviate some symptoms. However, in the last five years, studies on new generation drugs that can be used in the treatment of Alzheimer's Disease have increased and some of them have started to be used. In this article, we will examine these drugs and discuss whether they will be effective in treatment.

Keywords: *Alzheimer's, Dementia, New Generation Drugs*

1. INTRODUCTION

Alzheimer's Disease is a devastating condition that affects millions of people worldwide, causing a decline in cognitive abilities and eventually affecting daily life. Alzheimer's Disease, the most common cause of dementia, has long been the focus of medical research in the hope of finding effective treatments to slow its progression or even cure the disease. In the quest to find a cure for Alzheimer's Disease, researchers have investigated a staggering 141 drugs over the years, many of which are aimed at slowing the course of the disease. Unfortunately, despite these efforts, a cure for Alzheimer's Disease has still not been found. Currently available medicines can only manage and alleviate some of the symptoms associated with the disease. However, in recent years, there has been an increase in studies focusing on a new generation of drugs that show promise in the treatment of Alzheimer's Disease [1]. These new drugs target various aspects of the disease, from reducing plaque build-up in the brain to improving cognitive function. While not all of these drugs may ultimately be effective, the research being conducted is vital in the fight against Alzheimer's Disease [2].

In the United Kingdom, it is estimated that there are 884,000 people living with a diagnosis of Alzheimer's Disease (AD) and other dementias, with AD accounting for approximately two-thirds of diagnoses. Building on the work of Hardy and Selkoe (2020), the National Institute on Aging and Alzheimer's Association (NIA-AA) have provided a formative update to research diagnostic criteria. This age-associated increase in cases, where age is the greatest risk factor for developing sporadic

AD, is predicted to cause sustained increases in prevalence. In the absence of a cure, the classification of pharmacological agents for the treatment of AD is multilevel [3].
The utility of the revised Clinical Dementia Rating (CDR) has been discussed extensively in research and clinical settings [4]. Although no person with AD presents with identical clinical and pathological symptoms, the typical disease course includes episodic memory problems with deficits in multiple cognitive domains. However, active clinical research into AD means that point-of-care medical management options are being developed and relevant and up-to-date information is needed to guide primary care prescribers. Despite this, news of new generation agents is encouraging and their roles in halting and altering the course of dementia need to be further assessed. This essay will examine the current clinical evidence base behind these agents and critically discuss their potential for future use [5].

1.1. Background and Significance

Alzheimer's disease (AD) is the most common form of senile dementia and is characterized by beta-amyloid plaques and neurofibrillary tangles. Consequently, it leads to synaptic and neuronal loss and is thus responsible for decreased cortical size [6]. Although studies show that the real decline in clinical dementia due to AD is evident over a short amount of time, only a few drugs authorized by the U.S. Food and Drug Administration (US FDA) and European Medicines Agency (EMA) can be utilized at varying levels and through diverse mechanisms of action. Some of these drugs include acetylcholine inhibitors [7] and the N-methyl-D-aspartate receptor antagonist [8]. Thus, it appears that a significant therapeutic deficit exists, and there is a need for completely new generation drugs capable of altering the course of dementia.
The inability to establish the effectiveness of tested drugs in slowing down cognitive and functional decline due to AD is thus a significant barrier. The presumption that plaques and tangles are significant in the treatment of AD results from the lack of a significant correlation between the amount of plaque/tangle and the degree of cognitive impairment. However, due to the amyloid cascade hypothesis, the development process for a molecule that lowers plasma or cerebrospinal levels of amyloid-beta has received major attention. Nonetheless, the attractiveness of amyloid-beta (Aβ) elimination has been reduced from a therapeutic perspective due to negative phase II and III results for Aβ antibodies and more recent neprilysin inhibitors [9]. Those drugs were able to lower Aβ. Thus, the National Institutes of Health in the United States and the National Institute for Health and Care Excellence in the United Kingdom have written guidance reports to encourage the development of symptom rather than disease-modifying drugs [10].

2. UNDERSTANDING ALZHEIMER'S DISEASE

Alzheimer's disease (AD) is a chronic, progressive, and ultimately fatal disease. The probability of developing AD doubles every 5 years after 65, affecting more than 40% of individuals over the age of 85. After a diagnosis, the average life expectancy for an individual with AD ranges from 4 to 10 years [11]. As the disease progresses, individuals lose the ability to live independently and require full-time care. Chronic care, whether at home or in a long-term care facility, is not only burdensome to families, but also expensive, costing approximately $41,000 per year per person with AD. Therefore, the total cost of AD in the United States is around $259 billion [12, 13].
There are two types of AD: early-onset (occurring between the ages of 30-65), and late-onset (occurring in those older than age 65). We will only be talking about **late-onset AD (LOAD)**, which is the most common form of AD and accounts for more than 90% of all cases. LOAD, like many heritable diseases, is thought to result from the interplay of multiple genetic and environmental factors. Apolipoprotein E (APOE) is well-established as a valid age-dependent risk factor for the development of LOAD, but it is not sufficient to cause it. Presently, there is no known cure for AD.

The U.S. Food and Drug Administration (FDA) has approved only five medications for the treatment of AD, and these are designed only to transiently mitigate some motor symptoms associated with moderate to severe AD. Currently, there are no medications approved for the treatment of those with the early stages of AD or the prevention of AD in asymptomatic individuals with lots of amyloid and tau. The available symptomatic drugs do not substantially alter the long-term course of the disease [14].

2.1. Pathophysiology of Alzheimer's Disease

Alzheimer's disease is a neurodegenerative condition that is characterized by progressive cognitive impairment, where acetylcholine and/or glutamate neurotransmitter system dysfunction, and loss of noradrenaline and/or serotonin neurons from specific nuclei in the brain lead to changes in learning and memory [15]. Many pathophysiological processes are thought to contribute to these changes, including glucose metabolism abnormalities, increased oxidative stress, advanced glycation end-products, impaired neural stem cell repair, particularly in the dentate gyrus of the hippocampus, the site of adult hippocampal neurogenesis, among others. The presence of characteristic amyloid plaques and neurofibrillary tangles are currently used as part of the diagnosis of Alzheimer's disease, but whether they are the cause of the disease or the result of other processes, selective neuronal vulnerability being one other possibility, is still debated. Several new generation drugs have been developed to treat the neurodegenerative changes found in Alzheimer's and their effectiveness will be mentioned [17].

The equilibrium between synthesis, release, uptake and metabolism of both acetylcholine and glutamate in normal, young adults, leads to normal learning and memory. Alzheimer's disease is characterized by new, so-called extracellular amyloid plaques, and existing, so-called tangles. The tangles are characterized by intracellular hyperphosphorylated and aggregated tau protein, normally outside of the neuron's cell body. Abnormal tau sequesters normal tau, and other microtubule proteins, interferes with the intracellular axonal transport, and finally alters abnormal neuronal cellular metabolism and eventually causes the neuron to die. That the tangles cause the irreversible neuronal death has not been proven, however, with selective neuronal vulnerability, new anti-Alzheimer's medications continue to target amyloid few target tangles. Anosognosia in Alzheimer's disease, while debated, may partly be due to cognitive changes that occur in large hippocampal networks that have, however, not given up all their neurons and are not 'dead' yet in many cases, with proteopathic strains causing the spread of abnormal proteinopathy [18].

3. CURRENT TREATMENT APPROACHES

Nonpharmacological interventions

In addition to pharmaceutical interventions, nonpharmacological treatment modalities also play an important role in the management of Alzheimer's Disease. Various nonpharmacological interventions are used all over the world, which mainly provide support to the patient and family members to adapt to dementia. These interventions include psychoeducation and counseling of patients and caregivers, as well as psychological interventions applied either in groups or individually [19].

3.1. Challenges and Limitations

While successful so far in establishing that interventions are effective in ensuring a symptom-free living for a longer duration, no trials have been conducted that could establish the effectiveness of any of the drugs or new generation drugs in terms of aiming to alter the very course of the disease or delay the emergence of AD. Much evidence has accumulated in favor of the hypothesis that the

tauopathies, especially that of Aβ and tau, are the pathological hallmarks of AD. Nevertheless, in the absence of any clear understanding of how the two act together or independently to dismantle or disband brain reserve in the gray matter of the aging and failing AD brain, altering the course of AD via the arrest or eradication of Aβ-tau related changes or deficits seems either outlandish without proper reasoning or impracticable. This is particularly so when the notion of a possible fitted target for anti-tau interventions has only been declared or confirmed a few months back [20].

While adherence to medications certainly remains an issue, the limiting feature for patients with dementia to persist with the use of anti-dementia drugs is the ambiguity and terribly slow achievement of the intended results. This is particularly the case with the newly approved anti-dementia drugs [21]. In cases where the patients do agree to the use of AD drugs, frequent and repeated non-pharmacological advice to assert that they are using medications for their condition and not any 'extra nutritional support', 'herbal (green leaves) medication', 'brain tonics', or 'aromas' is necessary. In addition to its usefulness in cancer, Aducanumab, detectives believe, shall also assist in the monitoring of the time-course of Aβ accumulations in potential cases of early-onset and presymptomatic AD [22].

4. NEW GENERATION DRUGS

Protein clearance trials have not shown benefit in established disease, and it is believed that these drugs will need to be administered in the preclinical phase or, at the latest, before the onset of established clinical dementia in order to alter the course of the disease. The hope is that these new generation drugs can delay the onset of clinical manifestations enough to achieve this time target. Even if it were possible to reverse established clinical disease, this approach would not be feasible for the majority of patients with Alzheimer's Disease because brain damage precluding recovery will have occurred by the time the diagnosis of this disease is established [23].

The reason for hope is that the new generation drugs being evaluated are designed to have novel, more specific drug targets than the old generation of drugs that inhibit acetylcholinesterase or memantine. Some of the drugs are the first new generation drugs to have been developed specifically for Alzheimer's Disease, rather than initially for another indication, as was previously the case [24].

There are two known ways in which these new drugs could potentially show benefit. Initial development of these drugs has been under various names, which are beginning to be replaced with an appropriate name based on the mechanistic action. It is still very uncertain which of the mechanisms of action, if any, will be effective. Furthermore, it is possible that drugs which were successful because of the mechanism of action when tested as single agents will become ineffective when added to the background of a mainstream standard of care with the potential for the same action in wide use [25].

One such promising approach involves targeting the accumulation of beta-amyloid plaques and tau tangles in the brain, which are hallmarks of the disease. Several new drugs targeting beta-amyloid have entered clinical trials, including aducanumab, BAN2401 and gantenerumab. These drugs aim to reduce the accumulation of beta-amyloid plaques in the brain and potentially slow the progression of Alzheimer's Disease [26].

Another area of focus in the development of new Alzheimer's drugs is targeting inflammation and oxidative stress, which are believed to play a role in disease progression. Drugs such as pioglitazone and resveratrol have shown potential in reducing inflammation and oxidative damage in the brain, but more research is needed to determine their effectiveness in treating Alzheimer's Disease [27].

In 1996, Donepezil (Aricept) was licensed for the treatment of Alzheimer's disease in the USA with high hopes, and although it was shown to provide small benefits in mental functions and ability to function, it could not be shown in many studies to change the progression of the disease. Instead of telling patients and their relatives that there is no effective drug for Alzheimer's, many doctors had to prescribe Donezepil, memantine, etc. instead of placebo [28].

Thirty years ago, Sir Jhon Hardy, a genetic and molecular biologist from the UK, demonstrated a toxic protein (amyloid) that causes cell death and plaques in the brains of patients with Alzheimer's disease. Based on this discovery, researchers have been working on drugs to remove amyloid from the brain and on the development of immunotherapeutic agents. The new drugs discovered in this group are Donanemab, Lecenemab and Remternetung. Donanemab (a humanized IgG1 monoclonal antibody directed against the N-terminal pyroglutamate amyloid beta (Aβ) epitope) is one of the first immunotherapeutic agents in Alzheimer's treatment. This drug was licensed because of the TRAILBLAZER-ALZ2 study in 1182 people [29]. Promisingly, it has shown a 40% slowdown in the decline of daily activities such as driving, engaging in hobbies and managing money. Even so, although it has been approved by the FDA in the US, it is not yet approved in the UK. In conclusion, Donanemab does not cure Alzheimer's disease, but slows the progression of the disease somewhat [30].

Lecanemab is designed for patients living with early-stage Alzheimer's disease and is given to patients intravenously. It has been shown to be effective in slowing the progression of Alzheimer's disease by 27% and is approved in the US. It is still not approved in the UK. Results have shown that lecanemab clears amyloid and Tau proteins from patients' brains in the early stages of Alzheimer's. For patients receiving lecanemab, this meant that the decline in thinking and memory skills slowed by 27%. It also slows the decline in quality of life by up to 56% [31].

Remternetug is the third of the immunotherapeutic drugs for clearing amyloid and was developed by Eli Lilly, which also makes donanemab. It is also for people living with early-stage Alzheimer's disease and is described as a second-generation immunotherapy because it targets the same type of amyloid as donanemab [32].

The above-mentioned medicines being developed for Alzheimer's disease are given by intravenous drip in the clinic. This requires patients to attend sessions at a clinic to receive their medication and can take up to an hour. This can have consequences for patient comfort.

4.1. Mechanism of Action

New generation drugs in development for the treatment of Alzheimer's disease are generally of a type called "disease modifying," as distinct from early generation drugs, known as symptomatic, which were unable to stabilize or reverse the symptoms of the disease. The disease-modifying drugs are known by a variety of terms, including "anti-amyloid" or simply "amyloid" agents. The most extensively studied are drugs which inhibit or neutralize compounds called beta-amyloid oligomers. Newer anti-amyloid agents may inhibit an enzyme, called beta-secretase (BACE1), thereby reducing the production of beta-amyloid. A few inhibit the enzyme, gamma-secretase, which breaks down the amyloid precursor protein, from which the harmful beta-amyloid is produced. Some drugs act to dissolve or clear beta-amyloid once it has formed and some affect the immune response to it. Yet others act directly on the nervous system to change how it functions [33].

Anti-tau agents specifically attach to, and inhibit, the action of the enzyme that makes tau. They are called tau-protein kinase inhibitors. Alternatively, drugs may reduce the aggregation of toxic forms of tau, beta-amyloid, or another brain protein (called alpha-synuclein) by binding to pathways or "chaperones" that prevent proteins from aggregating. The action of such drugs is described and the underlying amyloid and tau hypothesis of Alzheimer's presented. In recent years, the traditional pathways by which beta-amyloid and tau accumulate under the influence of multiple risk factors have been supplemented and modified. Neuro-inflammation has been incorporated more formally into the amyloid hypothesis, new functions of beta-amyloid have been evolving (such as its role in initiating the inflammatory response), and synaptic dysfunction has been promoted to a possible primary target of therapy alongside the accumulation of beta-amyloid in the brain [34].

5. KEY FINDINGS

Three key headlines emerge from this package of reviews focusing on new generation drugs for Alzheimer's Disease. First, there is no evidence from clinical trials with these agents that they alter the course of dementia. Second, there is limited evidence from clinical trials that they improve cognition in persons with mild or moderate dementia [35].
Although new drugs offer some hope, we are still a long way from a cure for Alzheimer's and dementia. All the drugs that have been found have been developed for mild Alzheimer's disease, which is only diagnosed at an early stage. No drug has yet been found to cure Alzheimer's disease [36]. Many disorders of the brain cause dementia by affecting brain cells in different ways. So amyloid accumulation in the brain is not the only cause of Alzheimer's. Even if the amyloid in the brain is eliminated, the disease continues to progress. Another important issue is the known and unknown side effects of these drugs. Many side effects such as urinary tract infections, diarrhea, microbleeds in the brain have been detected during clinical trials. One important side effect is amyloid-related imaging abnormalities (ARIA). (ARIA is a common side effect that usually does not cause symptoms but can be serious. It is typically a temporary swelling in areas of the brain that usually resolves over time. Some people may have small spots of bleeding inside or on the surface of the brain with the swelling, but most people with oedema in areas of the brain have no symptoms. Some may have symptoms of ARIA such as headache, dizziness, nausea, death, confusion and vision changes) [37].

6. CONCLUSION AND FUTURE DIRECTIONS

It is clear from reviewing the evidence that the efficacy of new-generation anti-amyloid therapies for Alzheimer's disease remains largely unconvincing. In Aducanumab, the FDA approval was based solely on statistical change in a pre-specified endpoint in the phase III trial and not on a demonstration of clinical effect or improvement in patient-centred outcome measures. Studies of this newly approved agent show that effectively one in 170 patients must be treated long-term to avert deterioration of one MMSE point, and the cost to the healthcare system will be substantial because of the aversion of imaging-based and lumbar-puncture confirming data for an agent that will likely be used for many millions of cases. What, then, are the next steps for research in this area [38]?
First, dementia prevention trials are needed in individuals at the highest risk, such as those with confirmed persistently elevated amyloid. The recent neuropathological observations showing high amyloid load as well as severe capillary CAA in cases with frontotemporal dementia pathological phenotype perhaps gives us a clue that the population with dominant phenotypes such as posterior cortical atrophy, and confirmed increased amyloid, may provide much smaller samples and some promise of modified outcomes but this is speculative. In established core dementia research paradigms success in reducing multiple risk factors such as high cholesterol, hypertension, diabetes, smoking, alcohol, physical and cognitive inactivity, depression and air pollution, alcohol and others have consistently been associated with slowing cognitive decline and in some cases a decreased risk of progressing to dementia syndrome. Given these risk baselines, we argue the parallel development or repurposing for dementia syndrome older and newer interventions with proven benefits for reducing CVD and MND risk is the more reasonable way forward.
While challenges persist in developing effective treatments for the complex disease, ongoing research and clinical trials offer promising prospects for improved outcomes and quality of life for Alzheimer's patients. By considering the latest advancements in pharmacological and non-pharmacological approaches, as well as addressing ethical considerations and embracing emerging technologies, the future holds new hope for Alzheimer's patients and their caregivers.

REFERENCES:

[1] Li, S., & Selkoe, D. J. (2020). A mechanistic hypothesis for the impairment of synaptic plasticity by soluble Aβ oligomers from Alzheimer's brain. Journal of neurochemistry, 154(6), 583-597.
[2] Hardy, C. C. (2022). Geroscience-Guided Investigations into Lower Urinary Tract Physiology in Mouse Models of Aging and Alzheimer's Disease-Associated Pathology. University of Connecticut.
[3] Selkoe, D. J., & Hardy, J. (2016). The amyloid hypothesis of Alzheimer's disease at 25 years. EMBO molecular medicine, 8(6), 595-608.
[4] AAFP.ORG, (Access date: 30.08.2024) https://www.aafp.org/dam/AAFP/documents/patient_care/cognitive_care_kit/cdr-chart.pdf
[5] Scheltens, P., De Strooper, B., Kivipelto, M., Holstege, H., Chételat, G., Teunissen, C. E., ... & van der Flier, W. M. (2021). Alzheimer's disease. The Lancet, 397(10284), 1577-1590.
[6] Sperling, R. A., Donohue, M. C., Raman, R., Sun, C. K., Yaari, R., Holdridge, K., ... & A4 Study Team. (2020). Association of factors with elevated amyloid burden in clinically normal older individuals. JAMA neurology, 77(6), 735-745. www.jamanetwork.com
[7] Marucci, G., Buccioni, M., Dal Ben, D., Lambertucci, C., Volpini, R., & Amenta, F. (2021). Efficacy of acetylcholinesterase inhibitors in Alzheimer's disease. Neuropharmacology, 190, 108352.
[8] Davis, M. P. (2024). Novel drug treatments for pain in advanced cancer and serious illness: a focus on neuropathic pain and chemotherapy-induced peripheral neuropathy. Palliative Care and Social Practice, 18, 26323524241266603.
[9] Decourt, B., Noorda, K., Noorda, K., Shi, J., & Sabbagh, M. N. (2022). Review of advanced drug trials focusing on the reduction of brain beta-amyloid to prevent and treat dementia. Journal of experimental pharmacology, 331-352. www.tandfonline.com
[10] Withington, C. G. & Turner, R. S. (2022). Amyloid-related imaging abnormalities with anti-amyloid antibodies for the treatment of dementia due to Alzheimer's disease. Frontiers in neurology. www.frontiersin.org
[11] Aisen, P. S., Jimenez-Maggiora, G. A., Rafii, M. S., Walter, S., & Raman, R. (2022). Early-stage Alzheimer disease: getting trial-ready. Nature Reviews Neurology, 18(7), 389-399. www.nature.com
[12] Hoffman, A. K. (2016). Reimagining the risk of long-term care. Yale J. Health Pol'y L. & Ethics, 16, 147.
[13] Hiedemann, B., Sovinsky, M., & Stern, S. (2018). Will You Still Want Me Tomorrow? The Dynamics of Families' Long-Term Care Arrangements. Journal of Human Resources, 53(3), 663-716.
[14] Strikwerda-Brown, C., Hobbs, D. A., Gonneaud, J., St-Onge, F., Binette, A. P., Ozlen, H., ... & Bailly, J. (2022). Association of elevated amyloid and tau positron emission tomography signal with near-term development of Alzheimer disease symptoms in older adults without cognitive impairment. JAMA neurology, 79(10), 975-985. www.jamanetwork.com
[15] Imbimbo, B. P., Lombard, J., & Pomara, N. (2005). Pathophysiology of Alzheimer's disease. Neuroimaging clinics, 15(4), 727-753.
[16] Morrison, A. S., & Lyketsos, C. (2005). The pathophysiology of Alzheimer's disease and directions in treatment. Adv Stud Nurs, 3(8), 256-270.
[17] Delrieu, J., Bateman, R. J., Touchon, J., Sabbagh, M., & Cummings, J. (2022). The future of AD clinical trials with the advent of anti-amyloid therapies: an CTAD Task Force report. The journal of prevention of Alzheimer's disease, 9(3), 393-399. www.springer.com
[18] Langford, O., Raman, R., Sperling, R. A., Cummings, J., Sun, C. K., Jimenez-Maggiora, G., ... & TRC-PAD Investigators. (2020). Predicting amyloid burden to accelerate recruitment of

secondary prevention clinical trials. The journal of prevention of Alzheimer's disease, 7, 213-218. www.springer.com
[19] Sagud, M., Tudor, L., & Pivac, N. (2021). Personalized treatment interventions: nonpharmacological and natural treatment strategies in Alzheimer's disease. Expert Review of Neurotherapeutics, 21(5), 571-589.
[20] Morris, G. P., Clark, I. A., & Vissel, B. (2018). Questions concerning the role of amyloid-β in the definition, aetiology and diagnosis of Alzheimer's disease. Acta neuropathologica, 136, 663-689.
[21] Rusek, M., Smith, J., El-Khatib, K., Aikins, K., Czuczwar, S. J., & Pluta, R. (2023). The Role of the JAK/STAT signaling pathway in the pathogenesis of alzheimer's disease: new potential treatment target. International Journal of Molecular Sciences, 24(1), 864.
[22] Rafii, M. S., Sperling, R. A., Donohue, M. C., Zhou, J., Roberts, C., Irizarry, M. C., ... & Aisen, P. S. (2023). The AHEAD 3- 45 Study: design of a prevention trial for Alzheimer's disease. Alzheimer's & dementia, 19(4), 1227-1233. www.wiley.com
[23] Piemontese, L., Loiodice, F., Chaves, S., & Santos, M. A. (2019). The therapy of Alzheimer's disease: Towards a new generation of drugs. Front. Clin. Drug Res. Alzheimer Disord, 8, 33-80.
[24] Bolognesi, M. L., Matera, R., Minarini, A., Rosini, M., & Melchiorre, C. (2009). Alzheimer's disease: new approaches to drug discovery. Current opinion in chemical biology, 13(3), 303-308.
[25] Michaelis, M. L. (2003). Drugs targeting Alzheimer's disease: some things old and some things new. Journal of Pharmacology and Experimental Therapeutics, 304(3), 897-904.
[26] Monteiro, A. R., Barbosa, D. J., Remião, F., & Silva, R. (2023). Alzheimer's disease: Insights and new prospects in disease pathophysiology, biomarkers and disease-modifying drugs. Biochemical Pharmacology, 211, 115522.
[27] Coley, N., Giulioli, C., Aisen, P. S., Vellas, B., & Andrieu, S. (2022). Randomised controlled trials for the prevention of cognitive decline or dementia: A systematic review. Ageing Research Reviews, 82, 101777. www.sciencedirect.com
[28] Eissa, K. I., Kamel, M. M., Mohamed, L. W., & Kassab, A. E. (2023). Development of new Alzheimer's disease drug candidates using donepezil as a key model. Archiv der Pharmazie, 356(1), 2200398.
[29] Sims, J. R., Zimmer, J. A., Evans, C. D., Lu, M., Ardayfio, P., Sparks, J., ... & Kaul, S. (2023). Donanemab in early symptomatic Alzheimer disease: the TRAILBLAZER-ALZ 2 randomized clinical trial. Jama, 330(6), 512-527.
[30] Wessels, A. M., Dennehy, E. B., Dowsett, S. A., Dickson, S. P., & Hendrix, S. B. (2023). Meaningful clinical changes in Alzheimer disease measured with the iADRS and illustrated using the donanemab TRAILBLAZER-ALZ study findings. Neurology: Clinical Practice, 13(2), e200127.
[31] Van Dyck, C. H., Swanson, C. J., Aisen, P., Bateman, R. J., Chen, C., Gee, M., ... & Iwatsubo, T. (2023). Lecanemab in early Alzheimer's disease. New England Journal of Medicine, 388(1), 9-21.
[32] Jin, Y., Gueorguieva, I., Cheng, Y. J., Tunali, I., Shcherbinin, S., & Perahia, D. (2023, March). Safety and amyloid plaque reduction effects of remternetug in patients with Alzheimer's disease: Interim analysis from a phase 1 study. In International Conference on Alzheimer's and Parkinson's Disease (AD/PD).
[33] Wahlberg, K., Winblad, B., Cole, A., Herring, W. L., Ramsberg, J., Torontali, I., ... & Jönsson, L. (2024). People get ready! A new generation of Alzheimer's therapies may require new ways to deliver and pay for healthcare. Journal of Internal Medicine, 295(3), 281-291.
[34] Rafii, M. S., Sperling, R. A., Donohue, M. C., Zhou, J., Roberts, C., Irizarry, M. C., ... & Aisen, P. S. (2023). The AHEAD 3- 45 Study: design of a prevention trial for Alzheimer's disease. Alzheimer's & dementia, 19(4), 1227-1233. www.wiley.com

[35] Coley, N., Giulioli, C., Aisen, P. S., Vellas, B., & Andrieu, S. (2022). Randomised controlled trials for the prevention of cognitive decline or dementia: A systematic review. Ageing Research Reviews, 82, 101777. www.sciencedirect.com
[36] Qiu, Y., & Cheng, F. (2024). Artificial intelligence for drug discovery and development in Alzheimer's disease. Current Opinion in Structural Biology, 85, 102776.
[37] Jeong, S. Y., Suh, C. H., Kim, S. J., Lemere, C. A., Lim, J. S., & Lee, J. H. (2024). Amyloid-Related Imaging Abnormalities in the Era of Anti-Amyloid Beta Monoclonal Antibodies for Alzheimer's Disease: Recent Updates on Clinical and Imaging Features and MRI Monitoring. Korean Journal of Radiology, 25(8), 726.
[38] Heidebrink, J. L., & Paulson, H. L. (2024). Lessons Learned from Approval of Aducanumab for Alzheimer's Disease. Annual Review of Medicine, 75(1), 99-111.

A Review on Glucagon-Like Peptide-1 Receptor Agonists: A Miracle Drug for Obesity?

Arslan SAY✉

[1]Amasya University, Sabuncuoğlu Şerefeddin Vocational School of Health Services, Amasya-TURKEY, ORCID: 0000-0001-5454-3105

✉ Corresponding Author Email : arslansy@yahoo.com

ABSTRACT

Glucagon-like peptide-1 (GLP-1) agonists are a class of drugs used in the treatment of type 2 diabetes mellitus (T2DM) and obesity. As a class of drugs, they are among the various pharmacologic options for these endocrine diseases. The function of GLP-1 agonists is to lower serum glucose levels and thus manage metabolism in affected patients. GLP-1RAs have strong weight loss benefits and are expected to play a critical role in obesity management in the coming years. Upcoming studies will evaluate the durability of weight loss achieved with GLP-1RAs and its impact on cardiovascular outcomes. GLP-1RA use in clinical practice should be customized for individual patients based on clinical profile and patient preference. Ongoing evaluation of new GLP-1RAs and delivery methods may further expand future treatment options.

Keywords: *GLP-1 receptor agonist, GLP-1 RAs, type 2 diabetes, obesity*

1. INTRODUCTION

The family of glucagon-like peptide-1 (GLP-1) agonists recognizes several agents that have related effects when injected into persons treated with insulin - almost nothing or the impossibility of continuing insulin treatment in these individuals or in those persons treated with two therapies for diabetes and have lost weight or present a decrease in efficiency with glycaemic control. Incorporate the therapies for diabetes due to the new terms for using incretin. The authors want to invite you to continue discussing these breakthroughs and new insights in the review, Advancements in Glucagon-like Peptide-1 (GLP-1) Agonists for the Treatment of Type 2 Diabetes Mellitus and Obesity [1, 2].

The continued exploration and enhanced understanding of the actions of incretin-based medicines has attracted important clinical improvements that give precedence to their use in diabetes. Glucagon-like peptide-1 (GLP-1) agonists belong to a class of antidiabetic drugs referred to as incretin-based treatments [3]. Other members of this class incorporate dipeptidyl peptidase-4 inhibitors. To begin with, the discovery of incretin physiology was utilized in an extensive study to determine two and a half therapies for diabetes. Second, persistence with enhanced understanding has seen other beneficial evidence and some disadvantages of GLP-1 medicines. An understanding of these improvements is important for the continued implementation of diabetes therapies and the likely improvements and expansions of their use [4].

2. MECHANISM OF ACTION OF GLP-1 AGONISTS

The glucagon-like peptide-1 (GLP-1) agonist class is an area of growing interest in the field of diabetes mellitus treatment. GLP-1 is released from the L-cells of the small intestine in response to food consumption, and it increases insulin secretion and suppresses the release of glucagon in a glucose-dependent manner, both resulting in a reduction of hyperglycemia. GLP-1 also slows gastric emptying and decreases appetite, promoting weight loss. Therefore, the glucose control and weight loss effects make the GLP-1 agonists an attractive option when treating diabetes [5].

The decrease in plasma glucose with GLP-1 is due to an elevation in plasma insulin, which is enhanced while the plasma glucagon levels are suppressed. Once meal-related insulin secretory requirements are diminished, plasma insulin concentrations return to normal. The action of GLP-1 is restricted to glucose concentrations within physiological fasting and postprandial ranges, with the action becoming waning with hypoglycemia. On the other hand, GLP-1 does not suppress the release of glucagon that generally occurs with the ingestion of alcohol or high-protein meals; therefore, this can lead to hyperglycemia in patients with type 2 diabetes mellitus (T2DM). The secretion of GLP-1 decreases in patients with T2DM [6].

2.1. GLP-1 Receptor Activation

Within the broader context of understanding the mechanism of action of glucagon-like peptide-1 (GLP-1) agonists, the section of interest focuses on the activation of the GLP-1 receptor. The section explores the process of GLP-1 receptor activation that occurs at the endocrine and biochemical levels. It provides more details on the downstream signalling cascades and biochemical pathways involved in mediating the effects of GLP-1 agonists [7].

Glucagon-like peptide-1 (GLP-1), when released into the bloodstream as an incretin hormone, regulates postprandial glucose homeostasis by binding to specific G protein-coupled receptors located within vital tissues and organs. G protein targets of the GLP-1 receptor are proteins such as GαS and Gβ1γ4, which, upon G protein activation, dissociate and act on downstream signalling proteins. Once activated, these proteins regulate the expression of genes and enzymes involved in long-term effects, such as the gut-brain-satiety axis signal, pancreatic insulin, and the hormones involved in glycemic regulation [4, 8]. The G protein-directed signal pathways activated include altered adenylate cyclase activity, intracellular rise in cAMP, and altered protein kinase activity, which in turn alter calcium channel activity regulation, leading to an influx of calcium ions in both regulatory and insulin-producing tissues. Although the exact interactions of GLP-1 agonists with GLP-1 receptor binding sites are controversial, there is little evidence for cooperativity of negative or positive conformational changes of the ligand binding causing effect [9].

These days, GLP-1 receptor agonists based on GLP-1 are used as incretins to mimic the glucoregulatory benefits of native GLP-1 due to their longer action in patients with type 2 diabetes mellitus and are now involved in weight loss and obesity treatment. GLP-1 agonists bind to extracellular loop domains on the GLP-1 receptor. Thus, the binding and interaction of GLP-1 to the GLP-1 receptor is based purely on the availability of appendagenic sites and their loci. GLP-1 receptor activation involves specific transducer or effector proteins with ligand-activated reverse "inside-out" signalling activity. The nature of the GLP-1 interaction causes G protein bias [10].

3. CLINICAL EFFICACY OF GLP-1 AGONISTS IN TYPE 2 DIABETES MELLITUS

Incretin-based therapies are currently the most promising in the clinical management of patients with type 2 diabetes mellitus. Glucagon-like peptide-1 (GLP-1) agonists have been designed to provide effective glycemic control in a broader glycemic range (e.g., fasting and postprandial hyperglycemia) without significant hypoglycemia compared with oral antidiabetics. Compared to

basal insulin or other standard of care, food intake is reduced, and body weight is lost. The present review draws attention to the significant clinical evidence with GLP-1 agonists, which includes glucose-dependent insulin secretion, an expanded effect on glucagon suppression, lowering of gastric emptying, diuretic and weight reduction effects, the observation of long-term weight loss in face of controlled diabetes for up to 4.5 years is possible [11].

The secretion of GLP-1 in response to oral ingestion is greatly reduced in individuals with type 2 diabetes mellitus. Because of its glucose-dependent insulinotropic and hypoglycaemic actions, recombinant GLP-1 is a potential candidate for the treatment of type 2 diabetes. However, native GLP-1 has an extremely short half-life and, therefore, its therapeutic use in diabetes mellitus would be limited [12]. The loss of DPP-IV proteolytic cleavage of GLP-1 results in an increased half-life and prolonged duration of action. In humans, the administration of GLP-1 either by single injection or continuous infusion to healthy subjects or individuals with type 2 diabetes mellitus results in a significant glucose-dependent potentiation of glucose-induced insulin release and a suppression of glucagon release. Concomitantly, gastric emptying is slowed. In addition to these predominantly glucose regulatory actions, GLP-1 tending to delay gastric emptying could also reduce postprandial triglyceride absorption. The potency of GLP-1 to affect metabolic function makes its receptor an attractive target for pharmacological intervention in type 2 diabetes [13].

3.1. Blood Glucose Control

Once glucose enters the circulation, it has been shown to be able to stimulate the release of insulin, which is a major mechanism for insulin release. Interestingly, it has been reported that the insulinotropic effects activated by glucose in individuals with type 2 diabetes are dulled due to a reduction in β-cell number and function [14]. Blandino-Rosano et al. offered a further explanation, wherein a 10% reduction in pancreatic β-cell mass is reported in individuals with type 2 diabetes [15]. While in certain instances, the pancreatic β-cell count remains unaltered, mild or severe pancreatitis is induced in susceptible types by deranged lipid metabolism, which increases β-cell apoptosis and decreases the replication of β-cell replication. With β-cell loss, a decrease is observed in ongoing insulin secretion. Clinical trials have reported that both T2DM β-cell and gut incretin levels are reduced in people living with diabetes. Thus, it stands to reason that gut incretin levels would influence glucose levels that mirrors that of endogenous incretins. GLP-1, an incretin hormone, acts as a potential strategy to improve glycemic control in people with type 2 diabetes [16].

GLP-1 agonists have been shown to enhance insulin cell mass and prevent glucagon secretion by the hepatic α cells in humans, which has drawn particular interest. According to a recent study by Bierhaus et al., a heterodomain of insulin islet insulinomas derived from saducin-impaired β-cells decreases susceptibility to diabetes while preserving glucagon secretion [17]. Thus, insulin cell mass determines the quantity of endogenous insulin available at any given point. According to these reports, treatments that protect or boost β-cell mass are more likely to help patients with T2DM. Long-acting GLP-1 mimetic molecules can promote anti-apoptotic responses in human islets, resulting in a protective or potentially enhanced islet mass. It is well-known that chronic and acute glucose toxicity are associated with β-cell destruction or decreased replication and production, causing an imbalance in the regulation of their primary functions, including glucose homeostasis, which causes diabetes. These findings suggest that GLP-1 agonists may help improve insulin function. Furthermore, pharmacological treatment with a GLP-1 agonist results in improved insulin sensitivity in patients with type 2 diabetes [18].

4. WEIGHT LOSS BENEFITS OF GLP-1 AGONISTS

Glucagon-like peptide-1 (GLP-1) is an incretin hormone secreted from L-cells of the distal ileum in response to nutrient intake. It is an insulinotropic agent, and GLP-1 receptor agonists are indicated in the treatment of diabetes [19]. In comparison with other anti-diabetic agents, these agents have demonstrated marked benefits including reductions of weight, body mass index (BMI), systolic blood pressure, and triglyceride levels. Currently available agents in this class include exenatide, liraglutide, and semaglutide, in addition to the fixed-dose combination of semaglutide and naltrexone, which is currently under consideration with the Food and Drug Administration (FDA) [20]. Several studies suggest that the weight loss effects of a GLP-1 agonist are at least partially a function of its anti-hyperglycemic efficacy. In theory, if hyperglycemia is not driving weight gain, then agents with a role in appetite regulation should be more effective. This review aims to highlight the benefits of GLP-1 agonists on weight reduction and put forward a case for their use in obesity [21].

Clinical trial data from comparative efficacy studies (as anti-diabetes agents) have investigated the extent of weight loss for the GLP-1 agonists (exenatide, liraglutide, and semaglutide) and liraglutide in combination with the weight loss adjunctive obesity medication, orlistat. The effect of each agent on a labelled dose on weight loss was evaluated, and all drugs (apart from exenatide once weekly) provided some degree of weight loss as compared to sitagliptin. Recent studies are now investigating the potential of using these agents as combination therapy in the treatment of obesity. The STEP program (Semaglutide treatment effective in people with obesity), comprising 4 clinical studies, is the first to investigate the effect of an anti-diabetes agent (liraglutide) on a higher dose specifically in a cohort of patients with overweight/obesity. These include the STEP 1 study: A Randomized Controlled Comparison of Once-Weekly Semaglutide versus Placebo and/or Orlistat in the Treatment of People with Overweight or Obesity. Furthermore, the higher dose of semaglutide is currently being investigated in a global phase 3 clinical development program [22, 23].

4.1. Comparative Efficacy Studies

GLP-1 agonists were the first glucose-lowering medications to be evaluated for their weight loss benefits in head-to-head comparison trials. Between 2017 and 2018, four comparative efficacy studies were conducted for semaglutide using injectable comparators dulaglutide (0.75 mg and 1.5 mg once weekly), exenatide extended release (ER) or liraglutide (all 1.8 mg once weekly). The EVOLVE-1 trial found that for each of these three comparator agents, the percentage of patients with ≥5% body weight loss was significantly greater with the highest 2.4-mg dose of semaglutide than with the standard comparators. For example, for semaglutide vs. dulaglutide, the RR of achieving 5% body weight loss was 2.5 (95% CI 1.7–3.6). The EVOLVE-1 trial reported that 'almost all pairs of SAEs comparing the GLP-1 receptor analogues were within the estimates for noninferiority, except for semaglutide versus dulaglutide where 2 SAEs out of 36 could not be excluded [24].

Comparative efficacy trials have also been undertaken for the once-weekly subcutaneous and oral formulations of semaglutide. Across studies, both the subcutaneous and oral formulations of this agent were found to be superior to comparators regarding their ability to induce body weight loss measured after the first 12 to 68 weeks of treatment. Specifically, significantly more patients receiving subcutaneous semaglutide at a dose of 0.5 mg, 1.0 mg or 2.0 mg each week experienced ≥5% reduction in body weight compared to patients receiving comparators such as exenatide ER, liraglutide or placebo. Also, significantly more patients receiving daily oral semaglutide at a dose of 5 mg and 10 mg (but not 20 mg) experienced the same weight loss outcomes compared to patients treated with matching placebo. The STOP-NIDDM trial showed that another long-acting GLP-1 agonist, liraglutide 1.93 mg once weekly, is a better weight loss agent than sitagliptin [25].

5. FUTURE DIRECTIONS IN GLP-1 AGONIST RESEARCH

With the ongoing advancements in GLP-1 agonist development, it will be important to address whether decisions on treatment should be based on expected improvements of CVD, solid organ transplantation, improvements in sleep apnea, hypertension, NASH resolution, and fibrosis. This will need to be done in conjunction with individuals with obesity and T2D, who may be affected by improvements beyond weight and glucose lowering in making treatment decisions. In time, this may shed light on why there was no difference in overall effects on people with coronary disease between three GLP-1 receptor agonists of varying duration of action and Farxiga [26]. We always ask the drug-related question, yet the differences may have been between the groups rather than the agents. In addition to full characterization of the individual trials being undertaken across diabetes and obesity treatment regimens, future research will need to answer the above and to inform where medication sits in the treatment pathway, if not first, given the progressive nature of diabetes [27].
The evolving landscape of future research will potentially alter the next steps. We no longer think about primary endpoints of blood glucose, BP, or lipids, breaking examination of CVD and metabolic effects. In the future, we will consider sleep apnea and NASH resolution as primary endpoints that can lead to significant improvements in QOL and prevention of comorbidities. Yes, we are still thinking of BMI as an endpoint. Yes, we are still thinking about weight and metabolic improvements, but beyond this. The answer, for sure, remains to be seen [28].

5.1. Impact on Cardiovascular Outcomes

Additional future research in this area will specifically look for differences between long-term GLP-1 agonist intervention and more transient intervention on cardiovascular outcomes. Potential mechanisms underlying observed differences between the GLP-1 agonists in their impact on cardiovascular outcomes may arise out of the differing pharmacokinetics of each agent [29]. Theoretically, exenatide LAR (once weekly, 2 mg) may result in more continuous activation of GLP-1 receptors than once-daily injections, as may native GLP-1. Potential sex differences in the effects of long-acting GLP-1 agonists may also be of interest. Moreover, understanding the impact of the GLP-1 agonists on cardiovascular outcomes in different stages of their cardiometabolic disease course may also be of interest. Moreover, the effects of GLP-1 agonist therapy may extend to the vasculature where GLP-1 receptors have been identified. GLP-1-based therapy has been shown to reduce levels of both fasting arterial stiffness and postprandial augmentation index in hyperglycemic individuals and impact sympathetic drive-in healthy humans. Although the precise effect of incretin therapies on central nervous system satiety circuits remains unclear, studies examining neuroimaging surrogate markers have observed changes in hypothalamic activation with both GLP-1 agonists and DPP-4 inhibitors. The effects of CL316,243 administration on heart rate and heart rate variability in humans have not been investigated [29].

6. CUSTOMIZATION OF GLP-1 AGONIST THERAPY

Therapeutic decisions of patients with type 2 diabetes mellitus (T2DM) are greatly influenced by preferences, needs, and profile, such as comorbid conditions, social and economic constraints, and potential side effects. Similarly, the physician's behaviour is influenced by their own expertise, beliefs, and social constraints that may interfere with prescription indication and intensification. Thus, the choice of the most appropriate second-line drug strategy, after metformin first monotherapy failure in T2DM, is not only driven by the overall glucose-lowering effect but above all by the specific patient's characteristics, priorities, and expectations [30].

In this perspective, incretin-based therapy, particularly glucagon-like-peptide-1 (GLP-1) agonists, is associated with patient-rated outcomes such as weight loss, low risk of hypoglycemia, and the possibility of simplification by less frequent administration [31]. Thus, adding to or switching to a GLP-1 agonist is a choice to be considered in:

6.1. Obesity-focused strategy

If the glycemic goal has not been achieved, and the consideration of insulin is limited by comorbidities, weight, hypoglycemia, or other clinical characteristics, patients may start GLP-1 agonists, including their weekly or once-monthly injectable formulations, as their second or third glucose-lowering drug. The advice of injectable formulations may be useful for fostering treatment intensification [32].

After considering several clinical outcomes such as cardiovascular benefits, chronic kidney disease (CKD), fluoride Q, diabetic retinopathy or non-alcoholic steatohepatitis, the articles reviewed in this study recommended treatment of T2DM patients who may benefit from adjusting their weight to improve lipids (Prioritize Triglyceride Reduction).

The results from the articles we reviewed showed that metformin treatment significantly increased the risk of hypoglycemia (RR = 2.14, 95% CI 1.45, 3.16) compared to incretin-based treatment with low heterogeneity (I21 = 0%) [33].

Incretin-based treatment was significantly associated with a greater improvement in hyperuricemia than TZD treatment (MD = 117.38, 95% CI 2.46, 232.30) with moderate heterogeneity (I22 = 42%) [34].

SGLT-2 inhibitors may be a useful treatment option for the control of HbA1c, body weight and hyperuricemia in type 2 diabetic patients with hyperuricemia, and our results suggest the initiation of incretin-based therapy or SGLT-2 inhibitor therapy other than metformin in T2DM patients with a history of hypoglycemia [35].

7. CONCLUSIONS

As discussed, it is apparent that patients have unique responses to GLP-1 agonists, with different factors contributing to individual treatment variability. Moreover, there are also differences in individual patient preferences when it comes to dosing, frequency, and administration of treatment. These differences not only apply to country populations but also to different non-white race/ethnic populations. Moreover, these preferences may change with the duration of therapy, indicating that effective management of the complexities underlying treatment decisions may require ongoing patient-provider communication throughout therapy. Thus, a focus on patient profiles and preferences to utilize a GLP-1 agonist, given the various marked differences in patient preferences and factors driving patient decisions including treatment satisfaction, avoiding injections, achieving weight loss, or avoiding weight gain frequently also represents an important point of diversification in medical decision-making. It may be quite useful to explore the factors that directly impact treatment choices, tailored to the individual patient, to achieve improved and early therapeutic results.

REFERENCES:

[1] Hinnen, D. (2017). Glucagon-like peptide 1 receptor agonists for type 2 diabetes. Diabetes spectrum, 30(3), 202-210.

[2] Andreasen, C. R., Andersen, A., Knop, F. K., & Vilsbøll, T. (2021). Understanding the place for GLP- 1RA therapy: Translating guidelines for treatment of type 2 diabetes into everyday clinical practice and patient selection. Diabetes, Obesity and Metabolism, 23, 40-52.

[3] Vilsbøll, T., Christensen, M., Junker, A. E., Knop, F. K., & Gluud, L. L. (2012). Effects of glucagon-like peptide-1 receptor agonists on weight loss: systematic review and meta-analyses of randomised controlled trials. Bmj, 344.

[4] Igarashi, A., Bekker Hansen, B., Langer, J., Tavella, F., Collings, H., Davies, N., & Wyn, R. (2021). Preference for oral and injectable GLP-1 RA therapy profiles in Japanese patients with type 2 diabetes: a discrete choice experiment. Advances in Therapy, 38, 721-738. www.springer.com

[5] Nauck, M. A., Quast, D. R., Wefers, J., & Meier, J. J. (2021). GLP-1 receptor agonists in the treatment of type 2 diabetes–state-of-the-art. Molecular metabolism, 46, 101102. www.sciencedirect.com

[6] González-González, J. G., González-Colmenero, A. D., Millán-Alanís, J. M., Lytvyn, L., Solis, R. C., Mustafa, R. A., ... & Rodríguez-Gutiérrez, R. (2021). Values, preferences and burden of treatment for the initiation of GLP-1 receptor agonists and SGLT-2 inhibitors in adult patients with type 2 diabetes: a systematic review. BMJ open, 11(7), e049130.

[7] Górriz, J. L., Romera, I., Cobo, A., O'Brien, P. D., & Merino-Torres, J. F. (2022). Glucagon-like peptide-1 receptor agonist use in people living with type 2 diabetes mellitus and chronic kidney disease: a narrative review of the key evidence with practical considerations. Diabetes Therapy, 13(3), 389-421. springer.com

[8] Drucker, D. J., & Nauck, M. A. (2006). The incretin system: glucagon-like peptide-1 receptor agonists and dipeptidyl peptidase-4 inhibitors in type 2 diabetes. The Lancet, 368(9548), 1696-1705.

[9] Levin, P. A., Nguyen, H., Wittbrodt, E. T., & Kim, S. C. (2017). Glucagon-like peptide-1 receptor agonists: a systematic review of comparative effectiveness research. Diabetes, metabolic syndrome and obesity: targets and therapy, 123-139.

[10] Zimner Rapuch, S., Divino, V., Norrbacka, K., Boye, K., Lebrec, J., Rosilio, M., ... & Guerci, B. (2021). Treatment patterns and persistence with GLP-1 RA treatments among patients with type 2 diabetes in France: a retrospective cohort analysis. Diabetes Therapy, 12, 1553-1567. www.springer.com

[11] Levin, P. A., Nguyen, H., Wittbrodt, E. T., & Kim, S. C. (2017). Glucagon-like peptide-1 receptor agonists: a systematic review of comparative effectiveness research. Diabetes, metabolic syndrome and obesity: targets and therapy, 123-139.

[12] Ussher, J. R., & Drucker, D. J. (2023). Glucagon-like peptide 1 receptor agonists: cardiovascular benefits and mechanisms of action. Nature Reviews Cardiology, 20(7), 463-474.

[13] Eng, C., Kramer, C. K., Zinman, B., & Retnakaran, R. (2014). Glucagon-like peptide-1 receptor agonist and basal insulin combination treatment for the management of type 2 diabetes: a systematic review and meta-analysis. The Lancet, 384(9961), 2228-2234.

[14] Savarese, G., Sharma, A., Pang, C., Wood, R., & Soleymanlou, N. (2023). Patient preferences for newer oral therapies in type 2 diabetes. International Journal of Cardiology, 371, 526-532.

[15] Blandino-Rosano, M., Perez-Arana, G., Mellado-Gil, J. M., Segundo, C., & Aguilar, M. (2008). Anti-proliferative Effect of Pro-inflammatory Cytokines in Cultured Beta Cells is Associated with Erk1/2 Pathway Inhibition: Protective Role of GLP-1 2. diabetes, 21, 22.

[16] Savarese, G., Sharma, A., Pang, C., Wood, R., & Soleymanlou, N. (2023). Patient preferences for newer oral therapies in type 2 diabetes. International Journal of Cardiology, 371, 526-532.

[17] Bierhaus, A., Illmer, T., Kasper, M., Luther, T., Quehenberger, P., Tritschler, H., ... & Nawroth, P. P. (1997). Advanced Glycation End Product (AGE)–mediated induction of tissue factor in cultured endothelial cells Is dependent on RAGE. Circulation, 96(7), 2262-2271.

[18] Morieri, M. L., Avogaro, A., & Fadini, G. P. (2020). Long-acting injectable GLP-1 receptor agonists for the treatment of adults with type 2 diabetes: perspectives from clinical practice. Diabetes, Metabolic Syndrome and Obesity, 4221-4234. www.tandfonline.com

[19] Brunton, S. A. & Wysham, C. H. (2020). GLP-1 receptor agonists in the treatment of type 2 diabetes: role and clinical experience to date. Postgraduate medicine. tandfonline.com

Chun, J. H. & Butts, A. (2020). Long-acting GLP-1RAs: an overview of efficacy, safety, and their role in type 2 diabetes management. Jaapa. [HTML]

[20] Singh, G., Krauthamer, M., & Bjalme-Evans, M. (2022). Wegovy (semaglutide): a new weight loss drug for chronic weight management. Journal of Investigative Medicine, 70(1), 5-13.

[21] Stretton, B., Kovoor, J., Bacchi, S., Chang, S., Ngoi, B., Murray, T., ... & Horowtiz, M. (2023). Weight loss with subcutaneous semaglutide versus other glucagon- like peptide 1 receptor agonists in type 2 diabetes: a systematic review. Internal medicine journal, 53(8), 1311-1320.

[22] Novograd, J., Mullally, J., & Frishman, W. H. (2022). Semaglutide for weight loss: Was it worth the weight? Cardiology in Review, 30(6), 324-329.

[23] O'Neil, P. M., Birkenfeld, A. L., McGowan, B., Mosenzon, O., Pedersen, S. D., Wharton, S., ... & Wilding, J. P. (2018). Efficacy and safety of semaglutide compared with liraglutide and placebo for weight loss in patients with obesity: a randomised, double-blind, placebo and active controlled, dose-ranging, phase 2 trial. The Lancet, 392(10148), 637-649.

[24] Gallwitz, B. (2017). Receptor agonists of glucagon-like peptide 1: Common characteristics and differentiation between various compounds. Der Diabetologe, 13, 487-497.

[25] Astrup, A., Rössner, S., Van Gaal, L., Rissanen, A., Niskanen, L., Al Hakim, M., ... & Lean, M. E. (2009). Effects of liraglutide in the treatment of obesity: a randomised, double-blind, placebo-controlled study. The Lancet, 374(9701), 1606-1616.

[26] Yu, J. H., Park, S. Y., Kim, N. H., & Seo, J. A. (2022). GLP-1 receptor agonists in diabetic kidney disease: current evidence and future directions. Kidney Research and Clinical Practice, 41(2), 136.

[27] Jalleh, R. J., Rayner, C. K., Hausken, T., Jones, K. L., Camilleri, M., & Horowitz, M. (2024). Gastrointestinal effects of GLP-1 receptor agonists: mechanisms, management, and future directions. The Lancet Gastroenterology & Hepatology.

[28] Mehta, K., Behl, T., Kumar, A., Uddin, M. S., Zengin, G., & Arora, S. (2021). Deciphering the neuroprotective role of glucagon-like Peptide-1 agonists in diabetic neuropathy: current perspective and future directions. Current Protein and Peptide Science, 22(1), 4-18.

[29] Bethel, M. A., Patel, R. A., Merrill, P., Lokhnygina, Y., Buse, J. B., Mentz, R. J., ... & Holman, R. R. (2018). Cardiovascular outcomes with glucagon-like peptide-1 receptor agonists in patients with type 2 diabetes: a meta-analysis. The lancet Diabetes & endocrinology, 6(2), 105-113.

[30] Lyseng-Williamson, K. A. (2019). Glucagon-like peptide-1 receptor agonists in type 2 diabetes: their use and differential features. Clinical Drug Investigation, 39(8), 805-819.

[31] Honigberg, M. C., Chang, L. S., McGuire, D. K., Plutzky, J., Aroda, V. R., & Vaduganathan, M. (2020). Use of glucagon-like peptide-1 receptor agonists in patients with type 2 diabetes and cardiovascular disease: a review. JAMA cardiology, 5(10), 1182-1190.

[32] Pantalone, K. M., Rogen, B., Zirm, P., Xiao, H., Bena, J., Barnard, G., ... & Burguera, B. (2024). An Obesity-Centric Approach with and Without Anti-Obesity Medications Compared to the Usual-Care Approach to Management of Patients with Obesity and Type 2 Diabetes in an Employer Setting: A Pragmatic Randomized Controlled Trial (EMPOWER-T2D). Diabetes Therapy, 15(5), 1201-1214.

[33] Grunberger, G., Garber, A. J., & Mechanick, J. I. (2014). Obesity management: applying clinical trial data to clinical care. Endocrine Practice, 20, 6-19.

[34] Grammatikopoulou, M. G., Gkouskou, K. K., Gkiouras, K., Bogdanos, D. P., Eliopoulos, A. G., & Goulis, D. G. (2022). The niche of n-of-1 trials in precision medicine for weight loss and obesity treatment: back to the future. Current Nutrition Reports, 11(2), 133-145.

[35] Aktar, N., Qureshi, N. K., & Ferdous, H. S. (2017). Obesity: a review of pathogenesis and management strategies in adult. Delta Medical College Journal, 5(1), 35-48.

Transformation of Food Waste into Medical Products by Green Synthesis: AgNP-THK-Plaster Gel

Rumeysa ÇELİK[1], Pelin YİĞİT[2], Gizem Kaleli CAN[2], Emre UYGUR[3], F. Zümrüt B. MÜFTÜLER[1]

rumeyscelik1@gmail.com

[1] Department of Nuclear Applications, Institute of Nuclear Sciences, Ege University, Izmir, Turkey
[2] Department of Biomedical Engineering, İzmir Democracy University, İzmir, Türkiye
[3] Soma Vocational School, Manisa Celal Bayar University, Manisa

ABSTRACT

In recent years, the rapid increase in food consumption driven by population growth has resulted in a substantial rise in food waste, highlighting the urgent need for effective recycling methods. One promising approach to addressing this issue is the environmentally friendly green synthesis of nanoparticles (NPs) from food waste. In this study, it is aimed the synthesis of silver nanoparticles (AgNPs) from carrot peels, a widely consumed vegetable, using green synthesis techniques. The synthesized AgNPs from orange carrot peels (AgNP-THK) were characterized by High-Performance Liquid Chromatography (HPLC), Dynamic Light Scattering (DLS), Zeta Potential Measurement, and Scanning Electron Microscopy (SEM). The AgNP-THK exhibited a hydrodynamic diameter of 79.35 nm and a zeta potential of -27.4 mV. Antibacterial activity assays revealed inhibition zones of 4.5 mm and 3.5 mm against Methicillin-Resistant *Staphylococcus aureus* (MRSA) and *Staphylococcus aureus* strains, respectively, while no inhibition was observed against Vancomycin-Resistant Enterococcus. In wound healing studies conducted on dermal fibroblast cells, more than 94% healing was observed at 4 and 24 hours, with complete healing at 48 hours. Based on these promising results, further studies are recommended, including the encapsulation of AgNP-THK in a PVA-PVP-based plaster gel, prepared in various ratios, and experimental studies using an infected animal model to evaluate the bioactivity of AgNP-THK against infectious diseases.

Keywords: Green Synthesis, Food Waste, Wound Healing

1. INTRODUCTION

Every year, more than one billion tonnes of food is wasted or lost around the world. Although food waste is biodegradable, increasing consumption leads to a parallel increase in waste production, contributing to greenhouse gas emissions and creating a global environmental problem. Disposing of waste in environmentally harmful ways exacerbates negative impacts on health and ecosystems [1]. Scientists are exploring economic and sustainable approaches to reduce food waste and address environmental challenges. One promising method is the green synthesis of nanoparticles (NPs) [2]. Food waste, such as carrot peel, can serve as a reducing agent in nanoparticle (NP) synthesis due to its rich phytochemical content. Carrots are rich in vitamins, carotenoids and phenolic compounds [3]. The increasing consumption of carrots has resulted in their peel becoming a common biodegradable waste. Green synthesis offers an economical, simple and non-toxic alternative for the production of nanoparticles. Studies have shown that phytochemicals derived from food waste play an important role in the synthesis of silver nanoparticles (AgNPs). These AgNPs exhibit antimicrobial activity and photocatalytic properties with applications in various fields, including wound healing [4]. In particular, innovative wound care products containing NPs, such as plaster

gels, provide a modern alternative to traditional methods by keeping wounds moist and protected from external factors [5].

This study investigates the antibacterial activities of AgNPs synthesised from orange carrot peels (THK) against *S. aureus*, Methicillin-resistant *S. aureus* (MRSA) and Vancomycin-resistant *Enterococcus* (VRE) isolates. In addition, their wound closure effect on healthy fibroblast cell lines (BJ) and usability in a plaster gel wound dressing will be investigated. Quality control and characterisation of AgNP-THK were performed using high performance liquid chromatography (HPLC), dynamic light scattering (DLS), zeta potential measurement and scanning electron microscopy (SEM). This study is expected to provide solutions to the food waste problem and contribute to innovative applications of recycled products in healthcare. In addition, future studies are planned to evaluate its bioactivity in infected animal models.

2. MATERIALS AND METHODS

2.1 Extraction

Carrot peels (THK) were weighed on a precision balance (25.06 g) and 250 ml ultrapure water was added. The mixture was boiled for one hour in a heated magnetic stirrer. The boiling and softened shells were crushed and mixed overnight in a magnetic stirrer. The mixed extracts were filtered.

2.2 Green synthesis of Silver Nanoparticles

1 mM AgNO3 (7761-88-8) was weighed on a precision balance and placed in a beaker containing 90 ml ultrapure water. Ten ml of the THK extract obtained was added dropwise to the beaker and incubated overnight in a magnetic stirrer. After incubation, the solution was centrifuged at 8,000 rpm for 15 minutes. After centrifugation, the supernatant was removed and the AgNPs were dried overnight in an oven at 90°C.

2.3 Plaster Gel Preparation

PVA pellets were dissolved in hot water at a concentration of 10% w/w using a magnetic stirrer. A combination of ethanol, glycerin and PVP was used and AgNP was stirred until a clear plaster gel was obtained.

2.4 Determination of Antibacterial Activity

Tryptic soy agar (TSA) was prepared for the determination of antibacterial activities. 6 g agar was added to 13 g tryptic soy broth (TSB) and 250 mL ultrapure water was added. The prepared agar was autoclaved (121 °C) for 20 minutes, cooled to 50 °C and sterilised. The sterile TSA was poured into 9 cm diameter petri dishes and allowed to solidify at room temperature.

S. aureus, MRSA and VRE bacteria were inoculated using the line inoculation method. Bacteria were kept in an oven overnight for multiplication. S. aureus, MRSA and VRE bacteria were prepared according to 0.5 McFarland standard. 30 µl of bacteria were dropped into the agar agar Petri dishes and spread. AgNP-THK and THK extract were then impregnated onto 5x50 antibiogram discs and placed in the petri dishes. They were kept in an oven overnight to determine the antibacterial effect. The results were measured using ImageJ (Figure 1).

2.5 *in vitro* Wound Healing

A healthy fibroblast cell line (BJ, CRL-2522) was cultured in a flask with appropriate medium (DMEM, 10% FBS, 1% sodium pyruvate, 1% L-glutamine and 1% penicillin-streptomycin solution). BJ cells (5×103 cells/well) were grown to 80% confluence in 24-well plates. A mechanical wound was made horizontally in each well using a sterile pipette tip (100µl volume). The location of the mechanical wound was marked on the surface of the plate, the medium was removed from the wells and fresh medium supplemented with AgNP-THK was added. The well to which only medium was added was taken as the control group. Images were taken at specific time parameters (0h, 4h, 24h, 48h and 72h) and wound closure rate was measured using Image J software.

3. RESULT AND DISCUSSION

3.1 Dynamic Light Scattering (DLS) and Zeta Potential Analysis

AgNP-THK was diluted with ultrapure water and added to the zeta potential cuvette (DTS1060C-Clear disposable zeta cell). The cuvette was placed in a Malvern ZetaSizer Nano Series instrument and measurements were performed in triplicate. The hydrodynamic size of AgNP-THK was determined to be 79.35 nm, with a polydispersity index (PI) value of 0.406 and a zeta potential of -27.4 mV (Figure 2). The polydispersity index defines the quality of the size distribution in nanoparticles, with PI values ≤ 0.5 considered indicative of good distribution quality. The negative zeta potential value indicates that the particles do not aggregate and that the synthesised material is stable. Accordingly, the synthesised AgNP-THK showed good dispersibility and structural stability. In a study conducted by Baran et al [6], AgNPs synthesised from artichoke leaves exhibited a zeta potential of +6.68 mV. In another study, Rolim et al. [7] synthesised AgNPs using green tea extract and reported an average hydrodynamic size of 34.68 ± 4.95 nm, an average PDI value of 0.28 ± 0.01 and an average zeta potential of -35.5 ± 3.32 mV.

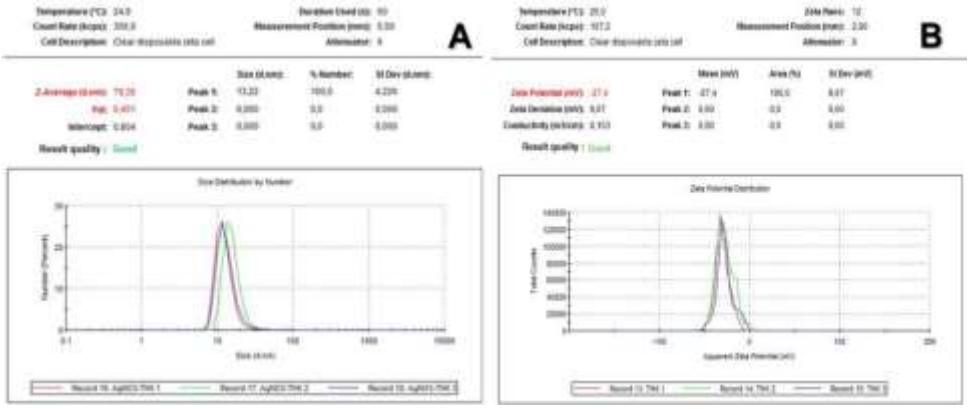

Figure 2. (A) Hydrodynamic size graph of AgNP-THK compounds as a result of DLS analysis (n=3). (B) Zeta Potencial distribution of AgNP-THK (n=3).

3.2 High- Performance Liquid Chromatography (HPLC) Analysis

HPLC (LC-10ATvp quadrupole pump, SPD-M20A DAD detector, CTO-10AS column oven, SIL 20A-HT autosampler, FRC-10A fraction collector and 5 micron C18-ODS) was used for quality control studies of AgNP-THK. HPLC system with C18 column was used. Methanol/water (60:40) was selected as mobile phase. The wavelength was determined as 215 nm in the UV detector and a temperature of 25 °C was applied. Samples were separated at a flow rate of 1 mL/min. The results showed that the Rt of AgNP-THK was 2.12 (Figure 3). Jan et al. [8] synthesised AgNP using aqueous extract of Aquilegia pubiflora and found the Rt to be 1.59.

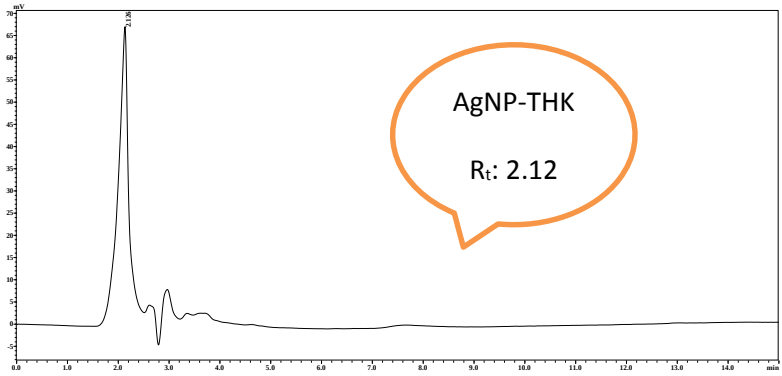

Retention Time (min.)

Figure 3. High Performance Liquid Chromatography (HPLC) of AgNP-THK.

3.3 Antibacterial Activity

AgNP-THK showed any zone on VRE isolate. A zone diameter of 3.5 mm was found on *S. aureus* isolate and 4.5 mm on MRSA isolate (Figure 4). According to the results, it was confirmed that the obtained AgNP-THK showed antibacterial activity.

Sumang et al. [9] obtained AgNP by green synthesis method using banana peels and found 19 mm zone diameter at different pH parameters in S. aureus isolate. Tasiu M. et al. [10] obtained extracts from pumpkin and guava peels and synthesised AgNP. The results were evaluated as 11 mm zone diameter in S. aureus isolate.

Figure 4. Investigation of the antibacterial activity of synthesised AgNP-THK compounds by disc diffusion method.

3.4 *in vitro* Wound Healing

The efficacy of AgNP-THK on the wound model created using dermal fibroblast cell line was observed to be over 94% at 4, 24 and 48 hours, respectively (Figure 5). In line with the results obtained, AgNP obtained compared to carrot extract was more effective in wound healing at similar times.

Shehabeldine A. et al. [11] obtained chitosan/AgNP and created a wound model in the BJ cell line. After 24 hours of exposure, it was reported that approximately 50.5% towards the opening to close the scratch wound greatly accelerated the wound healing process compared to 17.5% of the control. Veeraraghavan et al. [12] obtained AgNPs from Scutellaria barbata extract. In the L929 fibroblast cell line, both 5 µg and 7.5 µg of Sb-AgNP treatment was found to reduce cell migration.

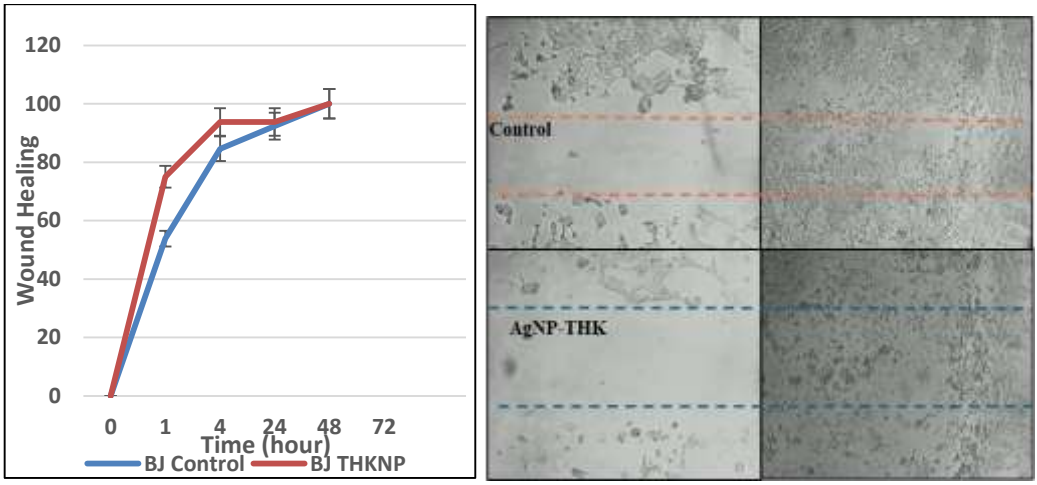

Figure 5. (A)The control group showed 84% wound healing and AgNP-THK showed 93% wound closure at 4 hours. (B) The wound healing activity of the control group and AgNP-THK on the BJ cell line after 4 and 48 hours, respectively.

4. CONCLUSION

In conclusion, it is predicted that this in vitro study, in which the bioactivities of AgNP-THK synthesised from food waste are evaluated for wound healing applications in the medical field, can contribute to the resolution of our country's food waste problem and the development of innovative ideas for its use as a new generation dressing product in the medical field.

5. REFERENCES

[1] Aswathi, V. P., Meera, · S, Maria, · C G Ann, & Nidhin, · M. (2023). Green synthesis of nanoparticles from biodegradable waste extracts and their applications: a critical review. Nanotechnology for Environmental Engineering, 8, 377–397. https://doi.org/10.1007/s41204-022-00276-8

[2] F. Rodríguez-Félix et al., "Review Article Trends in Sustainable Green Synthesis of Silver Nanoparticles Using Agri-Food Waste Extracts and Their Applications in Health," 2022, doi: 10.1155/2022/8874003.

[3] I. Uremis, S. Soylu, S. Kurt, E. M. Soylu, and E. Sertkaya, "Hatay ili havuç ekim alanlarında bulunan yabancı ot türleri, yaygınlıkları, yoğunlukları ve durumlarının değerlendirilmesi," Journal of Tekirdag Agricultural Faculty, vol. 17, no. 2, pp. 211–228, May 2020, doi: 10.33462/JOTAF.645336.

[4] M. R. Bindhu and M. Umadevi, "Synthesis of monodispersed silver nanoparticles using Hibiscus cannabinus leaf extract and its antimicrobial activity," Spectrochim Acta A Mol Biomol Spectrosc, vol. 101, pp. 184–190, Jan. 2013, doi: 10.1016/J.SAA.2012.09.031.

[5] M. Ovais et al., "Wound healing applications of biogenic colloidal silver and gold nanoparticles: recent trends and future prospects", doi: 10.1007/s00253-018-8939-z.

[6] Baran, A., Baran, M. F., Keskin, C., Kandemir, S. I., Valiyeva, M., Mehraliyeva, S., Khalilov, R., & Eftekhari, A. (2021). Evaluation of their Cytotoxic and Antibacterial Activities. https://doi.org/10.1155/2021/2270472

[7] Rolim, W. R., Pelegrino, M. T., de Araújo Lima, B., Ferraz, L. S., Costa, F. N., Bernardes, J. S., Rodigues, T., Brocchi, M., & Seabra, A. B. (2019). Green tea extract mediated biogenic synthesis of silver nanoparticles: Characterization, cytotoxicity evaluation and antibacterial activity. Applied Surface Science, 463, 66–74. https://doi.org/10.1016/J.APSUSC.2018.08.203

[8] Jan, H., Zaman, G., Usman, H., Ansir, R., Drouet, S., Gigliolo-Guivarc'h, N., Hano, C., & Abbasi, B. H. (2021). Biogenically proficient synthesis and characterization of silver nanoparticles (Ag-NPs) employing aqueous extract of Aquilegia pubiflora along with their in vitro antimicrobial, anti-cancer and other biological applications. Journal of Materials Research and Technology, 15, 950–968. https://doi.org/10.1016/J.JMRT.2021.08.048

[9] Sumang, R., Jarernsuk, S., Chutima, R., Vitayakorn, N., & Panpho, P. (2024). UTILIZING BANANA PEEL WASTE EXTRACT FOR GREEN SYNTHESIS OF SILVER NANOPARTICLES AND THEIR ANTIBACTERIAL APPLICATION. Suranaree Journal of Science & Technology, 31(3), 1–9. https://doi.org/10.55766/SUJST-2024-03-E05613

[10] Tasiu, M., Abdulmumin, Y., Abdulmumin, T. M., Murtala, M., Shehu, A., Abubakar, A. L., Zainab, S., Mustapha, R. K., & Binta, S. S. (2022). Antimicrobial Evaluation of Biologically Synthesized Silver Nanoparticles using Aqueous Peel Extracts of Guava (Psidium guavaja) and Pumpkin (cucurbita pepo). Asian Journal of Biotechnology and Genetic Engineering, 5(2), 20–29. https://www.sdiarticle5.com/review-history/86042

[11] Shehabeldine, A. M., Salem, S. S., Ali, O. M., Abd-Elsalam, K. A., Elkady, F. M., & Hashem, A. H. (2022). Multifunctional Silver Nanoparticles Based on Chitosan: Antibacterial, Antibiofilm, Antifungal, Antioxidant, and Wound-Healing Activities. Journal of Fungi 2022, Vol. 8, Page 612, 8(6), 612. https://doi.org/10.3390/JOF8060612

[12] Veeraraghavan, V. P., Periadurai, N. D., Karunakaran, T., Hussain, S., Surapaneni, K. M., & Jiao, X. (2021). Green synthesis of silver nanoparticles from aqueous extract of Scutellaria barbata and coating on the cotton fabric for antimicrobial applications and wound healing activity in fibroblast cells (L929). Saudi Journal of Biological Sciences, 28(7), 3633–3640. https://doi.org/10.1016/J.SJBS.2021.05.007

Investigation of occupational accidents in the metal industry using artificial neural networks

Seher ARSLANKAYA [1]✉

[1] Sakarya University, Industrial Engineering Department, Sakarya-TURKEY

ABSTRACT

The metal industry is an important business line that is the locomotive of all industries, economically and when defense, transportation, and similar sectors are considered. Metals are used as raw materials or end products in industrial establishments such as electrical-electronics, construction, transportation, and chemistry. Therefore, the metal industry leads all sectors worldwide, including Turkey.

Work accidents and occupational diseases continue to take lives and cause disabilities in the world and our country. Every year, a considerable number of people lose their lives or become disabled due to preventable work accidents and occupational diseases. Various safety measures are taken to prevent work accidents. One of the sectors where work accidents occur most frequently is the metal industry. This study aims to examine the work accidents experienced by workers working in the metal industry and to examine them by performing learning in an artificial neural network to predict the accidents that occur.

Keywords: *Work accidents, artificial neural networks, matlab applications*

✉ *Corresponding Author Email : aseher@sakarya.edu.tr*

1. INTRODUCTION

The metal sector can generally be defined as the metal melting and refining industry and the metal processing industry. Metal ores and scraps are processed to obtain pure metals in metal melting and refining processes. When the sectors of working life are evaluated in terms of hazards and risks, the metal, mining, construction, and textile sectors are at the forefront. These are among the heavy and dangerous sectors that require knowledge, experience, expertise, and continuous control due to the risks and dangers they contain due to their structure (Demir, 2009). Özoğlu et al. (2018) examined the expansion tank production line in a metal industry enterprise in their study. They determined the ergonomic risk levels to which the employees in the 7 line were exposed using REBA and OWAS methods. Güllüoğlu and Güllüoğlu (2019) analyzed the data on occupational accidents that occurred throughout Turkey between 2007 and 2016 and the accidents in the metal sector. Ergül (2018), Künteş and Bezek Güre (2024) conducted a study on the prediction of occupational accidents with artificial neural networks.

2. MATERIAL AND METHODS

Artificial neural networks are computer systems that automatically perform the human brain's abilities, such as deriving new information through learning, creating, and discovering new information without help. The minor units that form the basis of the operation of ANN are called artificial nerve cells (Sarı, 2016).

3. INVESTIGATION OF OCCUPATIONAL ACCIDENTS USING ARTIFICIAL NEURAL NETWORKS

Many factors impair the health of employees in workplaces around the world. Due to the conditions in workplaces, employees suffer from occupational accidents and occupational diseases. There is a possibility of suffering from an occupational accident in all work sectors.
Occupational accidents and occupational diseases continue to take lives and cause disabilities in the world and our country. Every year, a considerable number of people lose their lives or become disabled due to preventable occupational accidents and occupational diseases. Various safety measures are taken to prevent occupational accidents. Preventing occupational accidents is important for workers and employers. Occupational health and safety experts in this field apply the necessary measures and laws to prevent occupational accidents. One of the sectors where occupational accidents occur most frequently is the metal sector. This study aims to examine the occupational accidents experienced by workers working in the metal sector and to examine them by performing learning in an artificial neural network to predict the accidents that occur. The solution was reached by following the steps below to solve the problem.

1. Data collection: 100 data were obtained in Excel in the iron and steel factory for 365 days between January 2018 and December 2018. This data consists of work accidents that occurred that year. Work accidents that occurred are listed according to the body parts that were damaged. In work accidents, the injured and damaged areas vary depending on the accident. The accidents were randomly listed during the data entry phase.

Table 1. Some of the work accidents that occurred

Number of Accidents	Types of Accidents	Body Part of the Accident
1	Arm fracture due to fall	Arm
2	Electric shock	Arm
3	Ankle dislocation	Foot
4	Finger amputation	Hand
5	Arm injury due to fall	Arm
6	Foot sprain	Foot
7	Acute poisoning	Respiration
8	Foot fracture	Foot
9	Knee rotation	Leg
10	Elbow cut	Arm
11	Burn	Body
12	Load fall	Body
13	Crane hook breakage	Body
14	Finger amputation	Hand
15	Foot fracture	Foot
16	Slip fall	Body
17	Arm fracture	Arm
18	Burn	Body

2. Grouping of Collected Data: The regions where the 100 work accidents were grouped were determined. Groupings were made according to the injured areas. Listings were made in Excel according to the damaged limbs. Eight groupings were obtained.

Table 2. Grouping of Accidents

Accident Area	Numbering
Arm	1
Foot	2
Hand	3
Leg	4
Body	5
Fatal accident	6
Eye	7
Respiration	8

The experience and age of the workers in the accidents were examined, and their normalization was performed.

Table 3. Normalization of age and experience

Age	Experience	Norm age	Norm experience
42	20	0,741935	0,76
30	10	0,354839	0,36
22	2	0,096774	0,04
32	6	0,419355	0,2
45	15	0,83871	0,56
37	15	0,580645	0,56
48	20	0,935484	0,76
45	16	0,83871	0,6
33	11	0,451613	0,4
34	12	0,483871	0,44

The normalization process is applied to the data before starting training. This ensures that all inputs are between 0 and 1. Another benefit of normalization is that by bringing extremely large or extremely small values that occur in certain periods in the data to certain ranges, the network is prevented from being misdirected.

X'=(Xi-Xmin)/(XMax-XMin)
X': Normalized data
Xi: Input value
Xmax: Largest number in the input set
Xmin: Largest number in the input set

Table 4. Accident time period after starting work

Accident time zone	Grouping
0-2	1
2-4	2
4-6	3
6-8	4
8-10	5
10-12	6

Table 5. Some of the Reasons for the Accidents

Accident reason	**Grouping**	**Norm reason**	**Accident time zone**	**Norm hour**
Carelessness	1	0	1	0
Electric leakage	2	0,142857143	3	0,4
Slippery floor	3	0,285714286	2	0,2
Fall	5	0,571428571	2	0,2
Gas leakage	6	0,714285714	2	0,2
Equipment	4	0,428571429	2	0,2
Fall	5	0,571428571	2	0,2
Slippery floor	3	0,285714286	3	0,4
Equipment	4	0,428571429	2	0,2
PPE missing	7	0,857142857	1	0

The network type was determined as "Feed-forward backdrop"; the number of hidden layers was 2, and the number of neurons was 8. "TRAINGDX" was selected as the network training function, "LEARNGDM" as adaptive learning, and "MSE" as the performance function. Different ANN models were tried, and some of them are given below.

Table 6. Criteria tested in the artificial neural network

Trial	Training Function	Activation Function	Hidden Layer
1	Trainbr	Tansig	8
2	Traingda	Logsis	8
3	Traingdx	Logsis	10
4	Traingdx	Logsis	10
5	Traingdx	Logsis	8
6	Traindm	Logsis	10
7	Trainbr	Tansig	10
8	Traingdm	Tansig	10
9	Traingdx	Tansig	8
10	Trainbr	Tangig	10

Figure 1 shows the artificial neural network model.

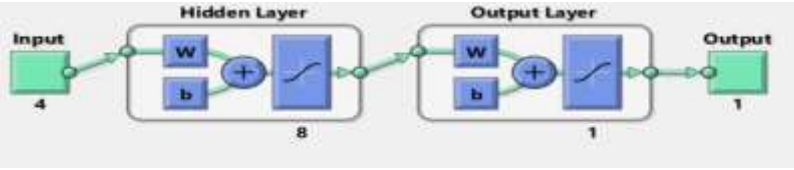

Figure 1. Artificial Neural Network Model

The artificial neural network model formed is shown in Figure 1. four input values, a hidden layer, an output layer, and finally, one output value are specified in the model. The graph of the error values for the training, validation, and test sets in each iteration as a result of training is given in Figure 1 as can be seen in the graph, the training of the network reached the optimum result in the 492nd iteration.

After the learning process starts, it is run several times, and its accuracy is evaluated by looking at the regression graphs. Regression graphs are shown in Figure 4.8. According to these graphs, 94% regression results were obtained in all clusters. It is seen that the data referred to as "data" is distributed over the training, validation, and test curves in the graph. This shows that the trained network structure's independent variables (inputs) affect the dependent variable (work accidents) by 94%.

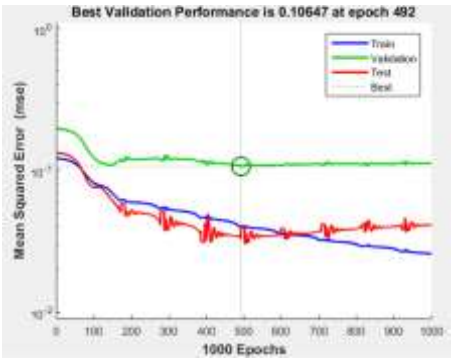

Figure 2. Error Performances

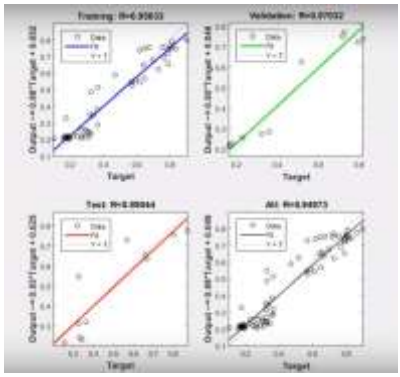

Figure 3. Regression Graphs

4. CONCLUSION

The causes of work accidents were classified using the data set. In this data set, we have the reasons why the accidents occurred, which body parts of the employees were affected, the ages and experiences of the employees, and the times the accidents occurred after they started working.

The data in hand was normalized and transferred to be examined in artificial neural networks. The employees' ages, their work-life experiences, the reason for the accident, and the times the accident occurred were examined, and a feedback estimate was obtained. As a result of the application, different causes of accidents were found, and the ANOVA test was applied to decide which of these causes of accidents would be selected as a priority. The iteration with the lowest standard deviation due to the test was selected and completed.

Learning was performed in artificial neural networks using the work accident probability data obtained with the Excel data normalization model. As a result of the learning performed, the probability of work accidents for new employees was predicted. As a result, a program was developed that gives the probability of having a work accident.

REFERENCES

Demir, E., (2009). Metal iş kolunda meydana gelen iş kazaları ve iş kazalarının oluşturduğu, kayıpların ekonomik yönden analizi. Yüksek Lisans Tezi, Marmara Üniversitesi Fen Bilimleri Enstitüsü, İstanbul

Özoğul B., Çimen B. Ve Kahya E. (2018). Bir metal sanayi işletmesinde ergonomik risk analizi. Mühendislik bilimleri ve tasarımı dergisi. 6 159-175 http://doi.org/10.21923/jesd.359123

Güllüoğlu, E. N., & Güllüoğlu, A. N. (2019). Türkiye'de Metal Sektöründe Meydana Gelen İş Kazalarının Analizi. International Journal of Advances in Engineering and Pure Sciences, 31(1), 70-82. https://doi.org/10.7240/jeps.486478

B. Ergül, "Türkiye'deki İş Kazalarının Zaman Serisi Analiz Teknikleri ve Yapay Sinir Ağları Tekniği İle İncelenmesi", kisgd, vol. 2, no. 2, pp. 63–74, 2018, doi: 10.33720/kisgd.395338

Künteş, Ö., & Bezek Güre, Ö. (2024). Yapay Sinir Ağı Kullanılarak Petrol Sektöründe Yaşanan İş Kazalarının İncelenmesi. Journal of the Institute of Science and Technology, 14(3), 1000-1012. https://doi.org/10.21597/jist.1502928

Prediction of Hepatitis Patients with Artificial Neural Networks

Seher ARSLANKAYA[1]✉

[1]Sakarya University, Industrial Engineering Department, Sakarya-TURKEY

ABSTRACT

Artificial Neural Networks (ANN) are computer systems that emerge by imitating the human brain and generate new information with the features of comprehending, learning, generalizing, and experiencing information.ANN contains different network structures for problems such as prediction, classification, data interpretation, data association, and filtering. It is an effective system for solving different and complex problems. With the increasing speed of technology use, the application of this technology to the health and medical field is carried out both to facilitate the work of doctors and employees and to prevent errors with overlooked results in the diagnosis of the disease and to create a minor error rate. In this study, the diagnosis of hepatitis disease and classification of whether people have hepatitis were made using Artificial Neural Networks. Data from 113 patients were used in the study. An artificial neural network was created considering 14 features, such as patients' personal information, medications used, detected effects, and laboratory results. A feed-forward backpropagation algorithm was used to diagnose hepatitis disease early and quickly.

Keywords: Prediction, hepatit, artificial neural networks

✉Corresponding Author Email : aseher@sakarya.edu.tr

1. INTRODUCTION

Technology, which is with us in every field and used in many places and sectors, is also used extensively in the health sector. The use of technology in the health sector has brought many developments in medicine. Technology is used in every field in the health sector. Technology is used to facilitate employees' work in studies such as findings, diagnosis, laboratory, and treatment and to obtain accurate results. In this case, patient and employee satisfaction is expected to increase. With these methods, physicians can make faster and more accurate decisions using the information obtained and analyzed based on patient information. (İlkuçar, 2015). It has been observed that Artificial Neural Network methods find solutions to many complex problems, such as prediction, classification, and clustering (Karaatlı, Helvacıoğlu, Ömürbek, Tokgöz, 2011). In this study, an analysis was made for hepatitis disease, and data obtained from the Hepatitis database from the UCI Machine Learning Repository was used. Hepatitis patients were classified using Artificial Neural Networks.

2. MATERIAL AND METHODS

Artificial Neural Networks collect information about examples, make generalizations, and then use the information they have learned to make decisions about examples they have never seen before (Öztemel, 2012).

ANN can be used to solve many different problems. Classification problems are one of them. Classification is the process of determining a class for data that is unknown. Classification can be used in a wide variety of areas. (Uslu, 2013).

3. CLASSIFICATION OF HEPATITIS PATIENTS WITH ARTIFICIAL NEURAL NETWORKS

This study aims to determine whether patients have hepatitis using artificial neural networks. Therefore, the dataset obtained from the UCI Machine Learning Repository includes 14 features of personal information and laboratory results of 113 patients. Using the hepatitis disease dataset, it was estimated whether the patients have hepatitis by classifying them with the Artificial Neural Network application. In this application, 80% of the 113 data were used for training the network and 20% for testing the network.

Table 1. Data set

Variables	Min-max
Age	7-72
Gender	1-2
Steroid	1-2
Antiviral	1-2
Fatigue	1-2
Weakness	1-2
Anorexia	1-2
Stiff liver	1-2
Spleen	1-2
Abdominal inflammation	1-2
Bilirubin	0,50-8
Alkaline phosphatase	26-295
Sgot	14-648
Albumin	2,4-5,2
Results	1-2

In this study, the Levenberg-Marquardt (TRAINLM) algorithm, which propagates the error backward as the learning function in the designed ANN model, and the Hyperbolic Tangent Sigmoid (TANSIG) function for the artificial nerve cells that perform the function as the transfer function in the intermediate layer were used. The Levenberg-Marquardt (backpropagation) algorithm is the most used algorithm in ANN because finding the error values reduces the errors by adjusting the neurons' weights. Since the sigmoid function is differentiable, it is frequently used with the backpropagation algorithm. Due to the structure of the transfer function used in the intermediate layer, the data is normalized between -1 and 1. The developed ANN model is given in Figure 1.

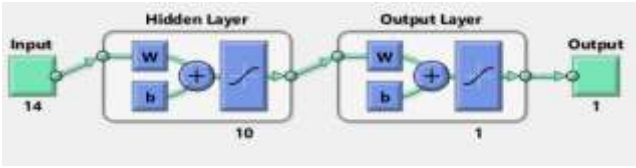

Figure 1. ANN model network topology

Mean Squared Error (MSE) was used as a performance measure. The MSE (sum of squares of the difference between the network's prediction and the actual data) value was aimed to be minimum. R is the correlation between the actual value and the network's predicted value. In other words, the square of the R-value is used to power the prediction, aiming to minimize the absolute deviation. The best result for the R-value is the one close to 1. R values vary between -1 and 1. A negative value is a negative result but shows an inverse proportion between the realized and predicted values. A value of zero means that there is no relationship between these values. The smallest MSE value for the 14-10-1 network was obtained in the second training. The performance graph and MSE value are shown in Figure 2.

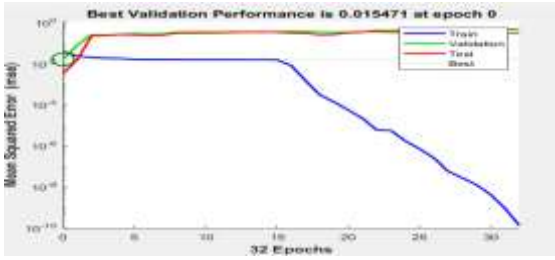

Figure 2. Classification Performances

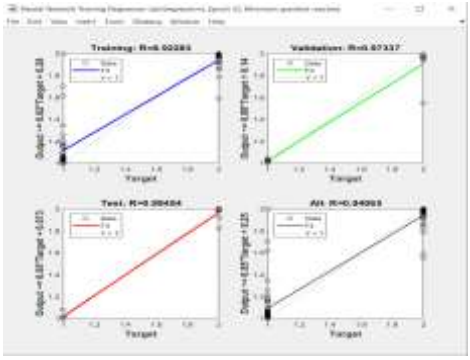

Figure 3. Relationship between output and target

As shown in Figure 3, the MSE value was 0.015. The maximum iteration number was 85, and the network training was completed in 32 iterations. The graphical representation of the R (correlation of the actual value and the estimated value of the network) values is as in Figure 3. When the evaluation was made according to the regression data, a regression value of around 94% was obtained. It was determined to be a usable network, although it is a good value for health data. The classification values formed by the trained network and the graphical representation of the actual values regarding whether or not there is a hepatitis patient are given in Figure 4.

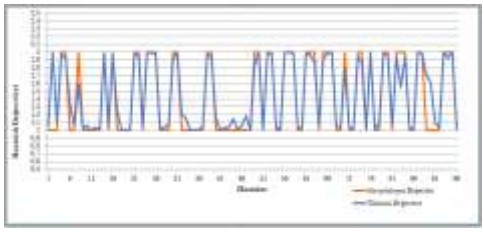

Figure 4. Graphical Representation of Values Estimated by the Network and Real Values

In Figure 4, a high level of similarity was achieved between the classification values obtained by the network with completed training and the actual values.

4. CONCLUSION

Hepatitis is an important cause of cirrhosis and liver cancer. Therefore, early diagnosis of hepatitis is an important effect of early treatment. In this study, classification was made using ANN to predict the disease early for both patients and physicians and to diagnose the disease. In this study, 113 patients were formed, 14 features were taken as basis, and the personal information of the patients, the diagnoses made, and laboratory result data (UCI) were used in the Matlab Package Program to classify whether the individuals had hepatitis using the feed-forward backpropagation multilayer ANN method. Different network structures were tried, and the results of these different networks were compared. The realized values and the values obtained in the ANN were found to be approximately consistent, and as a result of the classification, a high success rate of 94% was achieved. In line with the results of this study, it is possible to conduct medical diagnosis studies using the classification method of ANN, and many diagnostic studies have been conducted using the classification method in the literature.

REFERENCES

Öztemel E. (2012), "Yapay Sinir Ağları", Papatya Yayıncılık, 2012.

İlkuçar M., "Kronik Böbrek Hastalarının Yapay Sinir Ağı ve Radyal Temelli Fonksiyon Ağı ile Teşhisi", (2015), Mehmet Akif Ersoy Üniversitesi Fen Bilimleri Enstitüsü Dergisi 6(2): 82-88.

Karaatlı M, Helvacıoğlu Ö.C., Ömürbek N. and Tokgöz G. (2012), "Yapay Sinir Ağları Yöntemi ile Otomobil Satış Tahmini", Int. Journal of Management Economics and Business, Vol. 8, No. 17, pp. 87-100.

Determination of Occupational Health and Safety Risks in the Construction Industry

Seher ARSLANKAYA[1]✉

[1]Sakarya University, Industrial Engineering Department, Sakarya-TURKEY

ABSTRACT

When occupational accidents in Turkey are examined, it is among the countries with the highest occupational accident rates. The vast majority of these accidents occur in the construction sector. Precautions to be taken in this rapidly growing sector are of vital importance. The biggest reasons why occupational accidents occur more in the construction sector than in other sectors are that each project is unique, the continuous and rapid growth experienced in the sector, the sector spreading to large regions abroad, coming together with different cultures and establishing new business partnerships, and utilizing the labor force of that country, thus distributing more responsibilities to individuals than they can handle. In this study, a detailed study was conducted on what the risks related to occupational safety in the construction sector are and how they can be identified, what steps can be taken to reduce these risks, and if possible, how studies can be carried out systematically to eliminate the identified risks.

Keywords: Occupational health and safety, risk, construction sector

✉Corresponding Author Email : aseher@sakarya.edu.tr

1.INTRODUCTION

In parallel with industrialization and technological developments in the world and our country, some problems have emerged, mainly regarding workplace safety. Studies on determining and implementing safety measures based on scientific research in order to minimize work accidents and the losses they cause have been ongoing for years (Yanturalı, 2015).

A hazard is a source or situation that can cause injury, occupational disease, damage to property or the work environment, or a combination of these (Yılmaz, 2004). Risk is the combination of the consequences of a harmful event that will occur and the probability of occurrence. In order to talk about risk, it is necessary to predict the probability of the hazard occurring and the severity of the damage, harm, or injury that may occur due to this (Hull, 2012). See (Mukahy, 2010; Rejda, 2010) for more detailed risk information. Work accidents are classified in different ways depending on how the event occurs, the nature of the damage caused by the event, and the consequences of the accident (Bostan, 2012).

2. OCCUPATIONAL SAFETY IN CONSTRUCTION WORKS

People falling, material falling, material splashing, excavation edge collapse, collapse of a structure, electric shock, explosive accidents, accidents in construction machinery, limb entrapment in benches and machine elements, limb compression under/between materials, hand tool accidents, injuries with sharp-edged objects, traffic accidents on construction sites are the most common main accident types in the construction sector.

A sample application has been carried out below regarding the studies required to determine risks and hazards in the construction sector, to determine the degree and severity of risks, and to bring the identified risks to acceptable levels in terms of occupational health and safety.

In determining the units to be included in the Determination and Assessment of Risks, the units specified in Article 5 of the Regulation on Occupational Safety Boards, the Formation of Occupational Safety Boards, and people serving in the workplace for many years were selected.

This study was carried out in 5 stages (Ceylan and Başhelvacı, 2011).

Step 1: Recognizing the Hazard: First, all hazards and hazard sources were identified without distinguishing between major and minor, important and unimportant, and a hazard list was created.

Step 2: Assessing Risks: The severity and probability of the event caused by the hazard were considered. The 5x5 Risk Assessment Table was used for the identified risks. Here, Risk is calculated with the formula Risk = Probability x Intensity. The values in the tables below were used for the probability and intensity values in the formula.

Table 1. Probability values used in qualitative risk calculation

Frekans	Probability	Probability Value
Once a year	Very small	1
Once every three months	Small	2
Once a month	Medium	3
Once a week	High	4
Every day	Very high	5

Table 2. Intensity values used in qualitative Risk Calculation

Incident	Severity	Intensity Value
No loss of working hours, requiring first aid	Very mild	1
No loss of working days, requiring first aid	Mild	2
Minor injury, treatment required	Moderate	3
Death, serious injury, occupational disease	Serious	4
Multiple deaths, permanent disability	Very serious	5

Table 3. 5x5 Risk Assessment Table

Step 3: Determining Control Measures: In this step, the necessary control measures should be decided to reduce the risks to an acceptable level. The basic rule should be to eliminate the hazard.

Step 4: Completing Control Measures: Completing control measures should include the following:

- Developing working methods
- Communication (sharing the measures taken with employees)
- Providing education and training
- Supervision.

Step 5: Monitoring and Repeating: The following questions should be answered in this step. All listed activities should be recorded, and the effectiveness of the measures should be assessed.

- Were the selected control measures completed as planned?
- Are the selected control measures appropriate?
- Were these control measures implemented?
- Were these control measures implemented correctly?
- Was the exposure to the assessed risks eliminated? Or was it sufficiently reduced?
- Did the changes you made result in line with your objectives?

Table 4: Example of a matrix solution

Main activity	Hazard	Risk/impact	Affected	O	Ş	R	Precautions to be taken	P	V	R
Construction site dormitory	Use of inappropriate electric stoves	Fire	Employees Guests	2	4	8	Personnel should be informed about fire danger in dormitories	2	2	4
Construction site dormitory	Inadequate ventilation	Epidemic	Employees Guests	2	3	6	Increase the number of dormitories or improve the ventilation system	2	1	2
Construction site boiler room	Approaching the nitrogen tank area with fire	Fire	Employees Guests	3	4	12		2	1	2
Office activities	Non-ergonomic office furniture	Skeletal and muscular system diseases	Employees	4	3	12	Place warning and signage	3	1	3

3. Conclusion

In this project study conducted on the determination, analysis, probability, severity and effects of existing risks, elimination and control with Risk Management, which is one of the occupational health and safety applications of the Construction Sector; it has been determined that construction work includes many different risk factors, that many different dangerous situations occur in construction work starting from the project phase, during the implementation and delivery process, that if these situations are not taken into consideration and the necessary precautions are not taken, situations that will result in material and life loss can quickly occur, and it has been concluded that it is very important for the employees and their own interests for companies operating in the construction sector to receive technical support from expert and professional teams in terms of risk determination, elimination and control in order to avoid accidents, loss of life, material losses and loss of prestige in their said works.

The project study will also provide significant information to those working in the field and practitioners regarding risk management within the scope of occupational health and safety in the construction sector.

REFERENCES

Yılmaz, G. 2004. İş Güvenliğine Genel Bakış, Mühendis ve Makine Dergisi, Sayı 224,

Yanturalı, B., İş sağlığı ve güvenliğinde risk değerlendirmesi ve bir uygulama çalışması. Yayınlanmamış yüksek lisans tezi. Balıkesir Üniversitesi Fen Bilimleri Enstitüsü, 2015.

Bostan, H., İnşaat Sektöründe İş Güvenliği: Yeni Nesil Öğrenme Tekniği, Anadolu Üniversitesi Fen Bilimleri Enstitüsü İnşaat Mühendisliği Anabilim Dalı, Yüksek Lisans Tezi, Sf.17, Eskişehir 2012

Hull,J.C. 2012. Risk Managment And Financial Instıtutıons, 3rd Edition, Wiley .

Mukahy,R. 2010. Risk Management Tricks of the Trade For Project Managers,Rmc Publications.

Rejda,G. 2010. Principles of Risk Management And Insurance, 11th Edition,Prentice Hall

Türkiye ve dünyada hidroelektrik enerji potansiyeli, üretim durumu ve izlenen politikalar

Adil Ceylan, İpek Atik*

Gaziantep islam bilim ve teknoloji üniversitesi mühendislik ve doğa bilimleri fakültesi
[2] Name of Institution/Department, City, Country

**ipek.atik@gibtu.edu.tr*

Özet

Enerji, günlük hayat içerisinde her geçen gün önemi artan bir ihtiyaçtır. Bu ihtiyaç, insanlığı etkiler ve insanlığın yaşamsal faaliyetlerini oluşturup gerçekleşmesinde belirleyici bir konumdadır. Bu konumdan mütevellit enerji talebi ortaya çıkar ve bu talebin karşılanması çeşitli enerji üretim yöntemleriyle sağlanır.

Anahtar Kelimeler: Enerji, politika,hidroelektrik güç

1. Giriş

Enerji, günlük hayat içerisinde her geçen gün önemi artan bir ihtiyaçtır. Bu ihtiyaç, insanlığı etkiler ve insanlığın yaşamsal faaliyetlerini oluşturup gerçekleşmesinde belirleyici bir konumdadır. Bu konumdan mütevellit enerji talebi ortaya çıkar ve bu talebin karşılanması çeşitli enerji üretim yöntemleriyle sağlanır. Bununla birlikte enerji talebi toplumların gelişmişlik durumunu enerji tüketimini baz alarak sınıflandıran bir skala olarak kullanılmaktadır. Enerjiye olan talep gelişmekte olan ülkelerde %2-3, gelişmiş ülkelerde ise %10'a kadar varanmiktarlara çıkar [1].

Enerji talebini karşılayan en önemli kaynaklardan bir tanesi de günümüzde elektrik enerjisidir. Elektrik, üretim tesislerinde farklı ürün ve yöntemlerle elde edilir. Elektrik, termik santrallerde doğalgaz, kömür vb. fosil yakıtlar kullanılarak güneş enerji santrallerinde güneş ışınlarından faydalanılarak, hidroelektrik santrallerinde su gücü kullanılarak elde edilir. Yüksek kottan alçak kota düşürülen sudan veya akan sudan elde edilen kinetik enerji kullanılarak türbinler yardımıyla elektrik üretimi gerçekleştirilmesine hidroelektrik enerji, denir [2]. Bu üretimin yapıldığı tesise hidroelektrik santrali denir ve HES olarak kısaltılabilir.

HES yapıları barajlı ve barajsız olarak sınıflandırılabilir. Barajlı HES yapısında suyun belirli bir yüksekliğe ulaşana kadar birikmesi için bir yapıinşa edilir, bu yapı sayesinde suyun kazandığı potansiyel enerji ile elektrik üretimi yapılır. Barajsız HES yapılarında ise su seviyesini yükseltecek bir yapı mevcut değildir ayrıca bir regülatör ile akan su kabartılır ve kabarmış akan suyun enerjisi enerji üretiminde kullanılır. Barajsız HES yapılarına nehir tipi HES yapıları da denilmektedir. Bu yapılar dünyanın çeşitli yerlerinde elektrik üretiminde kullanılmaktadır. Hidroelektrik enerji üretiminde yaklaşık 700 TWh güç ile Çin ilk sırada yerini almaktadır, Çin'i yaklaşık 400 TWh güç üretimi ile Brezilya ve Kanada takip etmektedir [3]. Ülkemizde de su kaynakları elektrik üretiminde kullanılmaktadır.
Ülkemizde 20.yüzyılda başlayan HES yapılarından elektrik üretimi ilk olarak 1902 yılında Tarsus'ta küçük ölçekli bir hidroelektrik santralde başlamıştır [4]. 1913 yılında ilk büyük ölçekli santral İstanbul'da, 1933'te hidroelektrikle enerjisi sağlanan aydınlatma ve elektrik şebekesi Ödemiş'te kurulmuştur daha sonra 1935 yılında elektrik üretimi ile ilgili birkaç devlet kuruluşu tesis edilmiştir [4]. Ancak ilerleyen süreçte ülkemizin gelişimine paralel olarak artan elektrik ihtiyacını karşılama adına 2001 yılından sonra enerji sektöründe çeşitli düzenlemeler yapılmıştır [1].
Doğu Karadeniz Bölümü sahip olduğu yüksek hidroelektrik potansiyeli ile Türkiye'nin hidroelektriküretiminde önemli bir konumdadır. Bölümün sahip olduğu yüksek yağış miktarı ve akarsu miktarı su gücü ile elektrik üretiminde öne çıkmasında etkili olmuştur.
Bu çalışmada Türkiye ve dünyada bulunan HES'ler, için mevcut üretim ve tüketim durumu gibi konular incelenerek Türkiye'nin mevcut hidroelektrik durumu hakkında veriler sunulmuştur.

2. Yöntem

2.1. Hidroelektrik Santraller

Suyun potansiyel enerjisinin, bir mil ve kanatçığa sahip eleman olarak basitçe tanımlanabilecek, türbin ile mekanik enerjiye ve daha sonrasında jeneratör ile elektrik enerjisine dönüştürüldüğü tesise hidroelektrik santrali denir [5]. Şekil 1 'de bir HES yapısının çalışma sistemi basitçe gösterilmiştir.

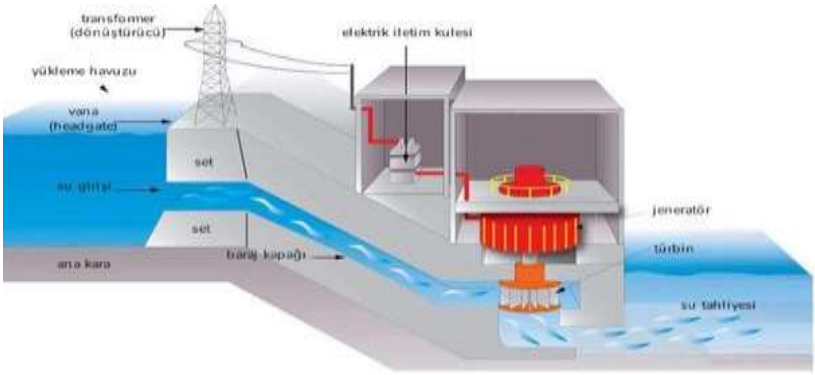

Şekil 1: HES çalışma sistemi. [6]

Bu santrallerde üretilen enerji genellikle suyun düşü ve debisine bağlıdır ve çeşitli kategorilerde sınıflandırılabilir. HES'ler depo yapılarına göre, düşülerine göre, kurulu güçlerine göre, ulusal elektrik sisteminin yükünü karşılama durumuna göre, baraj gövdesinin tipine göre, santral binasının yerine göre gibi kategorilerde sınıflandırılabilir. Bu sınıflandırma Tablo 1'de gösterilmiştir. Günümüzde dünya üzerinde hidroelektrik enerjisi üretimi rezervuarlı ve regülatör tip olarak kurulan HES'ler ile gerçekleştirilmektedir. Düşü ve debiye bağlı oluşundan ötürü HES tipi kurulacak yerin topoğrafik ve morfolojik özellikleri etkilenir [6]. Kurulacak bölgenin nüfusu, ticari yapısı, enerji ihtiyacı gibi çeşitli konulardan da HES tipinin seçimi etkilenir [7]. Ayrıca HES'ler taşkından korunma, turizm, sulama, enerji depolama, su ürünü yetiştirme amaçlarına hizmet etmesi için kullanılabilir. Bu ve bunun gibi genel ve özel ihtiyaçları karşılayabildikleri için birçok bölgede enerji ve elektrik üretiminde tercih edilir.

Dünya üzerinde altmıştan fazla ülke elektrik üretiminin yarısından fazlasını HES'lerden elde etmektedir [8]. Dünya'da hidroelektrik enerji üretiminde 694 TWh güç ile Çin ilk sırada, ikinci sırada 403 TWh güç ile Brezilya, üçüncü sırada ise 376 TWh güç ile Kanada yer almaktadır [3]. Çin'de Hubei eyaletinde bulunan Üç Geçit Barajı (Three Gorges Dam) dünyanın en büyük elektrik santralidir [9]. Dünya'nın en büyük nehir tipi hidroelektrik santrali ise ABD'de bulunan Chief Joseph hidroelektrik santralidir ve 2.620 MW güce sahiptir [3]

Resim 1: Üç Boğaz Barajı (Çin Hubei eyaleti)

Resim 2: Chief Joseph HES (ABD)

Türkiye'de nehir tipi ve depo tipi HES kullanılmaktadır. Yenilenebilir enerji kaynağı olan hidroelektrik santrallerde yakıt faktörünün olmaması, kurulum maliyetinin düşük olması ve çevreye zarar mekanizmasının çok az olması ülkemizde HES'lerin avantajlı yönleri olma konusunda önem arz eden hususlardır [1]. Hidroelektrik kaynaklarından elde edilen enerji toplam üretilen enerjinin %20,08 kadarıdır [10]. Enerji üretiminde yenilenebilir enerji kaynakları arasında en yüksek paya sahip olması HES'lere daha da önem kazandırır [10]. Türkiye'nin 2023 yılı elektrik tüketiminin 450 milyar kWh civarında olacağı öngörülmektedir [11]. Bu sebeple HES'ler tüm dünyada olduğu gibi ülkemiz içinde elektrik üretimi kapsamında değerli bir kaynak olarak düşünülebilir. Bu kaynağı ülkemiz adına değerlendirmek için yetkili makamlarca çeşitli çalışmalar yapılmış ve halen yapılmaya devam edilmektedir. 1932 yılında Türkiye'nin enerji talebini tahmin etmek, su kaynakları potansiyeli ile diğer enerji kaynaklarının potansiyellerini belirlemek ve geliştirmek için araştırma ve incelemeler yapmak maksadıyla EİE kurulmuştur [4]. 1954 yılında DSİ'nin kurulmasından sonra hidroelektrik kapasitesi 10 yıl içinde toplam enerji üretiminin %44'ünden sorumlu olan 412 MW (toplam kurulu kapasitenin %34'üne eşdeğer) değerine ulaşmıştır [4].

Türkiye'nin hidroelektrik üretimi, 1980'lerde %60'lar civarında enerji üretiminden pay alırken, sonraki yıllarda doğal gazın elektrik üretiminde kullanılmaya başlanması ve çeşitli yanlış uygulamalar sonucu büyük oranda azalmıştır [12].

HES SINIFLANDIRMASI
Depolama Yapılarına Göre:
➢ Depolamalı(rezervuarlı) HES'ler ➢ Nehir Tipi(regülatör) HES'ler
Düşülerine Göre:
➢ Alçak düşülü HES'ler(H<10m) ➢ Orta düşülü HES'ler(H= 10-50 m arası) ➢ Yüksek düşülü HES'ler(H>50 m den büyük düşülü
Kurulu Güçlerine Göre:
➢ Çok küçük (mikro) kapasiteli(<100 kW) ➢ Küçük(Mini) kapasiteli(100-1000 kW) ➢ Orta kapasiteli(1000-10000 kW) ➢ Büyük kapasiteli(>10000 kW)
Ulusal Elektrik Sisteminin YükünüKarşılama Durumuna Göre:
➢ Baz Yük HES ➢ Puant(Pik)Yük HES ➢ Hem Baz hem de Puant(Pik)Yük HES
Baraj Gövdesinin Tipine Göre:
➢ Ağırlıklı Beton Gövdeli Barajlı HES ➢ Beton Kemer Gövdeli Barajlı HES ➢ Kaya Dolgu Gövdeli Barajlı HES ➢ Toprak Dolgulu Gövdeli HES vb.
Santral Binasının Konumuna Göre
➢ Yer Üstü HES ➢ Yer Altı HES ➢ Yarı Gömülü veya Batık HES

Tablo 1: HES Sınıflandırması [2]

2001 yılında Enerji Piyasası Düzenleme Kurumu (EPDK) kurulmuş ve hidroelektrik dahil tüm enerji süreçleri için yeni bir dönem başlamıştır [4]. 2003 yılında Su Kullanım Hakkı Anlaşması yürürlüğe girdi ve özel sektörün enerji yatırımlarında önünün açılarak çok sayıda HES inşa edilmesi sağlanmıştır [1]. 2005 yılında çıkan kanun ile özel sektörün elektrik üretip satmasına izin verilmiştir ayrıca 2011 yılında düzenlene kanun ile küçük HES kurulumu sağlanmış ve mini ve mikro HES'lerin kurulumu için başvuru il özel idareleri tarafından alınmaya başlamıştır [4].

Doğu Karadeniz Bölgesi de dahil işletmeye alınan HES'lerin olduğu tüm şehirlerde sanayi açısından ihtiyaç duyulan enerji gereksinimine katkı sağlandığı görülmüştür [1]. Türk hükümetinin, 2023 yılına kadar hidroelektriğin önemli bir konumda olacağı yenilenebilir enerji kaynaklarından elde ettiği enerjiyi %30 seviyesine çıkarmayı amaçlayan planı vardır [13]. Bu planlamanın oluşmasında Avrupa Birliği (AB) topluluğunun yeşil enerjiyi desteklemeyi benimsemesi ve Türkiye'nin de üyelik adımları atması etkili olmuştur.

2.1.1 Hidroelektrik Potansiyeli

Bir akarsu havzasının hidroelektrik enerji üretiminin kuramsal üst sınırını gösteren brüt teorik hidroelektrik potansiyeli, deniz seviyesine kadar olan (sınır aşan sularda sınıra kadar) mevcut düşü ve ortalama debinin oluşturduğu potansiyelin %100 verimle türbinlenerek elde edileceği varsayılan yıllık ortalama enerji potansiyelini ifade etmektedir [12]. Teknik yönden değerlendirilebilir hidroelektrik potansiyel, bir akarsu havzasının hidroelektrik enerji üretiminin mevcut koşullardaki teknolojik üst sınırını göstermektedir [12]. Ekonomik olarak yapılabilir hidroelektrik potansiyel, bir akarsu havzasının hidroelektrik enerji üretiminin ekonomik olarak optimizasyonunun sınır değerini gösterir [12]. Türkiye'de brüt teorik hidroelektrik potansiyel 433 milyar kWh/yıl, teknik olarak değerlendirilebilir hidroelektrik potansiyel ise 216 milyar kWh/yıl, ekonomik olarak geliştirilen potansiyel ise 160,3 milyar kWh/yıl olup, yeni geliştirilecek projelerle birlikte 2023 yılı sonrasında bu potansiyel yaklaşık 180 milyar kWh/yıl'a ulaşacağı tahmin edilmektedir. 2019 yılı sonu itibarıyla işletmede olan 683 adet Hidroelektrik santralin toplam kurulu gücü 28.571 MW ve ortalama yıllık üretimi ise 99,6 milyar kWh olup, bu değer toplam geliştirilen potansiyelin yaklaşık %55,4'üne karşılık gelmektedir [14]

Tablo 2: Dünyanın Hidroelektrik Enerji Potansiyeli

Bölge	Brüt Hidroelektrik Enerji Potansiyeli (GWh/yıl)	Teknik Hidroelektrik Enerji Potansiyeli (GWh/yıl)	Teknik ve Ekonomik Hidroelektrik Enerji Potansiyeli (GWh/yıl)
Afrika	4.000.000	1.665.000	1.000.000
Asya	19.000.000	6.800.000	3.600.000
Avustralya / Okyanusya	600.000	270.000	105.000
Avrupa	3.150.000	1.225.000	800.000
Kuzey ve Orta Amerika	6.000.000	1.500.000	1.100.000
Güney Amerika	7.400.000	2.600.000	2.300.000
Dünya	40.150.000	14.060.000	8.905.000
Türkiye	433.000	216.000	127.820
Türkiye/Dünya (%)	1,07	1,54	1,84

2.1.2 Hidroelektrik Santrallerin Sınıflandırılması

Hidroelektrik santraller için yapılan sınıflandırmalardan depo tipine göre, düşülerine göre ve kurulu güçlerine göre kategorilerini göz önüne almak elektrik üretimi, elektrik üretiminde kullanılan yöntemleri ve yapıları daha iyi kavrama açısından fayda sağlayabilir. Depo tipine göre HES'ler ülkemizde nehir tipi ve barajlı tip olarak mevcuttur [5]. Barajlı tipte, akarsu sahil kısımlarından bir tanesi meteorolojik koşullara göz önüne alınarak ve gerekli düşü yüksekliği için memba kısmından rezervuar ile tamamen kapatılır [5]. Bu tip HES'ler yaygındır, bu yapıların işletme maliyetleri düşüktür, ekonomik ömrü uzundur ayrıca bu yapılar çevre dostudur, bulunduğu yerde halka çeşitli imkanlar sağlayan ve dışa bağımlılığı azaltan yapılardır [8].

Su alma yapısı, kuvvet tüneli, denge bacası, vana odası, cebri borular, santral binası, çıkış suyu kanalı, şalt sahası ve iletim hattı yapılar bu tip HES'lerde bulunabilir. Rezervuardan cebri boru içine akan su, potansiyel enerji ve akışta elde ettiği kinetik enerji ile türbini çevirir ve çıkar böylece elektrik enerjisi elde edilmiş olur [17].

Nehir tipte su depolaması söz konusu değildir bu sebeple mevsime bağlı olarak debi ve düşü etkilenir. Nehir tabanı kesitine tesisler yerleştirilir eğer kesit tabanı yeterince geniş değilse kazı işlemleri ile genişletilir [15]. Nehir santral yapılan; regülatör ve ilgili yapılar (nehir nakil araçları geçiş yeri, tomruk yolu, balık geçiş yeri) esik, ızgara, perde ve benzeri duvar, servis köprüsü, dalgıç perde, giriş yapısı ve bölme ayaklan, santral binası, kuyruk suyu kanalı, istinat duvarlarından ibarettir [15]. Düşülerine göre santraller alçak, orta, yüksek düşülü şekilde sınıflanır ve biriktirme haznesi genelde kullanılır ve Pelton ve Francis tip türbinler kullanılır [18]. Orta düşülü santraller nehir tipi ve biriktirmeli şekilde olabilir, Kaplan, Pelton ve Francis türbinleri kullanılabilir [18]. Alçak düşülü santrallerin genellikle debileri yüksektir ve nehir tipi şeklinde yapılır ve Kaplan,ve Francis türbinleri kullanılır [18]. Kurulu güçlerine göre HES'ler, mikro, mini, orta ve büyük kapasiteli olarak sınıflandırılabilirler. 50 MW ve daha üzeri güç üreten konveksiyonel güç santralleri sınıfında değerlendirilebilen, merkezi enerji nakil hatları ile ürettiği enerji bir ülkenin birçok bölgesine dağıtılabilen santrallere büyük kapasiteli hidroelektrik santraller denir [19]. Baraj gölü gibi maliyet oluşturacak yapılara gerek duymayan, 10-50 MW enerji üretebilen, yerel kullanılan ya da nakil hatları ile ulusal enerji şebekesine bağlanabilen, küçük, mini, mikro şeklinde isimlendirilebilen hidroelektrik santrallerine küçük hidroelektrik santralleri denir [19]. Küçük HES'lerin kurulmalarındaki asıl amaç, kırsal yerlerin enerji ihtiyacının karşılamak, sosyal ve ekonomik açıdan kalkınmalarına yardımcı olmaktır [5]. Çeşitli konularda değerlendirilerek kavranması için Tablo 3'de küçük HES'lerin sınıflandırılması detaylı olarak verilmiştir. Büyük yapıların tamamlayıcısı olarak da düşünebileceğimiz bu yapılar üretimde önemlidir.

Küçük hidroelektrik santrallerin sınıflandırılması aşağıda BM UNIDO tarafından belirtildiği şekilde yapılabilir [4].

• 100 kW gücü altında olanlar mikro,

• 101-1000 kW güçleri arasında olanlar mini,

• 1001-10000 kW güçleri arasında olanlar küçük hidroelektrik santraller olarak kabul edilmiştir.

Günümüzde küçük hidroelektrik santrallere yatırım yapmanın önünde olan en büyük engel maliyetin ne kadar tutacağıdır [20]. Ayrıca maliyet tahminleri ile var olan işletme yapılarının gerçek maliyetleri arasında sapmalar olabilmektedir. Bu santraller iç sulardan enerji elde etmek için ekonomik çözüm yöntemidir, santralin baş yüksekliği maliyeti etkiler ve türbin seçimi en önemli parametresidir [20].

Tablo 3: Küçük Hidroelektrik Santrallerin Ayrımı [20]

Küçük Hidroelektrik Santraller	**Enerji Edinim Kaynağı**	Denizler
		İçsular
		Birleşik Durumlar
	Başlık Yüksekliği	Yüksek Baş >100 m
		Orta Baş 30 m -100 m
		Düşük Baş <30 m
	ÇalışmaPrensibi	Suyu Depolamayan(Rezervuarsız)
		Kapasite Faktörüİle Çalışan
		Ara Sıra Çalışan(Zirve)
	Baraj YapılmaTarzı	Savak Yanında
		Baraj Yanında
		DerivasyonKanalı İle
		Basınç Derivasyon İle
		Birleşik Derivasyon İle

2.1.3 Hidroelektrik Santrallerin Avantajları

Hidroelektrik santrallerin elektrik üretiminde sağladığı avantajlar mevcuttur ve bu durum santrallerin tercih edilmesinde belirleyici bir konudur. Bu bölümde bu avantajlardan belirtilecektir. Üretilen enerji yerli enerjidir, yenilenebilir kaynaklardan üretilir ve HES yapılarından sulama, taşkın, içme suyu için yararlanılır, her mevsim verim alınabilir [21]. HES yapıları iklim ve hidrolik çevrime dahil süreçlerden etkilenen, yüksek verimli, benzer enerji üretim yöntemlerinden daha düşük işletme maliyetine sahip, işletme ömrü uzun olana enerji üretim sitemleridir [4]. Ulusal sistemden enerji alamayan kırsal yerler için ideal bir sistemdir, kullanılacak türbin ve makineler bu yapılara için tipleştirilerek aynı tipte santraller oluşturularak az sayıda personel ile denetlenebilirler, bölgesel olarak kullanıldığından uzun iletim hattı ve uzun inşa süreçlerine ihtiyaç duymayan yapılardır [7]. Santrallerde ihtiyaç duyulacak materyallerin endüstriyel üretimi yerli üretimle sağlanabilir [4]. Çevreye katı atık oluşturmaz, günlük ihtiyaç talebine kolay uyum sağlar, ucuz enerji üretimi sağlar, yüksek verimlidir [15]. Klimatolojik etki yapar (büyük yapılar biriktirme yapınca), balıkçılık, turizm ve su sporlarına katkı sağlar gibi belirtebileceğimiz avantajları da mevcuttur [5]. Santraller ile enerji depolaması yapılabilir bu depolama ile enerji ihracatı yapılabilir [22]. Bu yapılardan üretilen enerjinin birim maliyeti düşüktür, HES'ler rekabetçi piyasa ortamı sağlar ve ekonomik etkilerden kolay kolay etkilenmez [5]. Avantajların belli başlı olanları bu şekilde ifade edilmektedir.

2.1.4 HidroelektrikSantrallerin Dezavantajları

Hidroelektrik santrallerin elektrik üretiminde sağladığı avantajlar gibi dezavantajlar da mevcuttur. Hidroelektrik santraller, taşınmaz veya halkın santralin kurulduğu bölgeden uzaklaştırılmasına, bitki ve flora kaybına, yüksek miktarda hafriyat çıkışının meydana gelmesine, suyun kalitesinin bozulmasına sebep olabilir [15]. Küçük HES'lerin işletme giderleri ve 1Kw kurulu güç için yatırım maliyeti büyük santrallere göre daha yüksek gerçekleşir [7]. Biriktirmeli yapılardan kaynaklı olarak kurulan bölgede tarım alanı kaybı ve ekolojik dengede bozukluk görülebilir [22]. Depolama yapılmayan santrallerde elektrik üretimi kuraklıktan olumsuz etkilenir [15]. Belirlenen proje koşullarına uygun olmadan yapılan santral yapım yöntemleri, hafriyat uzaklaştırma vb. işlemler santralin kurulduğu bölgede erozyona ve çevre kirliliğine yol açabilir [16]. Akarsu yatağı ve çevresinden kaynaklı inşa problemleri oluşabilir ve yapıldığı bölgede gürültüye sebep olabilir [4].Dezavantajların belli başlı olanları bu şekilde ifade edilmektedir.

3. Türkiye de hes enerji üretiminde izlenen politikalar

3.1. 1950-1980 Dönemde

Akarsular enerji açısından değerlendirilmesi için gündeme gelmeye başlamıştır. Sarıyar, Seyhan, Kemer, Hirfanlı ve Demirköprü gibi hidroelektrik santraller kurularak elektrik üretilmeye başlanmıştır. Bu dönemde elektrik enerjisi üretimi %350 artmış ve 3560 milyon kW saate çıkmıştır hidroelektrik üretiminin tüm elektrik üretimi içindeki payı 1950 yılında %3,8'den 1962 yılında %31,6'ya yükselmiştir

3.2. 1980-2000 Döneminde

1980 sonrası özellikle devlet eliyle yapılan HES projelerinin özel sektör eliyle de yapılması gündeme gelmeye başlamıştır. Özel sektör HES yapma yetkisini alma isteğini sıklıkla dile getirmiştir. Çünkü Türkiye'nin gerçek anlamda hidroelektrik potansiyelini kullanmadığı tartışmaları gündemde olmuştur. Yani devlet tarafından hidroelektrik potansiyeli tam anlamıyla kullanılmadığı ifade edilmiştir.

2000'li yıllara kadar Türkiye'deki hidroelektrik potansiyelinin yeterince kullanılmadığı tartışmaları devam etmiştir. Bu durum nedeniyle çıkan kanunlarla birlikte hidrolik enerjinin serbest piyasa kurallarına göre değerlendirilmesi gerektiği konusunda önemli adımlar atılmıştır. Özellikle "Yenilebilir Enerji" ile alakalı kanunda alım garantisi ve birkaç destekleme mekanizmalarının bulunması özel sektörü harekete geçirmiştir. Bu dönemde sayısı hızla artmaya başlayan büyük ve küçük ölçekli HES projelerinin sayısı 2023 yılına kadar 1700 olacağı hesaplanmıştır.

İlerleyen zamanlarda özel sektörün bu alandaki faaliyetleri artmış ve 2001 yılında çıkartılan 4628 sayılı Elektrik Piyasası Kanunu ile yeni bir döneme geçilmiştir. Ardından 2005 yılında çıkartılan 5346 sayılı Yenilenebilir Enerji Kaynaklarının Elektrik Enerji Üretimi Amaçlı Kullanıma İlişkin kanunu ile birlikte özel sektöre HES'lerden elektrik üretip satabilme yolu açılmıştır.

3.3. 2000 -2023 Döneminde

Önceki dönemler de Devlet Su İşleri (DSİ), İller Bankası, Etibank, Sümerbank gibi kurumlar tarafından barajlar inşa edilmeye başlanmıştır. Daha sonra Dünya Bankası(DB)'nın da desteğinin artmasıyla Türkiye'de hidroelektrik yapılara olan ilgi artmıştır. Ancak Dünya Bankası'nın gerekli kıldığı masraf ve ileri teknoloji kullanılmasından dolayı DSİ, söz konusu olan hidroelektrik yapıları özel sektöre açmanın yollarını aramıştır. Bu bir ihtiyaç olarak görüldüğü için Yap-İşlet-

Devret(YİD) modeli işleme girmiş ve elektrik üretiminde özel sektör devrine geçilmiştir.
Yine aynı kanunla 2011 yılında yapılan değişikler sayesinde Türkiye'deki mikro ölçekli HES'lerin önü açılmıştır. Yapımları hızla artan bir şekilde devam eden HES'lerin giderek özel sektörü tarafından kurulup işletilmesine geçilmiştir.

4. Sonuç

Enerji, insanlığın ihtiyaç duyduğu çok önemli bir ihtiyaçtır. Bu ihtiyacın karşılanmasında çeşitli üretim süreçleri olan çeşitli enerji kaynakları vardır. Elektrik üretimi de bu ihtiyacı karşılamada önemli bir kaynaktır. Elektrik üretiminde kullanılan santrallerden su gücünü kullanan hidroelektrik santraller sağladığı avantajlar, çevreye verdiği minimum zarar, fosil yakıt kullanımına ihtiyaç duymama gibi özellikleriyle tercih edilebilen bir yapıdır. Bu yapıların Türkiye'de enerji üretiminde kullanıldığı belirtilerek bu yapıların mevcut durumu ve enerji sirkülasyonundaki durumu bu çalışmada araştırılmıştır. Çalışmada ülkemize ait çeşitli veriler kullanılarak Türkiye için hidroelektrik santrallerin önemi değerlendirilmiştir.
Sonuç olarak Türkiye'de bulunan hidroelektrik santraller, üretim lisansına sahip olan santraller, üretim tüketim verileri ve gelecek planlamaları değerlendirilerek hidroelektrik santrallerin Türkiye'de önemli bir enerji kaynağı olduğu, yüksek sayıda bulunduğu ortaya konmuştur. Hidroelektrik santrallerinin Türkiye'de için mevcutta gelişen enerji ihtiyacının karşılanmasında önemini artırarak sürdürebileceği sonucuna ulaşılmıştır. Ayrıca Türkiye'de bulunan hidroelektrik santrallerin enerji talebini karşılamadaki payının artabileceği sonucuna ulaşılmıştır.

Kaynaklar

[1] Bülbül, S. ve Çokluk, Y., Türkiye'de Gelişen Enerji Sektörü Hes'ler ve Kâr Kaybı Sigortalar,Finansal Araştırmalar ve Çalışmalar Dergisi,89-114, 2017.
[2] YGEM, Hidroelektrik Enerjisi Nedir?, Enerji Verimliliği ve Çevre Dairesi Başkanlığı, http://www.yegm.gov.tr/Yenilenebilir/H_Hidrolik_Nedir.Aspx#:~:Text=Hidroelektrik%20santrallar%20(HES)%20akan%20suyun,Y%C3%Bcksek%20miktarda%20enerji%20elde%20edilir, [Erişildi: 23 11.2023].
[3] Tunç, T., Artvin, Rize ve Trabzon İllerindeki Bazı Hidroelektrik Santrallerin Orman Alanları Üzerindeki Etkileri, Karadeniz Teknik Üniversitesi Fen Bilimleri Enstitüsü Orman Mühendisliği Anabilim Dalı, Yüksek Lisans Tezi, Trabzon, 2017.
[4] Gökdemir, M., Kömürcü, M. İ., ve Evcimen, T. U., Türkiye'de Hidroelektrik Enerji ve HES Uygulamalarına Genel Bakış, TMH, 471, 18-26,2012.
[5] Üçüncü, M. M., Enerji Kaynaklarımız Işığında Hidroelektrik Santrallerin Türkiye Ekonomisindeki Yeri ve Trabzon Örneği, Avrasya Üniversitesi Sosyal Bilimler Enstitüsü Yönetim Bilimleri Anabilim Dalı Yüksek Lisans Tezi., Trabzon, 2019.

[6] Uyar, F., HES Nedir? HES Hakkında Bilmeniz Gereken Herşey!, Enerji Beş Temiz Enerji Portalı, https://www.enerjibes.com/Hes-Nedir/,[Erişildi: 21 .11. 2023].

[7] Buttanrı, B., Türkiye'de Küçük Hidroelektrik Santrallerin Tarihsel Gelişimi ve Bugünkü Durum, İstanbul Teknik Üniversitesi Fen Bilimleri Enstitüsü İnşaat Mühendisliği Anabilim Dalı Yüksek Lisans Tezi, İstanbul2006.

[8] TMMOB İnşaat Mühendisleri Odası Antalya Şubesi., 4. Su Yapıları Sempozyumu, Retma Matbaa, Antalya, 2015.

[9] Wikipedia, https://en.wikipedia.org/wiki/Three_Gorges_D am , [Erişildi: 21 03 2020].

[10] Emeç, Ş., Adar, T., Akkaya, G., Delice, E. K., Efficiency Assessment of Hydroelectric Power Plant in Turkey by Data Envelopment Analysis(DEA), European Journal of Science and Technology, 34- 45, 2019. (DOI:10.31590/ejosat.594716)

[11] Atalay, Ö., Yılmaz Ulu, E., Hydropower Capacity of Turkey and Actual Investments,International Conference on Technology, Engineering and Science (IConTES), 162-164, 2018.

[12] Yılmaz, Ş., Türkiye Hidroelektrik Potansiyeli ve Gelişme Durumu, Türkiye'nin Enerji Görünümü, TMMOB Makina MühendisleriOdası, 203-225, 2016.

[13] Kankal, M., Akçay, F., Doğu Karadeniz HavzasıHidroelektrik Enerji Durumunun İncelenmesi, ÖHÜ Müh. Bilim.Dergisi, 892-901, 2019.(DOI:10.28948/ngumuh.598239)

[14] DSİ, Devlet Su İşleri Genel Müdürlüğü 2019 Faaliyet Raporu, DSİ, 2019.

[15] Gölbaşı, H., Karadeniz Bölgesi Küçük Hidroelektrik Santralleri ve Potansiyel Değerlendirmesi, Zonguldak Karaelmas Üniversitesi Fen Bilimleri Enstitüsü İnşaat Mühendisliği Anabilim Dalı Yüksek Lisans Tezi, Zonguldak, 2010.

[16] Aslan, H., ve Soğuksulu, Ş., Nehir Tipi Hidroelektrik Santralleri (NT-HES)'nin Neden Olduğu Sorunlar ve Rehabilitasyon Çalışmaları:Trabzon Örneği, KSÜ Doğa Bil. Dergisi, 20(1),67-74, 2017. (DOI:10.18016/ksujns.86536)

[17] Özbay, E., ve Gençoğlu, M.T., Hidroelektrik Santrallerin Modellenmesi, V. Yenilenebilir Enerji Kaynakları Sempozyumu, Diyarbakır, 2009.

[18] Mercan, B., Orta Ölçekli Hidroelektrik Enerji Tesislerinin İncelenmesi İçin Örnek Bir Çalışma Bağışlı Regülatörü Ve Hes, İstanbul Teknik Üniversitesi Enerji Enstitüsü Yenilenebilir Enerji Anabilim Dalı Yüksek Lisans Tezi, İstanbul, 2014.

[19] Akarçeşme, Y., Hidroelektrik Potansiyelin Türkiye Açısından Önemi, İstanbul Üniversitesi Sosyal Bilim Enstitüsü Coğrafya Anabilim DalıYüksek Lisans Tezi, İstanbul, 2019.

[20] Górecki, J., and Płoszaj, E., Cost Risk of Construction of Small Hydroelectric Power Plants, MATEC Web of Conferences, Krynıca, 262, 1-7,2018.(DOI https://doi.org/10.1051/matecconf/2019262070 0)

Rüzgar Enerjisinin Ülkemizdeki ve Gelişmiş Ülkelerdeki Durumu

Ayşenur SEKİN, İpek ATİK

Gaziantep İslam Bilim ve Teknoloji Üniversitesi, Elektrik-Elektronik Mühendisliği Bölümü GAZİANTEP, 27000, TÜRKİYE
* *sekinaysenur@gmail.com*

Özet

Enerji üretimi için kullanılan fosil yakıtların nüfus artışı, sanayileşme vb. konulardaki çevresel etkisi gelecekte tükenecek olması endişesine yol açmakta ve dünya genelinde yenilenebilir enerji kaynaklarına olan ilgi gün geçtikçe artış göstermektedir. Enerji tüketiminin büyük bir kısmının rüzgar enerjisinden karşılanması yenilenebilir enerji kaynaklarının kullanılmasına yönelik bir eğilim başlatmıştır. Yenilenebilir enerji kaynakları arasında en yaygın enerji olan rüzgar, elektrik üretimi açısından en umut verici olanıdır. Bu sebeple birçok ülke kısa ve uzun vadeli planlarda elektrik ihtiyacının en az %10'unu rüzgar enerjisinden karşılamayı hedeflemektedir. Rüzgar enerjisi alanında öncü olan ülkelerin kurulu gücü ile ülkemizdeki rüzgar enerjisi kurulu güçleri karşılaştırarak yıllar içinde meydana gelen değişimleri ve gelişmeleri incelenmiş , yenilenebilir enerji kaynakları içerisindeki rolü değerlendirilmiştir. Rüzgar enerjisi kinetik bir enerji kaynağı olup kolay elde edilebilir olması nedeniyle dünyanın en eski ve en sürdürülebilir enerji kaynaklarından biri olarak kabul edilmektedir. Bu çalışmada ülkemizde ve gelişmekte olan ülkelerde rüzgar enerjisinin mevcut durumu araştırılmıştır.

Anahtar Kelimeler: Rüzgar enerjisi , nüfus artışı , kurulu güç, çevresel etkiler.

1. Giriş

Günümüzde enerji kelimesi sosyal ve ekonomik yaşamda tüketimin vazgeçilmezi haline gelmiştir. Sanayi devriminden bu yana kullanılan fosil yakıtların miktarının kısıtlı olması, fiyatlarının her geçen gün artması ve çevreye verdikleri zararın geri dönülemez boyutlara ulaşması nedeniyle bu konuda bilimsel araştırma ve hassasiyet giderek artmaktadır. Bu bağlamda sürdürülebilir ekonomik modeller ve çevre güvenliğinin sağlanması açısından yenilenebilir enerji kaynakları enerji piyasalarının gündeminde yer almaktadır.

Yenilenebilir bir enerji kaynağı olan rüzgar enerjisi, hızlı teknolojik gelişimi nedeniyle son yıllarda çeşitli ülkelerin enerji portföyünde büyük bir yer işgal etmektedir. Rüzgar enerjisi çevre dostudur, dışa bağımlılık yaratmaz, yeni istihdam yaratmakta olup dünyanın birçok Ülkesinde ve Türkiye'de alternatif yenilenebilir doğal kaynak olarak kullanılmaktadır. Rüzgar enerjisinin tükenmez ve yenilenebilir bir doğal kaynak olması ve büyük rüzgar enerjisi potansiyelinden faydalanmanın Türkiye'nin artan enerji ihtiyacını karşılamanın ideal bir yolu olması rüzgar sektörü için teşvik edici bir faktör olup tartışmalar devam etmektedir.

Rüzgâr enerjisinin kullanımının tarihi çok eskilere dayanmaktadır. Rüzgar enerjisinin ilk örnekleri yelkenli gemiler ve yel değirmenleridir. Yelkenli gemiler, gemilerini hareket ettirmek için rüzgarın kinetik enerjisini kullanıyordu , aynı zamanda un değirmenlerde ise buğday gibi tahılları öğütmek için rüzgar enerjisini kullanıyordu. Zamanla enerji sorunları ortaya çıktı ve rüzgar türbinleri giderek daha fazla enerji üretimi için tasarlandı.

Dünyada mevcut enerji kaynaklarının çoğunun sınırlı olması ve fosil enerji kaynaklarının tüm ülkelerde politik bir araç olarak kullanılması nedeniyle rüzgar enerjisi geleceğin enerjisi olarak kullanılabilecek yenilenebilir enerji kaynaklarından biridir. Fosil enerji fiyatları, OPEC petrol ambargosu (1973), petrol krizi (1982) ve ardından gelen diğer enerji krizleri sonucunda yükseldi. Gelişmiş ülkelerde fosil enerji kaynaklarının sınırlı olması nedeniyle bu fiyat artışları rüzgar enerjisine olan ilgiyi yeniden gündeme getirmiştir. Yapılan araştırmalar sonucunda birçok yeni rüzgar türbini modeli üretilmiştir. Rüzgar enerjisinin öncelikli olarak ev ve işyerlerinde kullanılmaya başlanmasıyla birlikte gelişim devam etti ve dünya genelinde rüzgar türbinlerinin kurulu gücü hızla arttı.

Rüzgar enerjisi, sonlu enerjinin yerini alan, sera etkisinden kaynaklanan küresel iklim değişikliğinin önlenmesi açısından son derece önemlidir.

Gelişmekte olan ülkelerde ise , küresel ısınmaya neden olan sera gazlarından dünya çapında rüzgar enerjisi kullanımını yönlendirilmeli ve desteklemelidir.

Gelişmiş ve gelişmekte olan ülkeler tarafından Japonya'nın Kyoto kentinde imzalanan iklim değişikliği Kyoto Protokolü kapsamında AB, sera gazı emisyonlarını 2010 yılına kadar 1990 yılı seviyelerine indirme kararı aldı. Mevcut büyümenin aynı hızla devam etmesi halinde rüzgar enerjisi de artacak. 2020 yılına kadar yılda 109 milyon tonu kapsayacaktır. Bu miktar Kyoto Protokolü'nün belirlediği miktarın üzerinde olup bunlardan en önemlilerinden biri, Greenpeace uluslararası 2050 yılına kadar dünya elektrik üretiminin yaklaşık %7'sinin rüzgar enerjisinden elde edileceği tahmin edilirse, toplam 2.455 milyar ton karbondioksit tasarrufu sağlanacak; bu da karbondioksit emisyonlarının düşmesi anlamına geliyor.

2. Materyal ve Metot

Rüzgar enerjisi, Dünya yüzeyinin Güneş tarafından eşit olmayan şekilde ısıtılması, soğutulması ve hava basıncındaki farklılıklardan kaynaklanan kuvvetlerin neden olduğu havanın hareketidir. Bu hava akışının kinetik enerjisine rüzgar enerjisi denir. Rüzgar enerjisi sayesinde hava kütlesinin kinetik enerjisi mekanik enerjiye dönüştürülür. Bu anlamda rüzgar enerjisi de güneş enerjisine dönüştürülmüş olmaktadır.

2.1 Türkiye'de Rüzgar Enerjisi

Türkiye geçen yıl yaklaşık 1.750 Megavat ile tarihinin en yüksek yıllık rüzgar enerjisi kapasitesine ulaştı. Geçtiğimiz yıl işletmeye alınan yaklaşık 1.750 Megavatlık rüzgar enerjisi kapasitesi, Türkiye'de bir yılda işletmeye alınan en büyük kapasite oldu. Bu ilave ile birlikte Türkiye'nin toplam kurulu rüzgâr enerjisi kapasitesi 2021 yılı sonunda 270 projeyle 10 milyon 750 MW 'a ulaştı. Türkiye'nin bugüne kadarki en yüksek yıllık kapasite ilavesi 2016 yılında
1.248 MW oldu.
Pek çok ülke toplam üretiminin bir kısmını rahatlıkla rüzgar ve güneş enerjisinden sağlamaktadır.
İspanya ,Almanya ve Danimarka gibi enerji alanında önde gelen ülkeler enerjilerinin yaklaşık dörtte birini güneş veya rüzgar enerjisinden üretiyor. Danimarka ve Almanya sistem güvenilirliği açısından ilk sırada yer almaktadır. Ülkeler, rüzgar ve güneş enerjisinin enerji geçiş sürecinde daha büyük rol oynamasına olanak tanıyan esnek enerji sistemlerine yönelik kendi stratejilerini geliştirmişlerdir. Enerji üretiminde yaygın olarak kullanılan günümüz fosil yakıtlarının çevreye zararlı bileşikler üretmesi, pahalı olması ve doğal kaynakları hızla tüketmesi, teknoloji geliştikçe alternatif enerji kaynaklarının ve yenilenebilir doğal
kaynakların geliştirilmesine yol açmıştır. Rüzgâr enerjisi olarak güneş, su, jeotermal ve biyolojik kaynaklardan faydalanılmaktadır. Kaynağa dayalı bu enerji üretim cihazları arasında rüzgar türbinleri, diğer seçeneklere göre düşük risk, kısa kurulum süresi ve düşük yatırım maliyetleri nedeniyle dünya çapında tercih edilmektedir.
Rüzgar türbinleri; yakıt maliyeti gerektirmeyen, işletme maliyeti düşük, işletmesi ve bakımı kolay, dış kaynaklara bağımlı olmayan enerji santralleridir. Türkiye'nin ticari ölçekte elektrik üretebilen ilk rüzgar türbini, 1984 yılında Çeşme Otel Altınun Bahçe'ye kuruldu. O dönemde dünya henüz rüzgar enerjisi teknolojisini geliştirmekte büyük ticari rüzgar santralleri kuruluyor ve rüzgar santrallerinin inşaatı ise henüz başlamamıştı. Özellikle Avrupa'da rüzgar türbinleri 1990'lı yılların başında yapılmaya başlandı ancak ülkemizde ilk rüzgar santralinin inşası ancak 1998 yılında mümkün oldu.
Türkiye'de rüzgar enerjisi alanında asıl dönüm noktası, 1998 yılının Şubat ayında Çeşme'de üç adet 500 kW'lık Gelmiya RES türbininin kurulumuyla başladı. Santral, dönemin kanunlarına göre enerjiyi karşılayacak bağımsız bir elektrik santrali olarak inşa edildi. 600 kW kapasiteli 12 türbinden oluşan Ares RES, 1998 yılı Ağustos ayında Çeşme'de işletmeye alınmıştır. Bozcaada Res 2000 yılında kurulmuş olup her biri 600 kW kapasiteli 17 türbinden oluşmaktadır.

İstanbul Hadımköyde 2003 yılında kurulan 600 kW'lık iki türbinden oluşan Sunjut rüzgar santrali bulunmaktadır. Germiya RES'de olduğu gibi amaç kendi enerjini üretmektir. Yukarıda bahsedilen dört enerji santrali, yenilenebilir enerji kanunları veya düzenlemeleri olmadan inşa edilmiştir.
2000-2007 yılları arasında geliştirilmiş olan 4.000 MW değerindeki projeler onaylandı ve bunların çoğu rekabetsiz olarak devreye alındı.
21 Mayıs 2009 'da elektrik piyasası arz güvenliği belgesinde rüzgar enerjisi kurulu güç kapasitesinin 2023 yılı sonuna kadar 20.000 MW'a çıkacağı belirtildi.
Belirtilen hedefe ulaşmak için ülkemizde elektrik üretiminin desteklenmesine yönelik yasal bir mekanizma oluşturulmuştur. Yenilenebilir doğal kaynaklar kullanan enerji santrallerinin kurulması ve özel yatırımcıların rüzgar santralleri kurması teşvik edildi.
Enerji ve Tabii Kaynaklar Bakanlığından alınan verilere göre Nisan ayı itibari ile Türkiye'nin kurulu elektrik kapasitesi 104 bin 348 MW, rüzgar enerjisi kapasitesi ise 11 bin 426 MW'tır. Elektrik üretiminde yenilenebilir enerji kaynaklarının payı artmasına rağmen rüzgar enerjisinin Türkiye'nin kurulu elektrik kapasitesi içindeki payı yüzde 9,9'a yükseldi. Rüzgâr enerjisi kurulu gücünün çoğunluğu lisanslı santrallerden oluşmakta olup Türkiye'nin 47 iline dağılmıştır. 15 eyalette toplam 88,4 Megawatt kapasiteli lisanssız rüzgar türbinleri bulunuyor.
İzmir, 1.754,9 MW'lık üretimle rüzgar enerjisi alanında en büyük kurulu güce sahip ildir. İzmir'in yanı sıra diğer illerdeki rüzgar enerji kapasiteleri şu şekildedir;

- 1382,4 MW Balıkesir.
- 943,7 MW Çanakkale
- 838,7 MW İstanbul
- 701,7 MW Manisa

- 440,9 MW Bursa
- Hatay, 420,2 MW
- Aydın, 397,3 MW
- 394,5 MW Kırıklareli
- 338 MW elektrik üretim kapasitesiyle Kayseri, rüzgar enerjisi kapasitesi en büyük 10 şehirden biridir.

Türkiye Rüzgar Enerjisi Birliği'ne (TÜREB) göre rüzgar enerji sektörü hem kurulu üretim hem de kapasite açısından büyüyor. TÜREB 'e göre bu alanda faaliyet gösteren 100'ün üzerinde Türk firması, altı kıtada 44 ülkeye rüzgar türbini ihracatı yapıyor. Bu şirketlerin satışlarının yaklaşık yarısı rüzgar türbini ihracatından geliyor.
Türkiye'de 2022 ortalarına kadar rüzgar enerjisine ilişkin kurulu rüzgar türbini sayısı ve toplam kurulu kapasite dahil sayısal veriler Şekil 1'de gösterilmektedir.

Şekil 1. Türkiye'de 2022 yılı ortasına kadar rüzgâr enerjisi verileri

Türkiye'de rüzgâr enerjisinin güncel olan istatistiksel verileri aşağıda verilmektedir. Tablo 1'de Türkiye'de yer alan en büyük kapasitedeki 11 sahanın ayrıntıları verilmiştir.

Tablo 1. *Türkiye'de bulunan ve faaliyette olan en yüksek kurulu güce sahip rüzgâr santrallerinin verileri*

SANTRAL ADI	ŞEHİR	FİRMA	MW
Soma RES	Manisa	Polat Enerji	288
Karaburun RES	İzmir	Alto Holding	227
Dinar RES	Afyonkarahisar	Güriş Holding	200
İstanbul RES	İstanbul	Universal Wind Enerji	200
Geycek RES	Kırşehir	Polat Enerji	168
Balıkesir RES	Balıkesir	Enerjisa Elektrik	143
Osmaniye RES	Osmaniye	Zorlu Enerji	135 (150.6)
Saros RES	Çanakkale	Borusan EnBW Enerji	133 (138)
Kangal RES	Sivas	Ece Tur İnşaat	128
Şamlı RES	Balıkesir	Fernas Enerji	127
Bergama RES	İzmir	Bilgin Enerji	120

2.2 Türkiye'de Rüzgar Enerjisi Potansiyeli

Ülkemizde iklim değişikliğine bağlı olarak Meteoroloji Genel Müdürlüğü (DMİGM) rüzgar enerjisi ölçümleri yapmaktadır. Ancak ölçüm istasyonları çoğunlukla yerleşim bölgelerinde yer aldığından gerçek değer belirlenememektedir. Rüzgar enerjisi teknolojisinin dünya çapında gelişmesiyle birlikte Elektrik Enerjisi Araştırma Enstitüsü (EİE), ülkemizdeki rüzgar enerjisi potansiyelini ortaya çıkarmak amacıyla bir çalışma başlattı. On üç farklı gözlem noktası oluşturularak sonuçlar toplanmaya başlandı. 2020 yılında Türkiye'nin elektrik tüketiminin ortalama yüzde 100'ü rüzgar enerjisinden karşılanacaktır.
Ülkenin 2027 yılına kadar 16.000 MW rüzgâr kapasitesi işletmesi bekleniyor. Türkiye 'nin DMİGM 'ye göre ölçülen rüzgar enerji gücü131.756,40 MW olup, rüzgar hızı 50 metre yükseklikte 6,5 metre/s'nin üzerindedir.
Buna ek olarak ,Türkiye'nin en rüzgarlı bölgesi olan Marmara Bölgesi, Ege Bölgesi ve Güneydoğu Anadolu Bölgesi'nde rüzgarın hızını 6,5 m/s'yi aşması durumunda offshore rüzgar enerjisi Türkiye'de de kullanılabilmektedir.

Tablo 2 . *Rüzgarın yıllık olarak hızı ve yoğunluğu*

Bölge	Yıllık ortalama rüzgar yoğunluğu m/s2	Yıllık ortalama Rüzgar Hızı (m/s)
Marmara Bölgesi	51.91	3.29
Ege Bölgesi	23.47	2.65
Akdeniz Bölgesi	21.36	2.45
İç Anadolu Bölgesi	20.14	2.46
Karadeniz Bölgesi	21.31	2.38
Doğu Anadolu Bölgesi	13.19	2.12
Güney Doğu Anadolu Bölgesi	29.33	2.69
Ortalama	25.82	2.58

Tablo 2'de sunulan verilere bakıldığında, Marmara bölgesinde yıllık ortalama rüzgar hızı 3,29 m/s ve yıllık ortalama rüzgar yoğunluğu ise 51,91 m/s2 iken aynı değerler Ege Bölgesi'nde yıllık ortalama rüzgar hızı 2,65 m/s2 ve yıllık ortalama rüzgar yoğunluğu m/s2 23,47 m/s2'dir.
Rüzgar santrallerini yoğun olarak Balıkesir, Manisa, İzmir, Hatay, Osmaniye, Çanakkale ve İstanbul illerinde bulunmaktadır.
2020 yılında Türkiye'nin elektrik tüketiminin ortalama %100'ü rüzgar enerjisinden sağlanacak.

Ayrıca 2027 yılında rüzgar enerjisi potansiyelinin 16.000 MW gücünde faaliyete geçmesi bekleniyor. Türkiye'nin karada bulunan rüzgar enerji gücünün ise 37.000 MW, denizdeki rüzgar enerji gücünün 11.000 MW olacağı öngörülmektedir. Türkiye'nin 48.000 MW rüzgar enerjisi potansiyeli bulunuyor ve bu enerji kaynağı elektrik ihtiyacının yarısını karşılayabiliyor.

2.3 Rüzgar Enerjisine Dayalı Kurulu Güç

Haziran 2021 sonu itibarıyla rüzgâr enerjisi kurulu gücümüz 10.976 MW olup, toplam kurulu gücün % 0,81'ini oluşturmaktadır. Aşağıdaki Şekil 2'de kurulu kapasitedeki yıllık değişimler ile toplam kurulu kapasite arasındaki ilişki gösterilmektedir.

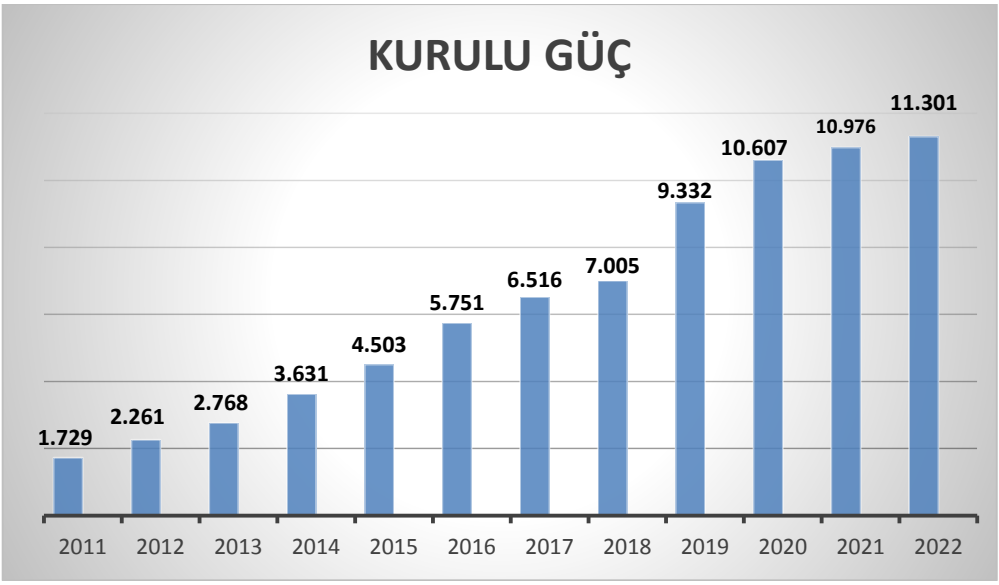

Şekil 2. Rüzgar enerjisinin kurulu gücü

2.4 Gelişmiş ülkelerde rüzgar enerjisi

Bölgelere bağlı olarak bazı unsurlar sonucu değişiklikler meydana gelmektedir. Rüzgar enerjisini etkileyen unsurlar: Ülkenin karayla çevrili olup olmamasına ve içinden ne tür hava akımlarının geçtiğine bağlıdır. Rüzgar enerjisi artık tüm dünyada popüler olacak gibi görünüyor.

Dünya çapında 100'den fazla ülke elektrik üretmek için rüzgar enerjisini kullanıyor. Rüzgar enerjisi kurulu kapasitesinin en yüksek olduğu ülkelere bakıldığında ise Çin, ABD ve Almanya ilk üçte yer alıyor.
Rüzgar türbini kurulu kapasitesi açısından Avrupa'da 7'nci, dünyada ise 13'üncü sırada yer alan Türkiye'nin en önemli rüzgar enerjisi satış bölgeleri Kuzey Amerika, Asya ,Avrupa Afrika ve Rusya'dır.
Araştırmaya göre bu bölgelerden Rusya, Afrika ve Kuzey Amerika'nın dünya rüzgar enerjisi potansiyelinin yarısından fazlasını barındırdığı belirlendi. Rüzgar enerjisi teknolojisi, son yıllarda 200 MW'lık rüzgar türbinlerinin inşa edilmesiyle büyük ilerleme kaydetti.
Resmi istatistiklere göre dünyanın kurulu rüzgar enerjisi kapasitesi 1995 yılında 4.843 MW, 1996 yılında ise 6.097 MW'tır.1997 ve 1998'de 7.500 MW'a ulaşıldı. 1999 yılı sonunda dünya rüzgar enerjisi kurulu gücü 2,8 daha artış göstererek 13.455 MW'a ulaşmıştır.
Dünyada rüzgar enerjisi kurulu gücü 2003 yılı itibari ile 33.400 MW, 2006 yılı itibari ile
74.000 MW, 2015 yılı sonunda ise 432.883,00 MW olarak gerçekleşmiştir (TÜREB, 2016).
Aralık 2015 itibarıyla dünya çapında işletmede bulunan rüzgar türbinlerinin kurulu gücü 432.883,00 MW'tır. Bunun 147.771 MW'ı Avrupa'da, 100.969 MW'ı ABD'de, 175.831 MW'ı
Asya'da, 4.823 MW'ı Güney Pasifik'te ve 3.489 MW'ı ise Kuzey Pasifik'te bulunmaktadır.(greenpea.org. 2016).

2040 yılına kadar dünya çapında 100.000'den fazla insanın elektrik ihtiyacının rüzgar enerjisiyle karşılanacağı tahmin ediliyor.
Kurulu rüzgar türbinlerinin çoğu Avrupa'da, ardından Amerika'da, geri kalanı ise Asya ve diğer kıtalarda bulunuyor. Avrupa'da en çok kurulu rüzgar türbinleri 23.025 MW ile İspanya, 13.603 MW ile İngiltere, 10.358 MW ile Fransa yer almaktadır. Asya'da rüzgar enerjisi üretimine odaklanan ülkeler Çin ve Hindistan'dır . Avrupa'da rüzgar enerjisinin kullanımı son yıllarda hızla artmıştır. Avrupa Rüzgar Enerjisi Birliği'ne (EWEA) göre 2004 yılında 34.205 MW olan rüzgar enerjisi üretiminin 2020 yılında 180.000 MW 'ı aşması bekleniyor. Rüzgar enerjisi kullanımı arttıkça birim maliyetlerin düşmesi bekleniyor. Bu nedenle Avrupa'da 2000 yılından bu yana rüzgar enerjisi kullanımı ve 2020 yılına kadar hedeflenen kapasite aşağıdaki Tablo 3'de gösterilmektedir.

Tablo 3. Avrupa'da rüzgar enerjisi üretiminin yaşı ve hedef kurulu gücü

YILLAR	KURULU GÜÇ (MW)
2000	12.880
2001	17.313
2002	23.159
2003	28.567
2004	34.205
2005	40.500
2006	48.000
2015	147.771
2020	180.000

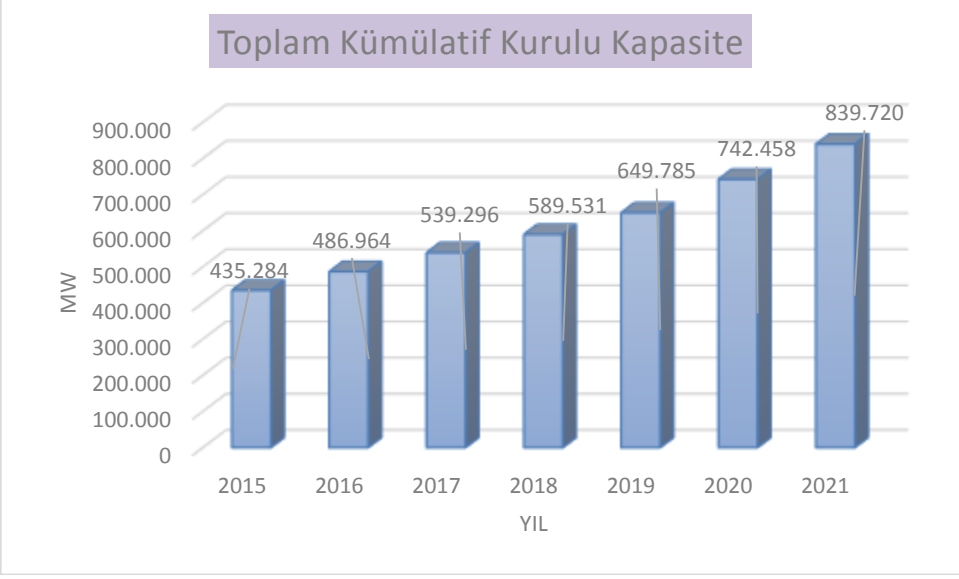

Şekil 3. AB ülkelerinde rüzgar enerjisinin mevcut durumu

Kurulu gücün büyüme hızı 2000-2001 döneminde 5 kat, 2000-2015 döneminde ise 11,5 kat artarak 147.771,00 MW'a ulaştı.
İstatistiksel verilere göre son yıllarda dünyanın rüzgar enerjisi 7 yılda ortalama 310 GW kapasitesi arttı. Dolayısıyla 2021 yılında toplam küresel yeni rüzgar enerjisi kapasitesinin ortalama 839 MW olduğu açık olup, yıllık rüzgar enerjisi kapasitesi artışı Şekil 3'te gösterilmektedir.

2.5 AB Ülkelerinde rüzgar enerjisinin durumu

Avrupa Birliğinde bulunan ülkeler en yaygın kullanılan enerji kaynağı olan rüzgar enerjisinin kullanımını artırmaya yönelik yatırımlar yapıyor.
Avrupa ülkeleri başta olmak üzere diğer bölgelerde de bu hedeflere ulaşmak için çeşitli pazar desteklerini benimsemiştir. Bu ülkelerde üretilen enerji başına tazminat ödenmesinden, yenilenebilir enerji kaynakları kullanan santrallere , özel tarifeler , teşvikler vb. pek çok yöntem kullanılıyor. Avrupa'da rüzgar enerjisi kullanımı 2009 yılında artmaya devam etti. Almanya liderliği korurken İspanya da onu takip etti.
AB'nin gelişmekte olan ülkelerinde rüzgar türbinlerinin kullanımı henüz istenilen seviyeye ulaşmadı. Avrupa'nın dört başkenti Fransa, İtalya, Almanya ve İspanya'dır. Ayrıca offshore yenilenebilir enerji kurulu gücü 2.061 MW olup, Avrupa'nın toplam 76.152 MW'lık kapasitesinin %2,7'sine tekabül etmekte olup, offshore yenilenebilir enerjinin önümüzdeki yıllarda artması beklenmektedir..

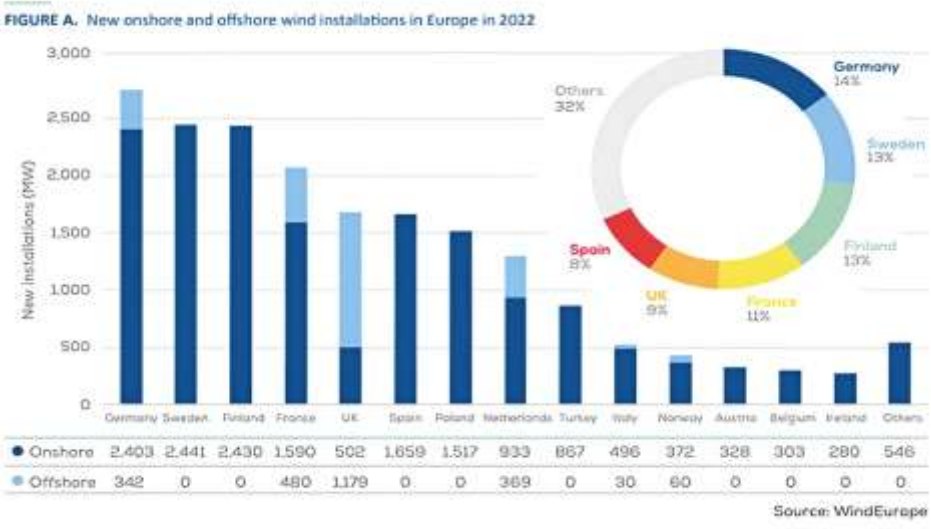

Şekil 4. *Karada ve denizde kurulu rüzgar enerjisi kapasite raporu*

Şekil 4'deki rapora göre Avrupa'da geçen yıl 454 MW rüzgar enerjisi üretildi. Ancak Wind Europe, önümüzdeki beş yıl içinde yaklaşık 5,6 GW 'ın devreye gireceğini öngörüyor.Bu arada Avrupa'da şu anda 255 GW kurulu rüzgar enerjisi kapasitesi bulunuyor. Bunun 225 GW'ı karada, 30 GW'ı ise açık deniz rüzgar türbinlerinde (RES) kurulacak.
Ülkelere göre geçen yıl inşa edilen yeni rüzgar türbinlerinin 16,7 GW karadaydı. Avrupa'daki yeni offshore rüzgar santrallerinin kapasitesi 2,5 GW'a çıktı. İsveç, Finlandiya, Almanya ve Fransa ülkede en fazla rüzgar türbini inşa eden ülkelerdir. Geçen yıl Almanya, 100'ü karada olmak üzere toplam 2,7 GW ile en fazla rüzgar türbini kuran ülke oldu.İsveç ve Finlandiya'nın her biri 2,4 milyon kW, Fransa 2,1 milyon kW ve Birleşik Krallık ve İspanya 1,7 milyon kW üretti.Aynı zamanda Ukrayna, savaşa rağmen yeni elektrik üretim kapasitesini 83 MW artırdı.Rapora göre Türkiye geçen yıl 867 MW kapasite kullandı. Bu, 2021'deki rekor olan 1,8 GW'ın yarısından azdır.
Türkiye'nin 2023-2027 yılları arasında ülkede 8,2 GW kurulum yapması bekleniyor. Geçen yıl Avrupa'daki rüzgar türbinleri 487 TWh elektrik üretti. Wind Europe, Avrupa'nın önümüzdeki beş yıl içinde 129 GW yeni rüzgar enerjisi kurmasını bekliyor.Plana göre bunun 98GW'ı 27 AB ülkesinde gerçekleştirilecektir.

3. Sonuçlar

Türkiye, nüfusun artması , kentleşme çabaları ve sanayileşmenin gelişmesi ile enerji talepleri nedeniyle enerji sıkıntısıyla karşı karşıyadır. Sonuç olarak enerji üretimi ile tüketimi arasındaki fark hızla açılıyor.
Türkiye'nin enerji ihtiyacını karşılamak için, birincil enerji kaynaklarının tükenme ihtimalini göz önünde bulundurarak rüzgar enerjisi kullanımına ağırlık vermesi ve bu alanda özel sektörü teşvik etmesi gerekmektedir.
Türkiye'nin sağlam altyapıya sahip yerli bir rüzgar enerjisi sektörü geliştirebilmesi için özel sektörün belirtilen alanda rekabet gücünü sağlaması gerekmektedir. Avrupa Birliği'nin Türkiye'ye ve üye devletlere sunduğu avantajlar doğrultusunda ülke, vergi teşvikleri yoluyla veya her şeyden önce vergi teşvikleri yoluyla belirli bir yüzde vergiyi düşürerek Türkiye ve üye devletlerine gerekli yatırım teşviklerini sağlayacaktır. Üreticilerin önünü açmamız gerekecektir.
Rüzgar enerjisinin olumlu yanlarının yanı sıra olumsuz yanları da mevcuttur. Gürültü, görüntü ve estetik kirliliği, kuş ölümleri, 2-3 kilometre yarıçapındaki radyo ve televizyon alıcılarına müdahale edilmesi ise rüzgar enerjisinin olumsuz yönlerindendir.
Ancak teknolojik gelişmeler sayesinde bu olumsuz etkiler önemli ölçüde azaltılmış veya ortadan kaldırılmıştır. Yenilenebilir enerji kaynaklarının araştırma ve geliştirilmesi üniversite, özel sektör ve sanayi işbirliğiyle yürütülmelidir.

Bu işbirliğinin amacı aynı zamanda rüzgar enerjisinin önemini ve ülkeye faydalarını toplumun her kesimine anlatacak projeler üretmektir. Ülkelerin önümüzdeki yıllarda alacağı kararlar dünyanın ekolojik ve ekonomik durumunu belirleyecektir.
Gelişmiş ülkelerin enerji stratejilerini yeniden düşünmesi, gelişmek üzere olan ülkelerin ise geçmişten ders çıkarıp sürdürülebilir enerji kaynaklarına dayalı ekonomik temeller oluşturması gerekiyor.

Kaynakça

[1] Enerji İşleri Genel Müdürlüğü Verileri, 2001.
[2] N. Öztürel, R. Zilan ve A. Ecevit, Türkiye 'de Yenilenebilir Enerji Kaynakları İçin İzlenmesi Gereken Strateji, Planlama Politikaları ve Bunların Sosyal ve Siyasi Etkileri. Yenilenebilir Enerji Kaynakları Sempozyumu, 28-32, İzmir, 2001.
[3]S.Dereli "Rüzgar enerjisi", Ankara; Tübitak Yayını; 2001
[4] Hayli, S. "Rüzgâr Enerjisinin Önemi Dünya'da ve Türkiye'deki Durumu," Fırat Üniversitesi Sosyal Bilimler Dergisi, cilt 11, sayı 1, s. 1-26 , 2001.
[5] Özgener, Ö. "Türkiye'de ve Dünya'da Rüzgâr Enerjisi Kullanımı," Dokuz Eylül Üniversitesi Mühendislik Fakültesi Fen ve Mühendislik Dergisi, cilt 4, sayı3, s.159-173. 2002.

[6] Tübitak, " Türkiye Bilimsel ve Teknik Araştırma Kurumu vizyon 2023 ön rapor",
Teknoloji Öngörüsü Projesi Enerji ve Doğal Kaynaklar Paneli, Ankara, Ocak, 2003
[7] History of wind energy, http://www.bergey.com/primer.html, 2003.
[8] Mathew, S. Wind Energy: Fundamentals, Resource Analysis and Economics.
Springer 2006.
[9] Turan, İ., Türkiye Rüzgar Enerjisi Sektörünün Durumu, Rüzgar Türbinleri ve Ekipmanlarının Yerli Kaynaklar Kullanılarak Tasarımı ve Üretim Paneli,7 Mayıs 2008,
İstanbul, Türkiye
[10] Durak M.," 2009 Yılı Sonu İtibari İle Dünya'da ve Ülkemizde Rüzgar Elektrik Santral Projelerinin Son Durumu" ,Türkiye Rüzgar Enerjisi Birliği Yayınları, s. 2-7, 2009 , Ankara.
[11] Koç, E., Şenel, M. C "Dünya'da ve Türkiye'de Enerji Durumu-Genel Değerlendirme," Mühendis ve Makine Dergisi, cilt 54, sayı 639, s. 32-44 . 2013.
[12] Gözen, M., "Renewable Energy Support Mechanism in Turkey: Financial Analysis and Recommendations to Policymakers", International Journal of Energy Economics and Policy, 4(2): 274-287, 2014.
[13] Dursun, B., Cihan Gokcol, "Impacts of the renewable energy law on the developments of wind energy in Turkey", Renewable and Sustainable Energy Reviews, 40: 318-325, 2014.
[14] Ilkılıç, C, Aydin, H. "Wind Power Potential and Usage in the Coastal Regions of Turkey," Renewable and Sustainable Energy Reviews, vol. 44, p. 78-86 2015.
[15] Kaplan, Y. A., "Overview of wind energy in the world and assessment of current wind energy policies in Turkey", Renewable and Sustainable Energy Reviews, 43: 562-568 , 2015.
[16] Şenel, M.C. ve Koç, E. "Dünyada ve Türkiye'de Rüzgâr Enerjisi Durumu-Genel Değerlendirme", Mühendis ve Makina, 56 (663), 46-56. 2015
[17] Buhan, S., Çadırcı, I., "Multi-Stage Wind Electric Power Forecast by Using a Combination of Advanced Statistical Methods", IEEE Transactıons On Industrial Informatics, 99, 2015.

[18] Turkish Wind Energy Association (TWEA). Wind power plants under operation in Turkey; 2015.
[19] Dickson, G. 2016. Türkiye Rüzgar Enerjisi Konferansı 2016. Ankara.
[20] Karagöl, E. T. & Kavaz, İ. "Dünya ve Türkiye'de Yenilenebilir Enerji", Analiz, 197, 1-31. 2017
[21] SETA Dünyada ve Türkiye'de Yenilenebilir Enerji, 197, 2017 İstanbul.
[22] Özalp, M. Küresel Ölçekte Türkiye'nin Enerji Arz Ve Talep Güvenliği 2019
[23] M. Ebrahimpour, R.Shafaghat, R. Alamian and M. S. Shadloo, "Numerical Investigation of the Savonius Vertical Axis Wind Turbine and Evaluation of the Effect of the Overlap Parameter in Both Horizontal and Vertical Directions on Its Performance", Symmetry, 11, 821, 2019.
[24] F., Pierre; J., Matthew W.; O., Michael; vd., "Global Carbon Budget 2019". Earth System Science Data. 11 (4): 1783–1838 , 2019
[25] TÜREB Türkiye Rüzgâr Enerjisi İstatistik Raporu, https://tureb.com.tr//yayin/turkiye-ruzgar-enerjisi-istatistik-raporu-ocak2020/128 .2020
[26] Y. Wittor, "Harvesting wind energy through electrostatic wind energy conversion - Comparison with common wind turbines and future possibilities", EGU Master Journal of Renewable Energy Short Reviews, 2021_09, 48, 2021
[27] Türkiye Rüzgar Enerjisi Birliği (TÜREB). "Türkiye Rüzgar Enerjisi İstatistik Raporu", https://tureb.com.tr//lib/uploads/55081baf3b9a1091.pdf 2021
[28] Akgün, N., ve Dündar, C. (2022, 15 Ekim). Türkiye Rüzgâr Atlası. https://www.kimyaegitimi.org/sites/default/files/kuresel_isinma_projeleri/probleme_dayali_ogrenme_modeli/turkiye_ruzgar_atlasi.pdf .2022
[29] Dvorak, P. Power performance upgrades to wind turbines. https://www.windpowerengineering.com/power-performance-upgrades-windturbines 2022
[30] Türkiye Rüzgâr Enerjisi Birliği Rakamlarla Rüzgâr Enerjisi. https://tureb.com.tr/anasayfa .2022
[31] Franke, D. I. Wind turbines in Galmsbüll, Deutschland. https://tr.m.wikipedia.org/wiki/Dosya:Gamsb%C3%BCll_repowering.jpg. 2022
[32] https://tureb.com.tr/haber/turkiye-ruzgar-enerjisi-istatistik-raporu-ocak-2023

Design of Grid-Connected Solar Power Plant in Gaziantep Province Using PV*SOL Premium

Samet Kayali*, İpek Atik

Gaziantep islam science and technology university faculty of engineering and natural sciences department of electrical and electronics engineering gaziantep-turkey
samtkayali@gmail.com

Abstract

Our country is highly dependent on energy imports, spending billions of dollars annually. The inadequacy of fossil energy sources has led us to seek new energy sources. While researchers work on more efficient use of existing energy sources, they also dedicate efforts to renewable energy sources. Solar energy is a significant energy production source for our country, with higher potential than European Union countries. EU countries are engaged in consumer awareness and promotion of electricity generation from solar energy through various incentive mechanisms. Recently, solar energy has become the most attractive renewable energy source due to high solar energy potential in the country and advancing photovoltaic (PV) technologies. Different PV production systems vary in efficiency, cost, and materials used. This study aims to present the performance analysis of a 500 kW capacity mono-crystalline photovoltaic power plant in the Dülük region of Gaziantep. Initially, detailed shading analysis was conducted to assess the suitability of the PV installation. Following shading analysis using PV*SOL Premium software, the performance of three different PV technologies was simulated and modeled. Performance evaluation parameters such as array efficiency, final efficiency, PV efficiency, and performance ratio were used. According to the results, the annual electricity production of mono-crystalline systems is projected to be 462.8 kWh, 436.4 kWh, and 433.64 kWh, with projected system utilization rates of 86%, 83.6%, and 83.1%, respectively. In the final stage of the study, the energy production of mono-crystalline photovoltaic technology, which performs well under different climate conditions in Turkey, was evaluated. The analysis reveals that regions with high solar radiation such as Gaziantep province demonstrate superior performance in PV energy production.

Keywords: Gaziantep, Solar Power Plant (SPP), Energy Efficiency, PV*SOL Premium, Grid-Connected Energy Production.

1. Introduction

Solar energy is the radiant energy released through the fusion process occurring in the Sun's core, wherein hydrogen gas is converted into helium. The Sun, which emits power at approximately 3.9×1026 Watts, represents a clean, inexhaustible renewable energy source. However, only a small fraction of this energy reaches Earth. On the outer surface of the atmosphere, an average of 1,367 watts of power is incident per square meter [1]. This incident radiation is partly absorbed and partly reflected by the atmosphere, with some components consisting of X-rays and ultraviolet rays. In an effort to mitigate the environmental damage caused by fossil fuels, nations have accelerated the transition to renewable energy sources. Consequently, numerous studies related to heat and electricity generation from solar energy are being conducted, and the utilization of solar energy has been increasing over the years. Despite the availability of multiple methods for generating electricity from solar energy, the general trend has focused on photovoltaic systems, which convert sunlight directly into electricity. Research on solar energy utilization has particularly gained momentum since the 1970s, leading to technological advancements and cost reductions in solar energy systems. Solar energy has established itself as a clean energy source environmentally [1]. The importance of solar energy is further highlighted by its status as a clean energy source and its low operational cost after installation. A solar power plant (SPP) is an energy facility that generates electrical energy from sunlight. Solar energy is a clean and sustainable energy source used globally. SPPs convert sunlight into electricity using photovoltaic (PV) panels or thermal energy collection systems.

Turkey is one of the leading countries in terms of solar insolation duration due to its geographic location. Considering that this situation indirectly influences the development of other alternative energies in Turkey, it is believed to provide a significant advantage in the country's efforts towards other renewable energy sources as well [2]. Turkey exhibits rapid development in the field of solar energy, not only due to its available resources but also because it is more environmentally friendly compared to other energy sources. However, there are certain challenges associated with solar energy, including high production costs, low efficiency, and

the lack of precise determination of solar energy parameters in installation areas. Addressing these issues could lead to increased investments in solar energy and indirectly enhance the potential for utilizing solar energy in other forms. Examination of the regional solar energy parameters in Turkey reveals that virtually every location has the potential for direct or indirect utilization of solar energy. Solar energy is commonly applied in methods such as providing hot water and space heating [2]. Additionally, it is used in heating swimming pools and fish farm waters, cooling buildings and agricultural product storage environments, drying agricultural products, and generating electricity. This study organizes and statistically analyzes data related to Turkey's general and regional solar energy parameters. According to the Solar Energy Potential Atlas of Turkey (GEPA) prepared by our Ministry, the average annual total sunshine duration is 2,741 hours, and the average annual total irradiance value is calculated to be 1,527.46 kWh/m² [3]. It is known that the average annual total sunshine duration in Turkey is approximately 2,737 hours, and the average daily sunshine duration is about 7.5 hours. According to other solar energy parameters, the total solar energy received per square meter annually is 1,527 kWh, and the daily solar energy value is 4.2 kWh/m². Additionally, the solar energy atlas suggests that the southern regions between the northeastern and southwestern extremities of the country receive more sunlight compared to other areas further north. As of the end of June 2022, the installed capacity for solar energy-based electricity is 8.479 MW, which constitutes 8.35% of the total installed capacity [3]. The variation in installed capacity over the years and its proportion within the total installed capacity are depicted in the graphs below. It has been determined that Turkey experiences the highest sunshine duration of 1,033 hours during the summer season, while the lowest sunshine duration of 321 hours occurs in the winter season.

2. Material and Method

The objective of the Gaziantep Solar Power Plant is to maximize the potential of solar energy and contribute to renewable energy production. By executing this project, a portion of Gaziantep's energy requirements can be met through solar power. Due to the differences in efficiency, cost, and materials associated with each technology, various photovoltaic (PV) systems are available. The aim of this study is to present a performance analysis of a 500 kW grid-connected

photovoltaic power plant, established using three photovoltaic technologies, monocrystalline, polycrystalline, and thin-film in the Dülük neighborhood of Gaziantep. The study employs the PV*Sol Premium program to conduct land application assessments for the increasingly utilized solar energy plants [4]. his is expected to lead to an increase in the land applications of small-scale solar power plants. When establishing a solar power plant, it is essential to first ascertain the irradiation values and annual sunshine duration of the proposed location. Understanding these parameters is crucial for determining the annual energy production of the plant. In this study, Gaziantep province is selected as the site for the plant. Gaziantep has an annual sunshine duration of 3,011 hours and a radiation value of 1,646 kWh/m²/year. Figure 1 illustrates the city where the solar power plant is installed, Figure 2 shows the annual solar radiation value for the location, and Figure 3 provides the PV*Sol Premium design layouts [5].

Figure Hata! Yalnızca Ana Belge.. *The Neighborhood Where the Solar Power Plant is Installed*

Figure 2. *Annual Solar Radiation Value of the Location*

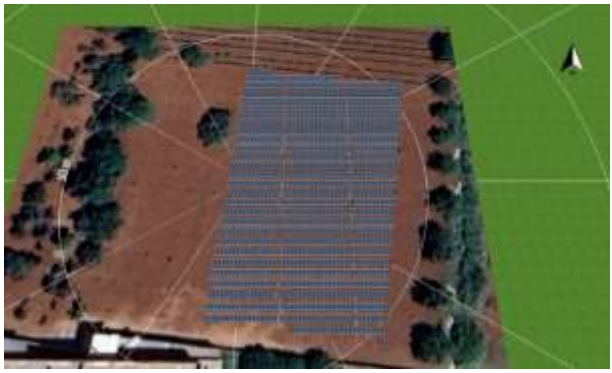

Figure 3. *PV*Sol Premium Solar Power Plant Design*

Accurate data on solar radiation and sunshine duration are essential for effective planning and optimization of solar energy systems. This study provides an overview of the monthly average daily global radiation values and sunshine durations for Gaziantep, using recent data.Global radiation, or solar irradiance, represents the total solar energy received per unit area. The monthly average daily global radiation values for Gaziantep are illustrated in Figure 4. This graph depicts the average daily global radiation values (in kWh/m²) for each month [5]. It shows a peak in solar radiation during the summer months, with July exhibiting the highest average of 7.8 kWh/m² and the lowest recorded in January at 3.4 kWh/m². Sunshine duration measures the total number of hours of direct sunlight per day [5]. The monthly average sunshine durations for Gaziantep are presented in Figure 5. This graph represents the average daily sunshine duration (in hours) for each month. It highlights that the longest sunshine durations occur during the summer months, with July averaging 9.5 hours per day, while January has the shortest average of 4.6 hours per day. The data presented in Figures 4 and 5 indicate that Gaziantep experiences significant solar energy potential, particularly during the summer months. The high global radiation values and extended sunshine durations are beneficial for solar energy production. However, the lower values during the winter months require careful consideration in system design to ensure consistent energy production throughout the year. the monthly average daily global radiation and sunshine duration data are critical for optimizing solar energy systems in Gaziantep. By considering the seasonal variations in these parameters, stakeholders can enhance the efficiency and effectiveness of solar energy projects in the region [6].

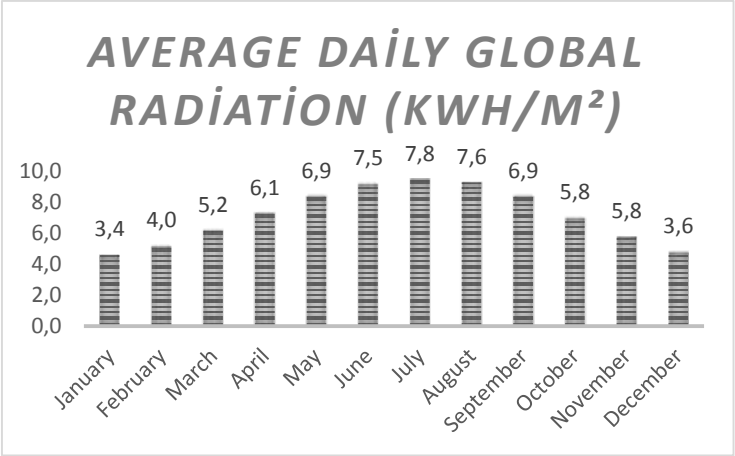

Figure 4. *Average Daily Global Radiation (kWh/m²)*

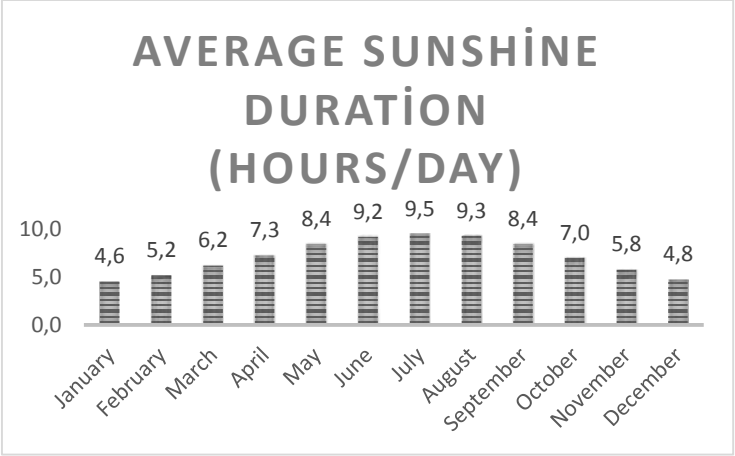

Figure 5. *Average Sunshine Duration (hours/day)*

Solar Power Plant Project: Types of Panels and Inverters Used

This project includes performance parameter analyses of three different panel brands connected to three different inverters. The performance parameters for the panels and inverters are detailed as follows:

1) In the project, I used LG Electronics' LG400Q1C-A6 (v2) Monocrystalline model panel. The inverter used was SMA Solar

Technology AG's Sunny Tripower X 25. A total of 1,157 panels and 11 inverters were installed [7].

2) In the project, I used CW Enerji Müh. Ticaret ve San. Ltd. Şti.'s CWT675-132PM12-V (v1) Monocrystalline model panel. The inverter used was Huawei Technologies' SUN2000 20KTL-M2 (v1). A total of 683 panels and 17 inverters were installed [8].
3) In the project, I used SunPower's SPR-X22-370 (v1) Monocrystalline model panel. The inverter used was Delta Energy Systems' SOLIVIA 8.0 EU T4 TL (v1). A total of 1,172 panels and 44 inverters were installed [9].

Each combination of panels and inverters was evaluated to determine the efficiency, cost-effectiveness, and reliability of the solar energy systems**.**

Each panel type offers distinct advantages depending on the specific requirements of the solar power system. The LG400Q1C-A6 and SPR-X22-370 are well-suited for environments with varying power needs and space constraints, while the CWT675-132PM12-V is designed for high-output applications and higher system voltages. Selecting the appropriate panel based on these specifications will enhance overall system performance and reliability.

Table 1. *Analysis of Panel Specifications Used in Gaziantep SPP Projects*

Panel Type	**LG400Q1C-A6**	**CWT675-132PM12-V**	**SPR-X22-370**
Peak Power (Pmax)	303 Wp	675 Wp	370 Wp
Module Efficiency	22.10%	25.72%	22.70%
Maximum Power Voltage (Vmp)	43.8 V	38.5 V	59.1 V
Maximum Power Current (Imp)	8.62 A	17.54 A	6.26 A

Open Circuit Voltage (Voc)	41.8 V	46.2 V	69.5 V
Short Circuit Current (Isc)	9.13 A	18.56 A	6.66 A
Power Tolerance	0~+3 W	0~+5 W	0~+5 W
Maximum System Voltage	1000 V DC	1500 V DC	1000 V DC
DFire Safety Class	C	C	C
Operating Temperature	-40 ~ +85°C	-40 ~ +85°C	-40 ~ +85°C
Maximum Series Fuse Rating	20 A	30 A	15 A

Table 2. *Analysis of Inverter Specifications Used in Gaziantep SPP Projects*

Inverter Type	**Sunny Tripower X 25 (SMA Solar Technology)**	**SUN2000 20KTL-M2 (Huawei Technologies)**	**SOLIVIA 8.0 EU T4 TL (DELTA)**
Maximum Generator Power	37,500 Wp	30,000 Wp	25,000 Wp
Measured DC Power	25,000 W	22,000 W	20,400 W
Maximum Input Voltage	1,000 V	1,080 V	1,000 V

MPP Voltage Range / Measured Input Voltage	430 V to 800 V	160 V to 950 V	250 V to 1,000 V
Minimum Input Voltage / Start-Up Input Voltage	150 V / 188 V	150 V / 188 V	350 V / 800 V
Maximum Input Current, A Input / B Input	36.2 A / 36.6 A	33.5 A / 44 A	60 A (2 inputs, 30 A/30 A)
Number of Independent MPP Inputs / Number of Strings per MPP Input	2/4	2/4	1/2

Choosing the appropriate inverter depends on the specific requirements of the solar power system, including the scale of the installation, voltage and current requirements, and flexibility in handling multiple panel strings. The Sunny Tripower X 25 is optimal for high-power applications, while the SUN2000 20KTL-M2 offers broad voltage range capabilities. The SOLIVIA 8.0 EU T4 TL is suitable for systems requiring higher input currents and simplified MPP input configurations [10].

Efficiency Analysis of Inverters and Panels Used in Gaziantep SPP Projects

In the project, it has been observed that the losses between the panels and inverters used are quite similar. In terms of efficiency, the most efficient panel and inverter types are as follows. LG400Q1C-A6 panel and Sunny Tripower X 25 inverter, CWT675-132PM12-V panel and SUN2000 20KTL-M2 inverter, and SPR-X22-370 panel and SOLIVIA 8.0 EU T4 TL inverter, with efficiency

percentages of 86.4%, 86.7%, and 87.2%, respectively. The table below provides the efficiency data according to panel and inverter types.

Table 3. *Efficiency Analysis of Inverters and Panels Used in SPP Projects*

Panel Type	**Inverter Type**	**Efficiency (%)**
LG400Q1C-A6	Sunny Tripower X 25	86.43%
CWT675-132PM12-V	SUN2000 20KTL-M2	86.71%
SPR-X22-370	SOLIVIA 8.0 EU T4 TL	87.16%

Table 4. *Depreciation Periods for Projects Designed in Gaziantep Solar Power Plant*

Panel Type	**Inverter Type**	**Depreciation Period (Years)**
LG400Q1C-A6	Sunny Tripower X 25	5,8
CWT675-132PM12-V	SUN2000 20KTL-M2	5,5
SPR-X22-370	SOLIVIA 8.0 EU T4 TL	5,7

The Gaziantep Solar Power Plant contributes significantly to reducing carbon dioxide (CO_2) emissions. By using solar panels and inverters, the plant generates clean energy, thereby avoiding CO_2 emissions that would otherwise be produced by burning fossil fuels. The projects at this solar plant are designed to prevent substantial amounts of CO_2 from entering the atmosphere. For example: LG400Q1C-A6 panels with Sunny Tripower X 25 inverters prevent 317,677 kg of CO_2 per year. CWT675-132PM12-V panels with SUN2000 20KTL-M2 inverters prevent 339,521 kg of CO_2 per year. SPR-X22-370 panels with SOLIVIA 8.0 EU T4 TL inverters prevent 310,504 kg of CO_2 per year. These reductions in CO_2 emissions are crucial for combating climate change and promoting environmental sustainability.

Table 5. *Prevented CO_2 Emissions for Projects Designed in Gaziantep Solar Power Plant*

Panel Type	**Inverter Type**	**Prevented CO_2 Emissions (kg/year)**
LG400Q1C-A6	Sunny Tripower X 25	317,677.00
CWT675-132PM12-V	SUN2000 20KTL-M2	339,521.00
SPR-X22-370	SOLIVIA 8.0 EU T4 TL	310,504.00

3. Conclusions

In the Dülük district of Gaziantep, various grid-connected ground-mounted solar power plant (SPP) designs have been developed using the PV*SOL Premium software. Three different scenarios were created to analyze the impact of

increasing the number of solar panels on the total power delivered to the grid and the corresponding CO_2 emissions avoided. Increasing awareness of solar panels and utilizing this energy source is crucial for reducing the energy costs in Gaziantep. The selection of panel and inverter types significantly influences the efficiency, capacity, and CO_2 emissions avoided in solar power plants. However, the most critical factor in this project is the total cost calculation of the chosen panel and inverter types. The site assessment results indicate that there are no obstacles to further developing the study. The research utilized mono-crystalline panel technology. This study focused solely on the comparison of simulation data. The most accurate results would be obtained by comparing the average production data over several years with the simulation data. Furthermore, additional research could be conducted to validate the increase in output energy by incorporating solar tracking systems, such as dual-axis tracking. Utilizing domestic resources for the installation of PV panels will reduce the country's increasing dependence on energy imports, contribute to energy security in Gaziantep, and significantly decrease the carbon footprint of the Organized Industrial Zone.

References

[1] TAKTAK, Fatih; ILI, Mehmet. Güneş enerji santrali (GES) geliştirme: Uşak örneği. Geomatik, 2018, 3.1: 1-21.

[2] GUNELI, Sadi Serdar; ARSERIM, Muhammet Ali; KENANOĞLU, Rıdvan. Dicle Üniversitesi Güneş Enerji Santralinin Şebeke İle Paralel Çalışmasında Olası Adalaşma Probleminin Matlab Simülasyon Ortamında Değerlendirilmesi. Dicle Üniversitesi Mühendislik Fakültesi Mühendislik Dergisi, 2019, 10.3: 863-877.

[3] DEMIR, Mucip. Kars İlinde Güneş Enerjisi Santrali Kurulum Potansiyeli Taşıyan Alanların, CBS Analizleri ve AHP Yöntemi Kullanılarak Belirlenmesi. Coğrafya Dergisi, 2023, 46: 93-109.

[4] ÖZTÜRK, Cemal. Güneş enerji sistemlerinde verim analizi ve enerji kayıplarının tespiti. 2020. Master's Thesis. Hasan Kalyoncu Üniversitesi.

[5] YAĞLI, Hüseyin; KOÇ, Yıldız. Gaziantep Bölgesi İçin Güneş Enerjisinden Elektrik Üretiminde Kurulacak Panellerin Optimum Eğim Açılarının Belirlenmesi. Avrupa Bilim ve Teknoloji Dergisi, 2020, 19: 475-483.

[6] AKGÜL, Batur Alp; CİNKİLİC, Mustafa Ersan; YEĞİNGİL, İlhami. GAZİANTEP BÖLGESİNDEKİ BİR EVİN ELEKTRİK ENERJİSİ İHTİYACINI KARŞILAYACAK ŞEBEKE DIŞI FOTOVOLTAİK SİSTEM TASARIMI VE MODELLENMESİ İLE TEKNİK ANALİZ VE TEMEL SİMÜLASYON YAPILMASI.

[7] OLGUN, Muhammed Süleyman; CENGIZ, Ebuzer; EVIN, Rifat. Güneş Enerjisi ile Aydınlanan Bir Yaşam: Siirt'te 15 Kw'lik Bağ Evi Fotovoltaik Sistemi. Hendese Teknik Bilimler ve Mühendislik Dergisi, 2024, 1.1: 19-27.

[8] ALAHMAD, Hamza; TAŞKESEN, Edip; BILEN, Elif Nur. Şırnak üniversitesi yerleşkesinde bulunan mühendislik fakültesi bina çatılarının örnek şebekeye bağlı (on-grid) bir fotovoltaik sistem tasarımı. In: International Conference on Scientific and Innovative Study.

[9] KUMRUOĞLU, Levent Cenk; ATEŞ, Salih Berkan. Türkiye'nin güneş enerjisi potansiyeli ve İskenderun için örnek üretim projeksiyonu. Çukurova Üniversitesi Mühendislik Fakültesi Dergisi, 2022, 37.1: 293-305.

[10] HENGİRMEN TERCAN, Şafak. Sürdürülebilir Ulaşım İçin Güneş Enerjili Teknelerin Kullanılması ve Çevresel Etkileri. Firat University Journal of Engineering Science, 2021, 33.1.

Design of grid-connected solar power plant with pv*sol premium in turkey

Ozan Hüseyin Kör*, İpek Atik

gaziantep islam bilim ve teknoloji üniversitesimühendislik ve doğa bilimleri fakültesi elektrik - elektronik mühendisliği bölümügaziantep-turkey

ozankor27@gmail.com

Abstract

Thanks to the high solar energy potential in our country and the advancing and developing photovoltaic (PV) technologies, solar energy is becoming the most attractive renewable energy source. There are various PV producing systems due to the differences in efficiency, price, and materials used by each technology. The aim of this study is to present the performance analysis of a 500 kW grid-connected photovoltaic plant established with monocrystalline photovoltaic technology in the Bodrum district of Muğla. Initially, a detailed shading study is conducted to examine the suitability of the area for PV installation. The shading study is carried out using the PVSOL Premium program, and then PVSOL Premium programs are used to simulate, model, and predict the performance of three PV technologies. The parameters used for performance evaluation are array yield, final yield, PV efficiency, and performance ratio. According to the results obtained, it is predicted that monocrystalline systems will generate 485.33 kWh, 420.53 kWh, and 417.6 kWh of electricity annually, and their system utilization rates will be 85.5%, 87.2%, and 88.6%, respectively. In the final stage of the study, the system is evaluated under different climatic conditions in Turkey using the high-performing monocrystalline photovoltaic technology with annual energy production. The analyses show that Muğla province, with its high solar radiation values, demonstrates superior performance in PV energy production. This research aims to analyze the process of incorporating this resource into Turkey's energy portfolio, which has strong potential for solar energy, and to evaluate solar energy applications in Muğla province as a local example.

Keywords: Photovoltaic system, grid-connected, energy production, solar power plan, photovoltaic panel, PV*SOL Premium, grid-connected energy production ,

1. Introduction

Solar energy is the radiant energy released through the fusion process in the core of the Sun, where hydrogen gas is converted into helium. The Sun, emitting approximately $3.9x10^{26}$ W of power, is a clean, inexhaustible source of renewable energy. Only a small fraction of this energy reaches Earth. On average, each square meter of the outer surface of the Earth's atmosphere receives about 1,367 W of power. Some of this radiation, primarily composed of X-rays and ultraviolet rays, is absorbed or reflected by the atmosphere. In an effort to avoid the environmental harm caused by fossil fuels, countries have accelerated the transition to renewable energy sources. As a result, research into generating heat and electricity from solar energy has increased, and its usage continues to grow over the years. Although there are several methods to generate electricity from solar energy, the primary focus has been on photovoltaic (PV) systems, which convert sunlight directly into electricity. Interest in solar energy utilization has particularly accelerated since the 1970s.

Technological advancements in solar energy systems have reduced costs and established solar energy as an environmentally clean energy source. The fact that solar energy is clean and operates with low costs after installation has further emphasized its importance.

A solar power plant (SPP) is a facility that generates electrical energy from sunlight. Solar energy, as a clean and sustainable energy source, is utilized worldwide. SPPs convert sunlight into electricity through photovoltaic (PV) panels or thermal energy collection systems.

Turkey is geographically located in the Northern Hemisphere, between latitudes 36-42° North and longitudes 26-45° East. Due to its advantageous geographic position, Turkey’s solar energy potential is significantly higher compared to many other countries. Despite being located within the solar belt, the production and utilization of solar energy in Turkey is far below the expected levels. Therefore, in the near future, it is crucial to implement solar energy as a significant and sustainable solution within the broader context of renewable energy sources to meet the country's energy demands.

Turkey is advancing rapidly in solar energy development, both due to its favorable solar energy potential and its environmental advantages compared to other energy sources. However, there are some challenges, such as high production costs, low efficiency, and the lack of precise solar energy parameter data for the areas where solar power plants are planned. Addressing these issues will lead to increased investment in solar energy and indirectly enhance other potential uses of solar power.

When examining the regional solar energy parameters of Turkey, it becomes clear that nearly every part of the country can benefit from solar energy either directly or indirectly. Solar energy is typically used for domestic hot water supply and space heating. In addition, it is employed in heating swimming pools and fish farm waters, cooling buildings and agricultural storage facilities, drying agricultural products, and generating electricity. This study statistically analyzes the general and regional solar energy parameters of Turkey by organizing relevant data.

Due to its geographical location, Turkey has significant solar energy potential. According to the Solar Energy Potential Atlas of Turkey (GEPA)e, prepared by the Ministry, the average annual total sunshine duration is 2,741 hours, and the average annual total radiation value has been calculated as 1,527.46 kWh/m². (TAKTAK & ILI)

2. Material and Method

The aim of the Muğla Solar Power Plant is to maximize the potential of solar energy and contribute to renewable energy production. With the implementation of this project, a portion of Muğla's energy needs can be met through solar energy. Due to the differences each technology brings in terms of efficiency, cost, and materials used, various photovoltaic (PV) systems are available. This study aims to present a performance analysis of a 500 kW grid-connected photovoltaic plant, established in Dalaman, Muğla, using three PV technologies: monocrystalline, polycrystalline, and thin-film.

In this study, the increasing use of solar power plants in land applications is explored through the PV*Sol Premium software. As a result, the expansion of land applications for small-scale solar power plants is expected. When setting up a solar power plant, it is essential first to determine the irradiation values and annual sunshine durations of the location. Knowing the sunshine duration and radiation values is crucial for estimating the plant’s annual energy production. For this study, Muğla was selected as the plant’s location. Muğla's annual sunshine duration is 3,043 hours/year, with radiation values of 1,621 kWh/m²-year.

Figure 1 shows the city where the solar power plant is located, Figure 2 presents the annual solar radiation value of the location, Figure 3 illustrates the location of the solar power plant. [2]

Figure 3: The City Where the Solar Power Plant is Established

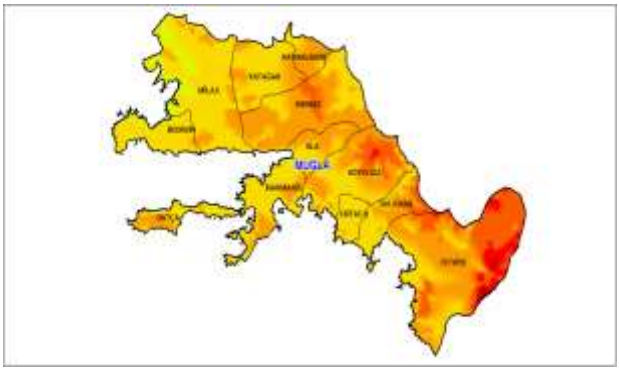

Figure 4: Annual Solar Radiation Value of the Location

Figure 5: Location of the Solar Power Plant

Muğla Province Solar Energy Potential Atlas (GEPA) Data:

The Solar Energy Potential Atlas (GEPA) provides a comprehensive overview of Muğla's solar energy capabilities. Key metrics for Muğla include:

- **Annual Total Sunshine Duration:** 3,043 hours/year
- **Annual Total Radiation Value:** 1,621 kWh/m²-year
- **Average Daily Radiation (Global):** Ranges from 2.22 kWh/m² in December to 7.58 kWh/m² in July
- **Best Months for Solar Energy Utilization:** May to August, with daily radiation values exceeding 6 kWh/m²
- **Geographic Location Benefits:** Muğla's position in the solar belt provides optimal conditions for solar power generation.

These data highlight Muğla's high potential for solar energy, positioning it as an ideal location for solar power plant installations. The annual sunshine duration and radiation values indicate that solar energy can be harnessed effectively throughout the year. [3]

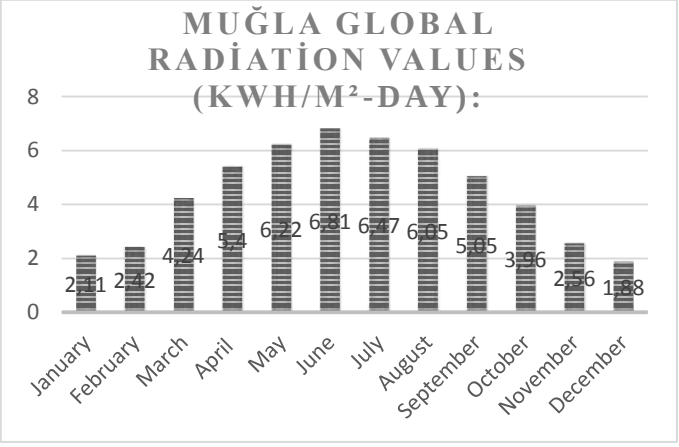

These values represent the average daily global solar radiation throughout the year in Muğla, showing a high potential for solar energy production, particularly in the summer months.

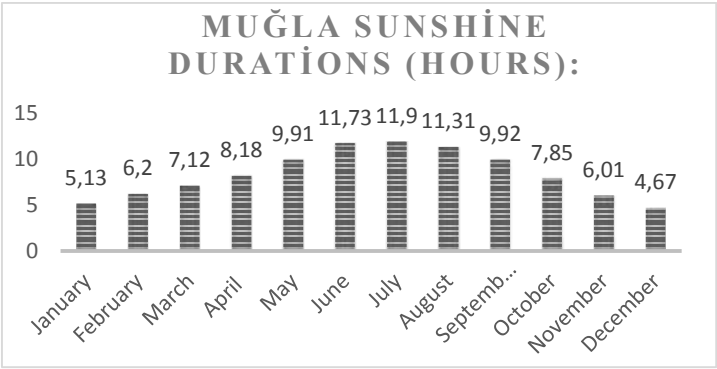

These values reflect the average monthly sunshine duration in Muğla, with the highest durations observed during the summer months, particularly in June and July. This makes Muğla a favorable region for solar energy utilization, as the extended sunshine durations allow for efficient solar power generation. [4]

Types of Panels and Inverters Used in the Solar Power Plant Project

This project includes performance parameter analyses of two different panel brands connected to three different inverters.

1. In the project, I used **SunPower's SPR-P5-530-UPP** model panel. The inverter used was **Delta Energy Systems' SOLIVIA 8.0 EU T4 TL** model. A total of **801 panels** and **45 inverters** were used.
2. In the project, I used **LG Electronics Inc.'s LG400Q1C-A6** model (monocrystalline) panel. The inverter used was **Huawei Technologies' SUN2000 20KTL-M2** model. A total of **1,044 panels** and **18 inverters** were used.
3. In the project, I used **CW Enerji Müh. Ticaret ve San. Ltd. Şti.'s CWT675-132PM12-V** model (monocrystalline) panel. The inverter used was **SMA Solar Technology AG's Sunny Tripower X 25** model. A total of **719 panels** and **17 inverters** were used.

Each combination of panels and inverters was evaluated to analyze performance parameters, considering factors such as efficiency, cost, and operational reliability. [5]

Specifications of Panels Used in Muğla GES Projects

The following table outlines the technical specifications of the solar panels used in the Muğla GES (Solar Power Plant) projects:

Panel Type	LG400Q1C-A6	CWT675-132PM12-V	SPR-P5-530-UPP
Peak Power (Pmax)	303 Wp	675 Wp	530 Wp
Module Efficiency	22.10%	25.72%	20.40%
Maximum Power Voltage (Vmp)	43.8 V	38.5 V	38.6 V
Maximum Power Current (Imp)	8.62 A	17.54 A	13.73 A
Open Circuit Voltage (Voc)	41.8 V	46.2 V	47.1 V
Short Circuit Current (Isc)	9.13 A	18.56 A	14.78 A
Power Tolerance	0 ~ +3 W	0 ~ +5 W	0 ~ +5 W
Maximum System Voltage	1000 V DC	1500 V DC	1500 V DC
Fire Safety Class	C	C	C
Operating Temperature	-40 ~ +85°C	-40 ~ +85°C	-40 ~ +85°C
Maximum Series Fuse Rating	20 A	30 A	25 A

These panels exhibit different power capacities and efficiencies, making them suitable for diverse

applications within the Muğla GES projects. The choice of panel influences the system's overall efficiency, energy output, and long-term performance

Specifications of Inverters Used in Muğla GES Projects

The following table outlines the key specifications of the inverters used in the Muğla Solar Power Plant (GES) projects:

Inverter Type	Sunny Tripower X 25	SUN2000 20KTL-M2	SOLIVIA 8.0 EU T4 TL
Max Generator Power	37,500 WP	30,000 WP	25,000 WP
Measured DC Power	25,000 W	22,000 W	20,400 W
Max Input Voltage	1,000 V	1,080 V	1,000 V
MPP Voltage Range / Measured Input Voltage	430 V to 800 V	160 V to 950 V	250 V to 1,000 V
Min Input Voltage / Start Input Voltage	150 V / 188 V	150 V / 188 V	350 V / 800 V
Max Input Current (A Input / B Input)	36.2 A / 36.6 A	33.5 A / 44 A	60 A (2 Inputs 30 A/30 A)
Number of Independent MPP Inputs / Strings Per MPP Input	2/4	2/4	1/2

This table highlights important details such as maximum power, voltage ranges, and current capacities of the inverters used in Muğla GES projects, demonstrating their suitability for different photovoltaic systems. [6]

Efficiency Analysis of Panels and Inverters Used in MUĞLA Solar Power Plant Projects

In this project, the observed losses among the panels and inverters were found to be very close to each other. In terms of efficiency, the most efficient panel and inverter combinations were observed as follows:

SPR-P5-530-UPP panel and SOLIVIA 8.0 EU T4 TL inverter,

LG400Q1C-A6 panel and SUN2000 20KTL-M2 inverter,

CWT675-132PM12-V panel and Sunny Tripower X 25 inverter.

The efficiency percentages were recorded as:

88.6% for the SPR-P5-530-UPP and SOLIVIA 8.0 EU T4 TL combination,

87.2% for the LG400Q1C-A6 and SUN2000 20KTL-M2 combination,

85.5% for the CWT675-132PM12-V and Sunny Tripower X 25 combination.

Cost Analysis of Panels Used in MUĞLA Solar Power Plant Projects

SPR-P5-530-UPP panels: The unit price is ₺12,100.00 with a total of 801 units used. The total cost amounts to ₺9,692,100.00.

LG400Q1C-A6 panels: The unit price is ₺9,500.00 with a total of 1,044 units used. The total cost amounts to ₺9,918,000.00.

CWT675-132PM12-V panels: The unit price is ₺6,500.00 with a total of 719 units used. The total cost amounts to ₺4,673,500.00.

This table presents the cost analysis of the panels used in the Gaziantep solar power plant projects. The total cost for each panel type is calculated based on the number of units used and their respective unit prices. The LG400Q1C-A6 panels have the highest total cost due to the larger quantity used, whereas the CWT675-132PM12-V panels offer the lowest total cost.

Cost Analysis of Inverters Used in MUĞLA Solar Power Plant Projects

Sunny Tripower X 25: The unit price is ₺90,000.00 with a total of 17 units used. The total cost amounts to ₺1,530,000.00.

SUN2000 20KTL-M2: The unit price is ₺85,000.00 with a total of 18 units used. The total cost amounts to ₺1,530,000.00.

SOLIVIA 8.0 EU T4 TL: The unit price is ₺56,000.00 with a total of 45 units used. The total cost amounts to ₺2,520,000.00.

Most Expensive Inverter: SOLIVIA 8.0 EU T4 TL with a total cost of ₺2,520,000.00.

Least Expensive Inverter: SUNNY Tripower X 25 and SUN2000 20KTL-M2 both with a total cost of ₺1,530,000.00 each.

The SOLIVIA 8.0 EU T4 TL inverter, while having the lowest unit price, results in the highest total cost due to the largest quantity used. The SUNNY Tripower X 25 and SUN2000 20KTL-M2 inverters have the same total cost despite differing unit prices, due to the different number of units required. [7]

Depreciation Periods for Designed Projects in MUĞLA Solar Power Plant

SPR-P5-530-UPP Panel with SOLIVIA 8.0 EU T4 TL Inverter: 8.7 years

LG400Q1C-A6 Panel with SUN2000 20KTL-M2 Inverter: 8.7 years

CWT675-132PM12-V Panel with Sunny Tripower X 25 Inverter: 8.2 years

Longest Depreciation Period: 8.7 years, applicable to both the SPR-P5-530-UPP panel with the SOLIVIA 8.0 EU T4 TL inverter and the LG400Q1C-A6 panel with the SUN2000 20KTL-M2 inverter.

Shortest Depreciation Period: 8.2 years, applicable to the CWT675-132PM12-V panel with the Sunny Tripower X 25 inverter.

The depreciation period indicates how long it takes for the investment in the solar power components to be recovered through the energy savings or revenue generated.

Prevented CO2 Emissions for Projects in MUĞLA Solar Power Plant

SPR-P5-530-UPP Panel with SOLIVIA 8.0 EU T4 TL Inverter: 301,904 kg/year

LG400Q1C-A6 Panel with SUN2000 20KTL-M2 Inverter: 299,562 kg/year

CWT675-132PM12-V Panel with Sunny Tripower X 25 Inverter: 335,638 kg/year

Highest Prevented CO2 Emission: 335,638 kg/year with the CWT675-132PM12-V panel and Sunny Tripower X 25 inverter.

Lowest Prevented CO2 Emission: 299,562 kg/year with the LG400Q1C-A6 panel and SUN2000 20KTL-M2 inverter.

The prevented CO2 emissions reflect the amount of carbon dioxide emissions that would be avoided by using solar energy instead of conventional energy sources.

3. Conclusions

This study examines the ground-mounted Solar Power System (GES) designs in Dalaman, Muğla, utilizing the Pv*sol Premium program. It explores three different scenarios with varying power capacities and investigates their effects on the total power delivered to the grid and the reduction of CO2 emissions. The research highlights the potential of using solar panels to lower energy costs and increase awareness of energy sources.

The selected panel and inverter types significantly impact the efficiency, capacity, and CO2 emission reduction potential of the GES. However, the study underscores that the most critical decision-making factor is the total cost of the panels and inverters. Therefore, cost-effectiveness has been a primary focus during the design process.

According to the field assessment results, there are no significant obstacles to further development of the project. Nonetheless, it is recommended to compare production data over several years with simulation data to obtain more accurate results. Additionally, further research is necessary to validate whether the integration of technologies such as solar tracking systems can enhance energy output.

Lastly, using local resources for the installation of PV panels will reduce dependence on energy imports, contribute to energy security, and significantly lower Dalaman's carbon footprint. Consequently, the implementation of Solar Power Systems (GES) is viewed as a crucial step toward achieving sustainable energy goals.

References

[11] TAKTAK, Fatih; ILI, Mehmet. Güneş enerji santrali (GES) geliştirme: Uşak örneği. Geomatik, 2018, 3.1: 1-21.

[12] KAYNAR, Nihal Kan. Yenilenebilir enerji kaynaklarından güneş enerjisinin Amasya ilindeki potansiyeli. *Bilge International Journal of Science and Technology Research*, 2020, 4.2: 48-54.

[13] ELDEM, M. Güneş Enerjisi. *TMMOB EMO Ankara Şubesi Haber Bülteni*, 2017, 5: 7-10.

[14] KIRBAŞ, İbrahim; ÇIFCI, Ahmet; İŞYARLAR, Barış. Burdur ili güneşlenme oranı ve güneş enerjisi potansiyeli. *Mehmet Akif Ersoy Üniversitesi Fen Bilimleri Enstitüsü Dergisi*, 2013, 4.2: 20-23.

[15] ALTINKÖK, Sevgi; KARADENIZ, Serdar; ALTINKÖK, Atılgan. Photovoltaic system design and analysis at faculty scale. Journal of Naval Sciences and Engineering, 2022, 18.1: 91-120.

[16] SARI, Vekil; ÖZYIĞIT, Fatih Yavuz. Sivas Cumhuriyet Üniversitesi yerleşkesinde güneş enerjisi santralinin ekonomik analizi. *Dokuz Eylül Üniversitesi Mühendislik Fakültesi Fen ve Mühendislik Dergisi*, 2020, 22.65: 517-526.

[17] SARI, Vekil; ÖZYIĞIT, Fatih Yavuz. Sivas ilinin farklı ilçelerinde şebeke bağlantılı güneş enerji santrallerinin tasarımı ve analizi. Avrupa Bilim ve Teknoloji Dergisi, 2020, 20: 425-437.

Yenilenebilir Enerji Sistemleri için PVsol Programı ile GES Santral Enerji Üretimi Analizi ve Karşılaştırmalı Tasarım

Mehmet KORKMAZ[1], İpek ATİK[2]

[1,2] *Gaziantep İslam Bilim ve Teknoloji Üniversitesi, Elektrik-Elektronik Mühendisliği Bölümü GAZİANTEP,27000, TÜRKİYE*
korkmazmehmet92@gmail.com

Özet

Türkiye'de şebekeye bağlı güneş enerjisi santralleri yaygınlaşarak enerji ihtiyacının önemli bir kısmını karşılamaktadır. Bu alanda en yüksek kurulu güce sahip şehir Konya'dır, 1722,2 MW ile öne çıkmaktadır. Onu sırasıyla 520,5 MW kapasiteyle Ankara, 435,1 MW ile Gaziantep, 414 MW ile Şanlıurfa, 392,4 MW ile Kayseri ve 338,8 MW ile İzmir izlemektedir. Bu çalışmanın amacı, PVsol programı kullanarak çatı üstü fotovoltaik güneş enerjisi santrallerini modellemek, simüle etmek ve bölge için analiz etmektir. PVsol, güneş enerjisi sistemlerinin verimliliğini artırmak için tasarım, optimizasyon ve analiz yapma imkanı sağlar. Program, çeşitli PV sistemlerini çatı üstü kurulumlardan büyük güneş tarlalarına kadar simüle etmek ve performanslarını değerlendirmek için kullanılmaktadır. PVsol, gerçekçi hava durumu verilerini kullanarak güneş ışığı yoğunluğu, hava sıcaklığı, rüzgar hızı ve yönü ile gölgelenme etkisini içeren faktörleri dikkate almaktadır. Proje kapsamında, Gaziantep ili İslahiye ilçesinde bulunan bir depo binası seçilmiştir. Çatı tipi PV güneş enerjisi santrali uygulaması yapılmış ve farklı panel tipleri ile yerleşim planı değişikliklerinin tesise etkileri incelenmiştir. Bir PV modülü genellikle 1000 W/m² altında ve 25°C'de değerlendirilir. Ancak güneş santrallerinde çalışırken, modüller tipik olarak daha yüksek sıcaklıklarda ve biraz daha düşük yalıtım koşullarında çalışırlar. PV modüllerinin beklenen çalışma sıcaklığını belirlemek, güneş hücresi güç çıkışını değerlendirmek için önemlidir. Bu nedenle, PV modüllerinin montajlandığı yapıların yüksekliği ve açısı PVsol ile analiz edilmiş ve sıcaklık etkisi detaylı olarak incelenmiştir.

Anahtar Kelimeler : *Güneş enerjisi santralleri, PVsol, Fotovoltaik sistemler, Çatı üstü güneş enerjisi, Enerji verimliliği*

GİRİŞ

PVSOL Programında Analiz İçin Konu Başlıkları

Proje Oluşturma: Analiz yapmak istediğiniz güneş enerjisi sistemini oluşturmanız gerekir. Bu yerel iklim koşulları, arazi topografyası, sistem bileşenleri ve bağlantı şeması gibi parametreleri içerir.

Sistem Tasarımı: PVSOL, kullanıcıların güneş paneli yerleşimi, eğim açıları, panel sayısı, inverter seçimi ve diğer sistem bileşenleri gibi tasarım parametrelerini belirlemelerine olanak tanımaktadır.

Simülasyon Ayarları: Analiz için gerekli olan simülasyon ayarlarını yapılandırarak , güneş ışığı yoğunluğu, hava sıcaklığı, gölgeleme etkileri ve diğer hava koşulları değişkenlerini içerir.

Analiz Çalıştırma: Oluşturulan sistem üzerinde analizi başlatarak PVSOL ile güneş paneli sistemlerinin elektrik üretimini ve performansını simüle ederiz. Bu, günlük, aylık veya yıllık enerji üretimi gibi çeşitli çıktıları içerebilir.

Sonuçları Değerlendirme: Analiz sonuçlarını inceleyip ve sistem performansını değerlendiririz. Bu, enerji verimliliği, finansal getiri, karbon ayak izi ve diğer kriterlerle ilgili olabilmektedir. Program bu çıktıları farklı konu başlıklarında sunmaktadır (Kazanç-Finansal analiz gibi) .

Optimizasyon ve İyileştirme: Analiz sonuçlarına dayanarak sistemi optimize etmek kullanacağınız panel gücü ve tipine karar verdikten sonra daha kolaydır. Bu, daha iyi performans, daha yüksek verimlilik veya daha düşük maliyetler gibi hedeflere yönelik çalışmanıza olanak sağlamaktadır.

Bölge Seçimi ve Koşullar

Güneş Işığı Potansiyeli: GES' nin verimli olabilmesi için bol miktarda güneş ışığına ihtiyaç vardır. Bu nedenle, Güneşin yoğun olduğu bölgeler, GES için en uygun olanlarıdır.

Arazi Durumu: GES için büyük bir alan gerekir. Toprak sahipleriyle anlaşma yapmak ve büyük bir arazi kiralamak veya satın almak gerekebilir. Bu nedenle, arazi uygunluğu ve erişilebilirliği önemlidir. Çatı GES tesisi uygulamaları şirketlerin ve kurumların inisiyatifi doğrultusunda yapılmaktadır.

İklim Koşulları: Yüksek sıcaklıklar ve düşük nem, GES' lerin performansını artırabilir. Sıcaklık faktörü sistemde kullanılan komponentler üzerinde olumsuz etki yapabilir , verimli sistemler için kabloların direk güneş ışığına maruz kalmaması ve panellerin havalandırılabilir yapılara montaj edilmesi gereklidir. Yoğun rüzgarlı alanlar ise panel temizliği açısından zorluklar çıkarabilir. İklim değişikliği senaryolarının da incelenmesi yatırımcı açısından önemlidir , amortisman süresi ve verimi doğrudan etkileyen faktörlerdir.

Altyapı ve Ulaşım: GES' nin inşası ve işletilmesi için altyapıya erişim önemlidir. Elektrik hatlarına yakınlık, ulaşım kolaylığı gibi faktörler dikkate alınmalıdır. Çatı GES ‘ ler hali hazırdaki mevcut alt ve üst yapıları kullandığı için bu konuda çok avantajlıdır.

Yasal ve Düzenleyici Faktörler: Her bölgenin güneş enerjisi projelerine yönelik farklı düzenlemeleri ve izin süreçleri olabilir. Bu faktörler de bölge seçimini etkileyebilir. Yenilenebilir enerji teşvikleri bölgesel veya zamana bağlı değişiklikler gösterebilir. Güncel mevzuat takip edilmelidir.

Toplumsal Kabul: GES' nin kurulacağı bölgedeki toplumun desteği veya direnci de önemlidir. Çevresel etkiler, yerel ekonomiye katkı ve istihdam gibi konular bölge halkının tutumunu etkileyebilir. Bu konunun içinde tesis güvenliği ve enerji arz güvenliği de değerlendirilmelidir.

Doğal Koruma Alanları ve Ekolojik Hassasiyetler: GES' nin çevresel etkileri değerlendirilmelidir. Doğal yaşam alanlarına, tarım arazilerine ve biyolojik çeşitliliğe etkisinin olmaması önemlidir. Verim değerlerini kaybetmiş ya da hasarlı PV panellerin geri dönüşüm ile geri kazanımı ya da bertaraf edilmesi kısmı da proje büyüklüğüne göre araştırılması ve değerlendirilmesi gereken diğer bir hususdur.

Projede çatı GES projesi Figür 6 ‘ da görülen mevcut yapının çatısı üzerinde modellenmiştir . Güneş enerjisi santrali sistemi analizinde panel tipi , yapının yönü ve panel sehpası montajı farklılıkları sonuçları incelenmiştir.

İklim projeksiyonları yapmak için kullanılan birçok uygulama ve sistem bulunmaktadır. PVSOL programı temelinde 1991-2010 yılları arasında yıllık verileri Figür 1 ‘ de görüldüğü üzere Google Earth üzerinden seçtiğiniz koordinatlar ile MeteoSyn aracı vasıtasıyla çıkarmaktadır . İlave olarak iklim parametre değişikliği yapılabilmektedir. Bu parametrelerin iklim değişikliğine göre tekrar revize edilmesi daha kesin sonuçlar almamızı sağlayacaktır .

İlave olarak Enerji ve Tabii Kaynaklar Bakanlığı ile Enerji İşleri Müdürlüğüne ait olan herkesin ulaşabildiği Figür 2 ‘ de görülen Güneş Enerjisi Potansiyel Atlası bulunmaktadır . İslahiye güneş enerjisi potansiyeli atlasından faydalanarak verimlilik ve güneşlenme sürelerinin analiz sonuçları PVSOL ile ay bazlı kıyaslanmıştır .

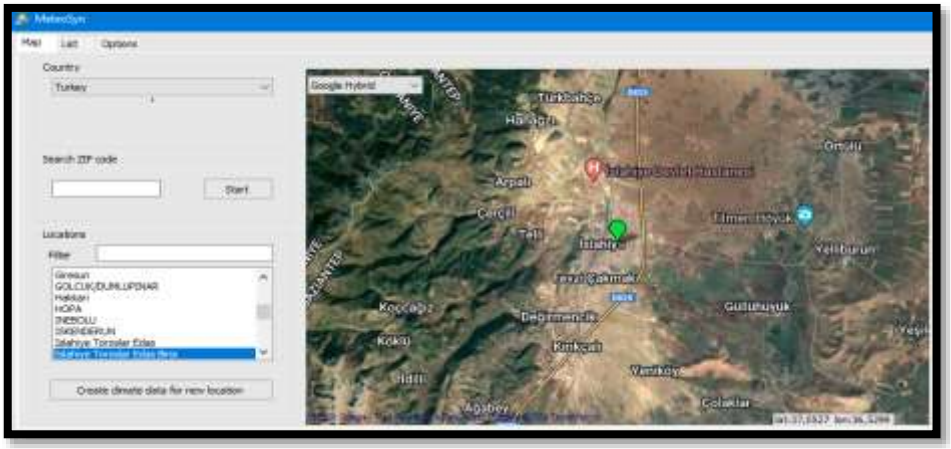

***Figür** Hata! Yalnızca Ana Belge.. Google Earth üzerinden seçilen proje uygulama bölgesinin PVSOL ekran görüntüsü*

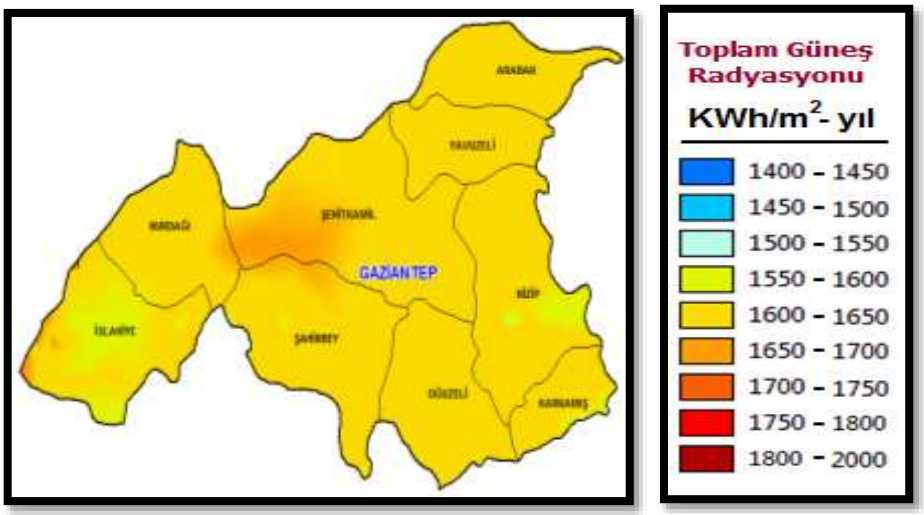

***Figür** Hata! Yalnızca Ana Belge.. Gaziantep Bölgesi GEPA Haritası*

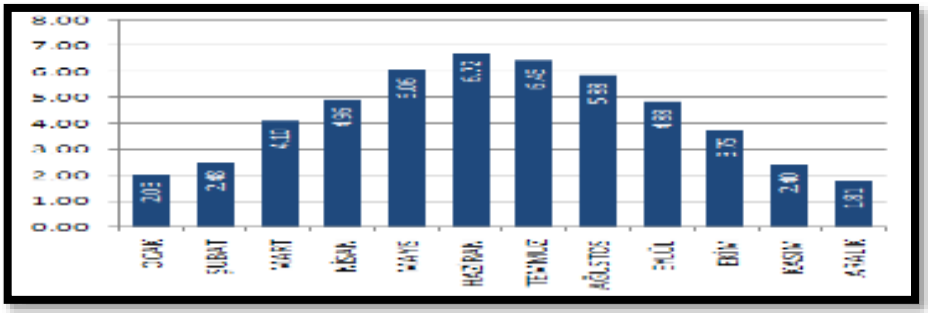

***Figür** Hata! Yalnızca Ana Belge.. GEPA İslahiye Global Radyasyon Değerleri (KWh/m2-gün)*

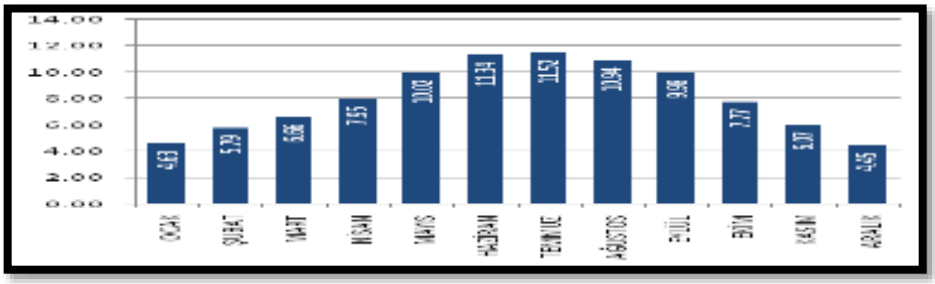

***Figür** Hata! Yalnızca Ana Belge.. GEPA İslahiye Güneşlenme Süreleri (saat)*

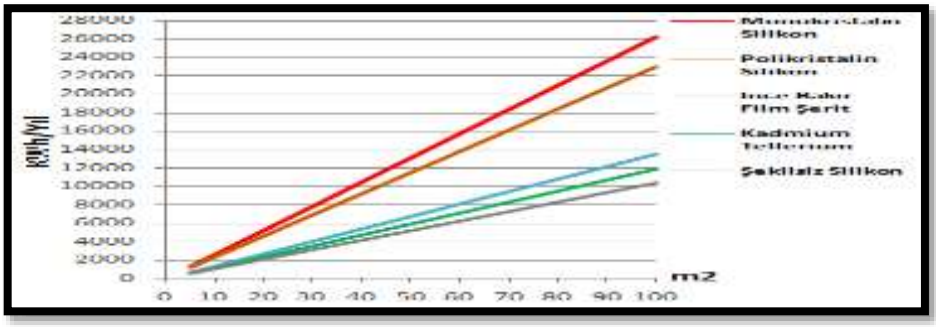

***Figür** Hata! Yalnızca Ana Belge.. GEPA İslahiye PV Tipi-Alan-Üretilebilecek Enerji (KWh-Yıl)*

Figür *Hata! Yalnızca Ana Belge.. Çatı GES ' in Uygulandığı Mevcut Yapı*

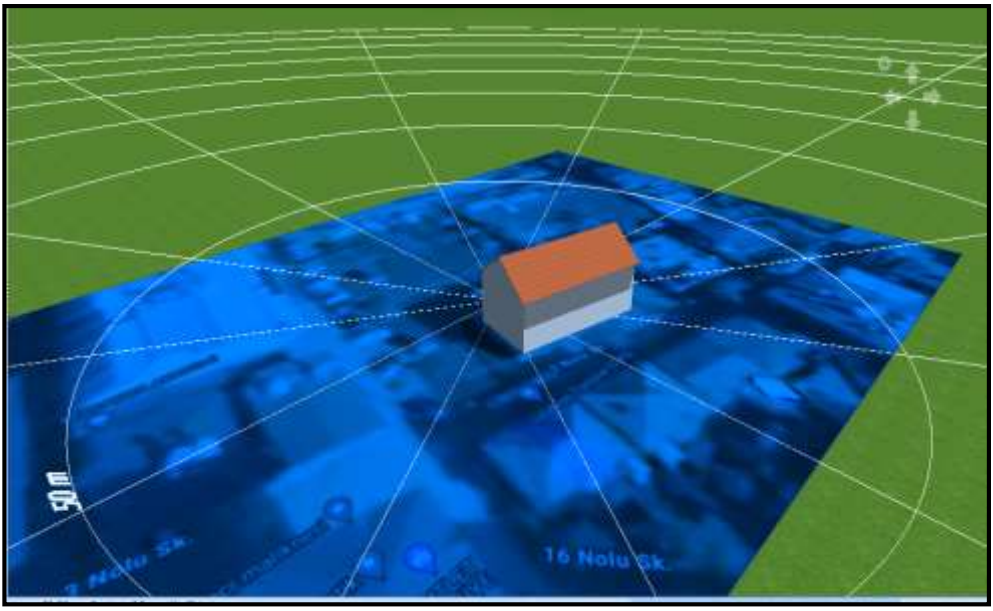

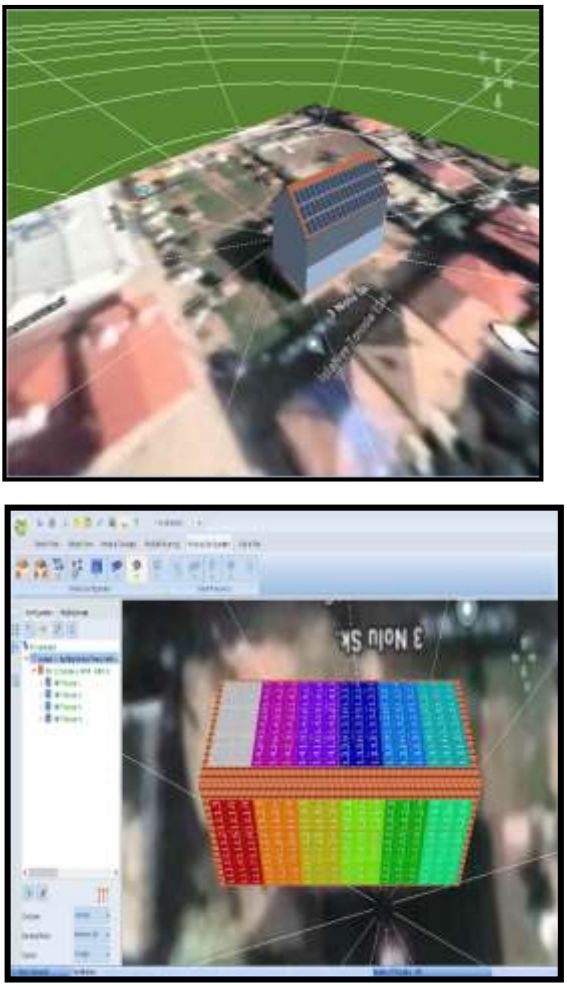

***Figür** Hata! Yalnızca Ana Belge.. PVSOL ile mevcut yapının modellenmesi , örnek panel yerleşimi ve örnek MPPT-String Grupları*

Sonuç

Konu	Açıklama	200W Mono Kristal / Kuzey 11°	200W Mono Kristal / Doğu 92°	200W Poli Kristal / Kuzey 11°
PV sistemi	PV jeneratör çıkışı (kW)	21,6	21,6	21,6
	PV jeneratör yüzeyi m2	175,3	175,3	181,1
	Sayı PV modülleri	108	108	108
	Evirici Sayısı	1	1	1
Kazanç	PV jeneratör enerjisi (AC şebekesi) (kW/h)	20,08	21,122	20,487
	Şebeke beslemesi (kW/h)	20,08	21,122	20,487
	Besleme noktasındaki düzenleme	0	0	0
	Kişisel Güç Tüketimi	0	0	0
	Güneş Enerjisi Oranı	0	0	0
	Yıllık Özgül Kazanç (kWh/kWp)	926,6	977,85	948,48
	Sistem kullanım oranı (PR) (%)	58,4	59,3	59,5
	Gölgelemeden dolayı oluşan kazanç kaybı (%/yıl)	0	0	0
	Önlenen CO_2 emisyonu (kg/yıl)	9,437	9,927	9,629
Finansal Analiz	Toplam yatırım maliyeti (TL)	32400	32400	32400
	Varlıkların Getirisi (%)	2,04	2,55	2,24
	Amortisman süresi (yıl)	18,3	17,3	17,9
	Elektrik üretim maliyeti (TL/kWh)	0,09	0,08	0,08
	Enerji Dengesi / Şebekeyi Besleme Kavramı	TAM	TAM	TAM

***Tablo** Hata! Yalnızca Ana Belge**.** PVSOL sonuç raporu Monokristal PV Panel açı değişimine göre kıyaslama ve Polikristal PV Panel Karşılaştırılması*

Simülasyonu yapılan projede güç artışı yapılmadan mevcut yapının kuzey cephede olan bina yerleşimi doğu cepheye çevrilerek daha fazla güç üretilmesi sağlanmıştır Tablo 1. ‘ de görülen karşılaştırılmalı sonuçlar yer almaktadır . Bina yerleşiminde değişiklik olduğunda güç artmış ve sonuçlar incelenmiştir. Bağlantı şekilleri , aynı güç ve tipteki PV modül sayısı değiştirilmeden (PV jenaratör yüzeyi aynı kalacak şekilde) yaptığımız değişiklik ile ışınım daha fazla olduğu için yıllık kazanç artmış ve amortisman süresi 1 yıl düşmüştür böylelikle önlenen karbondioksit emisyonunda arttığı gözlemlenmiştir.

Projede kullanılan 200 W Mono Kristal PV modül yerine yine aynı güç ve sayıda 200 W Poli Kristal PV modül kullanarak farklı tip ve özellikteki panel kullanarak aynı yerleşim planı ile daha fazla PV jenaratör yüzeyinin elde edildiği böylelikle aynı cephe ve aynı inverter ile ilgili projede maliyetin düştüğü gözlemlenmiştir , veriler Tablo 1 ‘ de verilmiştir . Projede 108 adet 200 W PV modül kullanılmıştır , Poli ve Mono Kristal PV modül kullanımının proje maliyet ve amortisman süresine etkisinin az olduğu gözlemlenmiştir.

PVSOL bir çok tasarım çeşidi sunmaktadır , PV panellerin montajlarının farklı versiyonları da PVSOL üzerinden modellendirilip incelenebilmektedir. AC ana şebeke bağlantısında voltaj seviyesi değiştirilerek verimli ve fiyat performans inverter seçimleri bile yapılabilir.

Güneş panellerinin montaj şekli büyük önem arz etmektedir. Sehpaların açı değerine göre güneş enerjisinden elektrik enerjisi üretim kazancı değişmektedir. Bu açı değeri de lokasyona göre farklılık kazanmaktadır.

Güneş panelleri, özellikle güneş ışınımının etkili absorbanı olarak tasarlanmıştır. Hücreler, genellikle modül kapsülleri ve arka sırt tabakasından daha yüksek ısı üretecektir. Bu nedenle güneş hücreleri daha fazla birim alan başına üretilen ısıyı arttırır.

Bir PV modülü tipik olarak 1000 W/m2 altında 25 °C'de değerlendirilmektedir. Ancak santralde çalışırken, daha yüksek sıcaklıklara maruz kalırlar , ortam sıcaklığının artması paneller için bir anlamda üretilen gücün artması demektir. Düşük yalıtım koşulları, panel ve kablolardaki sıcaklık artışı panel verimliliklerini düşürmektedir. Montajları çeşitlendirerek ilgili bölgede GES tesisinin verimi incelenmiştir.

İslahiye ilçesinin aylık ortalama sıcaklık verilerine göre sıcaklığın düşük olduğu aylarda Tablo 2 ve Tablo 3 ‘ te de görüldüğü şekilde panel verimliliğinin arttığı görülmüştür. Hava sirkülasyonunun düşük olduğu ve panel,kablolarda ısınmaya sebep olacak şekilde çatıya sıfır montaj yapılmış sonuçlar hava sirkülasyonunun yüksek olduğu sehpa üzerine montaj yapılan modelle karşılaştırılmıştır verimlilik sonuçları Tablo 3 ‘ de görülmektedir. Ortam sıcaklığı arttıkça verim azalmıştır.

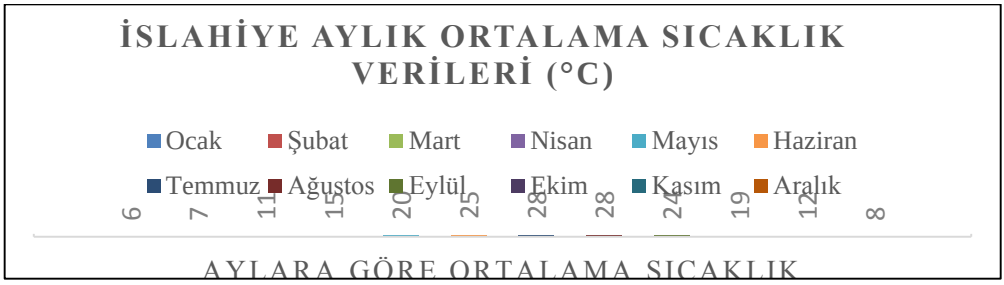

***Tablo** Hata! Yalnızca Ana Belge.. Gaziantep ili İslahiye ilçesi aylık ortalama sıcaklık verileri C °*

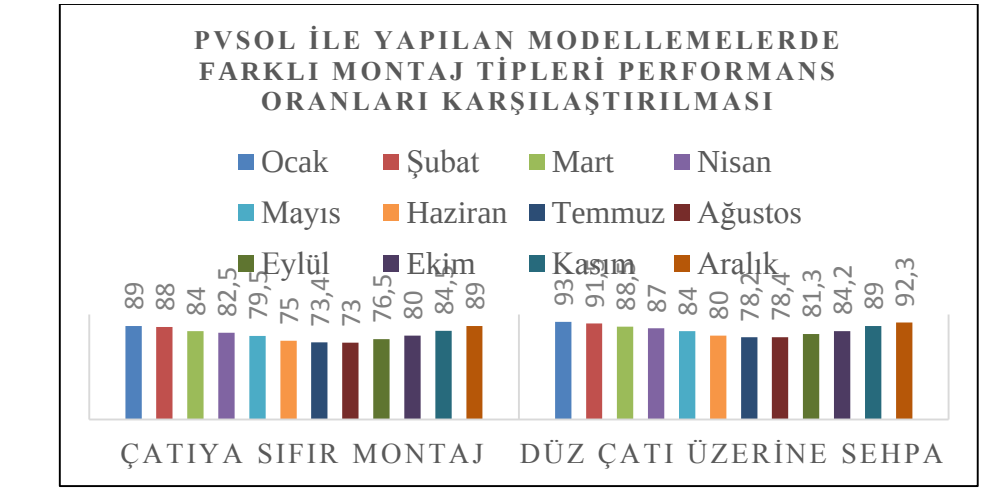

***Tablo** Hata! Yalnızca Ana Belge.. Farklı montaj tiplerinin sıcaklık-verim kıyaslaması verim oranı %*

Gaziantep İli Güneş Enerjisi Potansiyelinin Araştırılması ve Örnek Güneş Enerjisi Santrali Analizi

Akif AKINCI[1], Ipek ATIK[2], Ceren BILGIÇ[3]✉, Mesut BILGIC[4]

Son yıllarda ülkemizde enerji ihtiyacının artmasıyla birlikte Güneş Enerjisi Santralleri'nin (GES) kurulumu giderek artan bir trend haline gelmiştir. Yüksek maliyet gerektiren bu santrallerde, doğru malzeme seçimi ülke ekonomisi açısından önem arz etmektedir. Bu sebeple, yatırım öncesi çalışmalarında malzeme seçimi titizlikle yapılmalıdır. Gaziantep ilinde belirli bir arazi üzerine planlanan Güneş Enerjisi Santrali örneğinde, farklı güneş enerjisi santrali malzemeleri kullanılarak verimlilik analizi gerçekleştirilmiştir. Elde edilen sonuçlar, malzeme seçiminin santralin verimliliği üzerindeki etkili rolünü ortaya koymaktadır. Bu analizler, güneş enerjisi santrallerinin optimal performansı ve ekonomik verimliliği için önemli yönlendirmeler sunmaktadır. Gaziantep gibi güneş potansiyeli yüksek bölgelerde malzeme seçiminin doğru yapılması, santralin uzun vadeli başarısı açısından kritik bir faktördür.

Anahtar Kelimeler: Güneş Enerjisi, Verimlilik Analizi, Gaziantep, Güneş Enerjisi Santrali, Yenilenebilir Enerji

✉ *Corresponding Author Email : bilgiceren6493@gmail.com*

1. Giriş

Gaziantep, Türkiye'de güneş enerjisi potansiyeli yüksek olan illerden biridir. Genellikle yaz aylarında sıcak ve güneşli bir iklimi vardır. Bu özellikleriyle güneş panelleri için oldukça elverişli bir ortam sunar. Ayrıca, Gaziantep'in tarım alanlarının yanı sıra endüstriyel ve ticari faaliyetlerin yoğun olduğu bir şehir olması, elektrik tüketiminin de yüksek olmasına neden olur. Bu da güneş enerjisiyle elektrik üretimi için daha fazla potansiyel sağlar. Gaziantep için tipik güneşlenme süresi yılda yaklaşık 2.800 saat civarındadır. Bu, güneşlenme süresinin oldukça yüksek olduğunu gösterir. Ayrıca, yıllık ortalama güneş ışını yoğunluğu da yaklaşık olarak 1.600 kWh/m² civarındadır. Bu da bölgenin güneş enerjisi potansiyelinin oldukça yüksek olduğunu gösterir.

Gaziantep'te son yıllarda güneş enerjisi projelerine olan ilgi artmıştır. Belediyeler, kurumlar ve bireyler güneş enerjisi sistemlerine yatırım yaparak hem çevreyi korumayı hem de enerji maliyetlerini düşürmeyi hedeflemektedirler. Bu yatırımların artmasıyla birlikte Gaziantep'in güneş enerjisinden faydalanma potansiyeli de giderek artmaktadır.

Türkiye'nin Güneş Enerjisi potansiyelinin 380 milyar kWh/yıl olması (Topçu ve Yünsel, 2016), ve coğrafi konumunun güneşten faydalanma için oldukça elverişli olması (Uyan, 2016) araştırmacıları güneş enerjisi santralleri (GES) kurulumu çalışmalarına yöneltmiştir. Kurulum çalışmalarında fizibilite araştırması esnasında birçok kriterin etkili olması ve kurulum maliyetinin yüksek olması (Effat, 2013) sebebiyle mekânsal analizlerde zorluklar yaşanmaktadır. Çünkü GES yer seçiminde birçok kriterin ele alınması ve beraber değerlendirilmesi gerekmektedir.

Özdemir (2013) çalışmasında, Türkiye'de fotovoltaik sistemler için uygulanabilirliği araştırmak ve finansal değerlendirme yapmak için bu sistemlerin kurulumunun uygun olduğu bölgeler seçerek finansal yatırım teknikleri konusunda incelemelerde bulunmuştur. Araştırmasında seçtiği bölgelerdeki radyasyon oranlarını ve ortalama güneşlenme saatlerini kullanarak üretilecek enerji miktarını karşılamak için ne kadar panel gerektiği sorusuna yanıt aramıştır. Sonuç olarak finansal değerlendirme için bütçeleme tekniklerini kullanıp her bölge için maliyet, geri ödeme, verimlilik hesaplamalarını yaparak kıyaslama fırsatı bulmuştur. Hesaplamaların yapılmasında önemli faktörlerden biri de radyasyon değeridir. Fotonların uzay boşluğundan dünyaya gelene kadar ki yolculuğundan dünyanın farklı yer ve bölgelerine göre ışımaları da farklılık göstermektedir. Bu farklılardan dolayı, yatırımın en önemli evresinden biri de bu faktörün göz önünde bulundurulması ile gerçekleşmektedir

2. Materyal ve Metot

Bu çalışmanın amacı, güneş enerjisi sisteminin gerçek saha koşulları altında performansını değerlendirmek ve simülasyon sonuçlarıyla karşılaştırmaktır. Güneş enerjisi sistemlerinin tasarımı ve performans analizi için yaygın olarak kullanılan PVsyst yazılımını kullanarak gerçekleştirilen simülasyonlar, saha koşullarının dikkate alındığı bir senaryo üzerinden yapılmıştır. Bu çalışmanın hedefleri arasında, PVsyst programının kullanımının incelenmesi, güneş enerjisi sisteminin

tasarımının gerçekleştirilmesi, sistemin performansının simülasyonlarla değerlendirilmesi ve gerçek verilerle karşılaştırılması yer almaktadır. Gerçek saha ölçümlerinden elde edilen veriler, PVsyst tarafından sağlanan simülasyon sonuçlarıyla karşılaştırılacak ve sistem performansının doğruluğu değerlendirilecektir. Elde edilen sonuçlar, güneş enerjisi projelerinin planlanması, tasarımı ve performans optimizasyonu süreçlerinde yol gösterici olacak ve sektöre pratik bir katkı sağlayacaktır.

Öncelikle bölgenin coğrafi yapısı ve kurulması planlanan yapının arazi şartları göz önüne alınarak bölgesel bir araştırma yapmak gerekmektedir. Güneş enerjisi santrallerinde en önemli başlıca faktörlerden biri de radyasyon ve güneşlenme süresidir. Bu değerler ne kadar fazla olursa elektrik üretim değerleri ve verimlilikte o oranda fazla olacaktır. Yapılan hesaplamalar seçilen bölge üstünden yapılmakta olup en son halinde tesis tamamlandıktan sonra karşılaştırma fırsatı bulunacaktır.

Evirici sistemlerinde özellikle saha kurulumlarında merkezi inverter ya da bölünmüş inverter modelleri kullanılmaktadır. Merkezi inverterde kurulumu yapılan saha seri bağlantıları tek bir inverterde toplanıp şebekeye verilmek üzere gönderilebilmektedir. Ama bu tarz durumlarda paneller arasında bağlantıyı sağlayan DC kablolar daha uzun tutulacağı için ve bu kablolar AC kablolara göre daha hassas olduğu için ilerleyen zamanlarda sorun yaratabilmektedir. AC kablolar toprak altından nitekim daha korunaklı olarak ilerlemektedir. DC kablolarda maliyet düşük olabilir ama ufak çaplı sorunlar santralin ömrünü kısaltabilmektedir. Bu ufak çaplı sorunların neden ve nerede olduğunu bulmakta bakım onarım anlamında gecikmelere sebep olabilmektedir. Dizi şeklindeki inverter kullanımlarında ise DC kablolar üretim için kısımlara ayrılır böylece hem izlemesi hem de herhangi bir sorunda müdahale edilmesi daha kolay olacaktır. Merkezi inverterin sorun çıkardığı zamanlarda sistem tüm olarak kapatılması gerekmektedir. Dizi sisteminde ise sadece sorunlu olan kısım kapatılıp, onarımı yapılıp, devreye tekrardan sokulabilmektedir. Dizi sisteminde AC kablolar biraz daha uzun tutulmak zorunda kalınabilir. Bu durum kablolama için maliyet açısından daha fazla yatırım anlamına gelmektedir. DC kablolar panellerin birbirleri ile olan bağlantısında kullanılmaktadır. Santrallerin kullanım sürelerinin 25 yıl olduğu göz önünde bulundurulursa, kabloların bu konuda dayanıklı bir şekilde üretime destek vermesi çok mühimdir. Sıcaklık ve yüksek ışınımdan etkilenmemeleri için DC kablolar panel altlarından götürülmektedir.

AC kabloları da DC kablolara göre çap olarak çok daha büyük olduğundan, yer altından iletimi sağlanmaktadır.

Gaziantep İli GES Uygulanabilirliği Açısından Değerlendirilmesi

Gaziantep iline düşen yıllık ışınım miktarı 1 m2 alana 1550-1600 yer yer 1650 kWh/m2 -yıl dır. Ülke ortalamasının 1350kWh/m2- yıl olduğu düşünülürse Gaziantep güneş enerjisi alanında yatırım yapmak için uygun üretim koşullarına en uygun illerimizden biridir. Almanya en çok 1130 kWh/m2 -yıl ışınım miktarına sahiptir. Ancak, Dünyadaki güneş enerji sistemlerine en fazla yatırım yapan ülkedir. Gaziantep bölgesinde yapılan Şebekeye Paralel Fotovoltaik yatırımların mevcut teşvikler ve doğru tasarlanmış sistemler ile en fazla 10 yıl içerisinde kendisini amorti edeceği öngörülmektedir. Günümüz teknolojisi ile üretilen sistemlerin doğru tasarlanması halinde 25 yıl ömürlü sistemler olduğu düşünülürse, kurulan sistemler yatırımcıyı kara geçireceği bilinmektedir

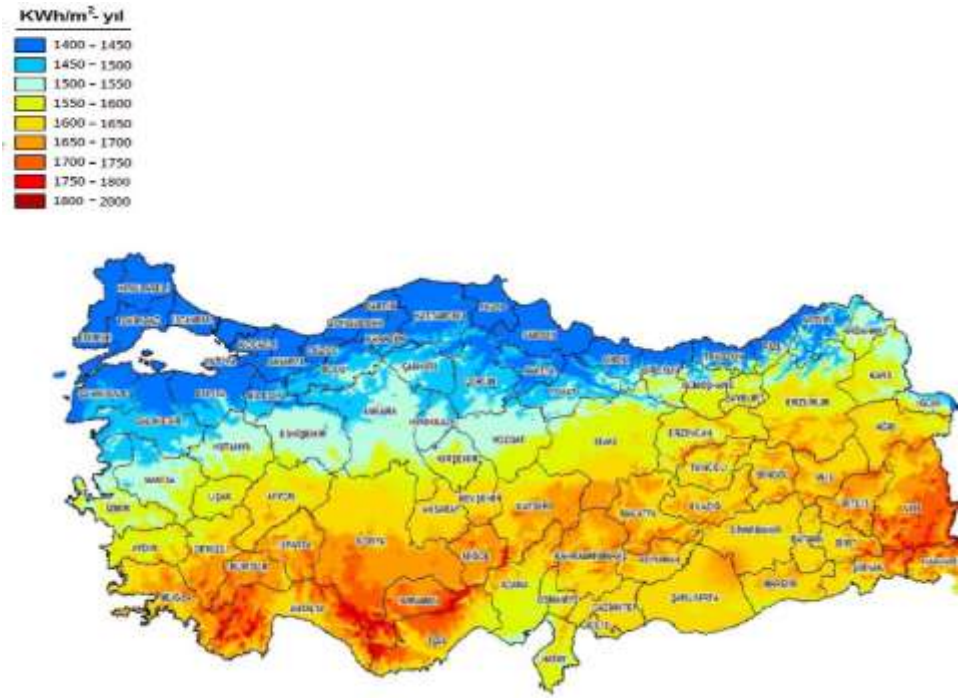

Şekil 1. Türkiye Güneş Radyasyon Haritası

Projenin Tasarlanması

Arazi tipi dağıtık güneş enerji santralinin tasarımı ve simülasyon uygulaması çalışmasında GES santrali yatırımı yapılmadan önce simülasyon çalışmalarının hem fizibilite çalışmalarında hem de daha uygun bir yerleşim planı oluşturmada faydalı bir yöntem olabileceği gözlemlenmiştir (Turan, 2022).
Ülkemizde fotovoltaik güneş panellerinden en iyi verimi alabilmek için optimum eğimde ve tam güneye bakacak şekilde konumlandırılmalıdır. Ancak arazilerde GES uygulaması yapılırken fotovoltaik güneş panelleri istenilen eğimde yerleştirilemezler çünkü mevcut arazi eğimine uyulmak zorunda kalınır. Ayrıca arazi alanı tam güney olmaya bilir bu durumda ise en uygun alan tercih edilmelidir. Projede kullanılacak olan malzeme listesi Tablo 1'de gösterilmiştir.
PVsyst, fotovoltaik sistemlerin kurulum öncesi üretim verilerini analiz etmek, boyutlandırmak ve modellemek amacıyla dünya genelinde yaygın bir şekilde kullanılan bir simülasyon programıdır. Program, off-grid (şebekeden bağımsız) veya on-grid (şebeke bağlantılı) santraller için panel, inverter ve kurulacak bölgenin ışınım ve meteorolojik verilerini kullanarak sistemle ilgili simülasyon sonuçlarını sunar. Bu şekilde, kullanıcıya sistemin potansiyel faydaları ve olası kayıpları hakkında bilgi verir. Ayrıca, programın 3D uygulamasıyla sistem üzerindeki gölgelemelerin modellemesi yapılmaktadır. Bu sayede, gölgelenmenin sistem üzerindeki etkisi de hesaplanabilmektedir (Çınaroğlu, 2021).

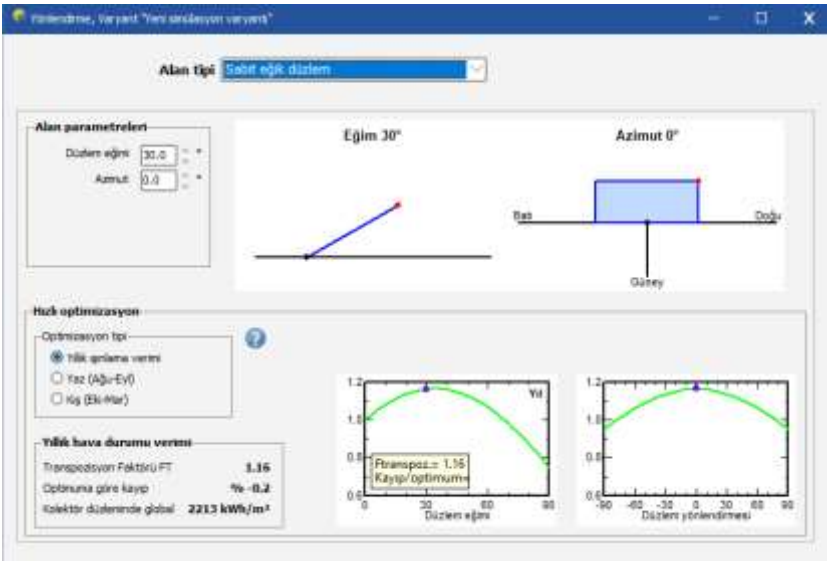

Şekil 2. Pvsyst Uygulaması

Sistem benzetiminin ilk adımında, projenin coğrafi konumu tespit edilmekte ve bu konuma özgü meteorolojik veriler benzetim programı aracılığıyla sentetik olarak oluşturulmaktadır. Ardından, sistemde panel açısı ve azimut değeri belirlenmekte olup, bu adım PVsyst programının "Orientation" seçeneği kullanılarak gerçekleştirilmektedir. Şekil 2'de görüntüsü sunulan ekran aracılığıyla panel açısı ve azimut verilerinin girilmesiyle orientation aşaması tamamlanmıştır. Bu değerler, güneş ışınlarının optimum verimlilikle yakalanabilmesini sağlamak amacıyla seçilmiştir.

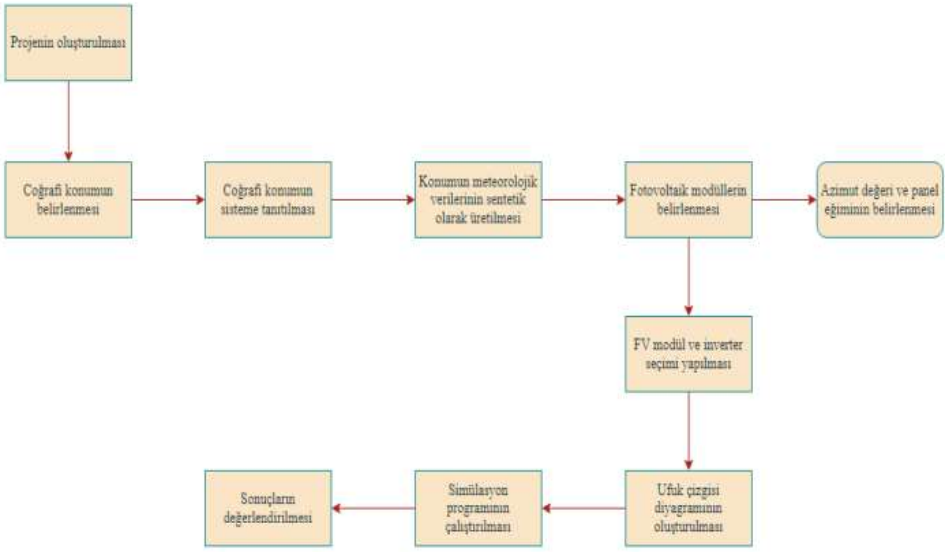

Şekil 3. Simülasyon programının akış diyagramı

FV paneller kullanılarak enerji eldesi yapılırken inverter seçimi çok önemlidir. Simülasyonu yapılan bu sistemde 3 farklı modül çeşidi ve inverter çeşidi kullanılmıştır. Sistemin toplam gücünü destekleyecek inverter seçimi yapılmıştır. Panel ve inverter seçimiyle ilgili olan bölümler "System" seçeneği altında gerçekleştirilmiştir. Bu işlemin ekran görüntüsü Şekil 3'te verilmiştir.

2. Bulgular ve Tartışma

PVsyst programında öncelikli olarak koordinatlarımız girilmiştir. Panel ve evirici bilgileri girilmiş olup dizi ve seriler oluşturulmuştur. Sistemde olabilecek kayıplar düşünülerek verileri sisteme işlenmiştir.

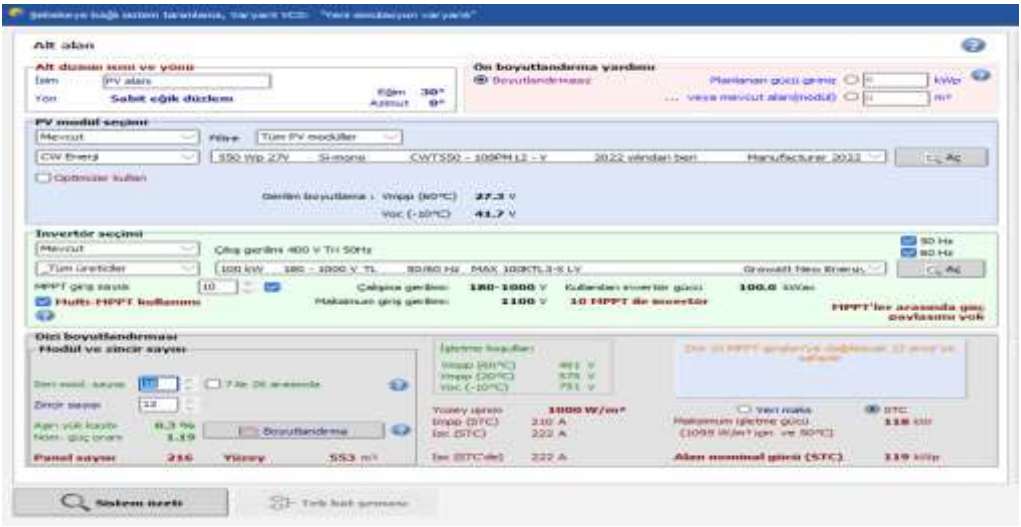

Şekil 3. Panel ve inverter seçim ekranı

Yaptığımız çalışmada PVsyst programı ile 3 farklı sistem modellemesi yapılmıştır. Ortalama 120 KWP sistem gücü için, 216-221 sayıda panel ve 99.9- 100 kW gücünde eviriciden oluşan sabit açılı ve çift eksen güneş takipli sistem modellemesi yapılmıştır. Paneller arasında 6 mm2 'lik DC güneş kablo, evirici çıkışında ise 120 mm2 'lik AC kablo kullanılmıştır. Buradaki amacımız üretim verilerini karşılaştırmak olduğu için modellenen tesislerin koşulları ve kullanılan ürünler nitelik ve nicelik olarak farklı seçilmiştir.

PVsyst programı ile üretim simülasyonu çalıştırıldığında kurulması planlanan sistemin Akif Akıncı GES projesinde, yılda yaklaşık 186,7 MWh enerji üretebileceği ve sistemin %85,44 performansla çalışacağı öngörülürken, Ceren Bilgiç GES projesinde yılda yaklaşık 180,4 MWh enerji üretebileceği ve sistemin %82,78 performansla çalışacağı öngörülmüş, Mesut Bilgiç GES projesinde yılda yaklaşık 184,1 MWh enerji üretebileceği ve sistemin %84,23 performansla çalışacağı öngörülmüştür.

Sonuç

Sonuçlar, PVsyst simülasyonunun tasarlanan güneş enerji santralinin performansını gerçek dünya koşullarına yakın bir şekilde tahmin etme yeteneğine sahip olduğunu

SİSTEM GÜCÜ (KWP)	PANEL SAYISI	MODÜL	EĞİM / AZİMUT	İNVERTÖR GÜCÜ (KWA	ÜRETİLEN ENERJİ (KWH/YIL)	ÜRETİLEBİLİR (KWH/KWP/YIL)	PERF. ORANI
				277 C)			

AKİF AKINCI GES	119	216	12 ZİNCİR X 18 SERİ	30 / 0	100	221792	1867	%85.44
CEREN BİLGİÇ GES	121	220	11 ZİNCİR X 20 SERİ	30 / 0	100	218342	1804	%82.78
MESUT BİLGİÇ GES	122	221	13 ZİNCİR X 17 SERİ	30 / 0	99.9	223718	1841	%84.23

Tablo 1. Performans Sonuçları

göstermektedir. Panel sayısı, inverter sayısı, panel ve inverter kapasiteleri, kurulumun yerleşim şekli, panel eğimi ve yönelimi gibi tasarım parametrelerinin enerji üretimine etkileri belirlenmiştir. Sistem performansının analizi, enerji üretimini optimize etmek için tasarım ve konfigürasyon değişiklikleri yapılması gerektiğini ortaya koymuştur.

Ayrıca, panel eğimi ve yönelimi üzerinde yapılan analizlerin enerji üretiminde önemli bir etkiye sahip olduğu görülmüştür. Optimal panel eğimi ve yönelimi seçimi, güneş ışığının en verimli şekilde kullanılmasını sağlar ve dolayısıyla enerji üretimini artırır. Güneş enerji santralinin performansı, panel ve inverterlerin kalitesiyle de doğrudan ilişkilidir. Yüksek kaliteli bileşenlerin seçimi, enerji verimliliğini ve sistemin güvenilirliğini artırır.

Bu çalışmadan elde edilen sonuçlar, güneş enerji santrali projelerinin planlama ve tasarım aşamalarında karar vericilere ve mühendislere rehberlik etmek amacıyla önemli bir katkı sağlamaktadır. Gerçek saha verilerinin simülasyonlarla birleştirilmesi, daha gerçekçi sonuçlar elde etmeyi mümkün kılarak projelerin başarısını artırır. PVsyst simülasyonu ve analizi, güneş enerji santrali projelerinin planlama aşamasında kullanılabilecek önemli bir araç olarak değerlendirilebilir.

Gerekli kaynağa sahip ve ihtiyaç duyacağı ek kaynağı temin edebilecek yatırımcılar, kaynaklarını kuşkusuz riski düşük ve getirisi büyük yatırım alanlarında değerlendirmek isterler. Bu itibarla öngörülen sermaye yatırımı için karar verilmeden önce “Gayrimenkul Geliştirme” çalışması yapılması mutlak zorunluluk arz etmektedir.

Günümüzde enerji maliyetlerinin düşürülmesi, kaynakların etkin ve verimli bir şekilde kullanılması çevre açısından büyük önem arz etmektedir. FV sistemler, yenilenebilir enerji kaynakları arasında yer alan sürdürülebilir enerji üretimi olanağı sağlayan teknolojilerdir. Güneş enerjisinin tükenmeyen ve ücretsiz bir kaynak olması,

FV sistemlerin kullanılmasıyla enerji maliyetlerini düşürmek ve firmaların karlılığını artırmak açısından büyük avantaj sağlamaktadır. Bu nedenle, güneş enerjisine yapılan yatırımların arttırılması ve FV sistemlerin yaygınlaştırılması, Türkiye gibi özellikle yaz aylarında yüksek miktarda enerji üretilebilecek ülkeler için çevresel ve ekonomik anlamda olumlu sonuçlar doğuracak önemli adımlardır Simülasyon sonuçları, FV panel sisteminin yüksek performans sergilemesi sebebiyle, Gaziantep ilinin güneş enerjisi açısından oldukça elverişli bir bölge olduğunu ve tasarımı yapılan bu projenin uygulanabilir olduğunu göstermektedir. Çalışma özellikle Gaziantep ilinde kurulacak arazi tipi fotovoltaik panel sistemlerinin tasarımı ve performans analizi açısından, sürdürülebilir enerji uygulamalarına yol gösterici olabilecektir. Yenilenebilir enerji kaynaklarının kullanıldığı bu tür sistemlerin ülke genelinde yaygınlaştırılmasının, maliyetleri düşürmenin yanı sıra konvansiyonel enerji kaynaklarına olan bağımlılığı da azaltacağı düşünülmektedir.

Kaynakça

Effat, H. A. (2013). Selection of Potential Sites for Solar Energy Farms in Ismailia Governorate, Egypt using SRTM and Multicriteria Analysis, International Journal of Advanced Remote Sensing and GIS 2013, Volume 2, Issue 1, pp.205- 220, Article ID Tech-125 ISSN 2320 – 0243.

Topcu, C., Yünsel DT. "Yenilenebilir Enerji Raporu". http://www.cka.org.tr/dosyalar/ enerji.pdf (09.05.2019).

Uyan, M., (2016). Güneş enerjisi santrali kurulabilecek alanların AHP yöntemi kullanılarak CBS destekli haritalanması. Pamukkale Üniversitesi Mühendislik Bilimleri Dergisi, 23(4): 343-351.

Özdemir, G., 2013. Investment Analysis of Solar Energy Systems. Bahçeşehir Üniversitesi, Fen Bilimleri Enstitüsü, Yüksek Lisans Tezi, İstanbul.